Modélisation du bilan hydrique à pas de temps mensuel pour l'évaluation de l'impact du changement climatique dans le bassin Amazonien du Pérou.

Waldo Sven Lavado Casimiro

Université de Toulouse

THÈSE

En vue de l'obtention du

DOCTORAT DE L'UNIVERSITÉ DE TOULOUSE

Délivré par *l'Université Toulouse III - Paul Sabatier (UT3 Paul Sabatier)*
Discipline ou spécialité : *Hydrologie*

Présentée et soutenue par *Waldo Sven LAVADO CASIMIRO*
Le *mardi 16 février 2010*

Titre :
Modélisation du bilan hydrique à pas de temps mensuel pour l'évaluation de l'impact du changement climatique dans le bassin Amazonien du Pérou.

JURY

M. Jérôme Viers (Professeur UPS, Toulouse)	*Président*
Walter Collischonn (IPH, Porto Alegre)	*Rapporteur*
Gil Mahé (IRD-MSE, Montpellier)	*Rapporteur*
Mme. Elizabeth Silvestre (SENAMHI, Lima)	*Examinateur*
M. Abel Mejia (Président UNALM, Lima)	*Examinateur*
Mme. Sandra Ardoin (IRD-MSE, Montpellier)	*Invitée*

Ecole doctorale : *Sciences de l'Univers, de l'Environnement et de l'Espace (SDU2E)*
Unité de recherche : *LMTG - UMR 5563 UR 154 CNRS Université Paul Sabatier IRD*
Directeur(s) de Thèse : *Jean-Loup Guyot,David Labat*
Rapporteurs : *Gil Mahé et Walter Collischonn*

Résumé

Les recherches entreprises au cours de la présente thèse s'intéressent à répondre aux questions suivantes:

• Quels sont les cycles annuels et saisonniers, ainsi que la variabilité interannuelle et intra-saisonnière à moyen et long terme, des principales composantes du cycle hydrologique sur les bassins des rios Huallaga et Ucayali ?
• Quelles sont les réserves disponibles en eau sur les bassins des rios Huallaga et Ucayali ?
• Quel est l'impact du changement climatique sur l'hydrologie des rios Huallaga et Ucayali ?

En premier lieu, nous décrivons les principales caractéristiques des bassins des rios Ucayali et Huallaga, ainsi que la base de données utilisée. Nous avons ainsi mis en évidence le réchauffement sur notre zone d'étude (estimé à +0.09°C par décade). De plus, les ruptures observées sur les séries de température moyenne à la fin des années 70 concordent avec les séquences d'événements de type « El Niño ». Nous avons aussi démontré une corrélation négative entre les températures et l'indice du Pacifique (Indice d'Oscillation du Sud, IOS). Par contre, aucune tendance n'est mise en évidence dans les séries de précipitation. Néanmoins, environ 10% des stations de notre région d'étude présentent des ruptures significatives dans la période 1991-2000.
La production des ressources en eau sur les bassins des rios Ucayali et Huallaga est évaluée pour 7 sous-bassins : 6 situés dans le bassin de l'Ucayali et un situé dans le basin du Huallaga. Pour quantifier ces ressources en eau, nous utilisons deux modèles hydrologiques au pas de temps mensuel (GR2M et MWB3). L'utilisation des données de capacité de rétention en eau des sols (maximum, moyenne et minimum) de la FAO, comme valeurs d'entrée dans les modèles hydrologiques, a contribué à rendre plus physique ces modèles. Les paramètres optimaux obtenus par calibration reproduisent raisonnablement bien l'écoulement observé à l'exutoire des bassins sélectionnés.
L'impact des changements climatiques sur l'hydrologie ont été évalué en utilisant comme données climatiques les sorties des modèles de l'IPCC (BCM2, CSMK3 et MIHR), correspondant aux scénarios A1B et B1. Les écoulements annuels simulés sur la période 2008-2099 suggèrent que les impacts du changement climatique sur l'hydrologie varient avec le bassin, le modèle hydrologique choisi, et le scénario: Le sous-basin Requena est caractérisé par une augmentation (respectivement une diminution) d'écoulement en utilisant les modèles GR2M (respectivement MWB3) en considérant les scénarios A1B et B. Les bassins de Chazuta, Maldonadillo et Pisac voient leurs débits diminuer tandis que les bassins de Puerto Inca, Tambo et Mejorada voient leurs débits augmenter.
Les changements simulés dans les écoulements mensuels sur la période 2008-2099 suggèrent une augmentation pour tous les sous-bassins, excepté le bassin de Pisac. Juillet, Août et Septembre sont en général les mois caractérisés par les changements les plus marqués, avec une augmentation des débits pour les bassins de Requena, Chazuta, Puerto Inca, Maldonadillo et Tambo.

Mots Clés : bassin Amazonien ; Pérou ; variabilité hydroclimatique ; modélisation hydrologique ; changement climatique.

Abstract

The researches developed during this study gives answers about three important questions:

• What are the annual and seasonal cycles, as well as interannual and intra-seasonal variability in the medium and long term hydrological cycle over the basins of Huallaga and Ucayali rivers?
• What are the water resources available in the basins of Huallaga and Ucayali rivers?
• What is the impact of the climate change on the hydrological cycle of Huallaga and Ucayali rivers?

First, we describe the main features of the basins of Huallaga and Ucayali rivers, as well as the hydrological database used an we put in evidence a warming in our zone of study (estimated at +0.09°C per decade). Moreover, the ruptures observed in the series of average temperature at the end of the Seventies are in accordance with the sequences of "El Niño". We showed a negative correlation between the temperatures and the index of the Pacific (Southern Oscillation Index, SOI). On the other hand, no tendency is highlighted in the precipitation series. Nevertheless, approximately 10% of the stations in our area of study present significant ruptures during the 1991-2000 decade.
Then, the production of water resources in the basins of Huallaga and Ucayali rivers is evaluated over 7 sub-basins: 6 located in the Ucayali basin and one located in the Huallaga basin. To quantify water resources, we use two hydrological models at monthly step (GR2M and MWB3). The use of water holding capacity data of FAO soils (maximum, mean and minimum) as input of the hydrological models, contributed to propose physical interpretations to these models. The optimal parameters obtained by calibration procedure reproduce reasonably well the flow observed in the selected basins. The impacts of climate change on hydrology were evaluated using as climatic data the outputs of the IPCC models (BCM2, CSMK3 and MIHR), corresponding to the scenarios A1B and B1. The annual flows simulated in the 2008-2099 period suggest that the impacts of climate change on hydrology vary with the basin, the hydrological model chosen, and the scenario: The Requena sub-basin is characterized by an increase (respectively a reduction) of flow using GR2M model (respectively MWB3) considering the A1B and B1 scenarios. The Chazuta, Maldonadillo and Pisac basins exhibit flows decreasing while the basins of Puerto Inca, Tambo and Mejorada show flows increasing. The changes simulated in monthly flows over the 2008-2099 period suggest an increase for all the sub-basins, except the Pisac basin. July, August and September are in general the months characterized by the most marked changes, with an increase in flows for Requena, Chazuta, Puerto Inca, Maldonadillo and Tambo basins.

Key words: Amazonas basin; Peru; hydroclimatic variability; hydrological models; climate change.

Resumen

Las investigaciones realizadas en la presente tesis se interesan en responder a las siguientes preguntas:

• ¿Cuáles son los ciclos anuales y estacionales, así como la variabilidad interanual e interestacional a mediano y largo plazo de los principales componentes del ciclo hidrológico sobre las cuencas de los ríos Huallaga y Ucayali?
• ¿Cuáles son las reservas disponibles de agua sobre las cuencas de los ríos Huallaga y Ucayali?
• ¿Cuál es el impacto del cambio climático en la hidrología de los ríos Huallaga y Ucayali?

En primer lugar, describimos las principales características de las cuencas de los ríos Huallaga y Ucayali, así como la base de datos utilizada. Así, observamos un calentamiento sobre nuestra zona de estudio (estimado en +0.09°C por década). Además, las rupturas observadas sobre las series de temperatura media al final de los años 70 están en concordancia con el aumento de las frecuencias de los eventos "EL Niño". También demostramos una correlación negativa entre las temperaturas y el índice del Pacífico (Índice de Oscilación del Sur, IOS). Para las series de precipitación, ninguna tendencia clara se pone en evidencia. Sin embargo, alrededor del 10% de las estaciones de nuestra región de estudio presentan rupturas significativas en el período 1991-2000. La producción de los recursos hídricos sobre las cuencas de los ríos Ucayali y Huallaga se evaluaron para 7 sub cuencas: 6 situados en la cuenca del río Ucayali y uno situado en la cuenca del río Huallaga. Para cuantificar estos recursos hídricos, utilizamos dos modelos hidrológicos al paso de tiempo mensual (GR2M y MWB3). La utilización de los datos de capacidad de retención en agua de los suelos (máximo, media y mínimo) de la FAO, como valores de entrada en los modelos hidrológicos, contribuyó a hacer más físico estos modelos. Los parámetros óptimos obtenidos por el procedimiento de calibración reproducen razonablemente bien los caudales observados en las cuencas seleccionadas. El impacto de los cambios climáticos en la hidrología se evaluó utilizando como datos climáticos las salidas de los modelos del IPCC (BCM2, CSMK3 y MIHR), considerando los escenarios A1B y B1. Los caudales anuales simulados en el período 2008-2099 sugieren que los impactos del cambio climático en la hidrología varían con la cuenca, el modelo hidrológico elegido, y el escenario: La cuenca de Requena es caracterizada por un aumento (respectivamente una disminución) de los caudales al utilizar los modelos GR2M (respectivamente MWB3) al considerar los escenarios A1B y B. Las cuencas de Chazuta, Maldonadillo y Pisac ven sus caudales disminuir mientras que las cuencas de Puerto Inca, Tambo y Mejorada ven sus caudales aumentar. Los cambios simulados en los caudales mensuales en el período 2008-2099 sugieren un aumento para todas las cuencas, excepto la cuenca de Pisac. Julio, Agosto y Septiembre son en general los meses caracterizados por los cambios más fuertes, con un aumento de los caudales para las cuencas de Requena, Chazuta, Puerto Inca, Maldonadillo y Tambo.

Palabras Clave: cuenca Amazónica; Perú; variabilidad hidroclimática; modelización hidrológica; cambio climático.

Remerciements

Je tiens en premier lieu à remercier très sincèrement et très chaleureusement mes deux directeurs Jean Loup Guyot et David Labat qui ont assuré la finalisation de cette thèse. Aussi je dois remercier très sincèrement à Josyane Ronchail pour m'avoir aidé pendant la fin de ma thèse. Finalement je remercie aussi Sandra Ardoin-Bardin par m'avoir aidé au début de ma thèse pendant mon premier séjour hors de Toulouse à la Maison de Sciences de l'eau de Montpellier.

Cette thèse financée par le Conseil National de Science et Technologie Péruvien (CONCYTEC), l'Ambassade de Françe au Pérou et l'Institut de Recherche pour le Développement (IRD) a été menée au sein du Laboratoire de Mécanismes et Transferts en Géologie (LMTG) à Toulouse et au sein du Service National de Météorologie et Hydrologie Péruvien (SENAMHI) à Lima. Je remercie leurs directeurs respectifs François Martin (LMTG) et Wilar Gamarra (SENAMHI) de m'avoir accueilli pendant le parcours de ma thèse.

Au Pérou, je remercie le SENAMHI de m'avoir permis de passer mes séjours en France et à mes collègues de la Direction Générale d'Hydrologie et Ressources en eau pour m'avoir soutenu pendant le parcours de ma thèse. Je remercie aussi mes amis péruviens et « Molineros » Wilson Suarez, Jhan Carlo Espinoza et Fernando Vegas pour leurs conseils et temps passé avec eux en discussions scientifiques, politiques et de soirées bières au Pérou et en France. Je remercie aussi les membres du projet HYBAM au Pérou : Pascal Fraizy, Phillipe Vauchel, Jean Sébastien avec lesquels nous avons effectué des missions en Amazonie Péruvienne.

Toute cette histoire a commencé au début de l'année 2003 lors que j'ai fais ma première mission de jaugeages sur les fleuves amazoniens péruviens en tant qu'ingénieur du SENAMHI avec Jean Loup Guyot et Pascal Fraizy, mes collègues de l'IRD. Ensuite, j'ai eu la proposition de Jean Loup pour faire des études en France. Après deux ans de bataille, nous avons obtenu une bourse pour passer la première année de thèse en France. Après une année difficile en France j'ai eu l'occasion de connaître de très bons amis qui on rendu plus agréable mon séjour en France (Carolina, Teresa, Marcelo, Juan Gabriel, Matias, Joecyla, Michelly, Natalia, Pierre et d'autres pour lesquels je m'excuse par avance auprès d'eux si je ne les ai pas mentionnés). Après une année au Pérou, je suis revenu en France pour passer ma deuxième année de thèse, c'est ici que j'ai rencontré le bataillon des amis dont la plus part sont Chiliens avec qui j'ai passé de superbes moments de sport, de soirées, de pause-café et de batailles pour savoir l'origine du Pisco. Alejandro, German, Damian, Salvador, Carola, Jocelyn, Ana, Augusto et la plupart des autres mentionnés ci-dessus. Je remercie aussi Benjamin pour les matchs de tennis dignes de Roland Garros sur le terrain de l'OMP. Je remercie également mes collègues de bureau Laure, Marie et François Xavier pour m'avoir soutenu et pour leur compagnie très agréable.

Je remercie aussi l'ensemble des personnes au LMTG et au SENAMHI dont le travail ou simplement les conseils m'ont permis de mener à bien cette thèse et dont la liste est longue : il est difficile de toutes les citer ici au risque d'en oublier certaines. Je suis persuadé qu'elles se reconnaitront parmi celles à qui j'exprime ma profonde gratitude et mes sincères remerciements.

À Flavia.

À Hector, Lourdes, Renan, Boris, Kenneth et Titi.

Table des matières

Liste de Figures

Liste des Tableaux

CHAPITRE 1

Introduction

I. CHAPITRE 1. Introduction

Très peu d'études hydrométéorologiques exhaustives ont été à l'heure actuelle menées sur le Pérou. Les études précédentes sont en général très localisées sur des régions spécifiques et se basent sur des données climatologiques parcellaires (par exemple Gentry et Lopez-Parodi, 1980 ; Rocha et al., 1989 ; Marengo, 1995; Marengo et al., 1998a ; Rome-Gaspaldy et Ronchail, 1998 et autres). Récemment, la fonte des glaciers péruvien qui incluent 71% des glaciers tropicaux est devenu un enjeu qui rentre dans le cadre plus général de la mise en évidence d'un réchauffement global (Pouyaud et al., 2005). Ces études d'impact sur la ressource en eau ont porté spécifiquement sur le bassin du Rio Santa situé sur le versant Pacifique (Pouyaud et al., 2005 et Kaser et al., 2003). La deuxième problématique concerne le bassin Amazonien, d'une superficie de 6 000 000 km^2 avec un débit moyen annuel de 209 000 m^3/s (Molinier et al., 1996), qui se caractérise récemment par des événements extrêmes tels que la sécheresse de 2005 et la crue historique de 2009. Au Pérou, le Bassin Amazonien (BA) couvre 74.5% du territoire péruvien et fait actuellement l'objet d'une déforestation rapide (Oliveira et al., 2007), entraînant des crues importantes dans les zones de piémont. Le BA au Pérou se caractérise par la présence de régions de hautes altitudes couplées à de fortes pentes (les Andes) et de régions de plaines (la Forêt). Les rivières dans les Andes sont utilisées pour des usages agricoles, domestiques et énergétiques, tandis que dans la plaine amazonienne les fleuves sont utilisés comme moyen de communication entre les villages. Pour ces raisons, nous nous proposons de préciser les processus hydrologiques impactant le BA péruvien, ainsi que d'évaluer les impacts du changement climatique sur les régimes hydrologiques.

1.1 Contexte général du Pérou

Le Pérou (1 285 220 Km^2) est un pays caractérisé par divers ensembles physiographiques (Figure I-1) et climatologiques (Figure I-2). Pulgar (1941) a proposé de grouper les différences altitudinales en 8 régions homogènes : Chala ou Costa (0 à 500 m.s.n.m.), Yunga (500 à 2300 m.s.n.m.), Quechua (2300 à 3500 m.s.n.m.), Suni ou Jalca (3500 à 4000 m.s.n.m.), Puna (4000 à 4800 m.s.n.m.), Janca ou Cordillera (4800 à 6768 m.s.n.m.), Rupa rupa ou Selva Alta (400 à 1000 m.s.n.m.) et Omagua ou Selva Baja (80 à 400 m.s.n.m.). Cette classification a été reprise par le SENAMHI (2005) en utilisant la classification climatique de Thornthwaite (Thornthwaite, 1948a), mettant ainsi en évidence 27 zones climatiques différentes au Pérou (voir Figure I-2 et Tableau I-1). Voici les caractéristiques de ces différentes zones :

- **Climat Semi - Chaud Très Sec (Désertique-Aride-Sous Tropical)** : ce type de climat constitue un ensemble climatique remarquable sur le Pérou et s'étend sur presque toute la région de la côte, depuis Piura jusqu'à Tacna et depuis le littoral Pacifique jusqu'à l'altitude de 2000 m.s.n.m. environ, et représente 14% de la surface totale du pays. Ce climat se distingue par une précipitation moyenne annuelle 150 mm, une température moyenne annuelle de 18° à 19°C qui diminue dans les zones les plus élevées de la région.
- **Climat Chaud Très Sec (Désertique ou Aride Tropical)** : Il comprend le secteur septentrional de la région côtière, qui inclut une grande partie des départements de Tumbes et Piura, entre le littoral marin et la côte approximativement jusqu'à 1000 m.s.n.m. Il représente moins de 3% (35 000 km^2) de la surface du pays. Ce climat est très sec et chaud, avec une précipitation moyenne annuelle autour de 200 mm et une température moyenne annuelle de 24.7°C, sans changement thermique hivernal défini.

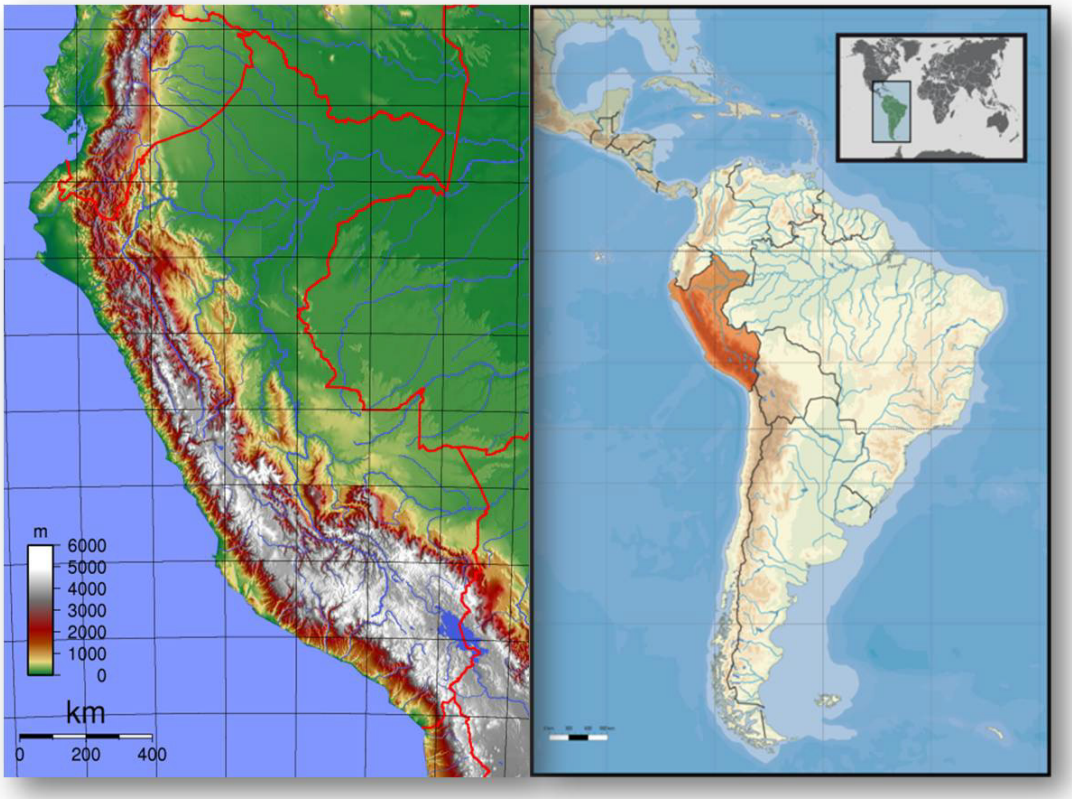

Figure I-1. Gauche : relief du Pérou en altitudes (http://geografia.laguia2000.com). Droite : république du Pérou en Amérique du Sud au 1er janvier 2009 (http://fr.wikipedia.org/wiki/fichier:south_america_location_per.png).

- **Climat Semi - Chaud Très Sec (Désertique-Aride-Sous Tropical)** : ce type de climat constitue un ensemble climatique remarquable sur le Pérou et s'étend sur presque toute la région de la côte, depuis Piura jusqu'à Tacna et depuis le littoral Pacifique jusqu'à l'altitude de 2000 m.s.n.m. environ, et représente 14% de la surface totale du pays. Ce climat se distingue par une précipitation moyenne annuelle 150 mm, une température moyenne annuelle de 18° à 19°C qui diminue dans les zones les plus élevées de la région.
- **Climat Chaud Très Sec (Désertique ou Aride Tropical)** : Il comprend le secteur septentrional de la région côtière, qui inclut une grande partie des départements de Tumbes et Piura, entre le littoral marin et la côte approximativement jusqu'à 1000 m.s.n.m. Il représente moins de 3% (35 000 km^2) de la surface du pays. Ce climat est très sec et chaud, avec une précipitation moyenne annuelle autour de 200 mm et une température moyenne annuelle de 24.7°C, sans changement thermique hivernal défini.
- **Climat Tempéré Subhumide (Steppe et Faibles Vallées Interandines)** : ce climat est propre à la région de montagne, correspondant aux vallées Interandines, d'altitude faible et intermédiaire, situées entre 1000 et 3000 m.s.n.m. Les températures dépassent les 20°C, et la précipitation moyenne annuelle est inférieure à 500 mm mais peut dépasser 1200 mm/an dans les parties les plus humides et orientales.
- **Climat Boréal (des Vallées Mesoandines) :** Ce climat s'étend sur la région de montagne entre 3000 et 4000 m.s.n.m. Il se caractérise par des précipitations annuelles de l'ordre de 700 mm et des températures moyennes annuelles de l'ordre de 12°C. Les étés sont pluvieux et les hivers secs avec de fortes gelées.

Figure I-2. Classification climatique du Pérou en utilisant la classification de Thornthwaite (d'après SENAMHI, 2005. Voir **Tableau I-1**).

Tableau I-1. Classifications des climats d'après Thornthwaite, 1948a.Voir Figure I-2.

Climats	
Pluie effective	**Efficience de température**
A Très pluvieuse	A' Chaud
B Pluvieuse	B'1 Semi-chaud
C Semi-sec	B'2 Tempéré
D Semi-aride	B'3 Semi-frais
E Aride	C' Frais
	D' Semi-froid
	E' Froid
	F' Polaire
Distribution de la pluie dans l'année	**Humidité Atmosphérique**
r Pluvieux pendant toutes les saisons	
i Hiver sec	H1 Très sec
p Printemps sec	H2 Sec
v Été sec	H3 Humide
o Automne sec	H4 Très humide
d Pas de pluies pendant tous les saisons	

- **Climat Froid (de Toundra)** : Ce type de climat, connu comme climat de Puna, correspond aux secteurs les plus élevés de la région andine compris entre 4000 et 5000 m.s.n.m. Il couvre environ 13% du territoire péruvien (170 000 km^2). Il se caractérise par des précipitations annuelles moyennes de 700 mm et températures moyennes annuelles de 6°C. Il comprend les collines, plateaux et sommets andins. Les étés sont toujours pluvieux et nuageux ; et les hivers (juin-août), sont extrêmes et secs.
- **Climat de Neige (Gélido)** : Ce climat correspond aux zones des neiges éternelles, avec des températures moyennes pendant tous les mois de l'année sous le point de congélation (0°C). Il est situé dans les secteurs dont l'altitude dépasse 5000 m.s.n.m. et qui sont recouvert par de grandes quantités de neige et de glace.
- **Climat Semi - Chaud Très Humide (Subtropical très Humide)** : Ce type de climat prédomine dans la forêt. Il se caractérise par son haut degré d'hygrométrie, avec des précipitations dépassant 2 000 mm/an et des valeurs extrêmes supérieures à 5 000 mm/an par exemple dans la région de Quincemil. Les températures sont inférieures à 22°C en général mais des températures plus élevées sont enregistrées dans les fonds des vallées et dans les zones de transition vers la plaine Amazonienne.
- **Climat Chaud Humide (Tropical Humide)** : Ce climat correspond aux plaines amazoniennes péruviennes. Il se caractérise par des précipitations moyennes annuelles de l'ordre de 2 000 mm et une température moyenne supérieure à 25°C, sans changement bien défini entre les saisons.

En conclusion, la présence de la Cordillère des Andes et de l'Altiplano divise les réseaux de drainage en trois bassins versants : Pacifique, Lac Titicaca et Amazonas (Atlantique) (Figure I-3). D'après un rapport de l' UNESCO (2006), la distribution moyenne annuelle du bilan hydrique (ruissellement) pour la période 1969-1999, calculée par différence entre les précipitations et l'évapotranspiration est de 16.4 mm sur le versant Pacifique, 129.8 mm sur le bassin du Lac Titicaca et 2696.5 mm sur le versant Amazonien. Ainsi, le ruissellement estimé par UNESCO (2006) est en opposition avec la distribution de la population au Pérou, où les plus grandes villes (Lima, Arequipa et Piura) sont situées sur le versant Pacifique.

1.2 A basin-scale trends in rainfall and runoff in Peru (1969-2004): Pacific, Titicaca and Amazonas drainage.

WALDO SVEN LAVADO CASIMIRO, JOSYANE RONCHAIL, DAVID LABAT, JHAN CARLO ESPINOZA & JEAN LOUP GUYOT

Cette section de la thèse sera présentée via un article en préparation. Il a été décidé de rajouter cette partie au document final car elle présente une vision globale et intégratrice du problème de la ressource en eau au Pérou.

Figure I-3. Versants du Pérou : Versant du Pacifique (ouest), Versant du Lac Titicaca (sud est) et Versant de l'Amazonas (est). (D'après UNESCO, 2006).

Résumé

Cette étude, basée sur des données s'étendant de 1969 à 2004, propose pour la première fois une analyse exhaustive des tendances hydroclimatologiques au Pérou. Cette contribution porte sur les trois principaux bassins versants du Pérou : Pacifique, Lac Titicaca et Amazonas, et porte sur les débits maxima (Qmax), moyens (Qmean) et minima (Qmin). Au total, une trentaine de bassins versants ont été étudiés : 29 dans la zone Pacifique, 3 dans la zone du Lac Tititcaca et 2 bassins versants (5 pour les pluies) dans la zone Amazonienne.

Les débits minima sont caractérisés en général par une tendance positive alors que cette tendance est négative sur la zone Pacifique. En effet, la plupart des bassins du nord de la zone

Pacifique sont caractérisés par des tendances négatives pouvant être reliées à la croissance des surfaces agricoles, et donc des besoins en eaux pour l'irrigation. Les débits minima mesurés dans les bassins des rios Chillon et Rimac présentent des tendances positives. En effet, ces ressources sont dédiées à un usage domestique, en particulier pour la population de la ville de Lima, capitale du Pérou. Des tendances opposées dans les débits minima observées dans la partie Sud de la zone Pacifique sont aussi imputables aux usages agricoles de l'eau. Enfin, les séries pluri-annuelles de Qmax, Qmean, Qmin et de précipitations mesurées sur la zone Pacifique sont comparées avec les principaux indices de circulation générale : L'index d'Oscillation du Sud (SOI), les températures superficielles de la mer (SST) dans l'Atlantique nord (NATL SST) et les différences des NATL moins la SST dans l'Atlantique Sud (SATL).

SUMMARY

According to the Peruvian Agricultural Ministry, the Pacific watersheds, where are located great cities and intense farming, only benefit from 1% of the available fresh water in Peru. That is why a thoroughfull knowledge of the hydrology of this region is of particular importance. In this study, it is completed by the analysis of the two other main Peruvian drainages, the Altiplano and the Amazon. Rainfall and runoff data collected by the National Service of Meteorology an Hydrology (SENAMHI) and controlled in the mark of the Hydrogeodynamics of the Amazon basin (HYBAM) program is the basis of this basin scale study that involve the 1969-2004 period. On the cost, runoff changes (increases or decreases) are detected during the low stage season. They mainly depend on human activities and infrastructures aimed at cities supplying and increasing agricultural exports that may remove water or on the contrary help sustain the minimum runoff. In the Amazon basin, natural causes as the long term warming of the northern tropical Atlantic explain the runoff diminution since the middle of the eighties.

Keywords: trend, rainfall, runoff, climate variability, Titicaca basin, Amazon, Pacific coast, Peru, tropical Atlantic.

INTRODUCTION

The North-South Andes cordillera in Peru (1 285 216 km^2) determines the presence of three main drainage basins (Figure 1), one toward the Pacific Ocean (Pd) on the western side of the Andes, another toward the Amazon basin on the eastern side on the Cordillera (Ad) and the southern endorheic Titicaca Lake basin on the Altiplano (Td). The Peruvian National Water Agency reports that Pd, Td and Ad represent respectively 21,7%, 3,8% and 74,5% of Peru and include 62, 13 and 84 main basins, respectively (Ruiz et al., 2008). The multi-annual water balance (difference between rainfall and evapotranspiration) has been computed for the 1969-1999 period by UNESCO (2006). It results that the available superficial water is 16.4 mm in Pd, 129.8 mm in Td and 2696.6 mm in Ad. Unfortunately, the availability of fresh water resources in Peru is opposite to population density, given that 88% of the population lives in along the Pacific coast, around the Titicaca lake and in the Andean zones of the Amazon basin, where there are only 2% of the Peruvian fresh water resources. Indeed, the greatest Peruvian cities (i.e. Lima, Arequipa and Piura) are in Pd where there is only 0.6% of the available fresh water of Peru. According to the Agricultural Minister (www.minag.gob.pe) Pd is an arid but fertile land. Agriculture has been developed thanks to irrigation that uses about 80% of the available water while domestic usages consume about 12% of the Pd available water. Private and public investments have been gathered in order to develop these infrastructures aimed at increasing agricultural exports.

Pd features small size basins with rivers initiating in the Andes cordillera and presenting a west to east direction, from the Andes toward the Pacific Ocean (Figure 1). These basins

exhibit bare and steep slopes that favour an important erosion and floods during the rainy season. Td is located on the Altiplano (Southeast of Peru) and its endorheic drainage is realized toward Titicaca lake (~ 3800 m a.s.l.), then Desaguadero river and finally Poopo and Salar de Coipasa lakes in Bolivia. The Ad is characterized by hot tropical lowlands near sea level and freezing cold tropical high mountain peaking at up to 6000 m a.s.l. of elevation;

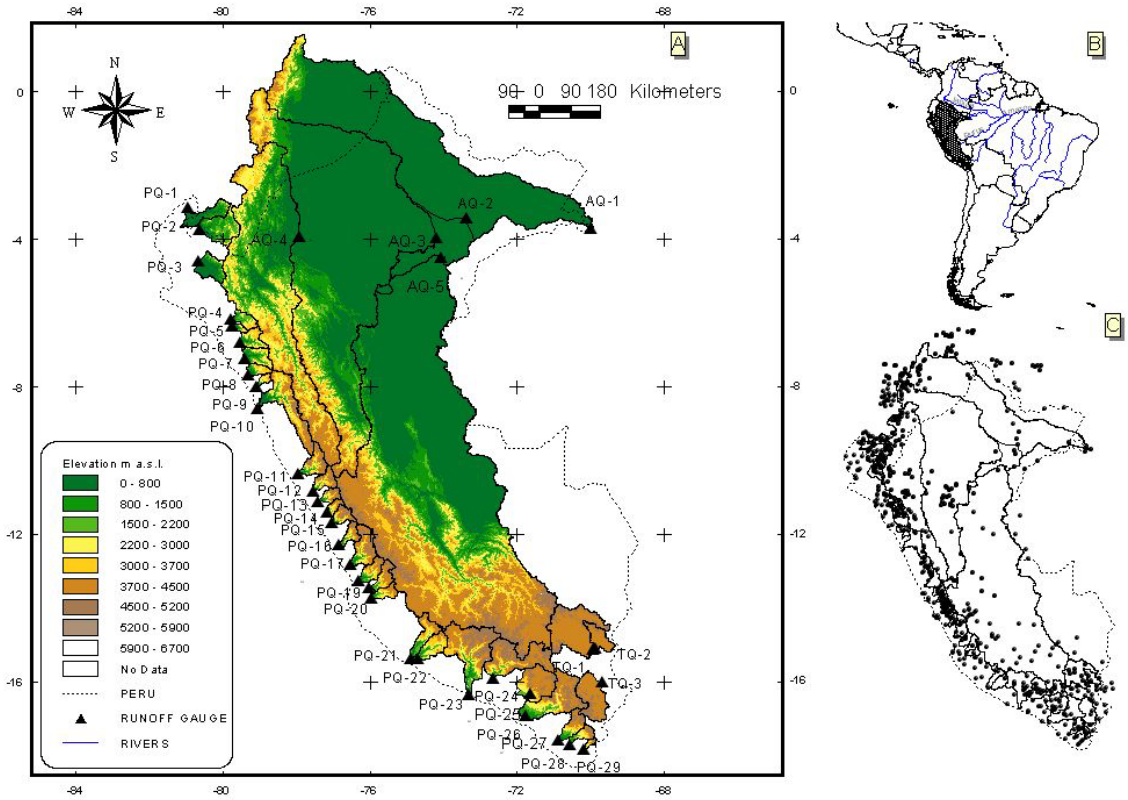

Figure 1. A) Elevation of the zone of study, mains rivers et limits of the selected basins. (see Table 1). B) Location of the zone of study in South America. C) Location of the rainfall gauges used in this study.

seldom in the world are such dramatic environmental contrasts lying closer together. Naturally, each of these two realms is subject to different, but in many aspects interrelated, sets of physical, geochemical and biologic parameters (ACTO, 2005). The rivers in the Ad exhibit steep slopes in the Andean western region while they are very smooth in the flat eastern lowlands.

Peruvian hydroclimatology is influenced by the disruption of the large-scale circulation patterns caused by the Andes cordillera, the contrasting oceanic boundary conditions and the landmass distribution (Garreaud et al., 2008). Low rainfall in Pd region is explained by the strong, large scale subsidence over the south-eastern subtropical Pacific Ocean and the southern Pd exhibits conditions of extreme aridity due to regional factors (Rutllant et al., 2003). Annual rainfall increases toward North in accordance with the seasonal southward displacement of the Pacific Intertropical Convergence Zone (ITCZ). UNESCO (2006) assesses that mean rainfall and runoff in Pd are about 274.3 mm and 168.1 mm respectively during the 1969-1999 period. Santa basin is an exception along the Pacific coast (PQ-10, Figure 1 and Table 1) as its water level is influenced by the melting of an upstream 600 km^2 glacier (Georges, 2004).

Table 1 Gauging stations used in this study. Lat. is latitude; Long. is longitude; Alt. is altitude and Dr. Ar. is Drainage Area

Gauging station	River	Code	Lat.	Long.	Alt. (m	Dr.Ar. (Km2)
El Tigre	Tumbes	PQ-1	3.72°S	80.47°W	40	4802
El Ciruelo	Chira	PQ-2	4.30°S	80.15°W	250	7760
Pte. Ñacara	Piura	PQ-3	5.11°S	80.17°W	119	4765
Racarumi	Chancay-Lambayeque	PQ-4	6.63°S	79.32°W	250	2401
Batan	Zaña	PQ-5	6.80°S	79.29°W	260	681
Yonan	Jequetepeque	PQ-6	7.25°S	79.10°W	428	3354
Salinar	Chicama	PQ-7	7.67°S	78.97°W	350	3651
Quirihuac	Moche	PQ-8	8.08°S	78.87°W	200	1918
Huacapongo	Viru	PQ-9	8.38°S	78.67°W	280	941
Pte. Carretera	Santa	PQ-10	8.97°S	78.63°W	18	11869
Yanapampa	Pativilca	PQ-11	10.67°S	77.58°W	800	4270
Sayan	Huaura	PQ-12	11.12°S	77.18°W	650	2896
Santo Domingo	Chancay-Huaral	PQ-13	11.38°S	77.05°W	697	1881
Larancocha	Chillon	PQ-14	11.68°S	76.80°W	120	1238
Chosica	Rimac	PQ-15	11.93°S	76.69°W	906	2339
La Capilla	Mala	PQ-16	12.52°S	76.50°W	424	2141
Socsi	Cañete	PQ-17	13.03°S	76.20°W	330	6003
Conta	San juan	PQ-18	13.45°S	75.98°W	350	3144
Letrayoc	Pisco	PQ-19	13.65°S	75.72°W	720	3107
Los Molinos	Ica	PQ-20	13.92°S	75.67°W	460	2154
Bella Union	Acari	PQ-21	15.48°S	74.63°W	70	4369
Puente Jaqui	Yauca	PQ-22	15.48°S	74.45°W	214	4245
Pte. Ocoña	Ocoña	PQ-23	16.42°S	73.12°W	122	16646
Huatiapa	Majes	PQ-24	16.00°S	72.47°W	699	13651
Pte. Del Diablo	Chili	PQ-25	16.41°S	71.50°W	236	8750
La Pascana	Tambo	PQ-26	16.99°S	71.64°W	281	12884
Pte. Viejo	Locumba	PQ-27	17.62°S	70.77°W	550	3639
La Tranca	Sama	PQ-28	17.73°S	70.48°W	620	1993
Aguas Calientes	Caplina	PQ-29	17.85°S	70.12°W	130	569
Pte. Ramis	Ramis	TQ-1	15.26°S	69.87°W	385	16229
Pte. Huancane	Huancane	TQ-2	15.22°S	69.79°W	386	3714
Pte. Ilave	Ilave	TQ-3	16.09°S	69.63°W	385	8714
Tabatinga	Amazonas	AQ-1	4.25°S	69.93°W	60	890308
Tamshiyacu	Amazonas	AQ-2	4.00°S	73.16°W	105	733596
San Regis	Marañon	AQ-3	4.51°S	73.95°W	80	359910
Borja	Marañon	AQ-4	4.47°S	77.55°W	450	115478
Requena	Ucayali	AQ-5	5.03°S	73.83°W	200	354316

On the contrary, very wet conditions are observed in the Amazon basin, on the eastern side of the Andes, due to the convection of moist and hot air that originates in the evapotranspiration of the rainforest and in the humid air advection from the tropical Atlantic. According to UNESCO (2006), mean rainfall over Ad during the 1969-1999 period is close to 2060 mm. But very high and low rainfall values (between 6000 and 250 mm/year) can be observed in nearby stations due to the leeward or windward position of rain gauges (Espinoza et al., 2009b). More, annual rainfall tends to diminish with altitude, being under 1500 mm above 2000 m.a.s.l. (Espinoza et al., 2009b). UNESCO (2006) estimates that on the Altiplano mean annual rainfall and runoff during the 1969-1999 period are 813.5 mm and 89 mm,

respectively. In this region, water vapour originates in the Amazon basin (Vuille et al., 1998; Chaffaut et al., 1998; Garreaud, 1999; Garreaud et al., 2003; Vizy et Cook, 2007) and it is locally enhanced around the Titicaca Lake (Roche et al., 1990).

In northern Pd and Td rainfall and runoff interannual variability are oppositely influenced by El Niño Southern Oscillation (ENSO). During El Nino, rainfall and runoff are higher than normal in Pd while there is an hydrologic drought in Td and over the high slopes of the Amazon basin (Waylen et Caviedes, 1986; Aceituno, 1988;Ropelewski et Halpert, 1987; Tapley et Waylen, 1989; Tapley et Waylen, 1990 ; Rome-Gaspaldy et Ronchail, 1998; Vuille et al., 2000;Waylen et Poveda, 2002; Espinoza et al., 2009b ; Romero et al., 2007, among others). Moreover, interannual rainfall variability in Southern Ad is indirectly related to the North Atlantic sea surface temperatures (NATL SSTs) (Lavado et al., Submitted-b) as well as runoff in the Amazonian basin, Tamshiyacu (AQ-2, Table 1; Espinoza et al., 2009a).

Long term rainfall and runoff variability has also been described in Peru. Marengo (1995) and Marengo et al., find decreasing runoff trends during the twentieth century in some gauging stations located in the northern Pd. They are often related to water catchment for irrigation and domestic usage in growing cities and farming zones. Also, Santa basin is in process of glacier retreat and lost mass (Kaser et al 2003, Mark et Seltzer, 2005; Pouyaud et al., 2005; Vuille et al., 2008a;Vuille et al., 2008b; among others), they have added to a temporary increase in runoff (Mark et Seltzer, 2005; Vuille et al., 2008a). On the Altiplano, a 13 years climatic period is observed in Quelccaya ice-cores (Melice et Roucou, 1998) and a recent decrease (since the end of the eighties) is detected in the level of Titicaca Lake that acts as a rainfall gauge for the Td region (Rigsby et al., 2003). In the Ad, Gentry et Lopez-Parodi (1980) associated upward (downward) trends in maximum (minimum) water levels in Iquitos (AQ-2, see Table 1) during the 1962-1978 period with deforestation as no clear rainfall change had been observed during the same period. Nordin et al.(1982) and Richey et al. (1989) discussed these results as well as Rocha et al. (1989) who find positive rainfall trends in Iquitos and Pucallpa stations during the 1955-1979 and 1957-1981 period respectively. On the contrary and more recently, Haylock et al.(2006) find a downward rainfall trend during the 1957-1994 period showing that the sign of long term variation changes with time. Marengo (2004) and Espinoza et al. (2006a; 2009a; 2009b) confirm this observation and propose a space variation of long term changes also within the Amazon basin, especially between the North and the South. Espinoza et al. (2007) describe upward runoff trends in the northern Ad (AQ-3, Table 2), whereas downward runoff trend over the southern Ad (AQ-5, Table 2) during the 1990-2005 period.

The studies mentioned above often involve a particular region of Peru and use few stations. That is why the aim of this study is to gather a comprehensive set of rainfall and runoff data in all the whole Peruvian territory (Pacific, Amazonas and Titicaca drainage) in order to propose, for the first time, a global outline about its mean hydrological characteristics and about its recent variability. This was made possible thanks to the collection, the validation and the completion of information through runoff gauging in big rivers of the Peruvian Amazon, in the mark of the Hydrogeodynamics of the Amazon Basin (Hybam) project that associate the Peruvian National Meteorology and Hydrology Service, SENAMHI (www.senamhi.gob.pe) and the French Institute for Reseach and Development (IRD).

This paper is organized as follow. After the introduction, the database and the methods used in this paper are described. The spatial distribution of rainfall and discharge and their annual cycles in the different basins are depicted. The relationship between annual rainfall and discharge is discussed and their interannual variability is addressed. We then comment on trends and breaks in discharge and annual series. Finally, hydrological variability is related to regional ocean-atmospheric indicators. A summary and concluding remark are provided in the

last section.

DATA AND METHODS

This work is based on monthly rainfall and discharge data in 33 basins (29 in Pd, 3 in Td and 2 in Ad), during the 1969/70 - 2003/04 period, with an hydrological year running from September to August (Table 1, Figure 1). Basins subdivision was made using the Digital Elevation Model (DEM) provided by the National Aeronautics and Space Administration, NASA through the Shuttle Radar Topography Mission, SRTM (www2.jpl.nasa.gov/srtm). The SRTM data is available as 3 arc second (~ 90m resolution), a description of this model is given by Farr et al. (2007).

Although being the largest part of the country, Ad holds a very small number of stations because measures generally began recently, during the eighties. In Ad long times series have been obtained in very large basins that almost reach 1 million km². On the contrary, basins in Pd and Td are more numerous and small, not surpassing 20 000km².

Monthly runoff data is from the SENAMHI and from the National Water Agency from Brazil (ANA, www.ana.gov.br) for the station of Tabatinga (AQ-1). Homogenisation was performed by SENAMHI using double-cumulative techniques. Cross correlations between all stations were calculated and missing data periods were filled using linear regression with nearby stations showing the highest correlation, always significant at the 99% level.

Monthly rainfall data from 1965 to 2007 are from the SENAMHI network and have been criticized by this institute. Pd and Td data (119 stations) have been already documented by UNESCO (2006), for the 1969-1999 period. In the mark of the Hybam program, rainfall data over Ad (48 stations) were preliminary controlled by Espinoza et al. (2009b) for the 1965-2003 period and by Lavado *et al.* (Submitted-b) for the 2003-2007 period. Both studies used the Regional Vector Method – RVM (Hiez, 1977 and Brunet-Moret, 1979),.

Rainfall stations are more abundant in Pd and Td than in Ad where they are concentrated in the Andes head basins that are more easily reached than the lowlands. To measure the average rainfall in each basin, the Kriging interpolation method is applied (Oliver et Webster, 1990, Deutsch et Journel, 1992). This method consists in establishing a variogram for each spatial point. This variogram evaluates the influence of the 16 closest stations according to distance. The Kriging method is the only one that takes into consideration a possible spatial data gradient which is very important in a mountainous region.

Annual maximum and minimum runoff (Qmax and Qmin respectively) are individualized and complement the mean annual runoff (Qmean). They are the monthly runoff values of the months with the highest and lowest runoff values respectively.

Seasonal variation coefficients (sVC) are calculated using the mean monthly rainfall and runoff. Likewise, interannual variation coefficients (VC) are computed using annual rainfall and runoff values.

Two trend tests were used in this work to analyze temporal fluctuations in hydroclimatic series. The Bravais-Pearson coefficient which is parametric measures the lineal correlation among variables, whereas Mann-Kendal coefficients is non-parametric and based on range probability of the data occurrence order (Mann, 1945 and Kendall, 1975a). Mann-Kendal test is considered as an excellent tool for trend analysis in climatic series (Zhang et al., 2001, Burn et Elnur, 2002). An index for trend measure is calculated using Eq. 1, where b is the slope of the linear trend and X is the mean value in the series (Espinoza et al., 2009a).

Table 2. Average Characteristics of Hydrometeorology variables, using the hydrological year (from September to August) in each case, for the 1970-2004 period except PQ-10 with 1970-1999 period for runoff. P: Rainfall; Q: Runoff; CV: coefficient of variation; r: Linear correlation coefficient (Rainfall-Runoff). Significant values (95%): bold characters.* only rainfall analysis. ** Non-calculated.

Code	P	Q	Q max.	Q min.	CV	CV	CV	CV	r	CV Seasonal	
	(mm)	(m3 s-1)	(m3 s-1)	(m3 s-1)	(P)	(Q)	(Q max.)	(Q min.)		P	Q
PQ-1	917	114	371	15	0.4	0.6	0.5	0.3	0.77	0.8	1.0
PQ-2	1011	115	321	24	0.4	0.6	0.7	0.6	0.57	0.7	0.8
PQ-3	618	28	120	0	0.8	1.5	1.2	3.3	0.96	1.3	1.3
PQ-4	722	34	91	7	0.4	0.3	0.4	0.4	0.79	0.7	0.7
PQ-5	750	8	22	2	0.7	0.6	0.9	0.4	0.89	0.8	0.7
PQ-6	681	28	97	2	0.9	0.6	0.6	0.7	0.75	0.9	1.0
PQ-7	744	25	113	2	0.4	1.0	1.1	0.8	0.93	0.9	1.2
PQ-8	517	9	35	0	0.4	0.9	1.1	1.2	0.90	0.9	1.1
PQ-9	583	4	19	0	0.4	1.3	1.3	1.2	0.68	0.7	1.4
PQ-10	489	201	550	49	0.2	0.4	0.4	0.3	0.36	0.7	0.7
PQ-11	521	43	115	12	0.3	0.3	0.4	0.5	0.59	0.9	0.6
PQ-12	493	29	85	10	0.3	0.4	0.6	0.3	0.61	0.9	0.8
PQ-13	460	18	61	5	0.3	0.4	0.6	0.4	0.75	1.1	0.9
PQ-14	455	6	18	2	0.3	0.4	0.4	0.9	0.47	1.1	0.8
PQ-15	515	31	70	17	0.2	0.3	0.4	0.3	0.52	1.0	0.5
PQ-16	409	15	59	1	0.3	0.5	0.5	0.6	0.65	1.1	1.2
PQ-17	407	49	155	9	0.2	0.5	0.7	0.3	0.64	1.0	0.9
PQ-18	184	10	45	0	0.3	0.7	0.9	1.2	0.57	1.3	1.2
PQ-19	500	21	82	2	0.3	0.5	0.7	0.7	0.44	0.9	1.1
PQ-20	357	1	3	0	0.4	0.5	0.5	NC	0.43	1.1	1.4
PQ-21	240	14	72	0	0.4	0.8	0.8	3.0	0.49	1.1	1.5
PQ-22	237	9	45	0	0.4	0.8	0.9	0.4	0.50	1.3	1.4
PQ-23	487	71	244	17	0.3	0.5	0.5	0.6	0.50	1.1	0.9
PQ-24	463	86	291	26	0.3	0.3	0.4	0.2	0.75	1.1	0.9
PQ-25	305	13	45	6	0.3	0.7	1.0	0.6	0.64	1.2	0.7
PQ-26	281	28	90	11	0.4	0.6	1.0	0.5	0.62	1.3	0.7
PQ-27	230	3	5	2	0.4	0.2	0.5	0.3	0.40	1.4	0.3
PQ-28	164	3	12	1	0.5	0.6	0.7	1.0	0.82	1.5	1.2
PQ-29	144	1	2	0	0.5	0.3	0.6	0.3	0.65	1.4	0.5
TQ-1	773	76	260	8	0.2	0.3	0.3	0.4	0.82	0.9	1.1
TQ-2	729	20	78	2	0.2	0.4	0.5	0.5	0.86	0.8	1.1
TQ-3	620	39	172	5	0.2	0.5	0.6	0.5	0.78	0.9	1.2
AQ-1	1913	38044	53710	22545	0.1	0.1	0.1	0.2	0.82	0.2	0.3
AQ-2	1701	32605	49238	16603	0.1	0.1	0.1	0.2	0.60	0.2	0.3
AQ-3*	1747				0.1					0.5	
AQ-4*	1463				0.1					0.3	
AQ-5*	1496				0.1					0.2	

$$Itrend = \frac{b}{X} \times 100 \qquad (1)$$

In addition, Pettitt non-parametric test for mean-change measure in temporal hydrological annual series was applied (Pettitt, 1979). It is based on changes in the average and the range of the series subdivided into sub-series and it is considered as one of the most complete test

to identify mean-change (Zbigniew et Robson, 2004). Significance level (a) is the probability that a test detects trend or other change when none is present (Robson et al., 2000). In this study, the null hypothesis in statistical tests is rejected using α equal 0.05 .

Several regional climatic indexes were used to characterize the time variability of rainfall and runoff. The Southern Oscillation Index (SOI) is the standardized pressure difference between Tahiti and Darwin. Monthly SSTs (1950–2000) are provided for the northern tropical Atlantic (NATL, 5–20°N, 60–30 °W) and the southern tropical Atlantic (SATL, 0–20 °S, 30 °W–10 °E). The standardized SST difference between the NATL and SATL is computed to feature the SST gradient in this oceanic basin. All these values are from the Climatic Prediction Centre of the National Oceanic and Atmospheric Administration (CPCNOAA: http://www.cdc.noaa.gov/).

Finally, the management of the rainfall and runoff databases, as well as the calculation of the average rainfall in the basins, have been carried out using the HYDRACCESS software, developed within the framework of the HYBAM programme (free download at www.mpl.ird.fr/hybam/outils/hydraccess en.htm; Vauchel, 2005b).

SPATIAL AND SEASONAL VARIABILITY OF RUNOFF AND RAINFALL

Mean annual rainfall values (1970-2005) in 167 stations, interpolated using the Kriging method, are displayed in Figure 2. A strong opposition appears between the rainy eastern lowlands in the Amazon basin (more than 1500 mm/year – see also Table 2) and drier conditions in the Andes and in the basins of the Pacific coast (less than 1000 mm/year).

Weak rainfall along the Pacific coast is related to the subsidence in the South East Pacific subtropical anticyclone that prohibits rainfall. Though, in Pd, rainfall increases while latitude diminishes, from very low values in the southernmost basins (144 mm/year in PQ29, Table 2) to nearly 1000 mm/year in the North (Figure 3a). This can be related to the diminution of the strength of the southern Pacific anticyclone toward North and to the seasonal southward displacement of the Pacific ITCZ that reaches the northern coast of Peru. This South-North gradient is also observed in the specific runoff of the river (Figure 3b) that has been computed in order to avoid the problem of dependence between runoff and size of the basin. The specific runoff increases regularly toward North. More, along the Pacific coast rainfall increases with altitude with very low values near the coast (much lower than 100 mm/year in the South) and higher values in the higher parts of coastal basins, above the inversion layer that blocks the convection at about 500-800 meters (Dollfus, 1964 and Johnson, 1976).

On the eastern flank of the Andes, on the contrary, rainfall is abundant. Though, local maximum and minimum are noticeable on Figure 1. In particular, very high annual rainfall (above 6000 mm/year) is recorded in regions where the concave form of the Andes favours convergence (Borja region) or in valleys opened toward North and oriented toward the humid north-western wind (High center Ucayali valley) (Figueroa et Nobre, 1990; Laraque et al., 2007; Espinoza et al., 2009b). They contrast with less rainy regions as the high Huallaga valley that is sheltered by relief and less exposed to moist air advection. Rainfall tends to increase when altitude diminishes as cool temperatures in the Andes do not favour a high moist content of the air.

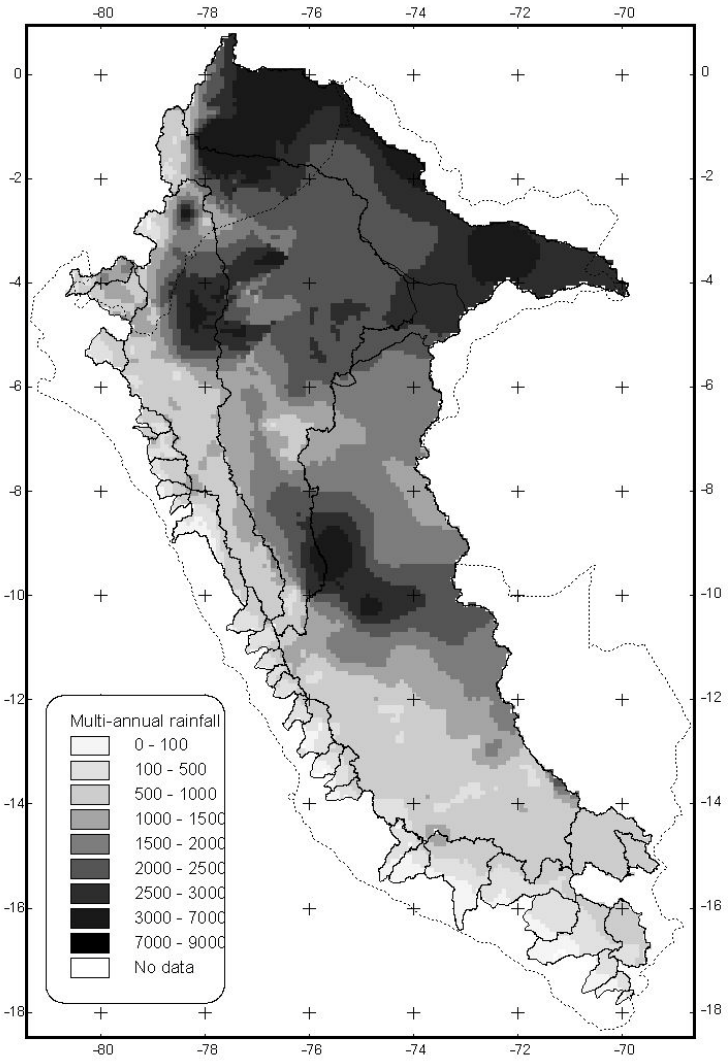

Figure 2. Mean annual rainfall values (mm) for the 1965-2007 period over Pacific (Pd), Amazonas (Ad) and Titicaca (Td) drainages.

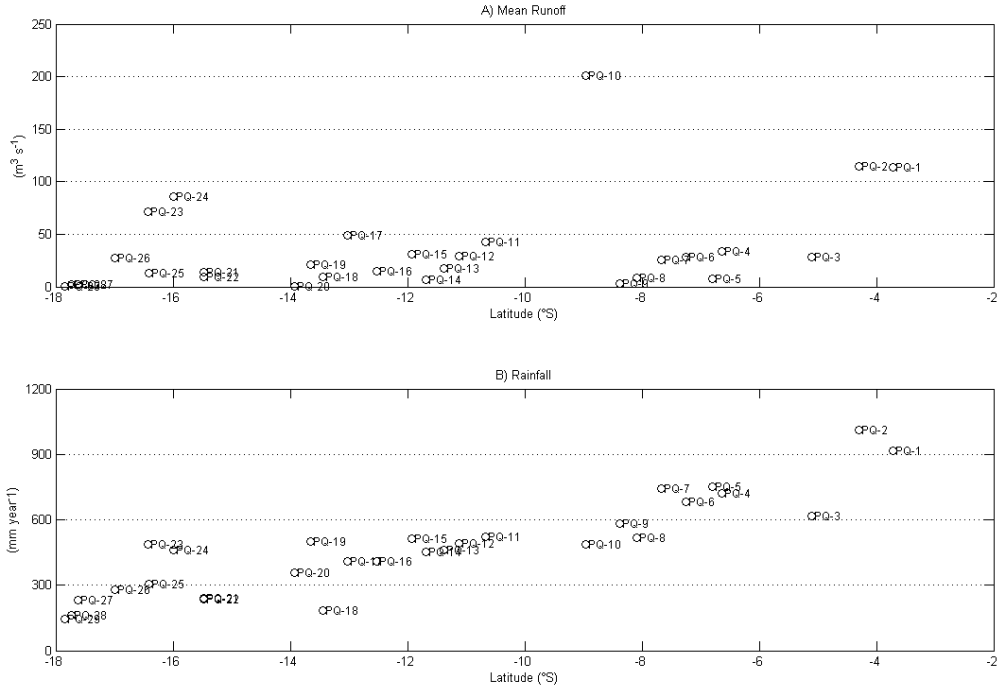

Figure 3. Relationship between latitude and mean multiannual A) specific runoff in Pacific drainage, B) rainfall. Labels and located of stations are described in Table 1.

Monthly rainfall and runoff values expressed as a percentage of the hydrological annual values are represented in Figure 4 for some selected gauging stations. There is a pronounced annual cycle along the Pacific coast and in the Altiplano, with a rainy season during austral summer and a dry season in winter. The rainy season on the coast corresponds to the southward displacement of the Pacific ITCZ. The rainfall seasonal coefficient of variation are often higher than 0.7 (Table 2) and increase from the northern to the southern Pacific coast, revealing a higher seasonal variability in the South. Moreover, many rivers in Pd, in the North as well as in the South, are non permanent and are characterized by null or near null low-level flow in austral winter; this feature, consistent with the strong seasonality of rainfall, may explain the very high seasonal discharge coefficient of variation in some basins (Table 2). On the Altiplano, the rainy season in austral summer is characterized by an intense convective activity combined with moisture advection from the Amazon basin (Montecinos et Aceituno, 2003; Garreaud, 1999). During austral winter, the eastern moist flux is replaced by westerly winds, which provide dry air related to the atmospheric stability over the Pacific Ocean. Consequently the seasonal coefficients of variation of rainfall and discharge are about 1. In contrast, rainfall is abundant all year round in the Amazon basin, with a maximum in summer during the South American Monsoon (Zhou et Lau, 1998) and the seasonal coefficients of variation are much lower than in Pd and Td, i.e. 0,2 in AQ1 and AQ2 (Table 2).

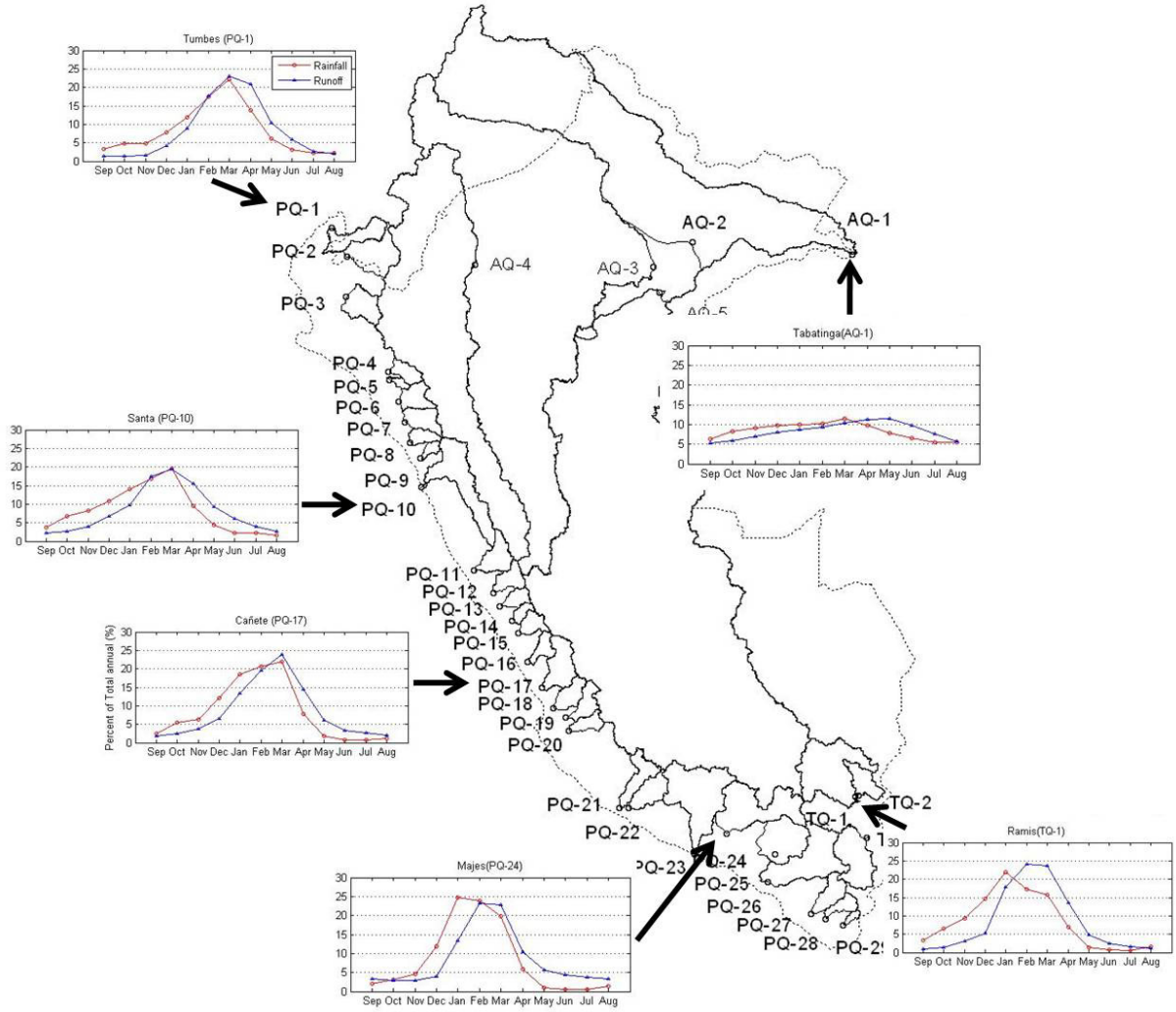

Figure 4. Mean monthly rainfall and runoff in percentage (ratio between monthly and mean annual values for runoff and ratio between monthly and total annual values for rainfall) in the selected basins in Peru.

In the small northern and center and probably southern Pd basins (e.g. Tumbes PQ-1, Santa PQ-10 and Cañete PQ-17) there is an immediate runoff response to rainfall with discharge peaks in March and low values in austral winter. Santa basin (PQ-10) shows singular characteristics (more runoff than rainfall in autumn and winter months, see Figure 3) due to glacier contribution (Pouyaud et al., 2005). In Southern Pd, there is one month lag between peaks in rainfall (January) and peaks in runoff (February) (e.g.). In greater basins there may be a month lag between the maximum rainfall and the high flow runoff (as in Majes PQ-24) In Td, there is one month lag between rainfall (January) and runoff (February) peaks in the large Ramis basin (TQ-1). As the sizes of the Amazonas basins are huge, there are two months lag between peaks in rainfall (Mars) and runoff (May) as in Tabatinga gauging station (AQ-1) (Espinoza et al., 2006a).

INTERANNUAL VARIABILITY OF RAINFALL AND DISCHARGE

Annual hydrological runoff and rainfall during the 1970-2005 period are plotted in Figure 5 for the same stations than in Figure 4. On average, mean annual rainfall and runoff present similar variability and are significantly correlated (Table 2). In some coastal basins (PQ10, PQ14, PQ15, from PQ18 to PQ23, PQ27), the correlations are low. This is due to the presence of underground water that sustain low flow runoff, to the melting of glaciers in upstream valleys as in the case of the Santa River (PQ10), to barrages or water derivation (for irrigation or city water supply, as in the case of the Rimac basin (PQ15) that drives water towards the city of Lima. Moreover, Tumbes river (PQ-1) shows huge rainfall and runoff anomalies during the last two ENSO extreme events (1982-1983 and 1997-1998) (Figure 4). This results in high rainfall and runoff interannual coefficients of variation (Table 2). Though, Qmin interannual coefficients of variation that are generally higher than Qmax CVs, experience a large set of values, from 0,3 in some basins until 3 in PQ3 and PQ21.

Correlation between rainfall and runoff are generally good in the Altiplano and in the Amazonas where the rivers are not equipped by man, except in AQ2. Interannual rainfall and runoff coefficients of variation (CVs) are very low in the Ad (see Tabatinga in Figure 5), indicating a low interannual variability, while they are a little higher in the Altiplano (see Ramis in Figure 5 and Table 2).

In summary, the Pd shows more rainfall and runoff variations than Td and Ad at seasonal and interannual time scale. This is particularly visible in Figures 6a and 6c where interannual coefficients of variation (MACV) of runoff and rainfall respectively are plotted against seasonal coefficients (SVC). Td and Ad stations are located near the origin of the graph while Pd basins are located higher, but occupying a wide range of values. Figures 6b and 6d show the ratio MACV / SVC in runoff and rainfall in Pd versus latitude. An opposition is evidenced between northern and southern stations, the northern Pd basins showing the highest interannual variation in rainfall and runoff, when compared to seasonal variation, probably in relation with the strong hydrological impacts of El Nino events in the northern coast. Another set of basins in the southernmost coastal region experiences a strong interannual runoff variability that is not observed in rainfall.

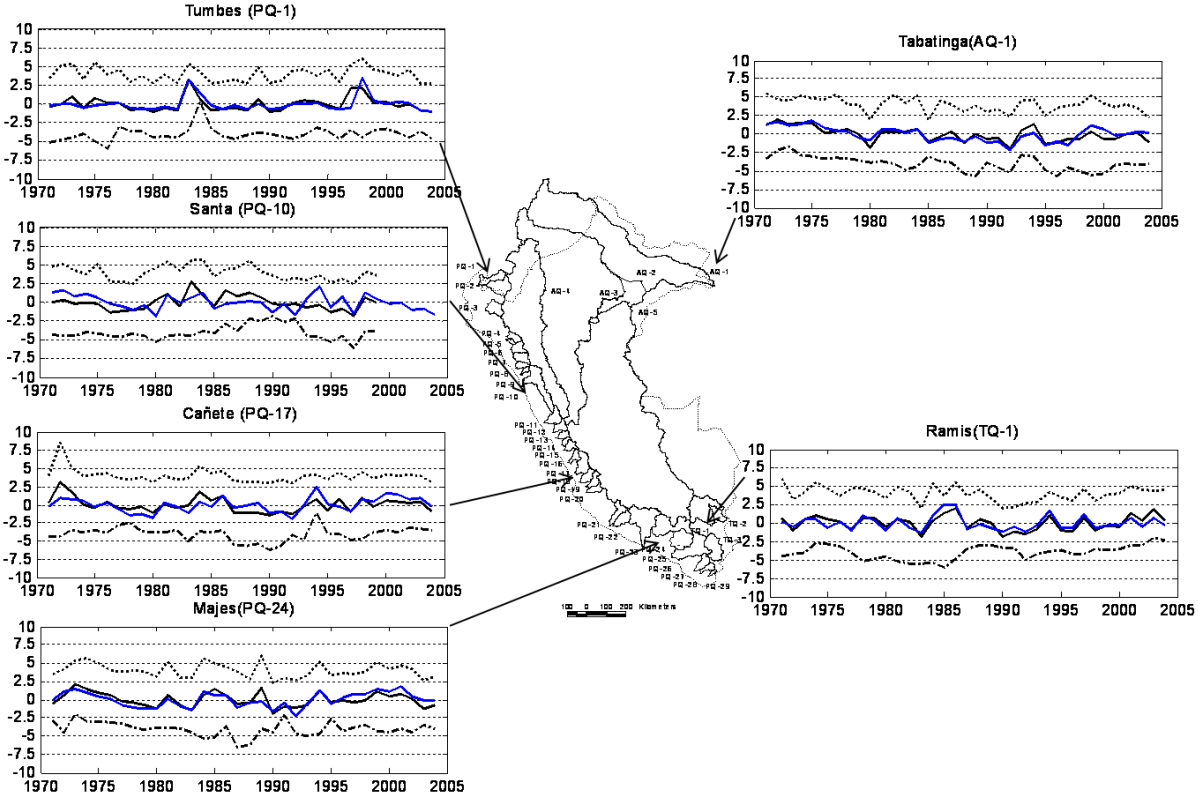

Figure 5. Annual series (September-August) for distinct basins over Peruvian drainages: the black lines are the mean annual runoff, the blue lines blue are the total annual rainfall, the black dotted lines are the maximum runoff and the black dashed lines are teh minimum runoff. Values are standardized and are corrected by coefficient in order to avoid confusion between the different lines. The coefficients are 4 for maximum runoff, 0 for mean runoff and -4 for minimum runoff.

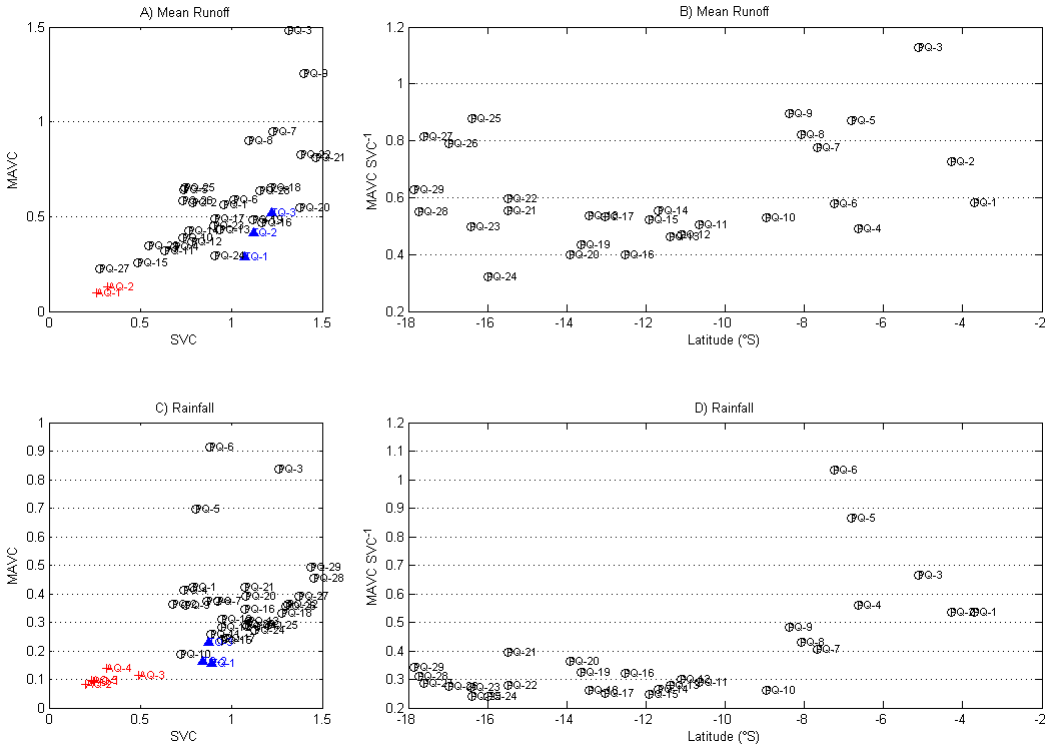

Figure 6. Relationship between multi-annual variation coefficients (MAVC) and the seasonal variation coefficients (SVC) in A) runoff and C) rainfall. Ratio between MAVC and SVC plotted in function of latitude in stations located in the Pacific drainage for B) runoff and D) rainfall. Circle black: stations located over Pacific drainage. Red plus sign: stations located over Amazonas drainage. Blue upward triangle: stations located over Titicaca drainage.

RUNOFF AND RAINFALL CHANGES AND TRENDS

The years of significant mean changes in runoff and rainfall in the Peruvian basins have been computed using Pettitt test. They are presented between parentheses in Table 3. Runoff and rainfall trend analysis have been computed using Bravais Pearson and Mann Kendal tests. For each basin, the best result between both methods is given in Table 3.

The main result is a change in all variables in the middle of the eighties in the two Amazonian basins, with rainfall and runoff decreases that have already been described by Espinoza et al. 2009. Itrend values, ratio between the slope of the linear trend and the mean value of the series, indicate that the stronger runoff decrease is observed in Tamshiyacu where there is no significant rainfall decrease, while in Tabatinga a moderate runoff decrease can be related with an important diminution of rainfall. In both stations the stronger runoff decrease is observed in minimum runoff.

In the Altiplano, on the contrary, there is an increase in minimum runoff. It is significant in the large Ramis basin (TQ-1), with a change in 1986, but it is not related to a change in annual rainfall. Is it associated with changes in winter rainfall that are not detected with our data and analysis.

Along the Pacific coast, the main changes and trends are observed in minimal runoff. The signals are different from a station to another and they are not related to change in annual rainfall. As there is no regional signal (the trends are as well positive or negative, the changes occur at very different dates, from the seventies until the late nineties), we can hypothesize that atmospheric circulation and rainfall do not originate these changes. On the contrary, they may be related to climatic change (glacier melting) or to constructions dedicated to sustain low flow when the trend is positive, and to the increase of water pumping installations for agriculture or city use, when the trend is negative. Positive trends are found in the Chillon (PQ-14), Rimac (PQ-15), Yauca (PQ-22) and Sama (PQ-28). The runoff of Chillon (PQ-14) and Rimac (PQ-15) rivers are mostly dedicated to urban use for the Lima city that according the last census 2007 from the National Institute of Statistic and Informatics from Peru, INEI (www.inei.gob.pe), bind 30.8% of total Peruvian population. Thus, the minimum runoff increase is due to runoff's control in the high rainy zones of these basins, which involve many reservoirs systems and include water transfer from the Amazon basin. Negative trends are observed in rivers Viru (PQ-9), Pativilca (PQ-11), Huaura (PQ-12), Acari (PQ-21), Ocona (PQ-23). In these basins agricultural activity may limit low flow discharge by surface and underground water pumping that has considerably increased since the 1990s, according to the Peruvian Agriculture Ministry (www.minag.gob.pe).

There is no trend in the big Santa River (PQ-10); on the one hand it benefits from the melting of the White Cordillera glacier but, on another hand, its water is intensely exploited for export agriculture production.

Table 3 Years of change (YC), when the Pettit test is significant at the 95% level, are between parentheses. Statistical trends for runoff (maximum, mean and minimum) and rainfall annual series (1970-2004 period except PQ-10 with 1970-1999 period for runoff). There is a trend if $p<0.05$, using the higher p value when using the linear Bravais-Pearson and the Mann-Kendall tests NEG. underlined values indicate significant negative trends (with $0>p>-0.05$) and POS. bold values indicate positive significant trends (with $0<p<0.05$). nt is for "no trend". Itrend is the ratio between the slope of the linear trend and the mean value of the serie. ** indicates that the trend has not been computed.

Code	Maximum Runoff		Mean Runoff		Minimum Runoff		Rainfall	
	TREND/YC	Itrend	TREND/YC	Itrend	TREND/YC	Itrend	TREND/YC	Itrend
PQ-1	nt	-0.218	nt	0.126	nt	0.494	nt	0.15
PQ-2	nt	0.422	nt	-0.584	nt	-1.525	nt	0.13
PQ-3	nt	2.464	nt	2.844	nt(1991)	2.105	nt	0.952
PQ-4	nt	-0.626	nt	-0.284	NEG.(1990)	-2.344	nt	1.082
PQ-5	nt	-0.151	nt	-0.082	NEG.	-1.687	nt	1.105
PQ-6	nt	0.692	nt	0.432	nt	-1.593	nt(1991)	1.7
PQ-7	nt	-0.071	nt	0.462	nt	-1.84	nt	0.237
PQ-8	nt	0.893	nt	1.409	nt	2.533	nt	0.816
PQ-9	nt	-0.975	nt	-0.324	NEG.(1976)	-5.738	nt	-0.518
PQ-10	nt (1989)	-1.756	nt	-0.323	nt	0.605	nt	-0.598
PQ-11	nt	1.113	nt	-0.009	NEG.(1980)	-2.232	nt	-0.529
PQ-12	nt	-1.622	nt	-0.893	NEG.(1988)	-1.56	NEG.	-1.496
PQ-13	nt	-1.77	nt	-0.893	nt(1988)	-1.18	nt	-0.184
PQ-14	nt	-0.953	nt	0.718	**POS.(1994)**	4.59	nt	-0.956
PQ-15	nt	-1.008	nt	0.447	**POS.(1994)**	**1.479**	NEG.	-0.904
PQ-16	NEG.	-1.956	nt	-0.662	nt	-0.543	nt(1992)	1.43
PQ-17	nt	-2.357	nt	-0.962	nt	-0.128	nt	0.614
PQ-18	nt (1976)	-4.349	nt	-1.622	nt	-1.601	nt	0.211
PQ-19	nt(1988)	-2.262	nt	-0.438	**POS.(1991)**	4.754	nt(1992)	1.409
PQ-20	NEG.	-2.148	nt	-0.828	**	**	nt	0.189
PQ-21	nt	-0.4	nt	1.193	NEG.(1982)	-11.922	**POS.(1992)**	**2.688**
PQ-22	nt	-0.097	nt	1.287	**POS.(1986)**	**2.031**	nt	0.476
PQ-23	nt	-0.51	nt	-1.1	NEG.(1989)	-3.921	nt	0.688
PQ-24	nt	-0.926	nt	-0.553	nt	-0.487	nt	0.41
PQ-25	nt	1.548	nt	1.102	nt	2.155	nt	0.271
PQ-26	nt	1.738	nt	0.975	nt	-0.206	nt	-0.407
PQ-27	nt	0.911	nt	-0.398	nt	0.061	nt	-0.737
PQ-28	nt	-0.641	nt	-0.588	**POS.(1997)**	5.159	nt	0.126
PQ-29	nt	1.722	nt	0.795	nt	0.124	nt	-0.15
TQ-1	nt	-0.671	nt	-0.141	**POS.(1986)**	**1.646**	nt	-0.102
TQ-2	nt	-0.574	nt	-0.023	nt	1.454	nt	0.143
TQ-3	nt	-1.033	nt	-1.203	nt	0.712	nt	-0.216
AQ-1	NEG.(1984)	-0.488	NEG.(1984)	-0.53	NEG.(1987)	-1.166	NEG.(1984)	-0.418
AQ-2	NEG.(1984)	-0.792	NEG.(1987)	-0.847	NEG.(1987)	-1.544	nt(1978)	-0.162
AQ-3							nt	-0.168
AQ-4							nt	-0.165
AQ-5							nt	-0.147

IMPACT OF OCEAN-ATMOSPHERIC INDICES ON PERUVIAN HYDROLOGY

In order to search explanation for the interannual and long term variability of runoff and rainfall, the hydrological series have been correlated to ocean-atmosphere indices as the Southern Oscillation Index (SOI) and Atlantic indexes constructed using Sea Surface Temperature (SST) in the southern and northern tropical Atlantic ocean. These indexes have been chosen because on the one hand coastal Peru is a key region for the El Nino – Southern Oscillation (ENSO) phenomena and because the tropical Atlantic SST is related to the strength of the trade winds and consequently to the water vapour advection from the Atlantic to the South America tropics (Marengo 1992, Marengo 2004). Their time series are presented in Figure 7a, b, c.

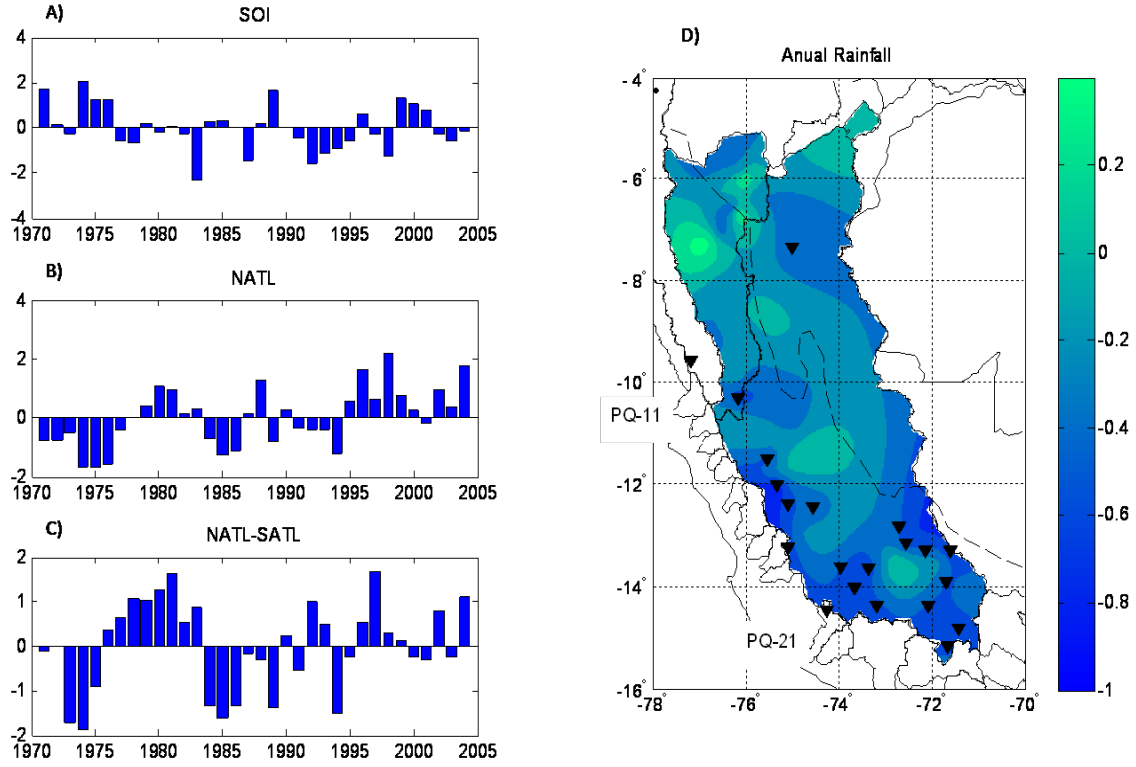

Figure 7. Standardized annual values (1969-2004 period) for A) the Southern Oscillation Index (SOI), B) the Northern tropical Atlantic SST (NATL, 5–20°N, 60–30 °W). C) the standardized difference between NATL and the southern tropical Atlantic SST (0–20 °S, 30 °W–10 °E), NATL-SATL. D) Interpolated correlation coefficients values in Ucayali and Huallaga basins. Stations with significant negative correlation between rainfall and NATL-SATL are represented by black downward triangles (95% of confidence level). Adapted from Lavado *et al.*(Submitted-b).

Correlations values using Bravais Pearson test are reported in Table 4. They are very similar to those computed using Mann-Kendall test (not shown). Correlation values are often low, explaining generally 25 to 30% of the hydrological series variability. But in some cases the relationship is much higher and half of the variance may be represented.

In the Amazon basin, there is a large discrepancy between runoff and rainfall results. Rainfall is positively related to SOI, with less rain during El Nino while there is no runoff-SOI signal. On the contrary, there is a negative signal between NATL and runoff indicating a higher runoff when the northern Atlantic SST is cooler than usual and no signal in rainfall. This discrepancy may be due to the rainfall gauge stations sampling that has been used to compute rainfall in the Amazon basin. Many stations were available in the Andes while few stations in the lowlands that represent the largest and rainiest part of the basins. Consequently, rainfall mainly represents the tropical Andes, while runoff the lowlands. That is why an Andean usual

ENSO signal (reference) is found in rainfall and no signal in runoff, consistently with the near-absence of ENSO signal in the western Amazon basin. NATL signal is strong in the Andes but is also present in the lowlands (Figure 7d, Lavado et al. Submitted); that is why it is present in runoff. The Amazonian basins downward runoff trend put in evidence in the former chapter may be related to the positive trend in NATL observed in Figure 7b, as high temperature in the northern tropical Atlantic inhibits water vapour transport toward tropical South America.

In the Titicaca basin, rainfall is usually lower during El Nino, but, surprisingly, this signal is observed in the Ilave basin (TQ-3) only. A better signal, with lower discharge during El Nino is observed in runoff, especially in Qmax in the Ramis and Ilave basins (TQ-1 and TQ-3). This is consistent with the timing of El Nino events that peak during austral summer. As in the Amazon basin, there is a negative relationship between NATL or the Atlantic SST gradient and hydrological series. Though it is rather weak and not all the basins or all the variables are affected.

Along the coast, as the basins have been largely modified by human activity or by climatic change, and as the runoff values may be null in austral winter, correlations between minimum runoff and ocean-atmospheric indexes are not considered as reliable. The relationship between SOI and rainfall changes along the Pacific coast, being negative (more rainfall during El Nino) in the North and positive (less rainfall during El Nino) in the Southern basins, largely influenced by the tropical Andes signal. A similar positive signal is observed in Qmean and Qmax values of the southern basins but surprisingly the northern runoff are not related to SOI. Is it because gauging scales are destroyed during El Nino flooding. A further examination of ENSO - hydrology relationships in Peru will highlight this feature.

Rainfall, Qmean and Qmax in all the southern basins (from PQ11 for rainfall and PQ-16 for runoff until PQ-29) are negatively related to the SST gradient in the tropical Atlantic (NATL-SATL). This means that runoff is higher when the southern tropical Atlantic is warmer than usual and/or the northern tropical Atlantic is cooler than usual. In certain cases the relationship is rather strong (near 50% of the variance explained). The physical mechanism explaining this feature needs to be investigated.

CONCLUSION

For the first time an analysis of rainfall and runoff mean conditions and variability is realized, at basin-scale, over the three principal drainages in Peru: Pacific, Titicaca Lake and Amazonas, during the 1969-2004 period. Annual data in 34 basins, 29 in the Pacific drainage, 3 in the Titicaca lake drainage and 2 in the Amazonas have been gathered from the Peruvian National Service of Hydrology and Meteorology (SENAMHI) in the mark of the Hydrogeodynamics of the Amazon Basin (HYBAM) program.

Beyond the well-know and strong opposition between the dry coastal basins and the rainy eastern lowlands, details are given about specific spatial rainfall distribution and opposite altitude-rainfall relationships. A strong South-North rainfall gradient prevails along the coast where rainfall increases with altitude while a patchwork of rainier and drier regions is observed in Amazonia along with a rainfall decrease with altitude. Over the Altiplano, annual rainfall experiences intermediate values. Discharge values and their annual cycle depend on the size of the basins, obviously; there is no lag between peaks in rainfall and runoff in the small coastal basins while a two months lag is observed in the huge Amazonian basins.

Runoff variability is strong in the coastal basins at seasonal and interannual time scales because rainfall variability is higher in this part of the country and also because the basins are small and the rivers often intermittent. On the contrary runoff is more regular in the Andes and in the Amazon.

Table 4 Linear regression coefficients between hydrological time series (maximum, mean and minimum runoff and rainfall) and large-scale circulation indexes (SOI: Southern Oscillation index, NATL: North Atlantic SST, N-S: NATL –SATL SSTs). Significant values (95%) are underlined (negative) or bold (positive)**.** ** Non-calculated

Code	Maximum Runoff			Mean Runoff			Minimum Runoff			Rainfall		
	SOI	NATL	N-S	SOI	NATL	N-S	SOI	NATL	N-S	SOI	NATL	N-S
PQ-1	-0.16	0.01	0.03	-0.33	0.07	0.09	-0.11	-0.03	-0.22	-0.35	0.12	-0.01
PQ-2	0.18	-0.12	-0.29	0.12	-0.32	-0.4	**0.35**	-0.55	-0.51	-0.35	0.12	-0.01
PQ-3	-0.28	0.24	0.01	-0.36	0.29	0.05	0.03	-0.08	-0.23	-0.41	0.2	0.1
PQ-4	0.12	-0.18	-0.25	0.18	-0.2	-0.32	**0.46**	-0.62	-0.49	0.06	0.15	-0.06
PQ-5	-0.28	0.2	-0.01	-0.18	0.14	-0.08	**0.58**	-0.46	-0.4	-0.32	0.19	0.01
PQ-6	-0.06	0.1	-0.09	-0.08	0.06	-0.19	0.32	-0.4	-0.42	-0.41	0.26	0.11
PQ-7	-0.19	0.27	-0.02	-0.21	0.24	-0.07	**0.57**	-0.51	-0.45	-0.12	0.1	-0.05
PQ-8	-0.09	0.3	-0.03	-0.13	0.29	-0.1	**0.47**	-0.33	-0.44	-0.07	0.14	-0.1
PQ-9	-0.11	0.25	0.01	-0.15	0.3	0	**0.39**	-0.41	-0.29	0.25	-0.12	-0.24
PQ-10	0.06	0.04	-0.18	-0.18	0.12	-0.18	0.06	-0.07	-0.29	0.19	-0.26	-0.45
PQ-11	-0.15	0.07	-0.18	0.1	-0.17	-0.3	**0.42**	-0.6	-0.15	0.26	-0.26	-0.42
PQ-12	-0.01	-0.28	-0.24	0.11	-0.39	-0.47	0.16	-0.58	-0.49	0.21	-0.44	-0.53
PQ-13	0.01	-0.25	-0.23	0.04	-0.23	-0.42	0.01	-0.24	-0.3	0.14	-0.18	-0.46
PQ-14	0.11	-0.22	-0.17	0.01	-0.12	-0.28	-0.03	0.14	0.03	0.25	-0.25	-0.46
PQ-15	0.12	-0.23	-0.14	0.01	-0.09	-0.28	-0.04	0.23	0.05	0.28	-0.35	-0.49
PQ-16	**0.41**	-0.63	-0.45	**0.35**	-0.53	-0.64	**0.39**	-0.24	-0.41	0.26	0.13	-0.3
PQ-17	0.13	-0.25	-0.25	0.11	-0.24	-0.37	0.03	-0.32	-0.13	0.27	-0.19	-0.55
PQ-18	**0.39**	-0.52	-0.43	**0.37**	-0.51	-0.64	0.27	-0.37	-0.58	0.19	-0.22	-0.4
PQ-19	0.13	-0.23	-0.37	0.16	-0.21	-0.5	-0.11	-0.03	-0.16	0.21	0.13	-0.22
PQ-20	**0.41**	-0.63	-0.45	**0.35**	-0.55	-0.62	**	**	**	**0.39**	-0.09	-0.33
PQ-21	0.12	-0.34	-0.51	0.12	-0.31	-0.57	0.3	-0.27	0.2	0.3	0.15	-0.24
PQ-22	0.09	-0.34	-0.57	0.1	-0.32	-0.61	0.03	-0.11	-0.5	0.27	-0.18	-0.46
PQ-23	**0.49**	-0.4	-0.53	**0.52**	-0.48	-0.64	**0.4**	-0.44	-0.38	0.29	-0.2	-0.56
PQ-24	**0.5**	-0.44	-0.59	**0.51**	-0.46	-0.68	0.28	-0.2	-0.08	**0.47**	-0.18	-0.49
PQ-25	**0.45**	-0.36	-0.37	**0.54**	-0.42	-0.47	0.16	-0.2	0.1	**0.44**	-0.28	-0.47
PQ-26	**0.46**	-0.32	-0.4	**0.56**	-0.42	-0.48	0.04	-0.42	0	**0.51**	-0.35	-0.39
PQ-27	0.09	-0.03	-0.4	0.15	-0.18	-0.29	-0.11	0.11	0.04	**0.5**	-0.45	-0.38
PQ-28	**0.35**	-0.51	-0.44	**0.43**	-0.57	-0.41	-0.04	0.06	-0.13	**0.48**	-0.4	-0.45
PQ-29	0.22	-0.1	-0.29	**0.36**	-0.24	-0.33	0.25	-0.33	-0.09	**0.49**	-0.33	-0.34
TQ-1	**0.5**	-0.31	-0.24	**0.46**	-0.41	-0.4	**0.37**	-0.08	-0.29	0.19	-0.37	-0.4
TQ-2	**0.37**	-0.33	-0.13	0.25	-0.39	-0.3	0.15	-0.4	-0.37	-0.01	-0.11	-0.1
TQ-3	**0.51**	-0.45	-0.4	**0.49**	-0.48	-0.42	-0.15	-0.21	-0.3	**0.52**	-0.43	-0.51
AQ-1	0.29	-0.33	-0.14	0.27	-0.51	-0.33	0.07	-0.57	-0.25	**0.44**	-0.32	-0.23
AQ-2	0.32	-0.44	-0.19	0.27	-0.58	-0.38	0.09	-0.63	-0.33	**0.36**	-0.19	-0.16
AQ-3										**0.37**	-0.11	-0.15
AQ-4										0.32	-0.13	-0.19
AQ-5										**0.37**	-0.29	-0.48

Significant trends and ruptures are observed in the runoff of Amazonian basins. Rainfall and runoff decrease, especially since the middle of the eighties and during the low stage season. Over the Altiplano and in some coastal basins increases in minimum runoff may be associated to the accelerated melting of the glaciers due to climate change. It is noticeable that almost all the coastal basins experience some change in minimum runoff during the last 35 years. As these changes are not related to rainfall changes and are not spatially organized they may be attributed to human activity. Increases in low stage runoff may concord with glacier melting as proposed before and with constructions dedicated to sustain low flow in the rivers that supply big cities or intensive farming. Minimum runoff decreases on the contrary may be related to water pumping.

The analysis of relationships between hydrology and oceano-atmospheric indicators as the Pacific Southern Oscillation Index (SOI) and the sea surface temperature (SST) over the tropical Atlantic Ocean gives some indications about the origin of rainfall and runoff variability. The strongest signal that had not been documented before is found between the Atlantic SST and the hydrology of the Amazon, the Altiplano and the southern Pacific basins. Rainfall and runoff (maximum and mean) decrease when the northern tropical Atlantic Ocean is warmer than usual. On the contrary, a cooler ocean may drive strong trade-winds and high water vapour fluxes towards the aforementioned regions. The long term warming of the northern tropical Atlantic may explain the significant downward trend of runoff observed in the Amazon. ENSO signal on the contrary is not so clear. As documented before, rainfall and runoff tend to decrease during El Nino events in the southern part of the country, in basins that depend on Andean rainfall. Thought there is no clear evidence of increased rainfall and runoff on the northern coast during El Nino, except for some extreme events (1982-83 and 1997-98). Further investigations may clarify and complete these first results.

1.3 Les programmes de recherche dans lesquels s'inscrit la thèse

1.3.1 Le programme HYBAM (Hydrogéodynamique du Bassin Amazonien)

HYBAM est un programme de recherche réalisé en partenariat entre l'Institut de Recherche pour le Développement (IRD-France) d'une part, et des institutions locales chargées du suivi hydrologique et météorologique, et des universités des pays amazoniens (Brésil, Pérou, Bolivie, Equateur et Colombie) d'autre part. Le programme HYBAM a débuté en 1994 et porte sur l'étude des régimes hydrologiques, sédimentaires et géochimiques des fleuves de l'Amazonie, avec pour objectif d'estimer :

- l'érosion et l'altération actuelle des Andes,
- le bilan des transferts de matière dans la plaine amazonienne par les fleuves, et les éventuels piégeages sédimentaires dans les zones humides,
- le rôle de la variabilité climatique actuelle sur ces transferts d'eau et de matière, l'impact de la pression anthropique sur le fonctionnement hydro-sédimentaire du bassin amazonien.

Les travaux de recherche se basent sur des observations acquises via un réseau de stations gérées par des institutions locales et sur des campagnes de terrain réalisées à différentes époques du cycle hydrologique le long des principaux affluents de l'Amazone.
Grâce à ce travail de terrain et à la présence simultanée du programme HYBAM dans 5 pays amazoniens, deux bases de données inédites des observations pluviométriques et des mesures de débits dans des stations qui constituent le plus important réseau hydro-pluviométrique de cette partie de la planète a été rassemblé. Ces bases de données font partie de l'Observatoire de Recherche en Environnement, ORE-HYBAM (www.ore-hybam.org).

Au Pérou jusqu'en 2003, les seules données hydrologiques disponibles étaient des hauteurs d'eau dans les fleuves amazoniens péruviens. Suite à un accord entre le Service National de Météorologie et Hydrologie de Pérou (SENAMHI), des mesures des débits sur les principaux fleuves amazoniens péruviens ont été réalisés et les résultats présentés dans le cadre de cette thèse se fondent sur ces données.
De façon complémentaire, le programme HYBAM favorise des actions de transfert de technologie et de formation scientifique entre l'IRD et les institutions locales. C'est dans ce cadre que se développe le présent travail de thèse.

1.3.2 Le SENAMHI (Service National de Météorologie et Hydrologie de Pérou)

Le SENAMHI a comme mission de conduire les activités météorologiques, hydrologiques, agrométéorologiques et environnementales au Pérou, de prendre part à la surveillance atmosphérique mondiale, et de produire de l'information dans le cadre du développement durable, de la sécurité et du bien-être péruvien. Aussi, ces activités consistent à :

- compiler, centraliser et traiter l'information des stations météorologiques, hydrologiques, agrométéorologiques et environnementales,
- organiser, favoriser et diriger des études techniques spécialisées dans le pays, exécutées par des organismes nationaux ou étrangers,
- divulguer une information technique et scientifique,
- effectuer et formuler des études de recherche, en accord avec les nécessités du pays et de la défense nationale,
- prendre part à des études scientifiques et à des projets portant sur l'environnement atmosphérique,
- organiser et maintenir le réseau des stations météorologiques et hydrologiques,
- développer des prévisions météorologiques et de la Surveillance Atmosphérique Globale (VAG - OMM),
- organiser et administrer le dossier national météorologique, hydrologique et environnemental (banque de données),
- conclure des contrats et des conventions de coopération technique avec des organismes publics et privés au niveau national et international,
- représenter le Pérou au sein de l'Organisation Météorologique Mondiale (OMM).

L'auteur de la présente thèse fait partie de l'équipe des professionnels du SENAMHI au sein de la Direction Générale de Hydrologie (DGH). La mise en place d'une nouvelle banque de données ainsi que l'accord du SENAMHI pour réaliser des séjours en France ont rendu possible ce travail de doctorat.

1.4 Sélection de bassins versants

Dans le cadre des programmes des recherche précédents, et en considérant que l'hydroclimatologie du basin amazonien péruvien demeurait peu étudiée, nous avons considéré dans notre étude deux bassins : les bassins des rios Huallaga et Ucayali, localisés sur le territoire péruvien. Ce choix a été dicté par la mise à disposition sur ces deux bassins d'une très importante base de données.

1.5 Objectifs de la thèse

L´objectif général de la thèse est de comprendre les impacts du changement climatique sur les régimes hydrologiques des fleuves du bassin amazonien péruvien, en utilisant des modèles de bilan hydrique à méso-échelle, au pas de temps mensuel. Aussi, les objectifs spécifiques suivant ont été identifiés :

- **Etudier** pour la première fois les cycles annuels et saisonniers ainsi que la variabilité interannuelle et intra-saisonnière, et à long terme, des principales composantes du cycle hydrologique sur les basins des rios Huallaga et Ucayali (précipitations, températures et évapotranspiration).

- **Modéliser la production des ressources en eau** sur les bassins des rios Huallaga et Ucayali en utilisant des modèles hydrologiques mensuels distribuées, afin d'identifier les liens entre les principales composantes du bilan hydrique : pluie, évapotranspiration et débit.

- **Quantifier les impacts du changement climatique sur l'hydrologie des bassins des rios Huallaga et Ucayali**. Pour répondre à cette question, des scénarios climatiques élaborés à partir de séries de pluies et de température issues de modèles de circulation générale seront appliqués, comme entrée aux modèles hydrologiques, afin d'analyser et de quantifier leur impacts sur l'hydrologie des bassins des rios Huallaga et Ucayali.

1.6 Organisation de la thèse

Notre travail s'articule de la manière suivante :

Après un chapitre introductif (Chapitre 1), le **Chapitre 2** décrit le contexte géographique et climatique des bassins des rios Huallaga et Ucayali, puis introduit la base de données sur laquelle s'appuie ce travail de thèse.

Le **Chapitre 3** présente les résultats obtenus en lien avec la variabilité hydroclimatique. Ces résultats sont basés sur des séries climatiques portant sur la période 1965-2007, sur lesquelles sont appliquées des tests de rupture ou de tendance. Des relations avec des indices de circulation océanique sont aussi présentées.

Le **Chapitre 4** présente les premières modélisations mensuelles hydrologiques sur sept sous bassins situés dans les bassins des rios Huallaga et Ucayali, et nous présentons les résultats des impacts du changement climatique sur l'hydrologie de ces bassins.

Finalement nous décrions les conclusions et perspectives dans le **Chapitre 5**.

CHAPITRE 2

Les bassins du Rio Ucayali et du Rio Huallaga

II. CHAPITRE 2 .Les basins de l'Ucayali et du Huallaga

Les bassins du Rio Ucayali (50% en région Andine et 50% en plaine amazonienne) et du Rio Huallaga (75% dans les Andes et 25% en plaine) sont situés en totalité sur le territoire péruvien (Figure II-1). Les superficies de ces deux bassins sont de 89 654 km^2 et 350 287 km^2 respectivement. Le fleuve Ucayali naît dans la Département de Ucayali, de la confluence des fleuves Tambo et Urubamba, au nord-est des Andes. Il coule en pente douce vers le nord-ouest du pays et finit par se joindre au fleuve Marañón, donnant ainsi deux sources à l'Amazone.

Le fleuve Huallaga nommé d'abord Huánuco, du nom de la ville qu'il arrose, capitale du Département de Huánuco, prend le nom de Huallaga à Muna. Il traverse le Département de Huánuco, puis celui de San Martín, puis pénètre dans celui de Loreto. Là, il se jette dans le fleuve Marañón, l'une des branches mères de l'Amazone, près de la localité de Puntilla.

2.1 Aspects climatiques

D'après SENAMHI (2005), sur notre zone d'étude, il existe différents types de climat (voir Figure II-2 et Tableau I-1). La classification climatique est en relation directe avec l'altitude, ainsi nous pouvons observer les climats suivants :

- Climat Tempéré Subhumide (Steppe et basses Vallées Interandines).
- Climat Boréal (des Vallées Méso-andines).
- Climat Froid (de Toundra).
- Climat de Neige (Gélido).
- Climat Semi - Chaud très Humide (Subtropical très Humide).
- Climat Chaud Humide (Tropical Humide).

2.1.1 Précipitations

Les précipitations constituent un paramètre climatique très variable, à la fois dans le temps et dans l'espace. Notre zone d'étude n'échappe pas à cette problématique. La Figure II-3a montre la distribution moyenne interannuelle de la pluie sur notre zone d'étude. La Forêt (vers l'est) est caractérisée par des totaux annuels de précipitation supérieurs à la partie Ouest des Andes, et de fortes pluies sont observées aussi dans la zone de transition Andes-Forêt (basin du Rio Pachitea). En résumé, sur les deux bassins d'étude, on note de fortes variations des précipitations en termes d'intensité, du sud vers le nord, et de l'ouest vers l'est. Les régimes de précipitation sur notre zone d'étude sont décrit par Espinoza *et al.* (2008) (voir Figure II-4). La partie méridionale du bassin montre un **régime tropical du sud** avec une longue saison sèche à partir de mai à septembre, comme à la station d'Antabamba (14.37°S 72.88°O ; 3900 m s.n.m. Figure II-4 a), avec un **début de cycle annuel en août et une période pluvieuse de décembre à mars**. Dans la partie supérieure des fleuves Huallaga et Ucayali, un **régime humide tropical** observé à la station de Quillabamba (12.86°S 72.69°O ; 1128 m s.n.m. Figure II-4b) indique une **période pluvieuse beaucoup plus longue et intense (à partir de décembre à mai)**. A Pozuzo (10.05°S 75.55°O ; 258 m s.n.m.) dans le nord, à une basse altitude, une **valeur plus élevée de précipitations et une période sèche plus courte (juin à aout)** (Figure II-4c). Dans le nord, dans la partie supérieure du fleuve Marañón (Figure II-4d), un **régime intermédiaire, entre les tropiques méridionaux et l'équateur comporte une période très pluvieuse à partir de janvier à avril**, qui s'observe par exemple à la station de Julcán (8.05°S 78.50°O ; 3450 m s.n.m.). Dans les

régions situées près de la ligne équatoriale, de plus longues saisons des pluies sont mises en évidence. Par exemple, la station de Gualaquiza (3.40°S 78.57°O ; 750 m s.n.m., Figure II-4e) près des Andes présente une **saison des pluies à partir de février à juillet et n'a aucune période sèche**. Vers l'est au niveau d'Iquitos (3.75°S 73.25°O ; 125 m s.n.m., Figure II-4f), on observe un **régime plus uniforme avec une légère diminution des précipitations à partir de juin à septembre**.

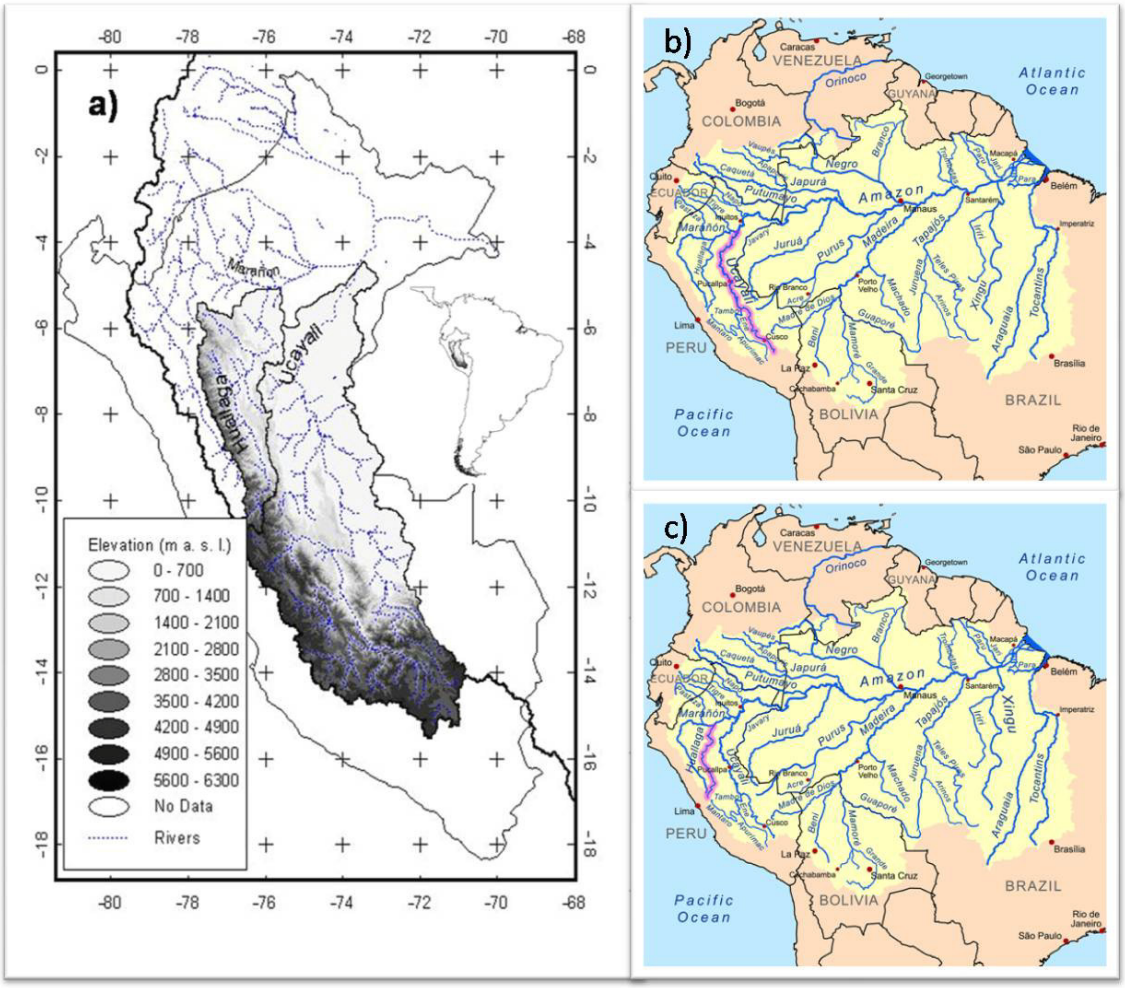

Figure II-1. a) Localisations des bassins de l'Ucayali et du Huallaga au Pérou. b) Fleuves sur le drainage du bassin Amazonien avec les fleuves Ucayali signalé (ligne violette) (d'après :http://fr.wikipedia.org/wiki/Fichier:Ucayalirivermap.png). c) Comme b mais pour le fleuve Huallaga (d'après http://fr.wikipedia.org/wiki/Fichier:Huallagarivermap.png).

2.1.2 Température et Evapotranspiration

Les moyennes interannuelles de température (moyenne Tmean; maximum Tmax et minimum Tmin en °C) ainsi que d'évapotranspiration sont indiquées en Figure II-3b, c, d et e respectivement. Globalement, pour les trois variables climatiques décrites, on observe des valeurs plus élevées sur zone de forêt que sur les Andes. Les variations entre l'été et les valeurs moyennes d'hiver sont de 1.7°C, 0.1°C, 3.5°C et de 0.8 millimètre par jour en considérant Tmean, Tmax, Tmin et l'évapotranspiration respectivement. Cette amplitude thermique très basse caractérise les régions tropicales où sont localisés les bassins des rios Ucayali et Huallaga.

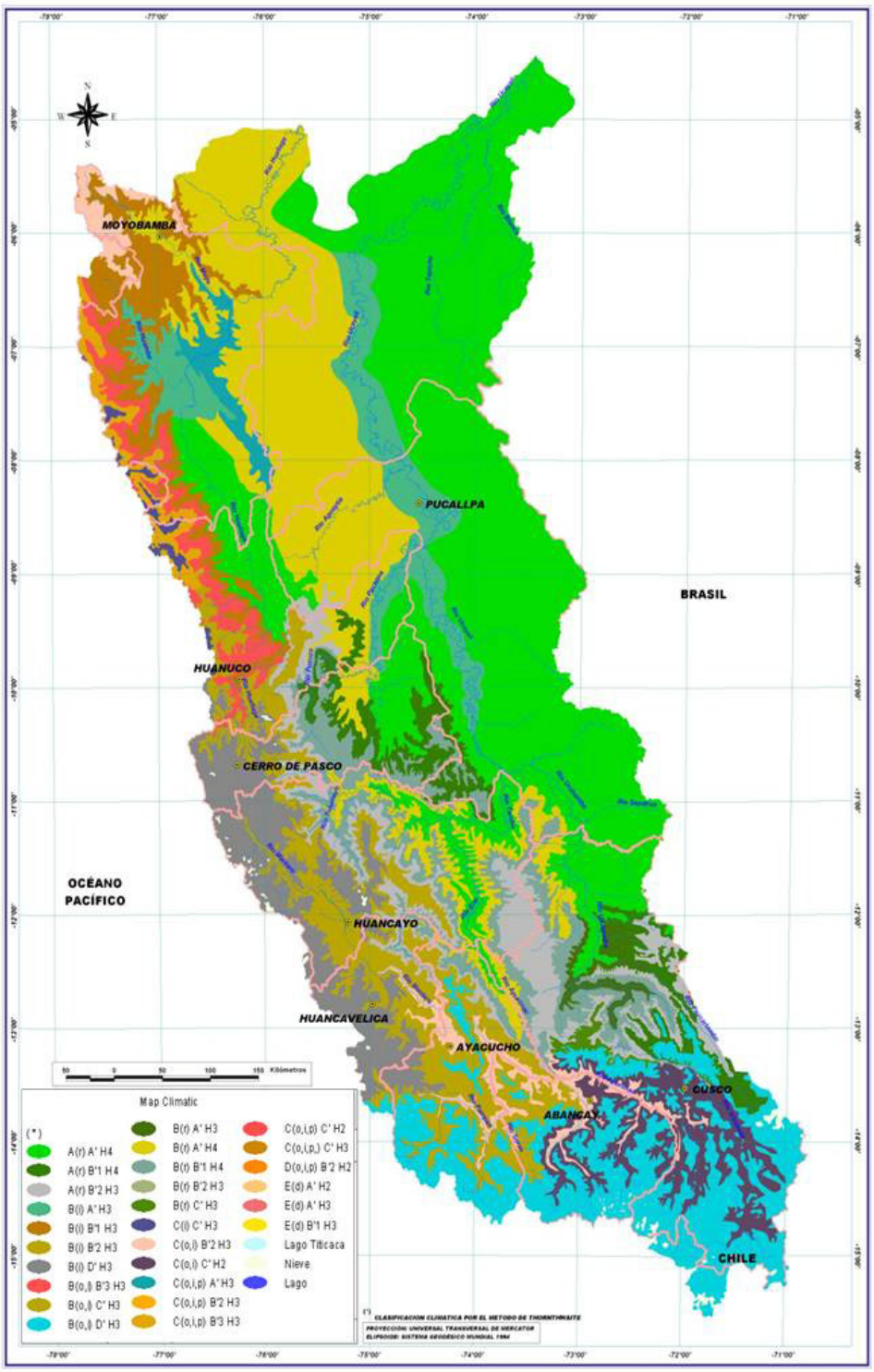

Figure II-2. Classification climatique des bassins Ucayali et Huallaga en utilisant la classification de Thornthwaite (d'après SENAMHI, 2005, voir **Tableau I-1**).

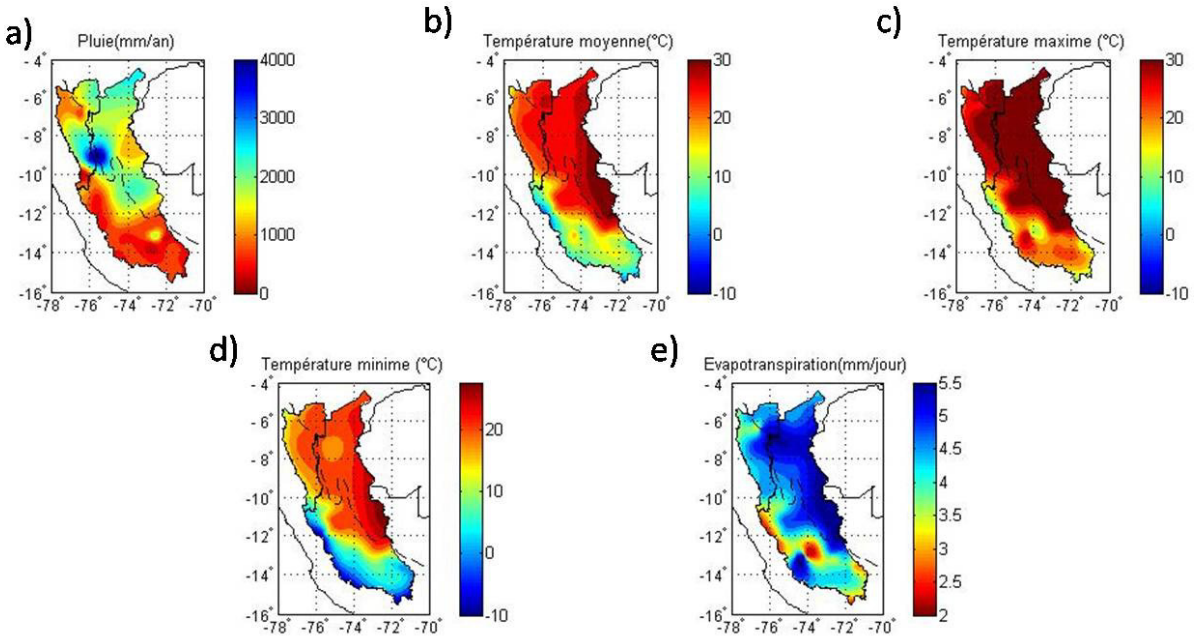

Figure II-3. Carte des climats moyens interannuels. a) Pluie ; b) Température moyenne ; c)Température maxime ; d) Température minime et e) Evapotranspiration. Ligne pointille divise les Andes (est) et la Forêt (ouest).

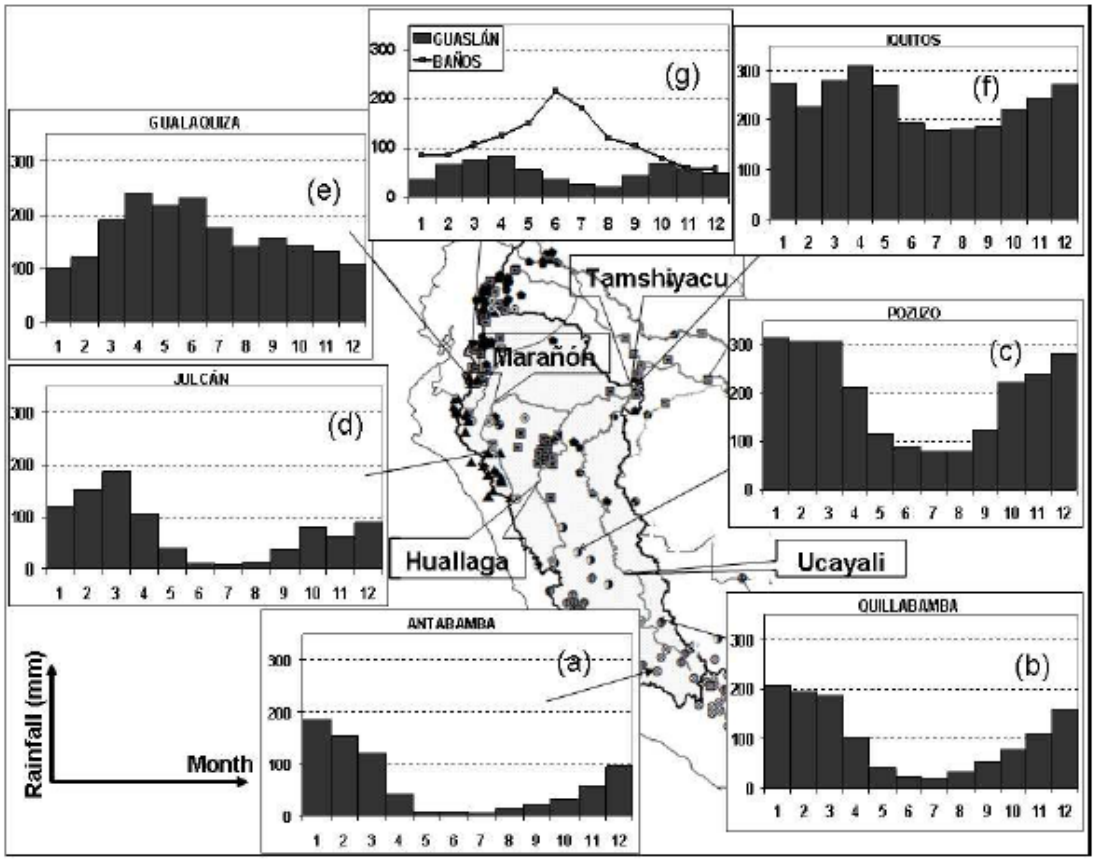

Figure II-4. Régimes de précipitation sur la basin amazonien péruvien (d'après Espinoza et al., 2008, voir Annexes).

Les températures paraissent évoluer en fonction de l'altitude. L'évapotranspiration est caractérisée par des valeurs élevées dans la zone de forêt mais plus contrastées dans les Andes, avec néanmoins des valeurs moins élevées que dans la zone de forêt. Tmean qui s'étend de 0°C à 30°C diminue avec l'altitude en moyenne de 0.48°C par 100 m, Tmax (de 10°C à 35°C) diminue d'environ 0.42°C par 100 m et Tmin (de -10°C à 25°C) de près de 0.54°C par 100 m. Comme attendu dans des régions tropicales, l'amplitude annuelle entre été et hiver est très faible tandis que l'amplitude quotidienne est plus élevée. Entre l'été et l'hiver, la différence de température est presque nulle pendant le jour mais plus élevée pendant la nuit, avec de plus grandes valeurs dans les Andes (4°C) que dans la Forêt (1.5°C). L'amplitude jour-nuit est aussi plus forte dans les Andes (14.4°C en considérant Tmean) que dans la Forêt (11.3°C). De plus, dans chaque région, cette amplitude est plus élevée pendant l'hiver que pendant l'été. Dans tous les cas, ces résultats sont compatibles avec la baisse de nébulosité i) dans les Andes que dans la zone de Forêt). ii) en hiver qu'en été. iii) pendant la nuit que pendant la journée.

2.2 Aspects géomorphologiques

2.2.1 Relief

Le relief des bassins des rios Ucayali et Huallaga est très contrasté du fait de la présence de la cordillère des Andes (altitudes élevées). Il est ainsi possible de différencier deux zones : une au-dessus de 1000 m, au relief escarpé, entaillé de vallées profondes, et présentant de fortes pentes. Sur ces pentes coulent des torrents, qui dans leurs parties andines plus sensibles à l'érosion, recueillent la plupart des sédiments qui arrivent à l'Atlantique via l'Amazone. On estime que 90% de ceux-ci proviennent des Andes. L'autre partie est située sous 1000 m d'altitude. La topographie, bien que faiblement accidentée, est assez escarpée à l'amont pour passer progressivement au domaine de la plaine amazonienne, lieu privilégié des fleuves à méandres.

Le modèle numérique de terrain a été calculé à partir des données fournies par le SRTM (The Shuttle Radar Topography Mission, voir http://www2.jpl.nasa.gov/srtm/) disponible à environ 30 arcs seconds. Il a permis de délimiter les bassins des rios Ucayali et Huallaga (voir Figure II-5).

2.2.2 Géologie

La géologie des bassins des rios Ucayali et Huallaga sera décrite à partir des données de l'Institut Géologique Minier et Métallurgique péruvien (INGEMMET, www.ingemmet.gob.pe).

Les Andes péruviennes comprennent un ensemble de cordillères parallèles placées entre la côte maritime et la plaine amazonienne. Ses stratigraphies, structure, magmatisme, minéralisation et sismicité sont le produit de plusieurs cycles orogéniques superposés, et de la "Subduction Andine", qui a démarré au Jurassique et qui résulte de la collision de la plaque tectonique sud-américaine avec la plaque tectonique océanique.

La Cordillère des Andes est constituée des roches métamorphiques du Protérozoïque, sur lesquelles se sont accumulées des séquences sédimentaires marine et continentale qui ont été déformées par la Tectonique Hercinique Paléozoïque, à laquelle ont été associées des intrusions plutoniques et du volcanisme pendant le Paléozoïque Supérieur. Le cycle andin commence dans le Mésozoïque; en définissant ses structures et en atteignant son développement maximal dans le Tertiaire, et en continuant son activité

jusqu'à aujourd'hui. L'activité sismique et volcanique est notoire dans les Andes péruviennes situées dans la partie active de la ceinture sismique.

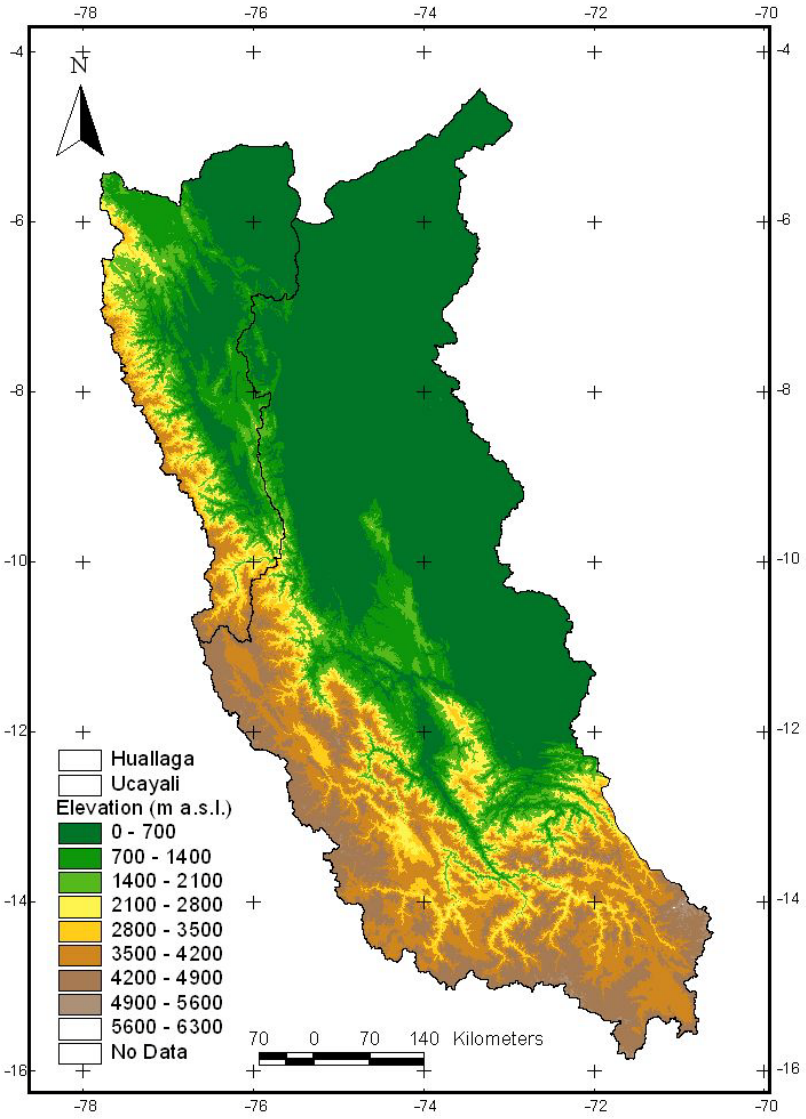

Figure II-5. Carte des altitudes sur les bassins des rios Ucayali et Huallaga.

Du fait de ce contexte géologique, le Pérou est un pays de ressources minérales abondantes, on trouve ainsi une grande variété de gites métalliques de diverses natures, créés principalement sous l'effet du magmatisme intrusif sous volcanique et extrusif. Ceci a permis la mise en place de gisements filoniens metasomatiques et disséminées, formés par des processus hydrothermaux metasomatiques et volcanogéniques, dont les caractéristiques dépendent des roches et de la nature des solutions minéralisantes qui leur ont donné naissance.

Durant les dernières années, l'exploration s'est orientée vers la recherche de gisements épithermales d'or et d'argent de haute et basse sulfinisation, comme à Yanacocha et Pierina. L'exploitation des gisements minéraux péruviens, pour l'or, l'argent et le cuivre, date de l'époque pré-inca. Actuellement le Pérou occupe le premier rang au niveau de la production d'or en Amérique latine, avec plus de 132 tonnes par année, et on projette d'atteindre des valeurs historiques jamais atteintes dans l'histoire nationale. Plus de 40

substances métalliques et non métalliques sont produites : antimoine, bismuth, cadmium, cuivre, étain, fer, indien, manganèse, mercure, molybdène, or, argent, plomb, sélénium, thallium, tellurien, tungstène, zinc ; d'autres minéraux chrome, cobalt, nickel, platine, titane, uranium et des terres rares, ont été identifiés dans diverses localités du pays, mais une plus grande exploration est nécessaire pour définir et quantifier ces possibilités. Parmi les minéraux non métalliques, on peut citer baryum, calcaire, plâtre, kaolin, argiles réfractaires, talc et roches d'ornement, orientées plus spécifiquement vers le marché intérieur.

Les gisements pétrolifères se trouvent dans les sédiments marins du Cénozoïque dans le Nord-ouest péruvien, qui forment des réservoirs avec des blocs faillés qui constituent des pièges structurels. Dans la Forêt, les bassins sédimentaires avec des faciès marins et mixtes contiennent aussi des hydrocarbures, en particulier dans les formations Chonta et Vivian des bassins Marañón et Ucayali. Il existe aussi d'importants gisements de gaz comme celui de Camisea, entre les mains d'investisseurs privés. Le bassin du Rio Madre de Dios offre aussi de bonnes possibilités pétrolière et gazière au sein des sédiments du Paléozoïque et Mésozoïque.

Une exploration systématique du pays, basée sur les nouvelles informations géologiques du territoire, les connaissances de la métallogénie andine et les nouvelles technologies d'exploration disponibles, rendront possible de localiser et de quantifier des ressources minérales et énergétiques nouvelles et de plus grande extension, sur tout le territoire national.

2.2.3 Sols

Le Pérou est un pays caractérisé par des sols pauvres malgré sa grande extension. De ses 128 521ha, seulement 25 525ha (19.86%) sont aptes pour l'agriculture et le bétail. De manière générale les sols du Pérou ont été classés dans sept types de sols ou régions géo-édaphiques. Sur les bassins des rios Ucayali et Huallaga, cinq de ces types de sols sont présents ONERN (1981) :

- **Région avec paramosols ou andosols** : Dans les zones dont l'altitude est supérieure à 4 000 m, il existe des sols favorables à une utilisation agricole, mais celle-ci est limitée par le froid. Les sols prédominant sont les sols riches en matière organique et acides (paramosols), mais il existe aussi des sols rocheux (lithosols), calcaires (rendzines), argileux profonds (chemozems), et organiques profonds (histosols).
- **Région avec kastanosols** : Dans les vallées inter-andines, entre 2 200 et 4 000 m, et dans la partie supérieure de la forêt d'altitude prédominent les sols calcaires de couleur rougeâtre et brune rougeâtre (kastanozems calciques), argileux (kastanozems luviques) et profonds et fins (phaeozems). Dans le sud prédominent les sols d'origine lacustre (planosols), parfois avec un mauvais drainage (gleysols), et des sols d'origine volcanique (andosols).
- **Région litho-cambisols** : Dans la forêt d'altitude, entre 2 200 et 3 000 m les sols sont pauvres et érodables. Aussi les sols superficiels (lithosols) et de formation naissante ou jeunes (cambisols) prédominent. Ils peuvent être acides ou calcaires, et sont fréquemment de couleur jaune.
- **Région avec acrisols** : Dans les zones d'altitude moyenne et basse de la forêt d'altitude, entre 500 et 2 800 m prédominent des sols profonds, de tons jaunes et rougeâtres, avec un bon drainage, et argileux très profonds (nitosols). Vers la

basse forêt apparaissent des sols argileux acides et contenant du fer (plintiques). Dans les fonds des vallées les sols sont alluviaux (fluviosols), parfois avec un mauvais drainage (gleysols) mais on rencontre aussi des sols argileux (vertisols).

- **Région acrisolique ondulée** : Dans la forêt de la plaine, on rencontre des sols rouges et jaunes, acides et de basse fertilité naturelle (ultisols), jeunes de profil peu différencié (entisols), jeunes avec différenciation dans des horizons (inceptisols), mal drainés (aguajales), modérément fertiles et bien drainés (alfisols, vertisols, mollisols), très infertiles sablonneux (spodosols), de sables blancs.

Sur nos bassins d'étude, on peut identifier d'après FAO/UNESCO (1981) 9 types de sols (voir Tableau II-1 et Figure II-6).

Tableau II-1. Typologie de sols. D'après FAO/UNESCO, 1981.

A : ACRISOLS	I : LITHOSOLS
Ao : Orthic Acrisols	
Ap : Plinthic Acrisols	K : KASTANOZEMS
	Kk : Calcic Kastanozems
B : CAMBISOLS	Kl : Luvic Kastanozems
Be : Eutric Cambisols	
	N : NITOSOLS
F : FERRALSOLS	Nd : Dystric Nitosols
Fx : Xanthic Ferralsols	Ne : Eutric Nitosols
G : GLEYSOLS	T : ANDOSOLS
Gd : Dystric Gleysols	Th : Humic Andosols
Gh : Humic Gleysols	Tv : Vitric Andosols
H : PHAEOZEMS	V : VERTISOLS
Hl : Luvic Phaeozems	Vc : Chromic Vertisols

2.2.4 Végétation

La carte de végétation des basins de l'Ucayali et du Huallaga est présentée en Figure II-7. Celle-ci est extraite d'UMD Global Land Cover Classification avec une résolution de 1 Kilomètre (Hansen et al., 1998). Sur les deux bassins d'étude, on observe que la forêt s'étend vers l'est avec des arbres à feuilles persistantes (environ 60% de la totalité des bassins de l'Ucayali et du Huallaga) tandis qu'au niveau des Andes, les deux bassins présentent des végétations variables.

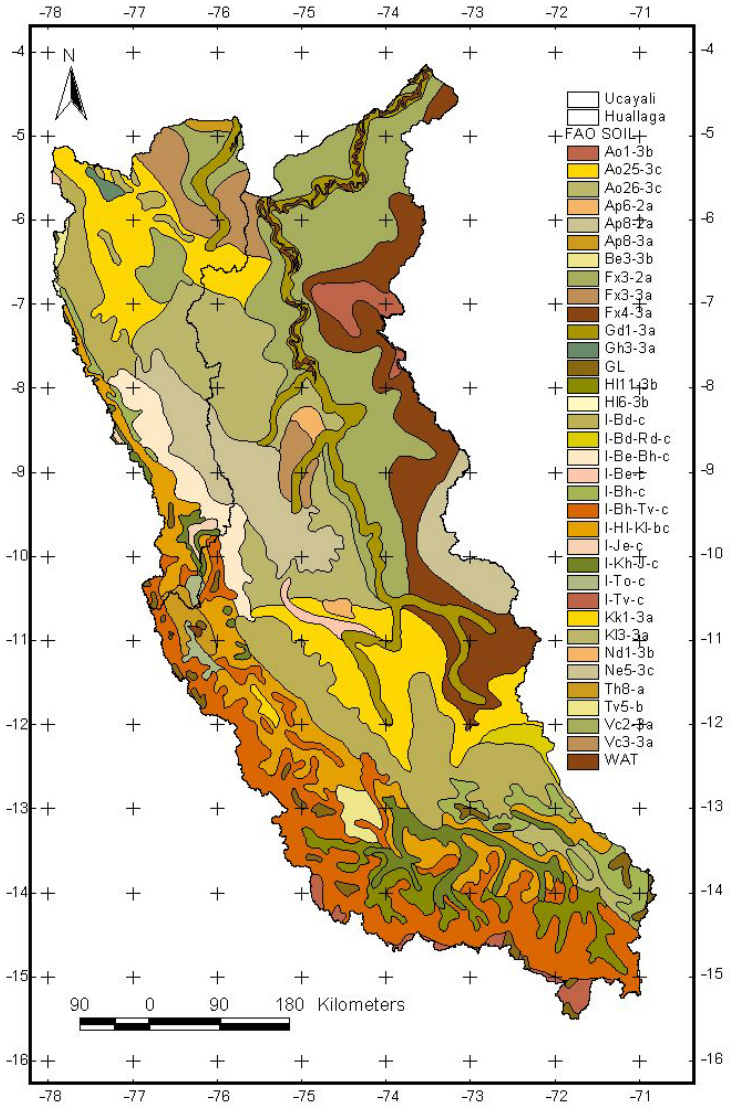

Figure II-6. Types de sols identifiés sur les bassins des rios Ucayali et Huallaga. Pour la légende voir **Tableau II-1**. D'après FAO/UNESCO (1981).

2.2.5 Aspects socio-économiques

Le bassin amazonien du Pérou est caractérisé par une densité de population faible (environ 7 habitants par Km^2). Notre zone d'étude comprend 13 régions politiques ou départements (du nord au sud) : Loreto, Amazonas, La Libertad, San Martin, Ucayali, Huánuco, Pasco, Junin, Ayacucho, Huancavelica, Cusco, Apurimac et Arequipa, au sein desquels existent 78 sous-régions (ou provinces) voir Figure II-8. Les régions avec les plus grandes densités de population sur les bassins de l'Ucayali et du Huallaga sont localisées dans les Andes, avec par exemple : Junin (26 habitants par Km^2) et Cusco (20 habitants par Km^2), tandis que les régions avec les densités plus basses sont celles de Loreto (avec 2.4 habitants par Km^2) et de l'Ucayali (avec 3.9 habitants par Km^2).

Le taux de croissance démographique annuel est estimé à 1.61%; le taux brut de natalité est estimé à 26% tandis que le taux brut de mortalité est estimé à 7 pour 1000 habitants. Les principales activités économiques sont l'agriculture, l'élevage et la pèche (environ 50%), puis vient le commerce (environ 11%). Le salaire moyen mensuel ne dépasse pas

100 euros. Pour ces raisons selon l'Institut National de Statistique et Informatique du Pérou, INEI (www.inei.gob.pe) la majorité de la population vit en condition de pauvreté, avec 60% d'habitants en pauvreté et 30% en condition d'extrême pauvreté.

2.3 Réseau hydrologique du SENAMHI et lesmesures hydrologiques récentes acquises dans le cadre du programme HYBAM

Le réseau hydrométrique du SENAMHI, qui comprend notamment les stations de mesure des débits jusqu'en 2001, est décrit dans la Figure II-9. La plupart des stations sont localisées sur les versants du Pacifique et du Lac Titicaca. Néanmoins, à partir de 2001, grâce à la coopération entre le SENAMHI et l'IRD au sein du programme HYBAM, des mesures de débit sur les fleuves du bassin amazonien péruvien ont été réalisées (Figure II-10). Au total, six stations de mesure des débits des fleuves (avec des courbes d'étalonnage) ont été installées sur le bassin Amazonien du Pérou.

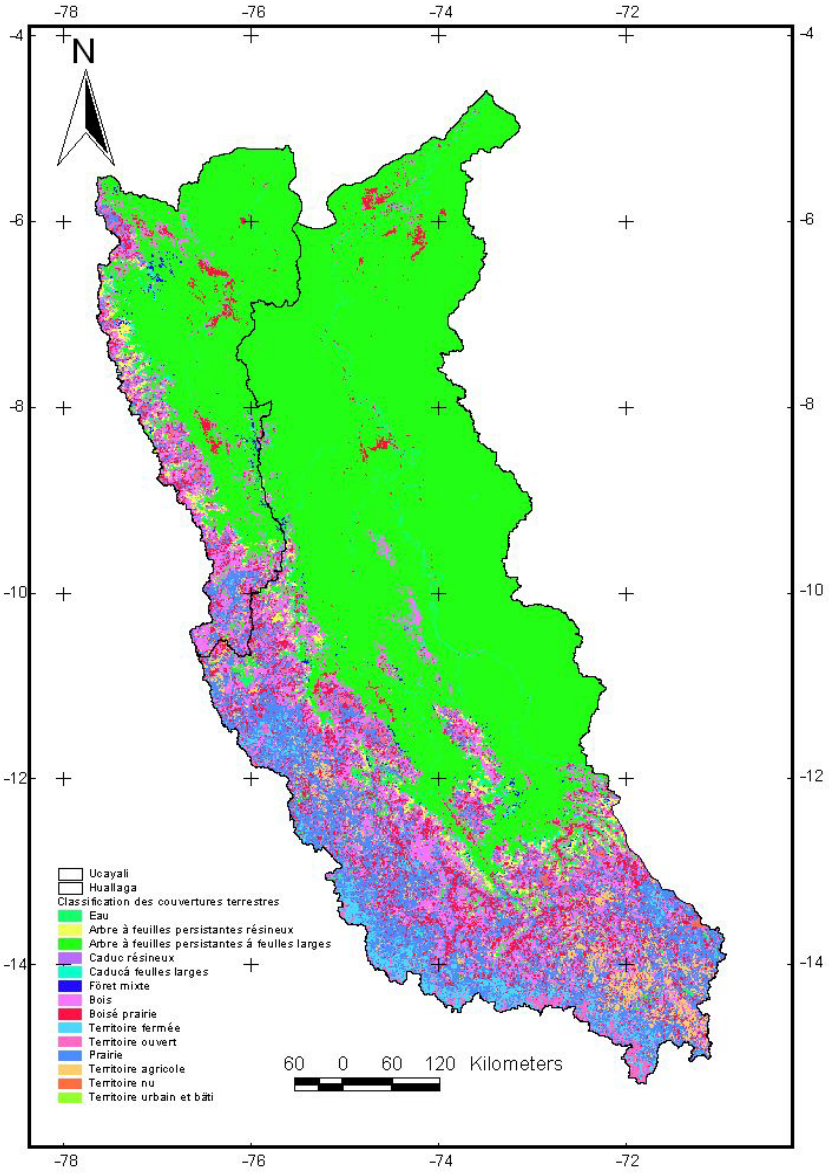

Figure II-7. Carte de végétation des bassins des rios Ucayali et Huallaga.

2.4 Sous basins sélectionnés sur les bassins Ucayali et Huallaga.

Les bassins des rios Ucayali et Huallaga ont été sélectionnés d'abord parce qu'ils sont entièrement situés sur le territoire péruvien, et que notre base de données météorologiques était donc limitée au seul réseau du SENAMHI péruvien. Les bassins de drainage des autres stations (San Regis, Tamshiyacu, Borja et Bellavista. Voir Figure II-10) sont situés à cheval sur les territoires péruvien et équatorien, et nous n'avons pas eu accès aux données météorologiques équatoriennes récentes (excepté pour les précipitations).

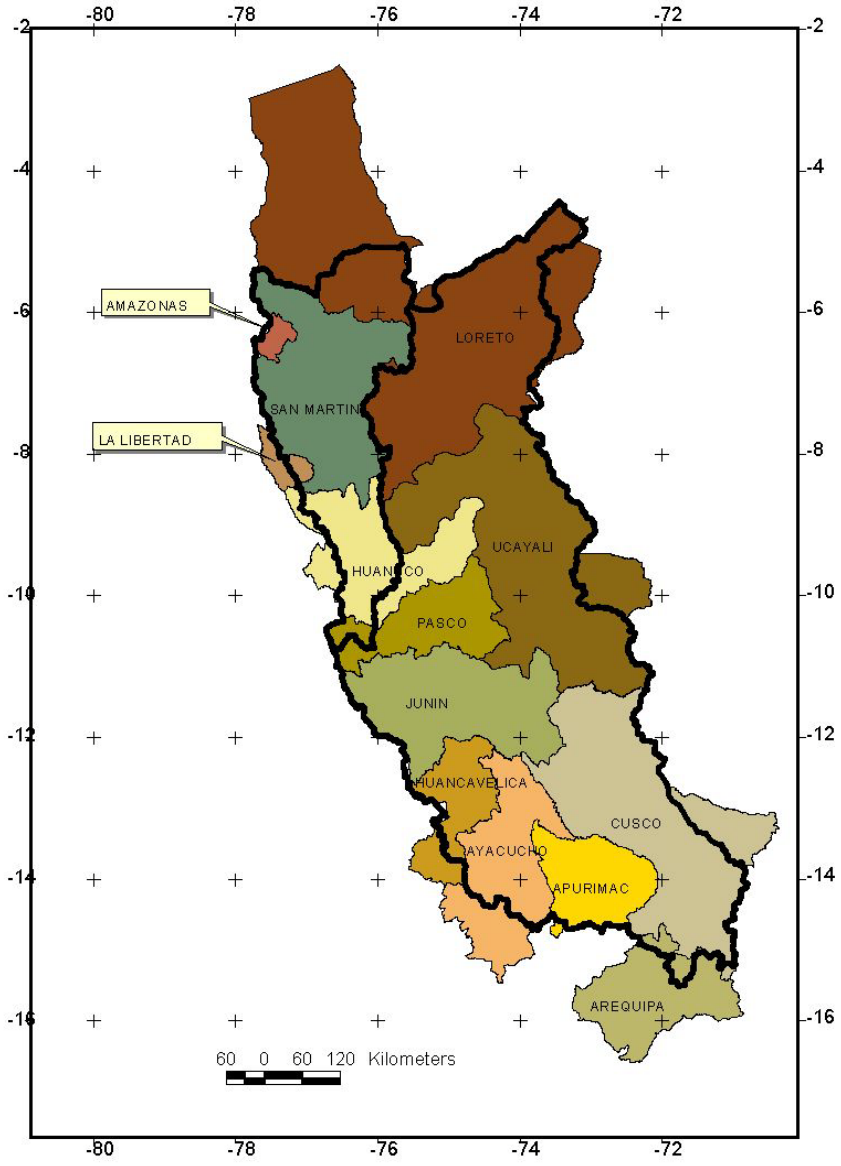

Figure II-8. Division politique des bassins des rios Ucayali et Huallaga. Les bassins de l'Ucayali et Huallaga sont limités par la ligne noire.

Ainsi, nous avons sélectionné 7 sous bassins en fonction de la disponibilité des données de débits. Les surfaces de drainage ont été délimitées au niveau des stations hydrologiques en utilisant le modèle numérique de terrain de la Figure II-5 (voir Tableau II-2 et Figure II-11), dont 5 sont situés en zone de forêt (Requena, Chazuta, Puerto Inca, Maldonadillo et Tambo) et 2 dans les Andes (Mejorada et Pisac).

Figure II-9. Réseaux des stations hydrométriques du SENAMHI avec mesures des débits jusqu'en 2001. Les stations sont identifiées par des carrés rouges et violets. D'après UNESCO, 2006.

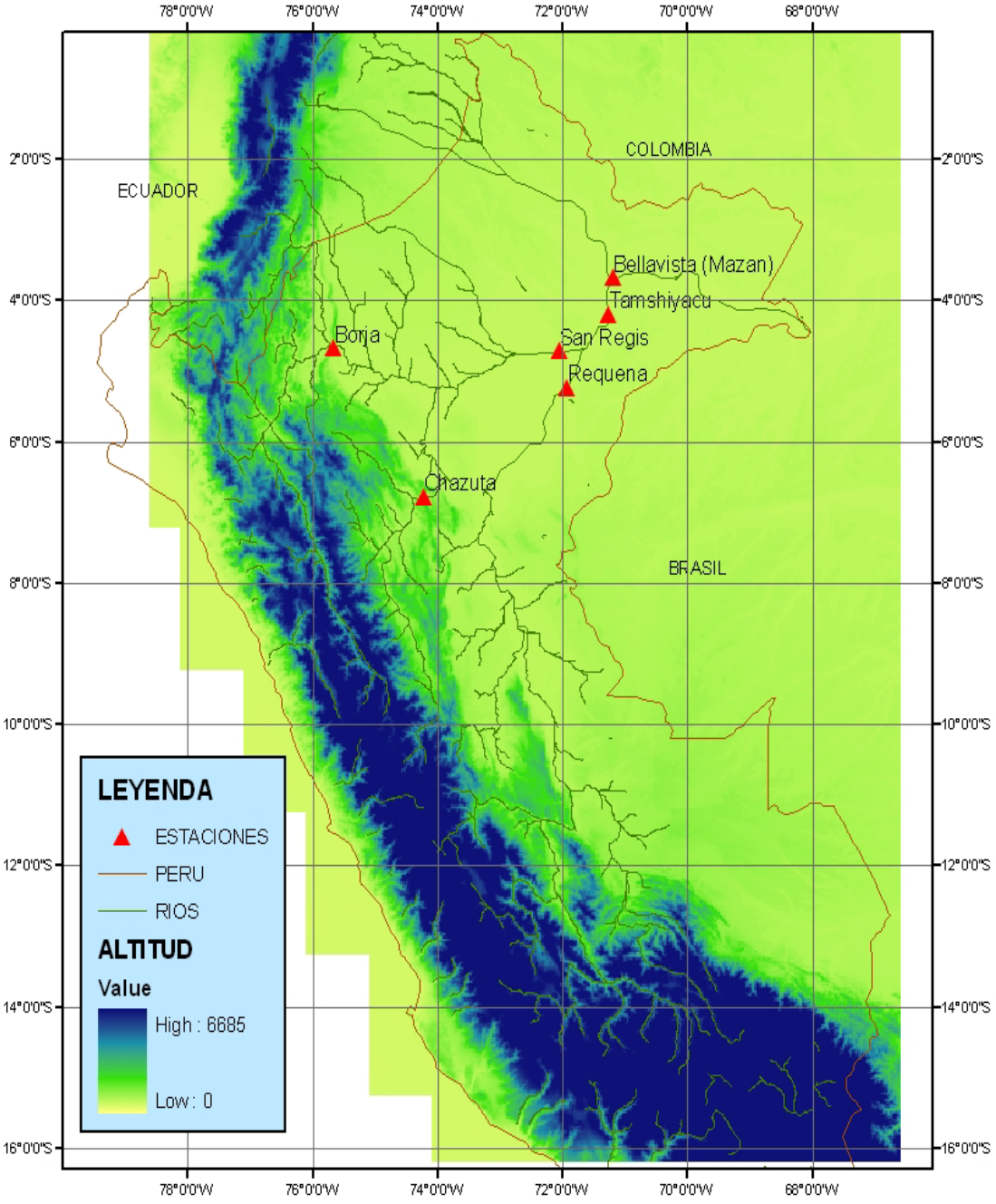

Figure II-10. Réseau des stations hydrométriques du SENAMHI avec mesures de débits, par le programme HYBAM (IRD-SENAMHI-UNALM).

Tableau II-2. Sous bassins sélectionnés sur les bassins des rios Ucayali et Huallaga. Ar. Dr. est la superficie drainée, et période est la période de données de débits disponibles pour chaque station.

N°	Station	Bassin	Lat. (°S)	Long. (°O)	Alt. (m s.n.m.)	Ar. Dr. (Km2)	Période
1	Requena	Ucayali	5.05	73.84	200	354416	janv.-1993/déc.-2007
2	Chazuta	Huallaga	6.58	76.18	200	69463	janv.-1999/déc.-2007
3	Puerto Inca	Pachitea	9.38	74.96	249	22661	janv.-1998/déc.-2007
4	Maldonadillo	Urubamba	10.74	73.71	287	60301	janv.-1988/déc.-2007
5	Tambo	Tambo	10.85	73.71	290	135252	janv.-1988/déc.-2007
6	Mejorada	Mantaro	12.52	74.93	2819	17244	janv.-1995/déc.-2007
7	Pisac	Vilcanota	13.43	71.84	2971	7129	janv.-1986/déc.-2007

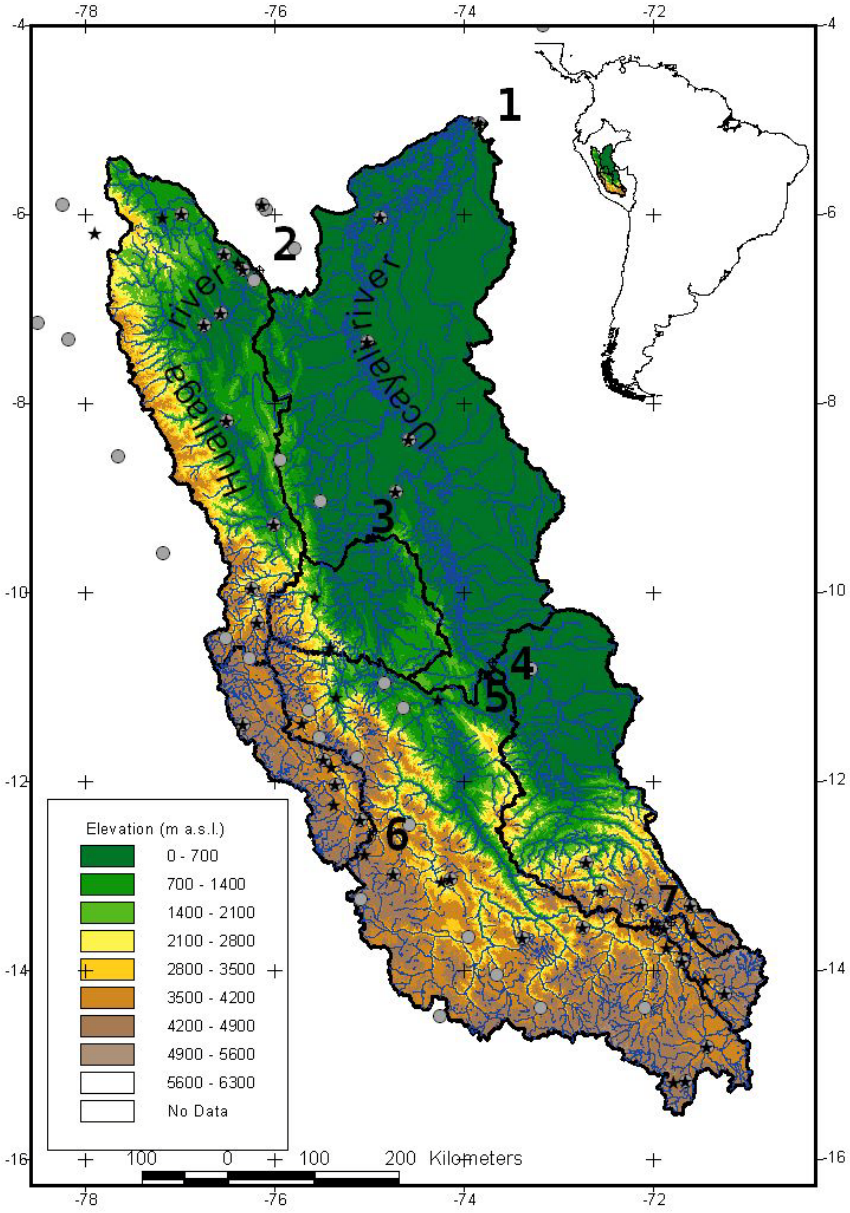

Figure II-11. Bassins sélectionnées pour notre étude. Pour la description voir la **Tableau II-2**. Les croix grises permettent de localiser les stations de mesure des précipitations tandis que étoiles noires indiquent les stations de mesure des températures.

2.5 Constitution de la banque de données

Les données nécessaires pour réaliser cette étude sont principalement les données de débit, de précipitation, d'évapotranspiration et la connaissance des types de sols. Les donnés journalières disponibles au SENAMHI au début de la thèse (2005) étaient stockées sous format papier, ou exceptionnellement sur format de feuille de calcul Excel, mais seulement au pas de temps mensuel. Ainsi, les données hydrométéorologiques sur le versant amazonien du Pérou étaient mal classées et surtout pas critiquées.

A partir de la collaboration du SENAMHI et de l'IRD dans le projet HYBAM, il a été décidé d'analyser les données de pluie au niveau mensuel dans tous les pays andins du bassin amazonien Espinoza *et al.* (2008).

Dans la présente étude, les bassins sélectionnés ont des surfaces variant de 7 129 à 354 416 Km^2 et nous présentons une modélisation du bilan hydrique distribué à la résolution de 0.25° par 0.25° (environ 27.8 par 27.8 Km^2).

2.5.1 Données hydrologiques

Comme mentionné dans la section 2.4, sept stations hydrologiques ont été choisies pour réaliser cette thèse : six sur le bassin du Rio Ucayali et une sur le bassin du Rio Huallaga. Quatre stations font partie du projet HYBAM (IRD-SENAMHI) dans la plaine amazonienne : Requena, Chazuta, Maldonadillo et Tambo, et les débits de ces deux dernières ont été estimés à partir des données de la station d'Atalaya (10.678°S, 73.8179°O). Les stations de Puerto Inca et Pisac font partie du réseau SENAMHI dans les Andes, et les valeurs ont été estimées par le Bureau de Statistique et Informatique. La station Mejorada fait partie du réseau géré par l'Entreprise d'Electricité péruvienne, et les débits naturels sont disponibles sur la page web du COES (Comité d'opération économique du système Interconnecté National, www.coes.org.pe). La localisation des stations ainsi que les surfaces de drainage et la période d'étude sont reportés dans le Tableau II-2. Toutes les données ont subis une critique statistique basée sur la technique du double cumul. La Figure II-12 montre les séries mensuelles de débits utilisées, et on observe déjà une grande variabilité de débits dans les sous-bassins de Chazuta et Puerto Inca.

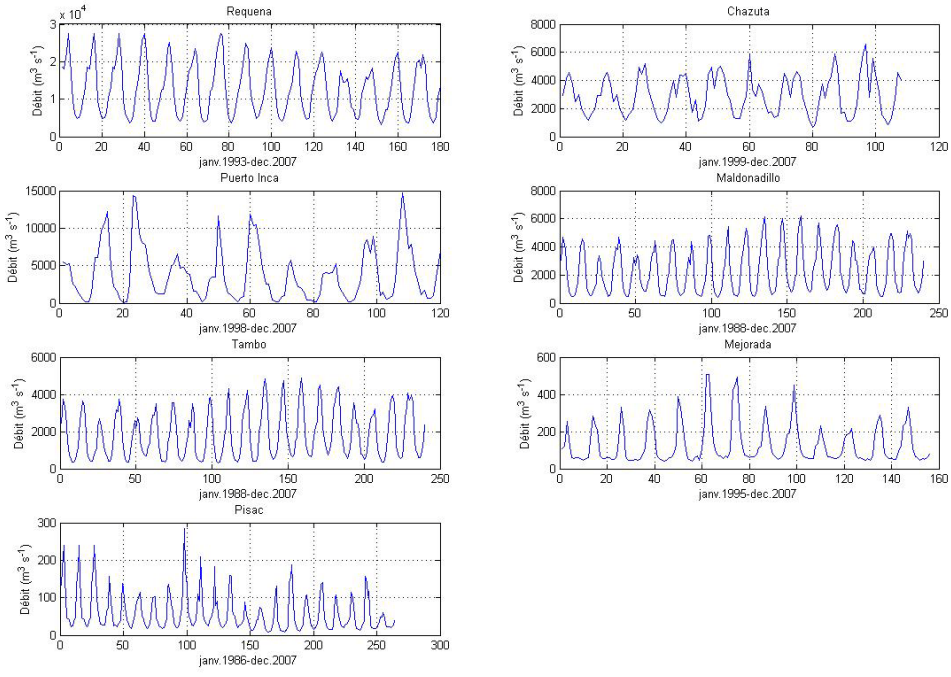

Figure II-12. Séries mensuelles des débits des stations hydrologiques retenues pour la présente étude.

La Figure II-13 présente les valeurs moyennes mensuelles sur les bassins étudiés. Les bassins de Chazuta et Puerto Inca présentent des crues marquées pendant les mois de novembre et décembre, tandis que les bassins d'altitude (Mejorada et Pisac) montrent des périodes sèches (de mai à décembre) et humide (janvier à avril) plus marquées.

2.5.2 Données pluviométriques

Les stations pluviométriques utilisées pour développer notre étude sont décrites en Figure II-11, et nous proposerons une analyse complète dans le **Chapitre 3**. En résumé, les données de pluies sont disponibles au pas de temps mensuel sur un réseau de 58 stations. Toutes les données ont été validées en utilisant le méthode du vecteur régional Hiez, 1977 et Brunet-Moret, 1979) pour les données compilées au sein du programme HYBAM (Espinoza et al., 2008) ainsi que par la méthode du double cumul pour les données utilisées dans l'étude de l' UNESCO (2006).

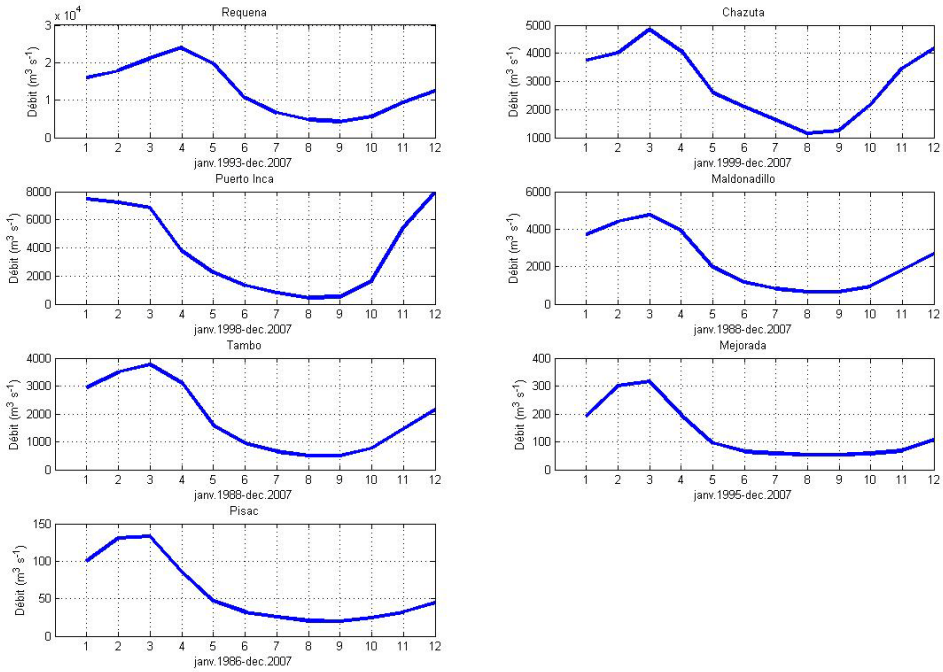

Figure II-13. Valeurs moyennes mensuelles des débits sur les sous bassins étudiés.

2.5.3 Données d'évapotranspiration

La variable évapotranspiration s'avère être la plus complexe à mesurer dans le cadre du cycle hydrologique. Différents types d'équations empiriques sont disponibles dans la littérature mais l'équation fournie par la FAO (FAO-Penman Monteith, Allen et al., 1998) est de loin la plus utilisée. Néanmoins, la principale difficulté de cette méthode est qu'elle requière plusieurs données météorologiques. Nous avons donc proposé une comparaison de méthodes empiriques d'estimation d'évapotranspiration sur huit stations au pas de temps journalier. Cette étude a été soumise à « Journal of Hydrology » et elle est en cours de révision.

2.5.3.1 Comparison of reference evapotranspiration models with the standard FAO Penman-Monteith model in the Peruvian Amazon-Andes basin

WALDO SVEN LAVADO CASIMIRO, DAVID LABAT, JEAN LOUP GUYOT, GILLES BOULET, JUAN JULIO ORDOÑEZ & OLIMPIO SOLIS

RÉSUMÉ

Plusieurs modèles sont disponibles pour estimer l'évapotranspiration de référence à partir des observations météorologiques. Le modèle de la FAO Penman-Monteith est de

loin le plus usuellement utilisé et on le considère généralement comme une méthode physique fiable, ainsi il est fréquemment utilisé comme référence pour comparer d'autres méthodes empiriques.

Douze modèles d'évapotranspiration de référence ont été comparés sur huit stations météorologiques à l'intérieur du bassin Amazonien Andin péruvien avec le but d'évaluer la performance de chaque modèle, comparé au modèle de FAO Penman-Monteith. Cette évaluation est basée sur plusieurs tests statistiques : coefficient de corrélation, indice de confiance, erreur aux moindre carrés, erreur relative biaisée et saisonnière.

Après avoir obtenu les performances des différents modèles d'évapotranspiration de référence pour chaque station météorologique, le modèle de Hargreaves-Samani apparaît comme le modèle le plus adapté. De plus, un recalibrage régional entre les modèles de Hargreaves-Samani et de Penman-Monteith de la FAO a été complété utilisant la régression linéaire, et en améliorant le test statistique basé sur des données journalières. Enfin avec la procédure de calibrage, un nouveau modèle de Hargreaves-Samani est obtenu, nommé dans ce travail Hargreaves-Samani modifié, mais ce dernier est seulement valide pour les bassins Amazoniens Andins du Pérou.

ABSTRACT

Several models are available to estimate reference evapotranspiration from standard meteorological observations. The FAO Penman-Monteith model is by far the most commonly used and it is generally considered as a physical and reliable method, so it is frequently used as a reference to compare other empirical methods.

Twelve reference evapotranspiration models were compared for eight weather stations inside the Peruvian Amazon-Andes basin, with the objective to evaluate the performance of each model compared to FAO Penman-Monteith model. This evaluation is based in several statistical tests: Correlation coefficient, Agreement Index, Root Mean Square Error, Relative Bias and Relative Seasonal Bias.

Once obtained the performances of the different reference evapotranspiration models for each weather station, Heargreaves-Samani model appears as the best suited model. In addition, regional recalibration between Heargreaves-Samani and FAO Penman-Monteith models was complemented using linear regression, improving the statistical test based on daily data. Finally with the recalibration procedure, a new Heargreaves-Samani model is obtained, called in this work Heargreaves-Samani modified, but this last is only valid over the Peruvian Amazon-Andes basin.

Key words: Evapotranspiration models, Peru, Amazonia, Andes, Regionalization.

INTRODUCTION

Evapotranspiration is defined as the amount of water that returns to the atmosphere through evaporation (moisture loss from the soil, standing water, etc.) and transpiration (biological use and release of water by plants). (Hansen et al., 1980).

Evapotranspiration is a function of temperature, solar radiation, relative humidity and wind speed (Dingman, 1994; Allen et al., 1998; Geiger et al., 2003; Fontenot, 2004 and others). In addition, specific vegetation and soil type are essential to calculate transpiration rates of different types of vegetation (Allen et al., 1998). Lysimeter and

eddycorrelation sensors can measure evapotranspiration directly. Pan evaporation measures the loss of a known quantity of water through evaporation (Fontenot, 2004) of a pan, but the direct measure of evapotranspiration is difficult and expensive using lysimeter and highly-sensitive sensors.

Because of the difficulty to estimate evapotranspiration, models are developed using as computing value the reference evapotranspiration (Eo) that provides a standard crop (a short, clipped grass) with an unlimited water supply so that a user can calculate maximum evaporative demand from that surface for a given day (Allen et al., 1998, Fontenot, 2004).

Generally, Eo models are categorized into three basic types: temperature, radiation, and combination (Jensen et al., 1990; Dingman, 1994; Watson et Burnett, 1995 and others). Models based on temperature generally require only mean daily air temperature measurements as the input to the model (e.g., Thornthwaite, 1948a,Hamon, 1961, Remanenko, 1961, Linacre, 1977, Hargreaves et Samani, 1985 and others). Radiation models (e.g., Abtew, 1996, Turc, 1961, Doorenbos et Pruitt., 1977, Hargreaves et Samani, 1985,Makkink, 1957, Jensen et Haise, 1963 and others) assume that radiation is the main driving variable.

Nevertheless, combination models (e.g., Penman, 1948) that combine elements from both the radiation regime and the vapor pressure deficit give very accurate results (Jensen et al., 1990), so currently the Penman family models are by far the most common combination model used (Jensen et al., 1990, Allen et al., 1998, Fontenot, 2004 and others). Over all the Penman's models, the FAO Penman-Monteith model (Allen et al., 1998) is considered to be the most physical and reliable method and is often used as a standard to verify other empirical methods (Chen et al., 2005).

Generally evaporation is measured with pan evaporation type 'A' and is frequently used to compare evapotranspiration models in homogeneous regions for different authors (e.g. Ali et al., 2007, Synder, 1992; Xu et Singh, 2001; Xu et Singh., 2000 and others) whereas for different regions the FAO Penman-Monteith model is used as a standard Eo model (e.g. Jensen et al., 1990; Chiew et al., 1995; Fontenot, 2004; Chen et al., 2005; Popova et Pereira, 2006; Fooladmand et Ahmadi, 2008; Jabloun et Sahli, 2008 and others).

Estimating Eo using FAO Penman-Monteith model is difficult because it requires many input data that are not easily accessible; the objective of this study is to compare several Eo models over the PAB region, using as a standard model of comparison the FAO Penman-Monteith model. It aims at obtaining a model that use limited but easily available data (e. g. temperature based model) and if possible, proposing recalibrations for regional purpose.

The present document is structured as follows: Introducing the theme of the paper in Section 1, Study area in Section 2, data availability, processing climatological and physical parameters are described in Section 3, description of Eo models in section 4, results are given in Section 5 and finally Conclusions in Section 6.

STUDY AREA

Several works about evapotranspiration over the Amazon basin have been made. Marengo (2006), reported many state-of-the-art works to compute evapotranspiration using global climate model reanalysis, climatonomic model, evapotranspiration models and some direct measurements, which in summary give an average evapotranspiration rate over the Amazon basin around 3.8 mm day^{-1}. According to Molion (1991), the solar radiation absorbed at the surface is primarily used for evaporating water (latent heat) and for heating the air (sensible heat) near the ground; also over the Central Amazonia, micrometeorological studies (e.g., Molion, 1987; Shuttleworth, 1988) have shown that 80% to 90% of the available energy is used for evapotranspiration and the rest for heating up the air. Consequently over the Amazon region, vegetation and climate is tightly coupled; evapotranspiration rate is believed to contribute to an estimated fifty percent of the annual rainfall (Salati, 1987).

The types of vegetation are very important to calculate Eo mainly to compute transpiration or soil evaporation, over our region of study exists many different types of vegetation: rain forest, savanna and grassland (Olson et al., 1985); moreover over the Amazonas basin a strong dependence between evapotranspiration and vegetation cover exists specially over the rainforest Costa et Foley (1997). Soil types play also a role in the evapotranspiration variability: Over the middle land and highland (around the Andes mountain) are predominantly lithosols (Viera, 1975a), where evapotranspiration is less than over the rainforest and evapotranspiration rates are parameterized like 20% of the rainfall (Costa et Foley, 1997), also this author mentions that mean annual rates of evapotranspiration by type of vegetation over the Amazon basin, is: about 4.18 mm day^{-1} for the rainforest; about 3.62 mm day^{-1} for the savanna and about 3.54 mm day^{-1} for the grasslands.

ACTO (2005), found five geographical regions over the Amazonas basin (Amazonia, Andes, Planalto, Guiana and Gurupi). The Peruvian Amazon-Andes basin (PAB), occupies about 856 751 km^2 (~ 74% from Peruvian territory) and is located in the western part of the Amazonas basin, with two distinct regions: Amazonia and Andes. Amazonia which is characterized by the presence of lowland rainforest biome, and the Andes region which correspond to western part of the Andes Cordillera with elevations over 6 000 m a.s.l. these two regions exhibit distinct types of land cover: humid forests, dry tropical forests, flooded tropical forests, agriculture, grass and shrub lands, little or sparse vegetation and water bodies.

The region of study exhibits several subregions (Peñaherrera, 2004); one can define altogether six natural regions Pulgar (1941): Quechua, Suni, Puna, Highland, High Jungle and Low Jungle. Each subregion shows contrasted characteristics of elevation, relief and climate; thus SENAMHI (2005), identify four distinct climate types over the PAB region using the Thornthwaite classification for climates types (Thornthwaite, 1948a), it is observed: Tropical, Warm Temperate, Highland and Polar climate.

In Peru, two works about evaporation inventory using pan type "A" (ϕ 1.20 m) were made, the first by MEM (1979) based on 90 stations found that evaporation increases with the altitude over the highlands, and associated the lower evaporation over rainforest to the higher relative humidity. The second work SENAMHI (1993) made the atlas of evaporation (1975-1985) from Peru using pan evaporation data from 64 stations,

majority localized over the Pacific and Titicaca basins. The main results consist in more evaporation over the highlands than over the rainforest for the PAB region.

According to UNESCO (2006), mean annual temperature characteristic over the PAB region exhibits relationship with elevation (lower altitude more temperature) and an higher seasonal amplitude of mean temperature than over the medium land and lowlands. Mean annual values of temperature exhibit range from 6 °C (highlands) up to 26 °C (lowlands). Mean annual rainfall is 2 060 mm over the PAB region ranging from 0 mm to 5500 mm. Evapotranspiration using Thornthwaite model (Thornthwaite, 1948a) shows annual mean of around 1 343 mm (~ 3.5 mm day^{-1}). Lavado *et al.*(2008) estimate evapotranspiration using the Thornthwaite model in sub basins over the Ucayali basin located inside the PAB region: Mean annual evapotranspiration rates are estimated over the 1969-1999 period, ranges from 613 mm (~ 1.7 mm day^{-1}) over the highlands to 1606 mm (~ 4.4 mm day^{-1}) over the rainforest.

Solar Radiation according to SENAMHI (2003) and Baigorria *et al.*(2004) over the PAB region ranges from about 5.5 kW h m^{-2} over the High Mountain and smaller amount to about 4.5 kW h m^{-2} over the rainforest.

DATA AVAILABILITY, PROCESSING CLIMATOLOGICAL AND PHYSICAL PARAMETERS

The FAO Penman-Monteith (PF) model (Equation 19, Table 3), following Allen *et al.*(1998) is used as the model of reference. It needs several meteorological data. Over the PAB region the Peruvian National Meteorology and Hydrology Service, SENAMHI (www.senamhi.gob.pe) has many weather stations mostly for precipitation and temperatures series but only eight weather stations exhibit the whole data required to run the PF model, overall meteorological variables to compute solar radiation.

Selected stations have daily data of pan evaporation using pan type "A" (ϕ = 1.20m) and daily meteorological data: temperatures, relative humidity and wind speed; in addition stations selected show valid empirical coefficient parameters to compute solar radiation with Bristow-Campbell method (Equation 9), already documented by Baigorria *et al.*(2004).

We removed the highest and lowest temperature data that can be considered doubtful. For this purpose we removed temperatures data out of range between lower and upper quartile. The weather stations (Table 1) are inside the PAB region (Fig. 1), and they are over the Highland (HU and AN stations), over the Medium Land (BA, BAM, AB and UR stations) and over the rainforest (CO and PO stations).

Mean climate characteristics of the weather stations are shown in Table 2, the principal characteristic over our region of study is a negative gradient for solar radiation and evaporation with respect to altitude; for minimum and maximum temperature series show larger values over the rainforest and smaller values over the highlands, according to the altitudinal lapse rate. Monthly seasonal variability in meteorological series over some selected weather station (Figure 2), exhibit larger seasonal range considering wind speed and relative humidity variables.

Table 1. Geographical location of weather stations used in this study.

Station	Code	Latitude (°S)	Longitude (°W)	Altitude m a.s.l.
Contamana	CO	7.21	75.00	185.00
El Porvenir	PO	6.35	76.19	230.00
Bagua Chica	BA	5.39	78.32	434.00
Bambamarca	BAM	6.40	78.31	2536.00
Abancay	AB	13.36	72.52	2750.00
Urubamba	UR	13.18	72.07	2863.00
Huayao	HU	12.02	75.19	3308.00
La Angostura	AN	15.11	71.39	4150.00

Methods for estimating Eo models from meteorological data require various climatological and physical parameters. Allen *et al.*(1998) describes methods to compute these parameters:

Atmospheric pressure (P) in kPa is given by:

$$P = 101.3\left(\frac{293 - 0.0065z}{293}\right)^{5.26} \quad (1)$$

Where, z is the elevation in meters; latent heat of vaporization (λ in MJ kg^{-1}, given by:

$$\lambda = 2.501 - 0.002361T \quad (2)$$

Where, T is the daily mean air temperature in ºC; psychrometric constant (γin kPa $°C^{-1}$, given by:

$$\gamma = \frac{C_p P}{\varepsilon \lambda} \quad (3)$$

Where, C_p is the specific heat of moist air at constant pressure (kJ kg^{-1} $ºC^{-1}$) and ε is ratio molecular weight of water vapour/dry air equal to 0.622; mean air temperature (ºC) is to compute as the mean between maximum and minimum temperature; saturation vapour pressure (e_s(T)) in kPa given by:

$$e_s = \frac{e^o(T_{\max}) + e^o(T_{\min})}{2} \quad (4)$$

$$\text{where } e_o(T) = 0.6108 \exp\left[\frac{17.27T}{T + 237.3}\right] \quad (5)$$

with Tmax equal to maximum temperature and Tmin is minimum temperature; slope of vapor pressure curve (Δ) in kPa $°C^{-1}$ given by:

$$\Delta = \frac{4098\left[0.6108 \exp\left(\frac{17.27T}{T + 237.3}\right)\right]}{(T + 237.3)^2} \quad (6)$$

Actual vapor pressure (e_a(T)) in kPa given by:

$$e_a(T) = 0.6108 \exp\left[\frac{17.27 T_{\min}}{T_{\min} + 237.3}\right] \quad (7)$$

wind speed of weather stations are generally measured up to 10 meters and Eo models require measures up to 2 meters above soil surface, Allen *et al.*(1998) suggests this equation (u_2) in m s^{-1}:

$$u_2 = u_z\left[\frac{4.87}{\ln(67.8z - 5.42)}\right] \quad (8)$$

Where, u_z is the wind speed at altitude z (m) above the ground surface in m s^{-1}; for this study z is 10 meters ; soil heat flux density (G) in MJ m^{-2} d^{-1} for daily step is considered around zero Allen *et al.*(1998) hence for this study G is equal to zero.

Table 2. Mean meteorological variables in the selected weather stations. n: number of data; Mean in mm day^{-1}; Std.: standard deviation in mm day^{-1}; Cv: coefficient of variation; RH: relative humidity; u_2: wind speed; R_s: solar radiation; PF: Eo PF model.

Weather	Statistic	Temperature (°C)			RH	u2	Rs	PF
Station		Maximum	Minimum	Mean	(%)	(m s-1)	(MJm-2day-1)	(mm day-1)
CO	Mean	32.15	19.26	25.71	67.82	1.78	17.57	4.37
n=1502	Std.	2.62	1.50	1.76	5.10	0.22	2.80	0.83
	Cv (%)	0.08	0.08	0.07	0.08	0.13	0.16	0.19
PO	Mean	32.39	20.50	26.45	70.16	1.71	14.65	3.89
n=9218	Std.	2.47	1.68	1.51	6.39	0.24	2.81	0.83
	Cv (%)	0.08	0.08	0.06	0.09	0.14	0.19	0.21
BA	Mean	32.17	20.02	26.10	69.60	1.99	20.20	4.81
n=2923	Std.	2.47	2.26	1.64	7.15	0.29	3.97	1.02
	Cv (%)	0.08	0.11	0.06	0.10	0.14	0.20	0.21
BAM	Mean	20.57	10.67	15.62	72.83	1.99	17.54	3.39
n=2983	Std.	1.91	2.51	1.28	8.56	0.32	2.46	0.56
	Cv (%)	0.09	0.24	0.08	0.12	0.16	0.14	0.17
AB	Mean	21.16	10.13	15.65	69.96	1.56	16.00	3.21
n=1865	Std.	2.58	1.49	1.62	6.29	0.24	3.11	0.70
	Cv (%)	0.12	0.15	0.10	0.09	0.15	0.19	0.22
UR	Mean	22.68	7.05	14.87	59.95	2.81	19.02	4.21
n=2639	Std.	2.16	3.22	1.85	8.46	0.44	2.40	0.68
	Cv (%)	0.10	0.46	0.12	0.14	0.16	0.13	0.16
HU	Mean	19.53	4.03	11.78	59.56	2.41	21.12	3.99
n=8030	Std.	2.07	3.48	1.79	9.48	0.16	2.82	0.64
	Cv (%)	0.11	0.86	0.15	0.16	0.07	0.13	0.16
AN	Mean	14.80	-2.97	5.91	53.55	2.43	21.70	3.65
n=2413	Std.	2.23	4.15	2.22	10.23	0.15	3.31	0.69
	Cv (%)	0.15	-1.40	0.38	0.19	0.06	0.15	0.19

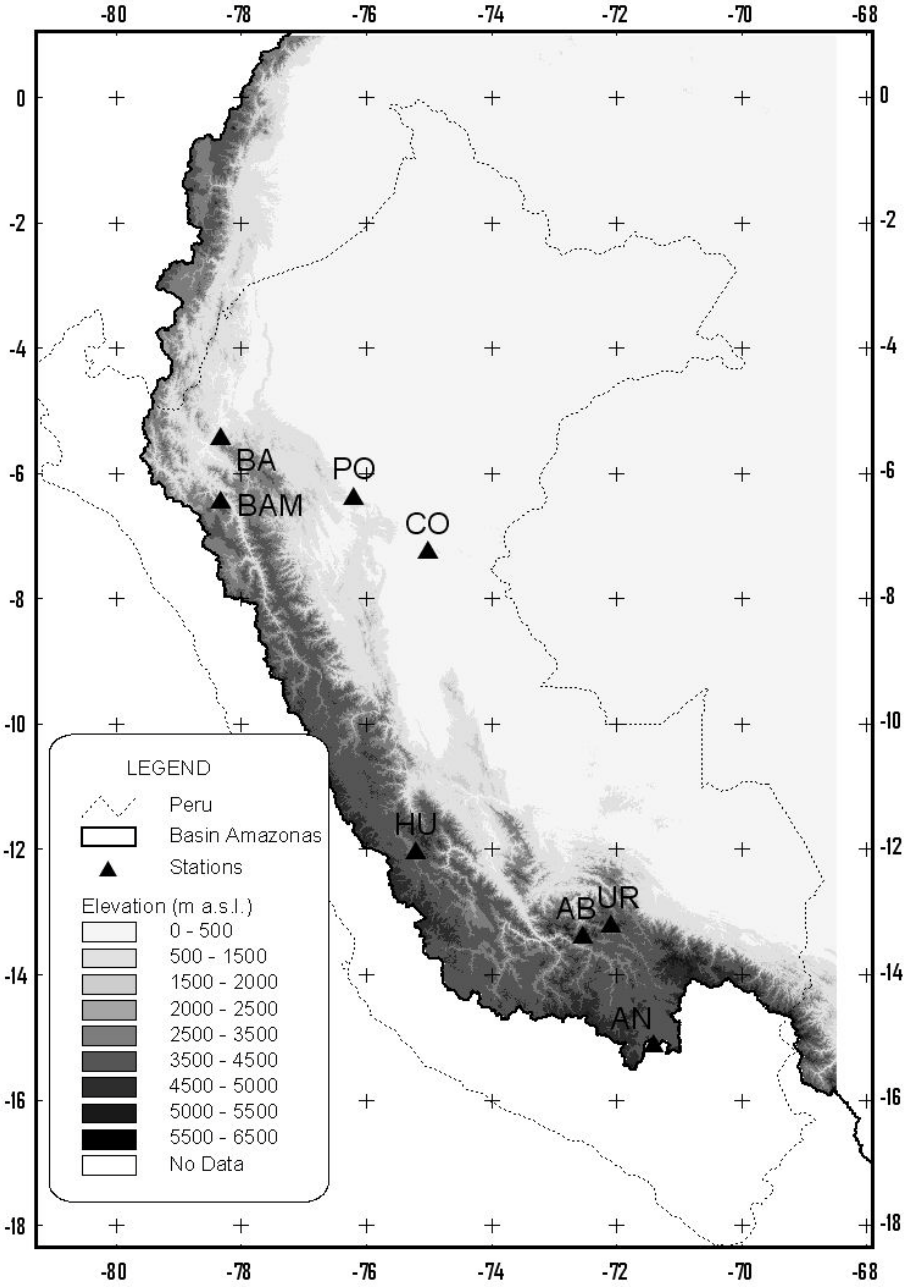

Figure 1. Location of the area of study, elevations, and used weather stations: Contamana (CO), Porvenir (PO), Bagua (BA), Bambamarca (BA), Abancay (AB), Urubamba (UR), Huayao (HU) and Angostura (AN).

To estimate the solar radiation (R_s), a Bristow-Campbell model (equation 9) is used (Bristow et Campbell, 1984), empirical coefficient parameters of Bristow-Campbell equation (a_B, b_B and c_B) of stations used in this study were validates by Baigorria *et al.*(2004), using observations from incoming solar radiation, sunshine observations and temperatures series of 15 weather station over Peru, we use these parameters to compute solar radiation of stations.

$$R_s = (a_B(1-\exp(-b_B \Delta T^{c_B}))R_a \qquad (9)$$

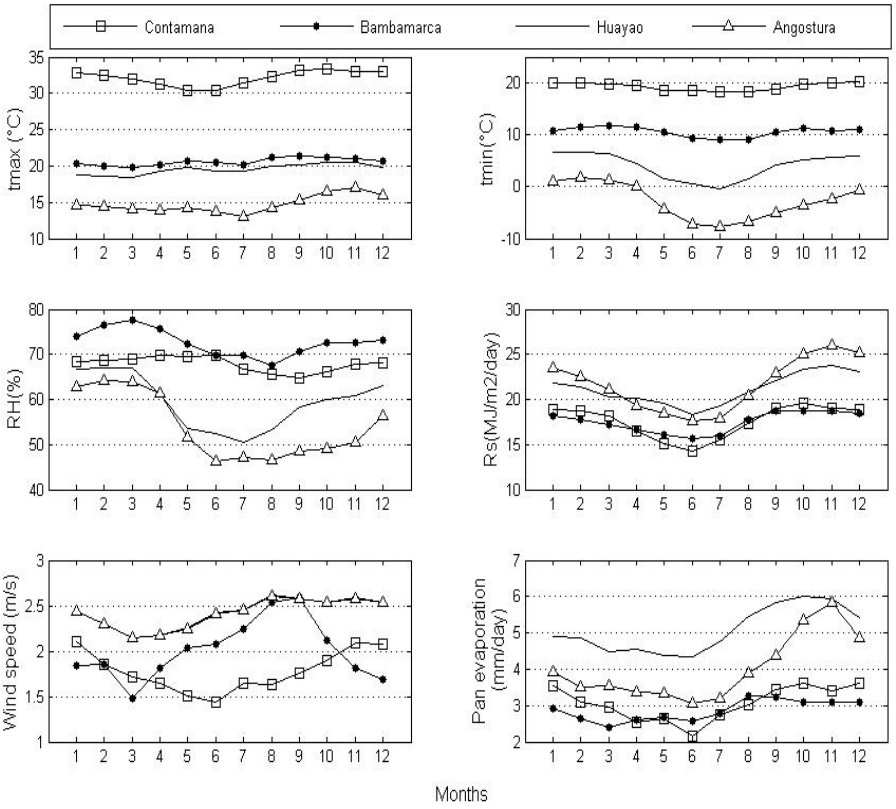

Figure 2. Monthly seasonal characteristics of Maximum Temperature (tmax), Minimum Temperature (tmin), Relative Humidity (RH), Solar Radiation (Rs), Wind speed and pan evaporation in four weather stations.

Where R_s is the solar radiation in MJ m^{-2} day^{-1}, R_a is the extraterrestrial radiation in MJ m^{-2} day^{-1}, ΔT is the difference between maximum and minimum temperatures in ºC and a_B, b_B and c_B are empirical coefficients of Bristow-Campbell model.

Extraterrestrial radiation is computed (Allen et al., 1998) as follow:

$$R_a = \frac{24*60}{\pi} G_{sc} d_r \left[\omega_s \sin(\varphi)\sin(\delta) + \cos(\varphi)\cos(\delta)\sin(\omega)\right] \qquad (10)$$

Where G_{sc} is solar constant equal to 0.0820 MJ m^{-2} min^{-1}; d_r is inverse the relative distance Earth-Sun (Equation 11); ω_s is sunset hour angle (Equation 13) in rad, φ is latitude in rad , δ is solar declination (Equation 12) in rad.

The inverse relative distance Earth-Sun, d_r , and the solar declination, δ, are solved how:

$$d_r = 1 + 0.033\cos\left(\frac{2\pi}{365} J\right) \qquad (11)$$

$$\delta = 0.409 sen\left(\frac{2\pi}{365} J - 1.39\right) \qquad (12)$$

Where, J is the number of the day in the year between 1 (January 1st.) and 365 or 366(31 December 31st.).

The sunset hour angle, ω_s, is given by:

$$\omega_s = \arccos[-\tan(\varphi)\tan(\delta)] \quad (13)$$

The daylight hours, N, in hours is given by (Allen et al., 1998):

$$N = \frac{24}{\pi}\omega_s \quad (14)$$

The clear sky solar radiation (R_{so}) in MJ m^{-2} day^{-1}, is given by (Allen et al., 1998):

$$R_{so} = \left(0.75 + 2\ 10^{-5} z\right) R_a \quad (15)$$

Where, z is station elevation above sea level in m; the net shortwave radiation (R_{ns}) in MJ m^{-2} day^{-1}, resulting from the balance between incoming and reflected solar radiation (Allen et al., 1998) is given by:

$$R_{ns} = \left(1 - \alpha\right) R_s \quad (16)$$

Where α is albedo (dimensionless), or canopy reflection coefficient, which is 0.23 for the hypothetical grass reference crop.

Stefan-Boltzmann law states quantitatively the relation between the rate of longwave energy emission and the absolute temperature of the surface raised to the fourth power, so we can compute Net longwave radiation (R_{nl}) in MJ m^{-2} day^{-1} as:

$$R_{nl} = \sigma\left[\frac{T_{\max}{}^4 + T_{\min}{}^4}{2}\right](0.34 - 0.14\sqrt{e_a})\left(1.35\frac{R_s}{R_{so}} - 0.35\right) \quad (17)$$

Where, σ is Stefan-Boltzmann constant equal to 4.903 10^{-9} MJ°$K^{-4}m^{-2}day^{-1}$, T_{max} and T_{min} is maximum and minimum temperature respectively in °K.

Finally, with the previous calculus, can compute Net Radiation (R_n) in MJ$m^{-2}day^{-1}$ as:

$$R_n = R_{ns} - R_{nl} \quad (18)$$

REFERENCE EVAPOTRANSPIRATION MODELS

Since the meteorological data available, twelve models were selected. Table 3 shows name, reference, symbol and equation of the Eo models used. In summary, PA model is observed pan evaporation type 'A', and recalibrated with wind speed and relative humidity; seven models are radiation-based (PT, TU, JH, MB, DO, AB, and MA) and four models are temperature-based (HE, HA, RO and LI). Table 4 shows the inputs of meteorological data required for the Eo models.

Table 3. Reference evapotranspiration models (Eo) used in this study.

Nº	Model (Reference)	Symbol	Equation (Eo)	
1	FAO Penman-Monteith Allen *et al.*(1998)	PF	$\frac{0.408\Delta(R_n - G) + \gamma \frac{900}{T+273} u_2 (e_s - e_a)}{\Delta + \gamma(1 + 0.34u_2)}$	(19)
2	Pan Evaporation Allen *et al.*(1998)	PA	$K_p * Ep$ $K_p = 0.108 - 0.0286 * u_2 + 0.0422 * \ln(FET) +$ $0.1434 * \ln(RH) - 0.000631 * [\ln(FET)]^2 * \ln(RH)$	(20)
3	Priestley-Taylor Priestley et Taylor (1972)	PT	$\frac{1.26 \frac{\Delta}{\Delta + \gamma} R_n}{\lambda}$	(21)
4	Turc Turc (1961)	TU	If RH>50 $0.013 \frac{T}{T+15} \cdot \frac{23.9R_s + 50}{\lambda}$ If RH<=50 $(0.013 \frac{T}{T+15} \cdot \frac{23.9R_s + 50}{\lambda})(1 + \frac{50 - RH}{70})$	(22)
5	Jensen- Haise Jensen et Haise (1963)	JH	$\frac{C_t (T - Tx) R_s}{\lambda}$ $C_t = (C_1 + 7.3C_h)^{-1} \quad C_1 = 38 - 2h/305$ $C_h = 5(e_o(T\max) - e_o(T\min))^{-1}$ $Tx = -2.5 - 7C_h^{-1} - h/550$	(23)
6	McGuinness-Bordne Jensen et Haise (1963)	MB	$\frac{R_s (T+5)}{68\lambda}$	(24)
7	Doorenbos – Pruitt Doorenbos et Pruitt (1977)	DO	$a \frac{\Delta}{\Delta + \gamma} R_s 0.408 - 0.3$ $a = 1.066 - 0.0013RH + 0.045u_2 -$ $0.0002RHu_2 - 0.0000315RH^2 - 0.0011u_2;$	(25)
8	Abtew Abtew (1996)	AB	$0.4081 R_s$	(26)
9	Makkink Makkink (1957)	MA	$0.61 \frac{\Delta}{\Delta + \gamma} R_s 0.408 - 0.12$	(27)
10	Hargreaves-Samani Hargreaves et Samani (1985)	HE	$\frac{0.0023(T + 17.8)(T\max - T\min)^{0.5} Ra}{\lambda}$	(28)
11	Hamon Hamon (1961)	HA	$\left(\frac{N}{12}\right)^2 \exp\left(\frac{T}{16}\right)$	(29)
12	Remanenko Remanenko (1961)	RO	$4.5\left(1 + \frac{T}{25}\right)^2 \left(1 - \frac{RH}{100}\right)$	(30)

13	Linacre Linacre (1977)	LI	$\frac{\left(\frac{500T_m}{100-A}\right)+15(T-Td)}{(80-T)}$ $T_m = T + 0.006h$	(31)

Weather data notations and units

Eo	=	Potential evapotranspiration (mm d-1)
Δ	=	Slope of vapor pressure curve (kPa °C^{-1})
λ	=	latent heat of vaporization (MJ kg-1)
γ	=	psychrometric constant (kPa °C^{-1})
$e_s(T)$	=	saturation vapour pressure (kPa)
$e_a(T)$	=	actual vapour pressure (kPa)
G	=	soil heat flux density (MJ m^{-2} d^{-1})
u_2	=	wind speed 2 meters above soil surface (m s^{-1})
r_a	=	aerodynamic resistance (s m^{-1})
r_s	=	surface resistance of reference crop (= 69 s m^{-1})
T	=	mean temperature (°C)
Tmax	=	maximum temperature (°C)
Tmin	=	minimum temperature (°C)
T_d	=	dew point temperature (°C)
R_s	=	solar radiation (MJ m^{-2} d^{-1})
R_a	=	extraterrestrial radiation (MJ m^{-2} d^{-1})
R_n	=	net solar radiation (MJ m^{-2} d^{-1})
N	=	Day length (hours d^{-1})
h	=	Elevation (m)
A	=	Latitude (degrees)
FET	=	Fetch (= 1000 m.)

Table 4. Input data requirement for evapotranspiration (Eo) models.

Models	Parameters				
	Solar Radiation	Air Temperature	Relative Humidity	Wind Speed	Atmospheric pressure
PF	✓	✓	✓	✓	✓
PA	▤	▤	✓	✓	▤
PT	✓	✓	▤	▤	✓
TU	✓	✓	✓	▤	▤
JH	✓	✓	✓	▤	✓
MB	✓	✓	▤	▤	▤
DO	✓	✓	✓	✓	▤
AB	✓	▤	▤	▤	▤
MA	✓	✓	▤	▤	▤
HE	▤	✓	▤	▤	▤
HA	▤	✓	▤	▤	▤
RO	▤	✓	✓	▤	▤
LI	▤	✓	✓	▤	▤

Parameter estimation and evaluation criteria

In order to evaluate the performance of models compared to the reference PF equation, different statistical tests are available in the literature. The correlation coefficient (R^2) is by far the most commonly used by the scientific community. Unfortunately, it exhibits some limitations that results in poor measure of model performance (Legates et McCabe, 1999). Therefore, it is essential to use other statistical tests to obtain the best goodness of fit. For these purpose four statistical values are used: the index of agreement (D), the root mean square (RMSE), the relative bias (RB) and the seasonal relative bias (SB) were used. The best model was chosen with the follow steps: (a) the maximum R and D values and (b) the least values of RMSE, RB and SB. The R^2 is the proportion of total variance in the observed data that can be explained by the model (Legates et McCabe, 1999), and is given by:

$$R^2 = \frac{\sum_{i=1}^{n}(Ev_i - \overline{Ev})(Em_i - \overline{Em})}{\left[\sum_{i=1}^{n}(Ev_i - \overline{Ev})\right]^{0.5}\left[\sum_{i=1}^{n}(Em_i - \overline{Em})\right]^{0.5}} \quad (35)$$

Where, Ev_i is the observed value (PF); $\overline{Ev}$ is the mean of the observed values; Em_i is the model estimated values; $\overline{Em}$ is the mean of the model estimated values; n is the number of data points.

R^2 is in the range from 0 to 1, where the highest values indicate the better agreement between estimates and the lowest value describes no agreement (Ali et al., 2007).

The D is given by Legates et McCabe, 1999:

$$D = 1 - \frac{\sum_{i=1}^{n}(Ev_i - Em_i)^2}{\sum_{i=1}^{n}\left(\left|Em_i - \overline{Ev}\right| + \left|Ev_i - \overline{Em}\right|\right)^2} \quad (36)$$

D has a similar interpretation as the R^2, so D varies from 0 (poor model) to 1 (perfect model), this statistical measure is an indication of deviation of data from the slope equal to 1 between observed and estimated values.

To measure the error between a pair of data set: RMSE and the RB are used. The RMSE is frequently used to measure the differences between values predicted by a model and the observed values, being the measure of non-systematic variation between two data series used as an index for performance evaluation (Ali et al., 2007). The RMSE is given by:

$$RMSE = \sqrt{\frac{1}{n}\sum_{i=1}^{n}(Ev_i - Em_i)^2} \quad (37)$$

The relative bias (RB) indicates the amount of underestimation (RB<0) and over estimates (RB>0), and is given by:

$$RB = \frac{1}{n}\sum_{i=1}^{n}(Ev_i - Em_i) \quad (38)$$

Finally, a seasonal relative Bias (SB) is used to compare seasonal values; this has a similar definition as the RB but is used with seasonal values.

$$SB = \frac{1}{n}\sum_{i=1}^{n}(Evs_i - Ems_i) \quad (39)$$

Where, Evs_i are the seasonal observed values (PF) and Ems_i is the model seasonal estimated values, n is equal to 12 (monthly averages of total data record).

Larger value of RMSE and also large absolute value of RB (RAB) and SB (SAB) indicate lesser accuracy of the model.

RESULTS

Statistical properties of Eo models

First the initial statistical properties were computed with respect to PF model. Table 5 shows the range between maximum and minimum, the mean plus and less standard deviation and the coefficient of variation for Eo models for each weather station, also Figure 3 exhibits statistical properties using boxplot graphics of weather station used in study.

PA model exhibits more differences in comparison to the PF model and the other models. Statistical properties of PA model shows a larger difference compared to PF model. The coefficient of variation (Cv) is the value that express these differences between the models. Larger values of Cv for PA model are shown chiefly over the rainforest (0.45 for CO station and 0.48 for PO station). AB model shows large differences for mean and standard deviation comparing to PF model, consequently PA and AB model underestimate and overestimate PF respectively.

Making a general evaluation of statistical properties, on average of the stations, PT, JH and HE models show less differences compared to PF considering the mean and standard deviation, Cv are similar for all the models except for PA, JH, HA and LI models.

In summary, HE model is more similar to PF model in five out of eight stations (BAM, AB, UR, HU and AN), based on mean and standard deviation properties. Then, CO, PO and BA stations show similar standard deviations for HE model. We will now perform a more robust analysis of the performance of the Eo models.

Table 5. Mean Statistical characteristics of the data series in weather stations for Eo models. n: number of dates; Range in mm day^{-1}; Mean in mm day^{-1}; Std.: standard deviation in mm day^{-1}; Cv: coefficient of variation in %.

Weather			Eo Models														
Station	Statistical	PF	PA	PE	PM	GA	PT	TU	JH	MB	DO	AB	MA	HE	HA	RO	LI
CO	Range	1.40-6.12	0.08-5.70	1.41-5.35	1.40-6.11	1.53-6.15	1.58-5.46	1.33-5.02	0.48-7.59	0.82-4.56	0.81-6.42	2.17-9.19	0.80-4.23	2.25-7.12	1.84-4.53	1.50-8.66	2.07-5.77
n=1502	Mean±Std.	4.37±0.83	2.53±1.14	3.97±0.70	4.35±0.83	4.52±0.82	4.15±0.72	3.86±0.61	4.58±1.26	3.25±0.63	4.48±0.95	7.16±1.14	3.15±0.56	5.23±0.86	3.42±0.45	5.99±1.15	4.44±0.56
	Cv	0.19	0.45	0.18	0.19	0.18	0.17	0.16	0.27	0.20	0.21	0.16	0.18	0.17	0.13	0.19	0.13
PO	Range	0.77-6.20	0-5.40	0.80-5.17	0.76-6.18	0.86-6.05	0.93-5.09	0.68-4.67	0.07-7.48	0.26-4.23	0.07-6.08	0.82-8.78	0.20-3.90	1.33-7.58	1.88-4.89	0.67-9.55	1.77-6.22
n=9218	Mean±Std.	3.89±0.82	2.28±1.09	3.51±0.67	3.87±0.82	4.00±0.80	3.65±0.65	3.32±0.59	3.90±1.21	2.77±0.60	3.66±0.93	5.97±1.14	2.64±0.55	5.09±0.88	3.57±0.41	5.71±1.33	4.45±0.57
	Cv	0.21	0.48	0.19	0.21	0.20	0.18	0.18	0.31	0.22	0.26	0.19	0.21	0.17	0.12	0.23	0.13
BA	Range	1.25-7.52	0.16-8.59	1.21-6.08	1.24-7.43	1.34-7.07	1.33-6.45	1.09-6.37	0.39-9.96	0.62-5.38	0.50-7.95	1.50-10.7	0.55-4.95	2.22-8.38	2.41-4.91	1.47-10.9	2.78-6.71
n=2923	Mean±Std.	4.80±1.01	4.31±1.51	4.45±0.85	4.79±1.01	5.02±1.00	4.78±0.88	4.40±0.81	5.51±1.71	3.78±0.81	5.25±1.32	8.24±1.62	3.69±0.77	5.11±0.90	3.50±0.41	5.72±1.38	4.52±0.57
	Cv	0.21	0.35	0.19	0.21	0.20	0.18	0.19	0.31	0.21	0.25	0.20	0.21	0.18	0.12	0.24	0.13
BAM	Range	1.76-5.08	0-4.98	1.93-4.54	1.75-4.97	2.03-5.33	2.28-4.82	1.76-4.21	0.53-6.77	1.10-3.04	1.62-6.40	3.85-9.91	1.48-3.91	1.76-5.58	1.26-2.37	0.86-5.99	2.60-5.04
n=2983	Mean±Std.	3.38±0.56	2.37±0.89	3.37±0.47	3.34±0.54	3.72±0.57	3.77±0.49	3.10±0.41	3.24±1.13	2.17±0.33	4.01±0.82	7.15±1.00	2.91±0.43	3.48±0.63	1.83±0.18	3.21±0.93	3.72±0.40
	Cv	0.17	0.38	0.14	0.16	0.15	0.13	0.13	0.35	0.15	0.21	0.14	0.15	0.18	0.10	0.29	0.11
AB	Range	1.15-5.44	0.03-5.66	1.26-5.07	1.14-5.39	1.33-5.68	1.47-5.47	0.96-4.63	0.22-9.38	0.50-3.62	0.75-6.69	2.27-9.88	0.75-4.34	1.33-6.19	1.09-2.74	0.73-6.60	2.51-5.90
n=1865	Mean±Std.	3.20±0.70	2.60±1.08	3.14±0.68	3.17±0.69	3.45±0.74	3.49±0.78	2.88±0.60	3.46±1.42	2.00±0.51	3.70±0.97	6.52±1.27	2.68±0.60	3.62±0.80	1.83±0.30	3.60±0.89	4.18±0.49
	Cv	0.22	0.42	0.22	0.22	0.22	0.23	0.21	0.41	0.26	0.26	0.19	0.22	0.22	0.17	0.25	0.12
UR	Range	1.01-6.27	0.22-6.16	1.14-5.33	1.00-6.13	1.25-6.41	1.30-5.35	0.74-4.57	0.16-9.04	0.38-3.34	0.68-7.34	2.17-10.2	0.66-4.39	1.12-6.11	0.94-2.54	0.72-6.61	2.22-5.76
n=2639	Mean±Std.	4.21±0.67	3.09±1.14	3.80±0.60	4.12±0.66	4.47±0.70	3.89±0.73	3.28±0.49	4.83±1.29	2.28±0.42	4.91±0.85	7.75±0.97	3.17±0.47	4.21±0.66	1.76±0.31	4.55±0.85	4.63±0.44
	Cv	0.16	0.37	0.16	0.16	0.16	0.19	0.15	0.27	0.19	0.17	0.13	0.15	0.16	0.18	0.19	0.10
HU	Range	1.25-6.00	1.00-7.26	1.44-5.42	1.24-5.87	1.51-6.36	1.72-5.67	0.93-4.83	0.20-10.1	0.51-3.35	0.94-8.01	2.73-11.7	0.90-4.77	1.38-5.78	0.80-2.21	0.63-6.10	2.44-5.65
n=8030	Mean±Std.	3.98±0.63	4.02±1.10	3.81±0.61	3.90±0.62	4.37±0.68	4.06±0.75	3.19±0.53	4.66±1.43	2.13±0.41	5.21±0.95	8.61±1.15	3.40±0.52	3.79±0.61	1.45±0.24	3.90±0.79	4.36±0.42
	Cv	0.16	0.27	0.16	0.16	0.16	0.18	0.17	0.31	0.20	0.18	0.13	0.15	0.16	0.17	0.20	0.10
AN	Range	0.83-5.52	0.50-5.84	1.03-5.06	0.82-5.35	1.07-6.08	1.23-5.32	-0.5-3.79	0.06-8.36	0.20-2.37	0.64-7.60	2.41-11.7	0.66-4.41	0.66-4.98	0.57-1.54	0.34-4.77	2.09-5.44
n=2413	Mean±Std.	3.65±0.69	3.16±0.96	3.56±0.73	3.55±0.68	4.13±0.81	3.78±0.91	2.12±0.76	3.76±1.39	1.44±0.42	5.06±1.04	8.85±1.34	3.20±0.60	3.22±0.69	1.01±0.22	3.15±0.57	4.25±0.41
	Cv	0.19	0.31	0.21	0.19	0.20	0.24	0.36	0.37	0.30	0.21	0.15	0.19	0.22	0.22	0.18	0.10

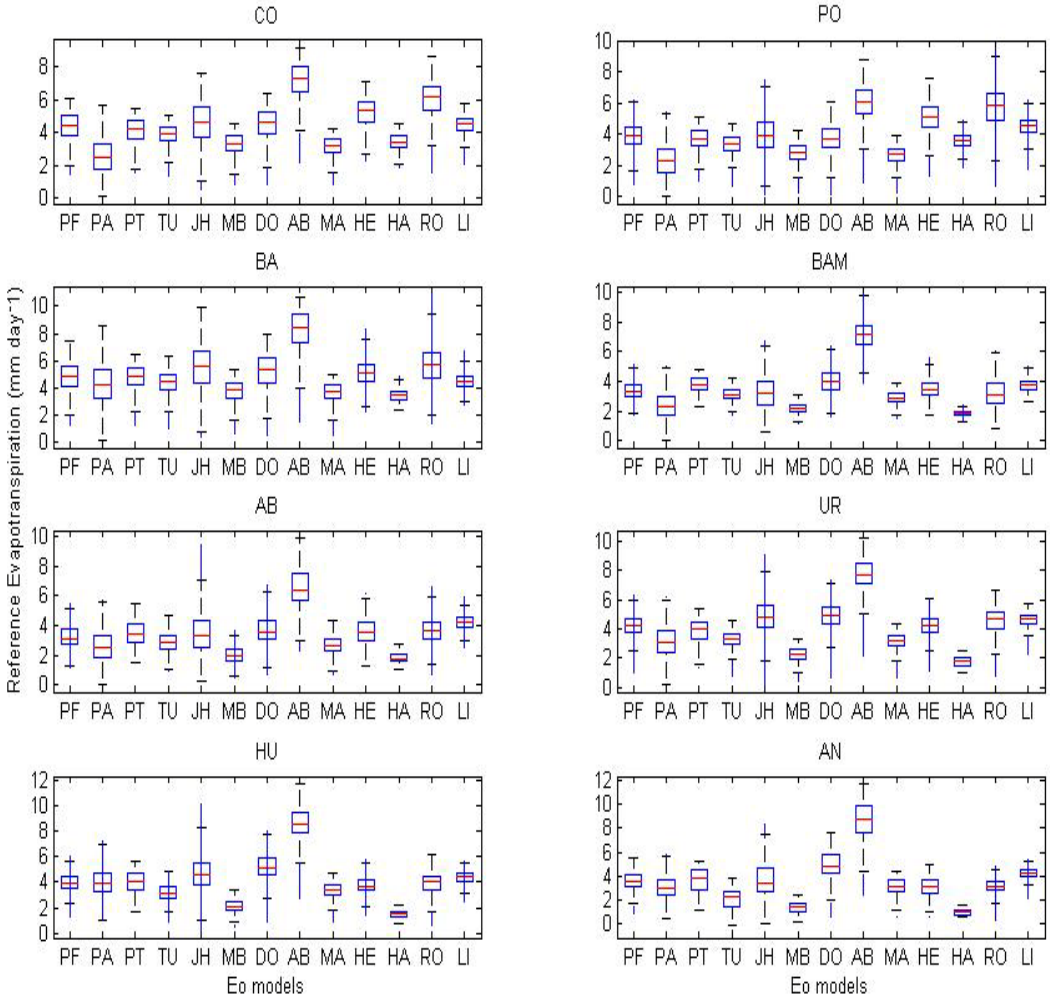

Figure 3. Boxplot comparison between Eo models used for Contamana (CO), Porvenir (PO), Bagua (BA), Bambamarca (BA), Abancay (AB), Urubamba (UR), Huayao (HU) and Angostura (AN) weather stations.

Performance of Eo models

In order to evaluate Eo models over the PAB region five statistical tests are used: R2, D, RMSE, RB, RAB and SAB. Table 6 shows the values of R2 and D, mostly HE and DO models exhibit the better performance considering R2 and D statistical tests, except for AB station with TU model like the best, better performance are shown considering statistical D for BA and AB stations. Close values to better performance of R2 and D statistical are observed between PT, TU, JH and MA models whereas PA, MB, AB, HA, RO and LI models show poor performance for R2 and D statiscal tests, i.e a good agreement are exhibited between standard model (PF) and Eo estimated by HE model for the most part of weather stations.

In relationship with errors of magnitude between PF model and Eo models RMSE, RB, absolute values of RB (RAB) and absolute values of SB (SAB) statistical tests were used. Results are shown in Table 7. The PA, TU, MB, AB, MA and HA models show lower performances considering all the stations. Values obtained for the other models exhibit smaller magnitudes. The HE model shows a better performance for BAM, UR, and HU stations, DO model is the better for CO station, JH model is the better for PO, AB and AN station and PT model is the better for BA station. In summary, Table 7 shows close RMSE, RB, RAB and SAB statistical tests considering first PT model and second HE model.

Table 6. Correlation coefficient (R^2) and Index of agreement (D) of selected weather stations.

		Eo Models											
Station	Statistic	PA	PT	TU	JH	MB	DO	AB	MA	HE	HA	RO	LI
	R2	0.64	0.98	0.99	0.98	0.99	0.99	0.98	0.99	1.00	0.84	0.88	0.90
CO	D	0.48	0.97	0.87	0.94	0.68	0.99	0.41	0.64	0.80	0.63	0.59	0.91
	R2	0.59	0.98	0.99	0.98	0.99	0.99	0.98	0.99	0.99	0.70	0.91	0.92
PO	D	0.50	0.95	0.84	0.96	0.66	0.98	0.51	0.62	0.69	0.70	0.56	0.81
	R2	0.66	0.94	0.98	0.98	0.97	0.99	0.97	0.98	0.98	0.49	0.93	0.91
BA	D	0.75	0.97	0.93	0.87	0.76	0.94	0.41	0.73	0.96	0.51	0.82	0.86
	R2	0.67	0.84	0.95	0.98	0.91	0.99	0.98	0.97	0.99	0.24	0.90	0.92
BAM	D	0.54	0.81	0.88	0.87	0.48	0.80	0.24	0.80	0.99	0.35	0.87	0.84
	R2	0.65	0.95	1.00	0.97	0.99	0.99	0.99	1.00	0.99	0.85	0.81	0.87
AB	D	0.69	0.94	0.94	0.85	0.58	0.89	0.33	0.86	0.92	0.47	0.84	0.62
	R2	0.70	0.67	0.88	0.95	0.81	0.99	0.94	0.90	0.91	0.41	0.77	0.83
UR	D	0.58	0.77	0.62	0.80	0.39	0.82	0.28	0.59	0.95	0.30	0.83	0.77
	R2	0.63	0.77	0.91	0.97	0.86	0.99	0.97	0.96	0.97	0.43	0.77	0.81
HU	D	0.73	0.86	0.67	0.76	0.39	0.63	0.22	0.78	0.96	0.28	0.86	0.78
	R2	0.83	0.84	0.80	0.97	0.80	1.00	0.98	0.95	0.98	0.62	0.79	0.78
AN	D	0.81	0.89	0.50	0.87	0.37	0.61	0.22	0.86	0.91	0.31	0.76	0.70

Top statistical values are in bold characters and the nearby values are in gray box.

Boxplot (Figure 4) shows the monthly seasonal comparison between PF model and the other models using SAB statistical test (Table 7), the better models are: PA model in HU station; PT model in BA station; JH model in PO, AB and AN stations; DO model in CO station and HE model in BAM and UR stations. Considering monthly seasonal characteristics, PT, JH and HE models show the better performances. In addition, seasonal cycle is better described by these models as shown in Figure 5, thanks to a better simulation of large spring and summer months (December to Mars) amplitudes and winter months (April to August) smaller values.

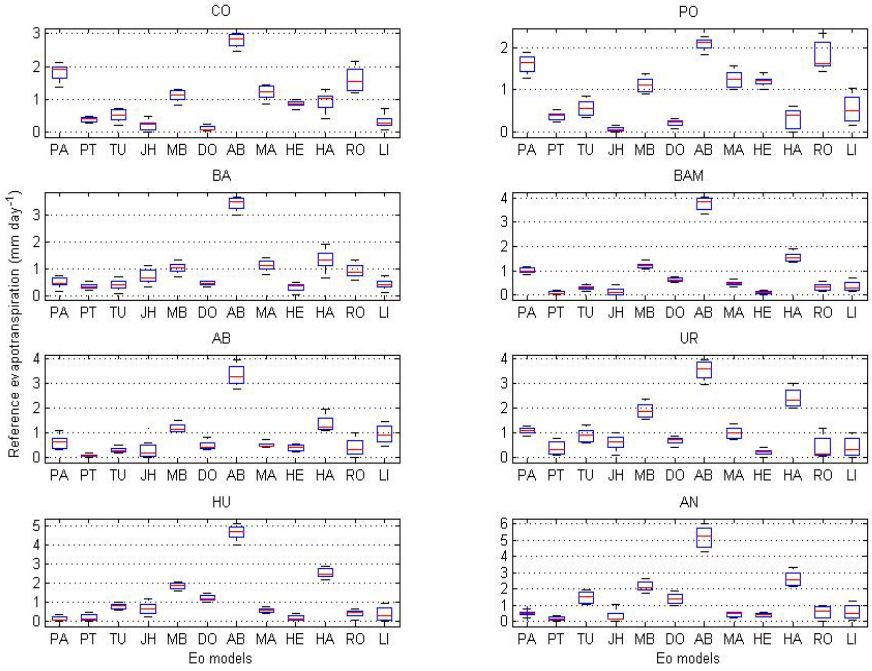

Figure 4. Boxplot comparisons between Eo models using Seasonal bias (SB) statitical for Contamana (CO), Porvenir (PO), Bagua (BA), Bambamarca (BA), Abancay (AB), Urubamba (UR), Huayao (HU) and Angostura (AN) weather stations.

In summary, three models exhibit better statistical properties and statistical test in comparison to PF model: two models based on radiation (PT and JH model) and one model based on temperature (HE model). From these Eo estimation models: HE model involves only temperature series contrary to PT and JH models that involve temperature and solar radiation series.

Best Eo model and recalibration for regional use

According to the results of statistical properties and statistical tests of comparison described above, the HE model appears as the better model out of the twelve models considered in this study. In order to improve the HE model over the PAB region compared to PF model, we aim at recalibrating the HE model using linear regression between HE and PF model.

Using a single station PF versus HE linear regression model, leads to several distinct recalibration coefficients. In order to propose a single set of valuable coefficients for the whole zone of study, we used the complete PF and HE models output data, thus the complete set of daily data for the 8 stations (i.e. 31573 observations).

Table 7. Root mean square (RMSE), Relative bias (RB), absolute real bias (RAB) and Seasonal absolute bias (SAB) of select weather stations.

		Eo Models											
Station	Statistic	PA	PT	TU	JH	MB	DO	AB	MA	HE	HA	RO	LI
	RMSE	2.03	0.29	0.56	0.52	1.13	0.20	2.82	1.25	0.87	1.08	1.73	0.42
	RB	1.84	0.21	0.51	-0.21	1.11	-0.11	-2.80	1.22	-0.86	0.95	-1.62	-0.07
	RAB	1.84	0.21	0.51	0.21	1.11	0.11	2.80	1.22	0.86	0.95	1.62	0.07
CO	SAB	1.84	0.21	0.51	0.21	1.11	0.11	2.80	1.22	0.86	0.95	1.61	0.32
	RMSE	1.84	0.33	0.62	0.43	1.14	0.28	2.11	1.28	1.21	0.69	1.94	0.68
	RB	1.61	0.23	0.57	-0.01	1.12	0.22	-2.08	1.25	-1.20	0.32	-1.82	-0.56
	RAB	1.61	0.23	0.57	0.01	1.12	0.22	2.08	1.25	1.20	0.32	1.82	0.56
PO	SAB	1.61	0.23	0.57	0.07	1.12	0.23	2.08	1.25	1.21	0.33	1.81	0.55
	RMSE	1.24	0.34	0.48	1.02	1.07	0.57	3.50	1.16	0.39	1.58	1.09	0.61
	RB	0.49	0.02	0.41	-0.70	1.03	-0.44	-3.43	1.12	-0.31	1.31	-0.92	0.28
	RAB	0.49	0.02	0.41	0.70	1.03	0.44	3.43	1.12	0.31	1.31	0.92	0.28
BA	SAB	0.49	0.15	0.41	0.71	1.03	0.44	3.43	1.12	0.31	1.31	0.92	0.43
	RMSE	1.21	0.49	0.35	0.62	1.25	0.68	3.80	0.50	0.14	1.65	0.53	0.42
	RB	1.02	-0.39	0.28	0.14	1.22	-0.62	-3.77	0.47	-0.10	1.56	0.17	-0.34
	RAB	1.02	0.39	0.28	0.14	1.22	0.62	3.77	0.47	0.10	1.56	0.17	0.34
BAM	SAB	1.02	0.37	0.28	0.15	1.22	0.62	3.76	0.47	0.09	1.56	0.33	0.35
	RMSE	1.02	0.37	0.34	0.81	1.22	0.58	3.37	0.54	0.43	1.45	0.66	1.05
	RB	0.60	-0.29	0.33	-0.26	1.20	-0.50	-3.32	0.52	-0.41	1.38	-0.40	-0.98
	RAB	0.60	0.29	0.33	0.26	1.20	0.50	3.32	0.52	0.41	1.38	0.40	0.98
AB	SAB	0.62	0.32	0.32	0.32	1.20	0.49	3.33	0.52	0.42	1.37	0.42	0.96
	RMSE	1.39	0.66	0.99	0.92	1.98	0.73	3.57	1.09	0.29	2.53	0.64	0.58
	RB	1.12	0.32	0.93	-0.62	1.93	-0.70	-3.55	1.04	0.00	2.45	-0.34	-0.42
	RAB	1.12	0.32	0.93	0.62	1.93	0.70	3.55	1.04	0.00	2.45	0.34	0.42
UR	SAB	1.12	0.47	0.92	0.62	1.92	0.70	3.54	1.03	0.23	2.44	0.45	0.44
	RMSE	0.86	0.49	0.84	1.08	1.89	1.27	4.66	0.61	0.24	2.60	0.51	0.54
	RB	-0.04	-0.08	0.80	-0.68	1.85	-1.23	-4.63	0.58	0.19	2.54	0.08	-0.37
	RAB	0.04	0.08	0.80	0.68	1.85	1.23	4.63	0.58	0.19	2.54	0.08	0.37
HU	SAB	0.13	0.38	0.80	0.68	1.86	1.23	4.63	0.58	0.20	2.54	0.43	0.38
	RMSE	0.74	0.51	1.60	0.76	2.25	1.45	5.24	0.50	0.45	2.70	0.66	0.75
	RB	0.49	-0.13	1.52	-0.11	2.21	-1.41	-5.20	0.45	0.43	2.64	0.50	-0.60
	RAB	0.49	0.13	1.52	0.11	2.21	1.41	5.20	0.45	0.43	2.64	0.50	0.60
AN	SAB	0.50	0.40	1.50	0.35	2.20	1.40	5.20	0.44	0.42	2.62	0.54	0.59

Top statistical values are in bold characters and the nearby values are in gray box.

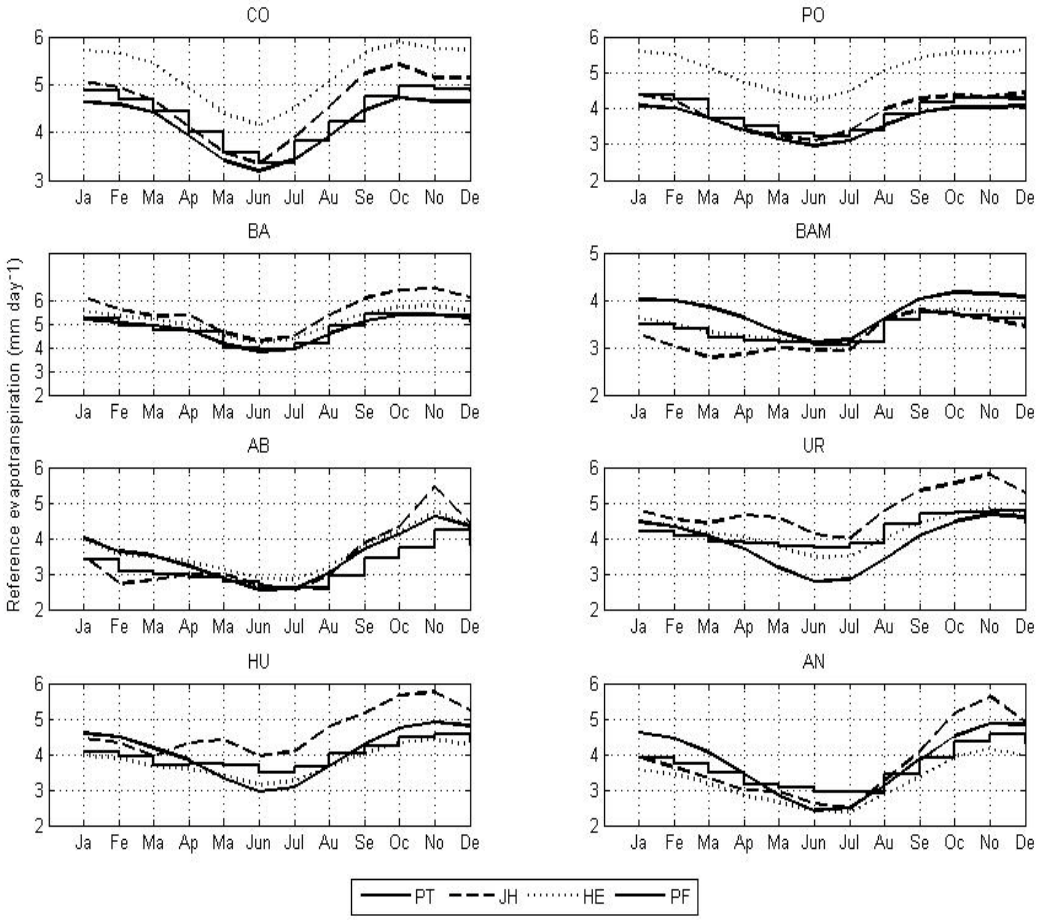

Figure 5. Seasonal monthly of PF, PT, JH and HE models, PF model is in stair step plot for Contamana (CO), Porvenir (PO), Bagua (BA), Bambamarca (BA), Abancay (AB), Urubamba (UR), Huayao (HU) and Angostura (AN) weather stations.

Linear regression to get one set of statistical parameters between PF and HE model was made using the following equation:

$$PF = a_1 * HE + a_2 \qquad (32)$$

Which is the general expression of polynomial equation, where, to solve equation (32) is required only to compute constant coefficients a_1 and a_2.

To solve equation (32) Matlab routine with algorithm QR factorization was used, values obtained, with 95% confidence bounds of coefficient and statistical test R^2 and RMSE are shown in Table 8.

Table 8. Coefficients values for modified Heargreaves-Samani model (HEm) for the total data.

Coefficient		95% confidence bounds
a1	0.6484	0.6432, 0.6536
a2	1.146	1.123, 1.169
R2	0.6543	
RMSE	0.4988	

Finally, we have the next equation valid for our zone of study:

$$HEm = 0.6484 * HE + 1.146 \qquad (33)$$

Where, HEm is new Hargreaves model modified valid over our region of study; data notations and units are similar to Hargreaves model (see equation 30); in fact, HEm model improve the original HE model for rapport to PF model.

Table 9 shows the performance of HEm model for rapport to other models, exhibiting the better performance of HEm model for almost all the stations i.e., HEm model has improved original HE model and is a good model for regional purpose over the PAB region. Figure 6 shows performance of HEm model comparing to PF model of the stations in study.

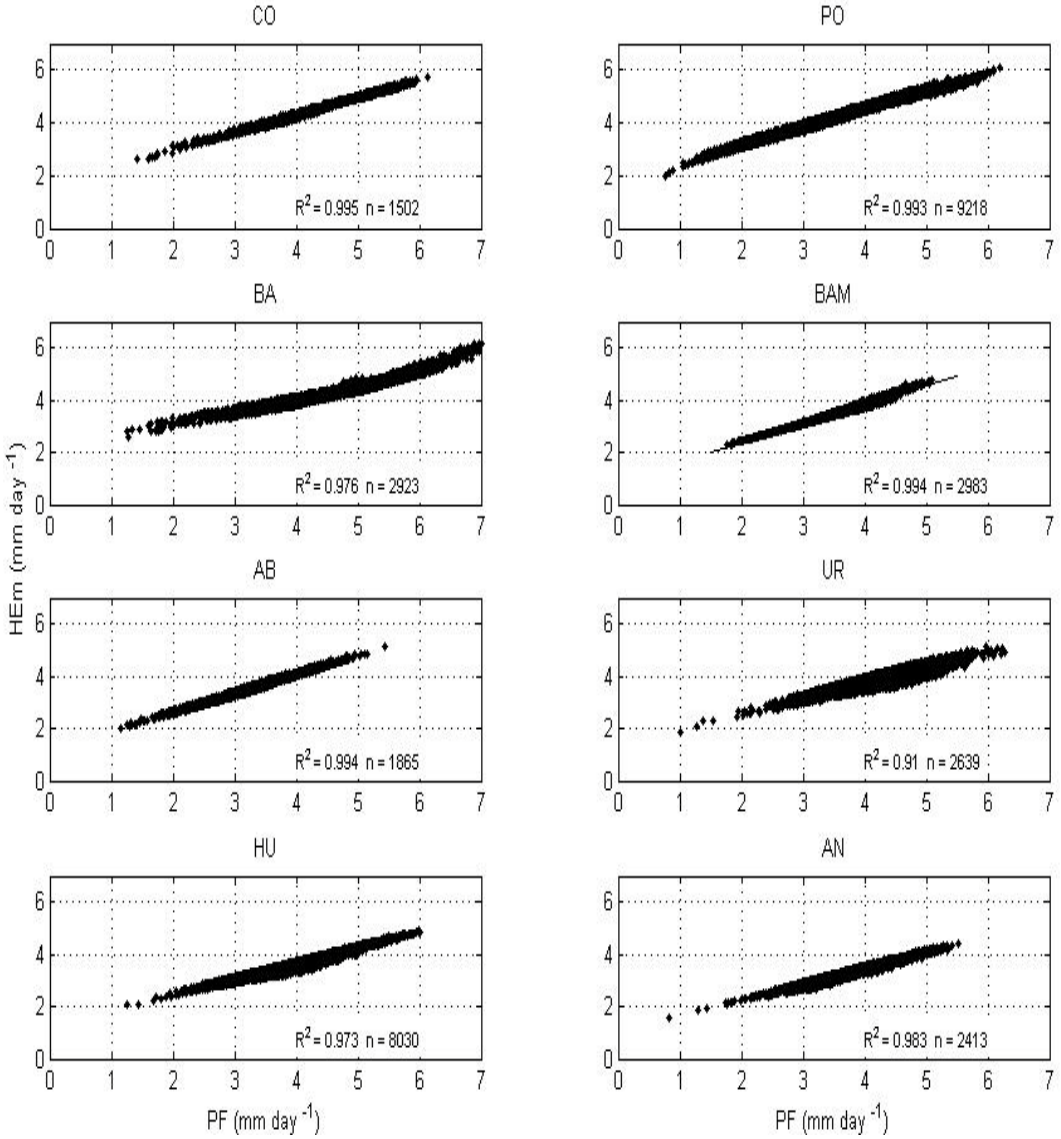

Figure 6. Comparison of PF model with Heargreaves-Samani modified model (HEm) for Contamana (CO), Porvenir (PO), Bagua (BA), Bambamarca (BA), Abancay (AB), Urubamba (UR), Huayao (HU) and Angostura (AN) weather stations.

Table 9. Statistical tests (R^2 D RMSE RAB and SAB) for four Eo models and comparison with Heargreaves-Samani modified model (HEm).

		Eo Models			
Station	Statistic	PT	JH	HE	HEm
	R2	0.98	0.98	1.00	1.00
	D	0.97	0.94	0.80	0.95
	RMSE	0.29	0.52	0.87	0.33
	RAB	0.21	0.21	0.86	0.17
CO	SAB	0.21	0.21	0.86	0.18
	R2	0.98	0.98	0.99	0.99
	D	0.95	0.96	0.69	0.84
	RMSE	0.33	0.43	1.21	0.62
	RAB	0.23	0.01	1.20	0.56
PO	SAB	0.23	0.07	1.21	0.56
	R2	0.94	0.98	0.98	0.98
	D	0.97	0.87	0.96	0.88
	RMSE	0.34	1.02	0.39	0.58
	RAB	0.02	0.70	0.31	0.34
BA	SAB	0.15	0.71	0.31	0.35
	R2	0.84	0.98	0.99	0.99
	D	0.81	0.87	0.99	0.97
	RMSE	0.49	0.62	0.14	0.16
	RAB	0.39	0.14	0.10	0.02
BAM	SAB	0.37	0.15	0.09	0.07
	R2	0.95	0.97	0.99	0.99
	D	0.94	0.85	0.92	0.93
	RMSE	0.37	0.81	0.43	0.34
	RAB	0.29	0.26	0.41	0.29
AB	SAB	0.32	0.32	0.42	0.29
	R2	0.67	0.95	0.91	0.91
	D	0.77	0.80	0.95	0.83
	RMSE	0.66	0.92	0.29	0.48
	RAB	0.32	0.62	0.00	0.34
UR	SAB	0.47	0.62	0.23	0.33
	R2	0.77	0.97	0.97	0.97
	D	0.86	0.76	0.96	0.83
	RMSE	0.49	1.08	0.24	0.46
	RAB	0.08	0.68	0.19	0.38
HU	SAB	0.38	0.68	0.20	0.39
	R2	0.84	0.97	0.98	0.98
	D	0.89	0.87	0.91	0.84
	RMSE	0.51	0.76	0.45	0.49
	RAB	0.13	0.11	0.43	0.42
AN	SAB	0.40	0.35	0.42	0.41

Top statistical values are in bold characters and the nearby values are in gray box.

CONCLUSIONS

This study is the first that compare reference evapotranspiration (Eo) models, using FAO Penman-Monteith (PF) model as standard over the Peruvian Amazon-Andes basin region.

Out of the twelve models used to compute Eo, the Hargreaves-Samani (HE) model appear as the best Eo model over the Peruvian Amazon-Andes basin region based over statistical comparison tests. This corroborates that HE model can be used as PF estimator, already documented for different authors (see e. g. Allen et al., 1998;Gavilán et al., 2006; Popova et Pereira, 2006; Jabloun et Sahli, 2008; among others).

HE model involves only maximum and minimum temperature series to compute Eo whereas PF model involves several meteorological variables. Hence, HE model allows computing Eo using limited data which was one of the main objective of this work.

Another objective of this study is to recalibrate the selected model (HE) for regional purpose. Linear regression was made between PF and HE model leading to a modified model, called in this work Hargreaves-Samani modified (HEm) model that improves consequently the HE estimations over the PAB region.

Temperature data is by far the most available parameter in the SENAMHI network. Then the model that estimates Eo values using only air temperature (HEm) appears well suited the PAB region making possible a better spatial distribution of Eo.

2.5.4 Données des sols FAO

A partir de la couverture pédologique décrite dans la Figure II-6, nous avons calculé la capacité de rétention en eau des sols, en utilisant les valeurs fournis par la Maison de Sciences de l'Eau (MSE) de Montpellier (voir Dieulin, 2005 et Dieulin et al., 2006): Sur la couverture mondiale, les unités de sols sont au nombre de 4930. À chaque unité est associé un champ intitulé FAO soil, constitué :

- du symbole de l'unité pédologique dominante ;
- d'un chiffre qui spécifie la composition des associations de sols ; quand les associations de sols sont dominées par des Lithosols, la composition de l'association est indiquée par un hachuré ;
- d'un chiffre indiquant la classe texturale des sols dominants de l'association (1 : grossière, 2 : moyenne, 3 : fine) ;
- d'une lettre minuscule indiquant la classe de pente de l'association de sols (a : plat à ondulé, b : vallonné à accidenté, c : fortement disséqué à montagneux).

Le libellé des symboles cartographiques est le suivant :

Exemples : Ag1-3a : acrisols gleyiques, de texture fine, et acrisols plinthiques, plats à ondulés.

Lc6-3b : luvisols chromiques, de texture fine, lithosols et vertisols chromiques avec solonets orthiques, vallonnés à accidentés.

La FAO a défini 7 classes de « profondeur » d'infiltration, classes déterminées par la granulométrie des types de sols. Les 7 classes sont rapportées en la Tableau II-3. Chaque unité de sol contient 7 valeurs correspondant au pourcentage de présence de l'unité de sol dans chaque classe. Le total atteignant obligatoirement 100.

Tableau II-3. Classification des sols selon la capacité de rétention en eau en mm (d'après FAO/UNESCO, 1981)

W(Wetlands)	A	B	C	D	E	F
N.C	200-300	150-200	100-150	60-100	20-60	0-20

Par exemple, pour la classe de sol Albic Arenosol dont le code FAO est Qa5-1a, les valeurs sont : Qa5-1a, 10, 0, 0, 40, 25, 25, 0 ce qui correspond à : 10% dans la classe Wetlands, 0% dans la classe A, 0% dans la classe B, 40% dans la classe C, 25% dans la classe D, 25% dans la classe E, et 0% dans la classe F. La FAO définit pour chaque classe une fourchette de valeur : la classe F par exemple correspond à une profondeur allant de 0 à 20 millimètres. Nous avons choisi de calculer pour chaque classe les profondeurs pour le minimum de la fourchette (pour la classe F, 0 millimètres), pour la valeur moyenne (10 pour la classe F) et pour la valeur maximale (20 pour la classe F) et nous avons donc attribué une valeur absolue (en millimètres) pour chaque SMIN, SMOY et SMAX de chaque unité de sol.

Seule la classe Wetlands n'est pas chiffrée dans les données de la FAO, elle concerne des types de sols marécageux. Nous lui avons arbitrairement donné la valeur de 1 000 mm. Le premier calcul que nous avons effectué fut de transformer en valeur absolue les pourcentages du tableau de la FAO. Reprenons l'exemple de l'unité de sol Qa5-1a, nous avons obtenu les valeurs de le Tableau II-4.

Tableau II-4. Valeurs obtenues pour estimer la capacité de rétention en eau pour l'unité de sol Qa5-1a.

Qa5-1a	Wetlands	A	B	C	D	E	F
	1000	200-300 mm	150-200 mm	100-150 mm	60-100 mm	20-60 mm	0-20 mm
Pourcentages	10	0	0	40	25	25	0
Valeurs (Min-Moy-Max)	10-10-10	0-0-0	0-0-0	40-50-60	15-20-25	5-10-15	0-0-0

Nous avons alors totalisé les valeurs pour chaque classe pour n'obtenir qu'une valeur minimum, moyenne et maximum pour chaque unité de sol. Soit pour l'unité de sol Qa5-1a, on a obtenu :

Smin = 10 + 0 + 0 + 40 + 15 + 5 + 0 = 70,

Smoy = 10 + 0 + 0 + 50 + 20 + 10 + 0 = 90,

et Smax = 10 + 0 + 0 + 60 + 25 + 15 + 0 = 110.

Ainsi pour nos basins d'étude, on a calculé les valeurs de rétention en eau minimum (FAO SMIN), moyenne (FAO SMOY) et maximum (FAO SMAX) des sols à partir des données de sol de la FAO (voir Figure II-14).

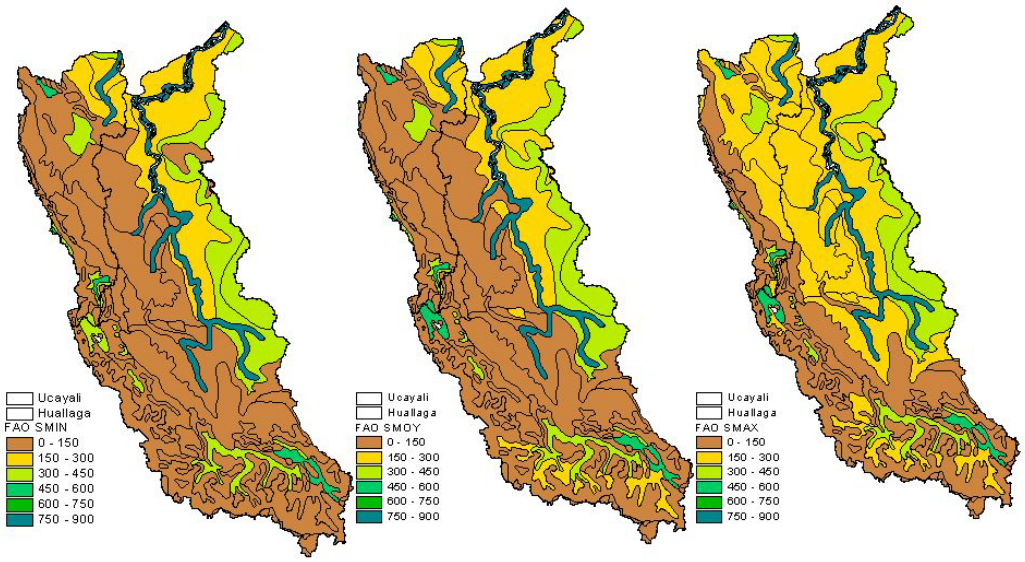

Figure II-14. Capacité en eau des sols (SMIN, SMOY et SMAX), exprimés en millimètres sur les basins de l'Ucayali et du Huallaga.

2.5.5 Constitution des grilles

En tenant compte des données décrites dans les sections antérieures, et en considérant qu'on va travailler à pas de temps mensuel et à l'échelle semi-distribuée avec une résolution de 0.25° par 0.25°, on doit utiliser une méthode d'interpolation pour les donnés de pluie et d'évapotranspiration. Ainsi pour l'interpolation nous utilisons la méthode de Kriging. Cette méthode consiste à établir un variogramme pour chaque point distribué dans l'espace. Ce variogramme évalue l'influence des 16 stations les plus proches selon la distance. La méthode de Kriging est la seule qui prenne en compte un possible gradient spatial de données. Pour développer cette méthode, on a utilisé le logiciel Hydraccess (Vauchel, 2005a). Les données de sols décrits dans la section antérieure doivent être interpolées à une résolution de 0.25° par 0.25°, pour réaliser cette interpolation on a suivi la méthodologie de Dieulin et al., 2006. D'abord on a intersecté le maillage de 0.25° par 0.25° sur toute notre zone d'étude avec les polygones de capacité de rétention en eau, comme le montre la Figure II-14. Sur cette carte, nous pondérons les valeurs Smax, Smoy, Smin en multipliant la valeur de ces champs respectifs par la valeur de surface de chaque polygone à l'intérieur de la maille. Nous obtenons ainsi la valeur pondérée pour chacun de ces champs qui deviennent Smaxp, Smoyp et Sminp, valeurs que nous additionnons par maille pour n'obtenir qu'une seule valeur de capacité de rétention en eau par quart de degré carré.

Enfin pour notre étude, on a développé les grilles suivantes avec une résolution de 0.25° par 0.25°: une grille pour la précipitation, une grille pour l'évapotranspiration et 3 grilles pour la capacité de rétention en eau à partir des données FAO (Maximum, Moyenne et Minimum).

2.6 Conclusions

Les basins des rios Ucayali et Huallaga présentent deux régions caractéristiques : les Andes et la plaine amazonienne. Les Andes se caractérisent par ses altitudes élevées, des bassins à fortes pentes, et des vallées profondes (canyons) dans lesquelles les fleuves andins s'écoulent, tandis que la plaine amazonienne se caractérise par des pentes faibles qui contribuent à l'écoulement fluvial sous forme de méandres. Aussi la géologie, la végétation et les sols sont différenciés entre ces deux régions.

La plupart de la population sur notre zone d'étude vit dans des conditions de pauvreté, et sont ainsi très vulnérables aux événements hydrologiques exceptionnels, ce qui rend cette étude

importante, car elle permet d'acquérir des connaissances sur les effets possibles du changement climatique sur les régimes hydrologiques de la région.

La différence contrastée entre les Andes et la plaine amazonienne génère des valeurs particulières de pluviométrie, car ces valeurs sont très différentes d'une région à l'autre, avec des pluies intenses localisées surtout dans la zone de transition des Andes vers la Forêt (zones de piedmont).

Pour la première fois une étude sur la comparaison entre méthodes empiriques de calcul de l'évapotranspiration a été réalisée en prenant comme base la méthode de FAO Penmann-Monteith. Nos résultats montrent que l'équation d'Hargreaves peut être appliquée, et qu'un recalage à la place de l'équation de FAO Penmann-Monteith est nécessaire sur notre zone d'étude. Spatialement les valeurs de l'évapotranspiration se distribuent en fonction de l'altitude, c'est-à-dire qu'il y a plus d'évapotranspiration dans la forêt que dans les Andes.

Une banque de données unique qui se résume à la constitution de grilles de pluie (1), d'évapotranspiration (1) et de capacité de rétention en eau des sols (3) à été développée pour la première fois sur le versant de l'Amazone au Pérou (bassins des rios Ucayali et Huallaga). Ce travail a requis presque 50% du temps de la réalisation de cette thèse.

Grâce à la méthodologie de transformation de données de sols FAO en capacité de rétention en eau des sols, nous pensons diminuer les variables d'entrée dans le modèle de bilan hydrique.

Les données hydrologiques rassemblées pour notre étude ne sont pas nombreuses et ne concernent que sept (7) stations hydrométriques, les uniques stations existantes. Au début de la thèse, seules les données de la station de Requena sur le fleuve Ucayali était disponibles, alors qu'à l'issue de ce premier travail, nous disposons maintenant de séries temporelles sur 7 bassins, ce qui est déjà un grand succès.

CHAPITRE 3

Variabilité hydroclimatique sur les bassins des rios Ucayali et Huallaga

III. CHAPITRE 3 .Variabilité hydroclimatique sur les bassins des rios Ucayali et Huallaga

Connaître la variabilité hydroclimatique en terme de tendances, ruptures et connexions avec indices océan-atmosphériques sur les bassins des rios Ucayali et Huallaga constitue le premier pas vers une compréhension plus fine du comportement hydrologique. La variabilité hydroclimatique du bassin de l'Amazone a été largement étudiée, néanmoins ces études sont centrées surtout au Brésil, c'est-à-dire dans les régions de la plaine amazonienne tandis que les pays Andins (Equateur, Pérou, Colombie et Bolivie) restent peu étudiés. Dans le cadre du programme HYBAM, les études récentes développées par Espinoza et al. (2008a ; 2008b) ont permis de mieux expliquer la variabilité spatio-temporelle des pluies et des débits, en particulier pour les régions Andines.

Dans ce chapitre, nous évaluons la variabilité des pluies, des températures et de l'évapotranspiration en prenant en considération les deux régions caractéristiques qui existent sur les deux bassins : Les Andes et la plaine amazonienne. Cette section est présentée sous la forme d'un article scientifique en révision pour « International Journal of Climatology ».

3.1 Recent trends in rainfall, temperature and evapotranspiration in the Peruvian Amazonas-Andes basin: Huallaga and Ucayali basins.

WALDO SVEN LAVADO CASIMIRO, DAVID LABAT, JEAN LOUP GUYOT, JOSYANE RONCHAIL, JHAN CARLO ESPINOZA, & JUAN JULIO ORDOÑEZ

RÉSUMÉ

L'hydroclimatologie du bassin Amazonien des Andes péruviennes, qui englobe environ 10% du bassin amazonien est encore mal documentée. Dans cette contribution, les évolutions temporelles des précipitations mensuelles (R), de la température moyenne (Tmean), de la température maximale (Tmax), de la température minimum (Tmin) et de l'évapotranspiration (Ev) estimée sur deux bassins péruviens (Rios Huallaga et Ucayali) sont analysées en identifiant en particulier les tendances sur les quarante dernières années. L'analyse de la base de données qui comprend 77 stations météorologiques pour la période 1965-2007 est réalisée en distinguant la région montagneuse des Andes, de la Forêt en plaine amazonienne (en-dessous de 500 m d'altitude).

Notre étude se focalisera tout d'abord sur les séries chronologiques météorologiques annuelles, et sur les moyennes saisonnières, par application des tests de Mann-Kendall et Bravais-Pearson pour la détection de tendances, et du test de Pettitt pour quantifier les ruptures de moyenne.

Il a été mis en évidence une tendance positive (statistiquement significative) pour les températures moyennes annuelles (+0.09°C par décennie) pour la région globale (en incluant les deux bassins) avec des valeurs identiques dans les Andes et la Forêt de la plaine amazonienne. Cette valeur est plus élevée que le réchauffement global moyen au cours des 100 dernières années (estimé à environ +0.07 °C par décennie). Un pourcentage important des stations caractérisées par des tendances significativement positives de Tmean est situé dans les Andes. Les ruptures de moyenne se sont produites plus tôt dans les séries Tmax (pendant

les années 70) que dans les séries Tmin (pendant les années 80). Ils coïncident avec un changement important dans la fréquence de « El Niño » dans l'océan. Des résultats similaires sont acquis en utilisant les données d'évapotranspiration.

Toutefois, un nombre restreint de séries pluviométriques présentent des tendances significatives. Les séries de précipitations sont caractérisées par une variabilité pluriannuelle, avec des ruptures importantes au début des années 1980 et au milieu des années 1990, qui coïncident avec les changements à long terme des températures de surface de la mer (TSM) des océans Pacifique et Atlantique tropicaux. Plus précisément, les corrélations les plus fortes concernent les séries annuelles et les séries moyennées sur les périodes été et automne mesurées sur le sud des Andes et la TSM sur l'Océan Atlantique tropical. On observe des résultats opposés dans les séries pluviométriques mesurées dans les zones des Andes et dans la Forêt de la plaine amazonienne.

ABSTRACT

The hydroclimatology of the Peruvian Amazon-Andes basin that corresponds to about 10% of the Amazonian basin is still poorly documented. In this contribution, the temporal evolution of monthly rainfall (R), mean temperature (Tmean), maximum temperature (Tmax), minimum temperature (Tmin) and evapotranspiration (Ev) series over two Peruvian Amazon-Andes basins (Huallaga and Ucayali) are analyzed in term of trends over the last forty years. The analysis of the extended database that includes 77 weather stations in the 1965-2007 period is realized distinguishing the Andes and Rainforest (below 500 m a.s.l.) regions.

We focus our attention on both annual and seasonal means meteorological time series, applying Mann-Kendall and Bravais-Pearson for trend detection and Pettitt test for mean-change estimations.

Positive significant trend in Tmean (+0.09°C per decade) has been calculated in the Global region (both regions) with similar values in the Andes and Rainforest. This value is higher than the mean global warming that is about +0.07 °C per decade over the last 100 years. A major percentage of stations with significant Tmean positive trends is located in the Andes. Main changes occurred earlier in Tmax (during the 1970s) than in Tmin (during the 1980s). They coincide with a major change in El Nino frequency in the Pacific Ocean and this is consistent with the relationship between the SOI index and Tmean, especially observed in the Northern Andes. Similar results are acquired using evapotranspiration data.

Very few stations exhibit significant rainfall trends as rainfall fluctuates at pluriannual time scales, with important changes at the beginning of the eighties and the mid nineties that coincide with long term changes in the tropical Pacific and Atlantic oceans SST. Opposite features are observed in the Andes and in the lowlands. More, the stronger correlations are found between the southern Andes annual, summer and autumn rainfall and the SST in the tropical Atlantic Ocean.

Key words: Amazon basin, hydroclimatology, trend, climatic change, Peru.

INTRODUCTION

In the 4th report of the Intergovernmental Panel on Climate Change (IPCC) (Trenberth et al., 2007) describe a rate of warming over the last 50 years that is almost the double when compared to the last 100 years (0.13°C ± 0.03°C vs. 0.07°C ± 0.02°C per decade), and also downward trends in rainfall over the tropics since the 1970s. Our contribution concentrate upon the recent climate changes over the Peruvian Amazon-Andes basin (PAB). Previous

studies on rainfall, temperatures and evapotranspiration trends on the Amazon basin mainly focus on Brazilian zone (see e.g. Marengo et al., 1998b; Costa et Foley, 1999; Marengo, 2004 among others) while few studies are dedicated to the PAB region. More, they are usually restricted to the identification of trends in rainfall and temperature time series whereas evapotranspiration time series fluctuations over the PAB region remain poorly documented. Gentry et Lopez-Parodi (1980) identify significant decrease differences in 3 out of 8 PAB weather stations datasets during the 1970-1978 period (compared to the 1961-1969 reference period) and associate these differences with deforestation. Their results are then discussed by Nordin et al.(1982). More recently, Vuille et Bradley (2000) show a warming trend of 0.10–0.11 °C per decade between 1939 and 1998 and of 0.32–0.34 °C per decade between 1974 and 1998 i.e. a tripling of the warming rate over the last 25 years. Vuille et al.(2003) based on CRU data (New et al., 2000), ECHAM-4 model simulations and data collected over the 1950-1994 period put in evidence a non-significant rainfall trend over the PAB region (but with slight increasing trend over northern Peru between 5° and 11°S and a slight decreasing trend in precipitation over southern Peru). Also, the temperature time series indicate an average warming around 0.09–0.15 °C per decade for the 1950-1994 period with an intensification of the warming over the 1975-1994 period.

Considering the high mountains zone of Ucayali basin (i.e. the Mantaro basin), IGP (2005) outlines a downward rainfall trend of 3% per decade over the 1964-2003 period, a positive trend of 0.2°C per decade for maximum temperature and no trend for minimum temperature using the 1965-2002 period data, leading to similar conclusions than Vuille et Bradley (2000).

More recently and restrained to the specified region of study, Espinoza *et al.*(2006b) described a 0.83% per year downward trend in mean rainfall over the 1970-1997 period in the Peruvian-Ecuadorian Amazon basin. Consistently, Haylock et al.(2006) identify a downward trend in annual precipitation in one meteorological station located in the Ucayali basin in the 1960-2000 period.

Annual precipitation is likely to decrease in the southern Andes (Trenberth et al., 2007). Although, changes in atmospheric circulation may induce large local variability in precipitation response in mountainous areas over the Amazon basin; that is why annual and seasonal mean rainfall changes remain under debate.

Recently the collaboration of HYBAM program (www.ore-hybam.org) with the Hydrometeorological services of the Andeans countries have made possible for the first time the development of an extended on-site climatological data bank already documented by Espinoza et al.(2008). That is why this study follows two objectives. The first part of the study is devoted to the time-space analysis of rainfall, temperatures and evapotranspiration time series and spatial distribution over the Huallaga and Ucayali basin, in order to identify mean-changes or trends. In the second part, one main process that can be related to these changes is examined: Climatic forcing fluctuations such as ENSO in the Pacific Ocean and Sea Surface Temperature in the Atlantic Ocean, that explain temperature and rainfall in many regions of tropical South America (Aceituno, 1988; Marengo, 1992 and more recently Ronchail et al., 2002 and Marengo et Camargo, 2008).

STUDY AREA CLIMATOLOGY (RAINFALL, TEMPERATURE AND EVAPOTRANSPIRATION)

Huallaga basin (with 75% of its total area in the Andes region and 25% in the Rainforest region) and Ucayali basin (with 50% of its total area in the Andes region and 50% in the Rainforest region) are part of the Amazonas basin and they are totally within Peru. Basins

areas are 89654 km^2 and 350287 km^2, respectively (Fig. 1a), both representing 10% of the Amazon basin. The PAB basin is located in the western zone of the Amazonas basin where two regions can be distinguished topographically: the Andes (~ over 500 m a.s.l.) and the Rainforest (~ below 500 m a.s.l.). The Andes region includes some of the steepest and tallest mountain ranges on earth whereas the Rainforest region is constituted by relatively flat lowland plains. Nowhere in the world such dramatic environmental contrasts lie close together with hot tropical lowlands near sea level versus freezing cold tropical high mountain peaks up to 6000 m a.s.l. of elevation. Naturally, each of these two regions is subject to different, but in many aspects interrelated, sets of physical, geochemical and biologic parameters (ACTO, 2005).

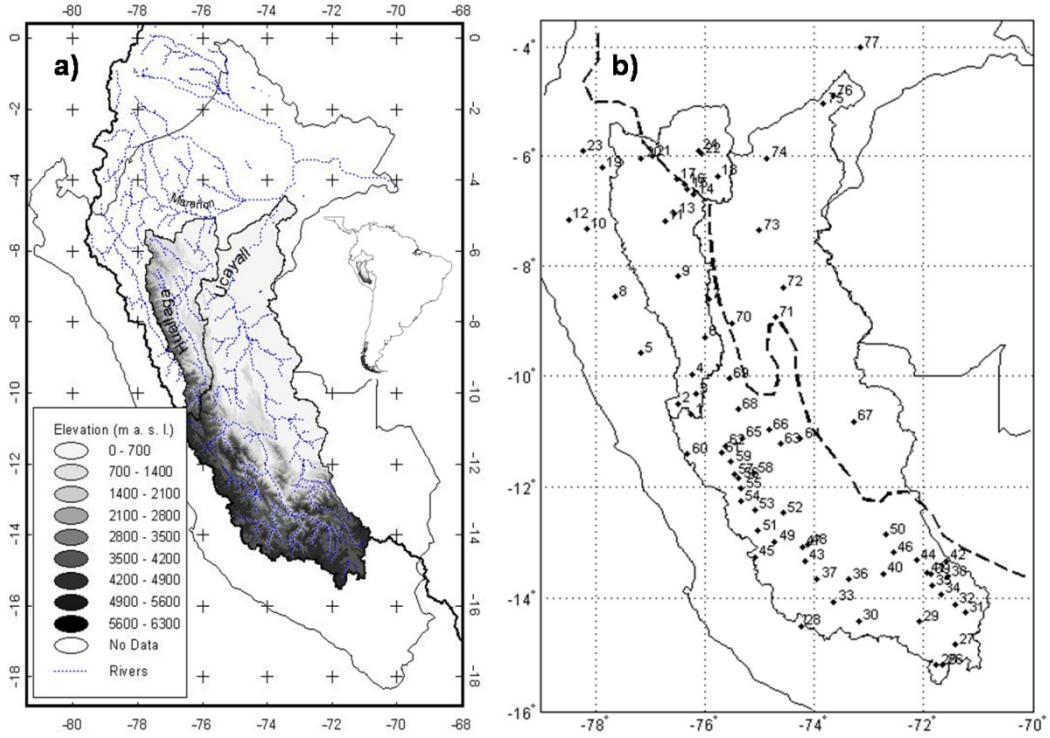

Figure 1. a). Localization and elevation of the region under study, left: Huallaga basin and right: Ucayali basin. b). Localization of the weather stations with number corresponding to codes given in the Table 1. The Ucayali and Huallaga basins are separated by a plain line. The Andes and Rainforest regions are limited by a black dashed line.

According to UNESCO (2006) mean annual rainfall over the PAB region in the 1969-1999 period is estimated to nearly 2060 mm/year. Moreover, very high and low rainfall values (between 6000 and 250 mm/year) can be observed in close stations due to the leeward or windward position of stations (Espinoza et al., 2008). Maximal rainfall rates occur between November and March. Considering the high Andes region, most of the rainfall is produced by convection (Garreaud et al., 2003). The moisture supply for this convection is predominantly the Atlantic and the Amazon basin (Fuenzalida et Rutllant, 1987; Vuille et al., 1998; Chaffaut et al., 1998; Garreaud, 1999; Garreaud et al., 2003; Vizy et Cook, 2007). According to Vuille et al. (2003), the climate in the tropical Andes is closely related to SST in the central equatorial Pacific on interannual time scales, with rainfall and temperature showing distinct departures from mean during El Niño and La Niña events. Thus, interannual rainfall variability over the Amazon basin depends in some measure on ENSO (Aceituno, 1988; Liebmann et Marengo, 2001; Ronchail et al., 2002; Espinoza et al., 2008 among others). In the Southern zone of the PAB region, rainfall rates are below normal during El Niño event (Aceituno, 1988; Tapley et Waylen, 1990; Rome-Gaspaldy et Ronchail, 1998; Vuille et al., 2000; Espinoza et al., 2008) whereas no clear signal is exhibited during La Niña events. In the center and northern zone of the PAB region rainfall variability is not associated with ENSO

(Tapley et Waylen, 1990; Rome-Gaspaldy et Ronchail, 1998; Kane, 2000; IGP, 2005; Espinoza et al., 2008).

Mean annual temperature fluctuations over the PAB region appear indirectly related to elevation (lower altitude leading to higher temperature). Higher seasonal amplitude of mean temperature is observed over the highland in the Andes cordillera than over the Rainforest region. Mean annual temperature over the PAB region considering the 1969-1999 period is estimated around 23 °C with ranges of temperature from 6 °C to 19°C between 500 to 6 780 m a.s.l. (highlands) and from 19 °C to 30°C between 400 to 1 000 m a.s.l. (lowlands) (UNESCO, 2006).

Marengo (2006), reported many state-of-the-art works to compute evapotranspiration using reanalysis global climate model outputs, climatologic model, evapotranspiration models and some direct measurements, which in summary give an average evapotranspiration rate over the Amazon basin around 3.8 mm day-1 Soil types play a crucial role in the evapotranspiration variability. Over the middle altitude land and highland (in the Andes mountain) where lithosols predominate, evapotranspiration is less than over the Rainforest (Viera, 1975b). Using Thornthwaite method (Thornthwaite, 1948a) evapotranspiration is estimated around 1343 mm/year (~3.7 mm per day) over the PAB region (UNESCO, 2006).

DATA AVAILABILITY

Basins subdivision is based on the Digital Elevation Model (DEM) provided by the National Aeronautics and Space Administration (NASA) through the Shuttle Radar Topography Mission (SRTM - www2.jpl.nasa.gov/srtm). SRTM data is available at 3 arc second (~ 90m resolution). A detailed description of this DEM can be found in Farr et al.(2007).

Weather stations used in this work are part of the Peruvian National Meteorology and Hydrology Service, SENAMHI (www.senamhi.gob.pe) network. 77 weather stations are used in this study: 58 stations with rainfall data and 48 stations with temperature data. 24 stations are located in the Huallaga basin and 53 in the Ucayali basin. Since both basins are characterized by highly heterogeneous climatic conditions, the forthcoming analysis is based on the distinction between Andes and Rainforest regions and not in term of hydrographic basins. It must be noted that stations located over Andes region are more numerous (45 stations with rainfall data and 37 stations with temperatures data) than over Rainforest region (37 stations with rainfall data and 11 stations with temperatures data) (Table 1).

Table 1. Characteristics of the stations: Name, Code reported in figure 1b, Geographical location, basin and measured variables at the weather stations. R: Rainfall; T: Temperature.

Weather Station	Code	Latitud (°S)	Longitud (°W)	Altitud (m a.s.l.)	Basin	Variable
Cerro De Pasco	1	-10.694	-76.254	4260	Huallaga	R
Yanahuanca	2	-10.491	-76.508	3170	Huallaga	R
San Rafael	3	-10.322	-76.169	2600	Huallaga	R,T
Huanuco Cayhuayna	4	-9.966	-76.237	1947	Huallaga	R,T
Chavin	5	-9.586	-77.176	3160	Huallaga	R
Tingo Maria	6	-9.288	-76.000	686	Huallaga	R,T
Aucayacu	7	-8.600	-75.934	600	Huallaga	R
Sihuas	8	-8.567	-77.650	2716	Huallaga	R
Tocache	9	-8.184	-76.500	508	Huallaga	R,T
San Marcos	10	-7.322	-78.169	3200	Huallaga	R
Juanjui	11	-7.175	-76.734	280	Huallaga	R,T
Augusto Weberbauer	12	-7.152	-78.491	2536	Huallaga	R
Bellavista	13	-7.051	-76.559	247	Huallaga	R,T
Sauce	14	-6.694	-76.203	620	Huallaga	R
El Porvenir	15	-6.593	-76.322	230	Huallaga	R,T
Tarapoto	16	-6.513	-76.372	282	Huallaga	T

Lamas	17	-6.424	-76.525	920	Huallaga	R,T
Navarro	18	-6.356	-75.779	190	Huallaga	R
Chachapoyas	19	-6.203	-77.881	2490	Huallaga	T
Rioja	20	-6.034	-77.169	880	Huallaga	T
Moyobamba	21	-6.000	-76.967	860	Huallaga	R,T
San Ramon	22	-5.949	-76.085	184	Huallaga	R
Jamalca	23	-5.898	-78.237	1200	Huallaga	R
Yurimaguas	24	-5.894	-76.118	187	Huallaga	R,T
Caylloma	25	-15.184	-71.767	4420	Ucayali	T
La Angostura	26	-15.180	-71.649	4150	Ucayali	R,T
Yauri	27	-14.817	-71.417	3927	Ucayali	R
Pampahuasi	28	-14.484	-74.250	3650	Ucayali	R
Santo Tomas	29	-14.399	-72.089	3253	Ucayali	R
Chalhuanca	30	-14.393	-73.179	3358	Ucayali	R
Sicuani	31	-14.254	-71.237	3574	Ucayali	R,T
Combapata	32	-14.100	-71.433	3464	Ucayali	T
Paucaray	33	-14.051	-73.644	3250	Ucayali	R
Acomayo	34	-13.917	-71.684	3160	Ucayali	R,T
Paruro	35	-13.768	-71.845	3084	Ucayali	T
Andahuaylas	36	-13.657	-73.371	2866	Ucayali	R,T
Vilcashuaman	37	-13.644	-73.949	3590	Ucayali	R
Ccatcca	38	-13.610	-71.560	3729	Ucayali	T
Granja Kcayra	39	-13.557	-71.875	2360	Ucayali	R,T
Curahuasi	40	-13.553	-72.735	2763	Ucayali	R,T
Cusco	41	-13.537	-71.944	3399	Ucayali	T
Paucartambo	42	-13.324	-71.591	3042	Ucayali	R,T
San Rafael	43	-13.321	-74.169	2600	Ucayali	R
Urubamba	44	-13.311	-72.124	2863	Ucayali	R,T
Tunel Cero	45	-13.254	-75.085	4700	Ucayali	R
Machu Picchu	46	-13.167	-72.546	2563	Ucayali	R,T
Wayllapampa	47	-13.068	-74.220	2500	Ucayali	T
La Quinua	48	-13.034	-74.135	3232	Ucayali	R,T
Lircay	49	-12.983	-74.729	3150	Ucayali	R,T
Quillabamba	50	-12.856	-72.692	990	Ucayali	R,T
Huancavelica	51	-12.779	-75.034	3676	Ucayali	T
Paucarbamba	52	-12.467	-74.567	3000	Ucayali	R
Pilchaca	53	-12.406	-75.085	3570	Ucayali	T
Laive	54	-12.252	-75.355	3990	Ucayali	R,T
Huayao	55	-12.034	-75.339	3308	Ucayali	R,T
San Lorenzo	56	-11.850	-75.384	300	Ucayali	T
Jauja	57	-11.779	-75.474	3322	Ucayali	R,T
Comas	58	-11.745	-75.118	3300	Ucayali	R
Ricran	59	-11.542	-75.525	3500	Ucayali	R
Marcapomacocha	60	-11.405	-76.325	4479	Ucayali	R,T
Tarma	61	-11.389	-75.695	3000	Ucayali	T
Huasahuasi	62	-11.254	-75.627	2737	Ucayali	R
Satipo	63	-11.220	-74.627	607	Ucayali	R
Puerto Ocopa	64	-11.136	-74.254	788	Ucayali	T
San Ramon	65	-11.117	-75.334	904	Ucayali	T
Pichanaky	66	-10.966	-74.830	547	Ucayali	R
Sepa	67	-10.817	-73.284	307	Ucayali	R
Oxapampa	68	-10.593	-75.390	1814	Ucayali	T
Pozuzo	69	-10.051	-75.559	798	Ucayali	T
Aguaytia	70	-9.034	-75.508	338	Ucayali	R
Tournavista	71	-8.932	-74.711	185	Ucayali	R,T
Pucallpa	72	-8.384	-74.576	160	Ucayali	R,T
Contamana	73	-7.353	-75.006	185	Ucayali	R,T
Juancito	74	-6.034	-74.867	150	Ucayali	R,T
Requena	75	-5.043	-73.836	128	Ucayali	R,T
Genaro Herrera	76	-4.900	-73.650	132	Ucayali	R
Tamshiyacu	77	-4.003	-73.161	141	Ucayali	R

Fig. 1b shows the spatial distribution of stations over the PAB region. Stations are rather scarce in the Huallaga basin and in the lowlands of the Ucayali basin (10 stations out of 53). On the contrary, the Andean region of the Ucayali basin is well documented. Rainfall (R) and temperature data (mean (Tmean), maximum (Tmax) and minimum (Tmin)) are available at

monthly time scale from January 1965 to December 2007. A procedure for quality analysis in temperature data is first applied. After a visual detection of suspect outliers in monthly plots, box plots graphics are computed for the suspect month; doubtful temperature values are those that exceed the third quartile plus three times the interquartile range. Suspect outliers values are compared to values of the corresponding period in nearby stations (over similar physiographic zone). The data is discarded only if a mismatch is detected through both criteria. Gaps were filled up by a multiple correlation method between nearby geographical stations.

Rainfall data over the 1965-2003 period are also validated using the Regional Vector Method – RVM (Hiez, 1977 and Brunet-Moret, 1979) : four homogeneous regions with similar interannual variability are found over Ucayali and Huallaga basin (Espinoza et al., 2008).

The lack of meteorological data (e.g. solar radiation, wind speed, daylight hours) over PAB does not allow using the classical FAO Penman-Monteith method (Allen et al., 1998) to estimate evapotranspiration (Ev). Then, Hargreaves-Samani (HE) method (Hargreaves et Samani, 1985) is used here as an alternative one to compute reference evapotranspiration. HE Ev is given by:

$$HE = \frac{0.0023(T + 17.8)(T\max - T\min)^{0.5} Ra}{\lambda} \quad (1)$$

Where HE stands for Ev (mm per day), λ stands for the latent heat of vaporization (MJ kg^{-1}), T for Tmean (°C), Tmax for maximum temperature (°C), Tmin for minimum temperature (°C). Ra that stands for extraterrestrial radiation (MJ m^{-2} d^{-1}) is computed following Allen et al.(1998) method . One notes that λ in this study is assumed as 2.45 MJ Kg^{-1} as suggested by Allen et al.(1998).

Interpolation of climatic variables in this study was made using Thiessen method through Hydraccess software (Vauchel, 2005b). The different distribution of climatic stations in the Andes (more stations) and the Rainforest (less station) may produce some over and under estimations when we work with specifics zones (areas) but these results are clarified when we work a station scale.

METHODOLOGY

According to Robson et al. (2000), three types of assumptions over the form of the distribution, the seasonality of the distribution and the independence of the variables are commonly made when carrying out statistical tests and these assumptions are used taken into account in this study. Three statistical tests are used in this work to identify spatio-temporal fluctuations in climates series:

(1) The Bravais-Pearson correlation (parametric trend test) to analyze the linear trend.

(2) The Mann-Kendall non parametric trend test (Mann, 1945 and Kendall, 1975b). Burn & Elnur (2002), consider this test as the most commonly used for detecting trend in climatic variables.

(3) A Pettitt non-parametric test (Pettitt, 1979) for mean-change detection in temporal series.

For all these tests, the significance level (α) is the probability that a test detects non-null trend or mean-changes when none is present (Robson et al., 2000). Null hypothesis in statistical tests for this study is rejected using α equal 0.05 (i.e. statistically significant at 95% level).

Temporal series are averaged over five periods: the year (January to December), Summer (December to February), Autumn (Mars to May), Winter (Jun to August) and Spring (September to November). Main climate values are shown in Table 2. Seasonal rainfall rate values in the whole region of study, with respect to annual rainfall, are around 38%, 28%, 11%, and 24% in summer, autumn, winter and spring temporal series, respectively. These values reflect two regimes that coexist over Huallaga and Ucayali basins (Espinoza et al., 2008). The first one is a south tropical regime with a dry season from May to September and a wet season from December to March and the second is an intermediate regime between southern Tropics and the equator that features a very rainy period from January to April and a drier one from June to October. Variations between summer and winter mean values are 1.7°C, 0.1°C, 3.5°C and 0.8 mm day^{-1} when considering Tmean, Tmax, Tmin and Ev respectively. The very low thermal amplitude characterizes tropical regions.

In order to explain the temporal patterns resulting from the analysis of R, temperatures and Ev, several regional climatic indexes were used. The Southern Oscillation Index (SOI) is the standardized pressure difference between Tahiti and Darwing. SST data at monthly scale (1965–2007) are provided for the northern tropical Atlantic (NATL, 5–20°N, 60–30 °W) and the southern tropical Atlantic (SATL, 0–20 °S, 30 °W–10 °E). The difference between the NATL and SATL is computed to feature the SST gradient in this oceanic basin. Indexes are from the Climatic Prediction Centre of the National Oceanic and Atmospheric Administration (CPC-NOAA: http://www.cdc.noaa.gov/).

Table 2. Mean (1965-2007) seasonal climate values for the entire zone, the Andes region (under 500 m a.s.l.) and the Rainforest region (above 500 m a.s.l.).Max. Tem.: Maximum Temperature; Min. Tem.: Minimum Temperature; Mean. Tem.: Mean Temperature; Evp: Evapotranspiration

		Rainfall (mm)	Mean Tem. (°C)	Max. Tem. (°C)	Min. Tem. (°C)	Evp (mm/day)
Total	Anual	1296.2	17.6	24.1	11.1	4.2
	Summer	490.7	18.2	23.9	12.5	4.4
	Autumn	357.3	17.7	23.9	11.5	3.9
	Winter	138.5	16.5	23.9	9.0	3.7
	Spring	309.7	18.1	24.8	11.4	4.6
Andes	Anual	1024.9	15.2	22.0	8.4	3.9
	Summer	427.4	15.9	21.6	10.1	4.2
	Autumn	275.6	15.3	21.7	8.8	3.7
	Winter	86.9	13.9	21.8	6.0	3.4
	Spring	235.0	15.8	22.7	8.8	4.4
Rainforest	Anual	2235.3	25.7	31.4	20.1	4.9
	Summer	709.7	26.0	31.4	20.6	5.2
	Autumn	640.0	25.7	31.0	20.4	4.6
	Winter	317.4	25.1	31.1	19.1	4.4
	Spring	568.3	26.1	32.0	20.2	5.3

FLUCTUATIONS IN THE WHOLE PAB REGION

Spatial distributions of mean annual R, temperatures and Ev are shown in Fig. 2. R rates exhibit no linear elevation-dependent pattern. Thought, little rainfall is observed over high terrains while very different rainfall rates are observed at low altitude, in accordance with

Espinoza et al. (2008). Temperatures time series appear in fair relationship with elevation while Ev time series seem with majors values in the lowlands (Rainforest) and with variable values in the Andes, but on average with minor values than in the Rainforest. Therefore, Tmean which ranges from 0°C to 30°C decreases with altitude by - 0.48°C per 100 m, Tmax (from 10°C to 35°C) by about -0.42°C per 100 m and Tmin (from -10°C to 25°C) by roughly -0.54°C per 100 m. Ev which ranges from 2 mm day^{-1} to 5.5 mm day^{-1} decreases along altitude ~ -0.04 mm day^{-1} per 100 m. As expected in tropical regions, the annual amplitude between summer and winter temperature is very low while the daily amplitude is higher. Between summer and winter, the temperature difference is nearly null during daytime and higher during nigh time, with greater values in the Andes (4°C) than in the lowlands (1.5°C). The amplitude between day and night is stronger in the Andes (14.4°C when considering Tmean) than in the lowlands (11.3°C). More, in each region, it is higher during winter than during summer. In all cases, these results are consistent with less cloud cover density 1) in the Andes than in the lowlands, 2) in winter than in summer, 3) during night than during daytime.

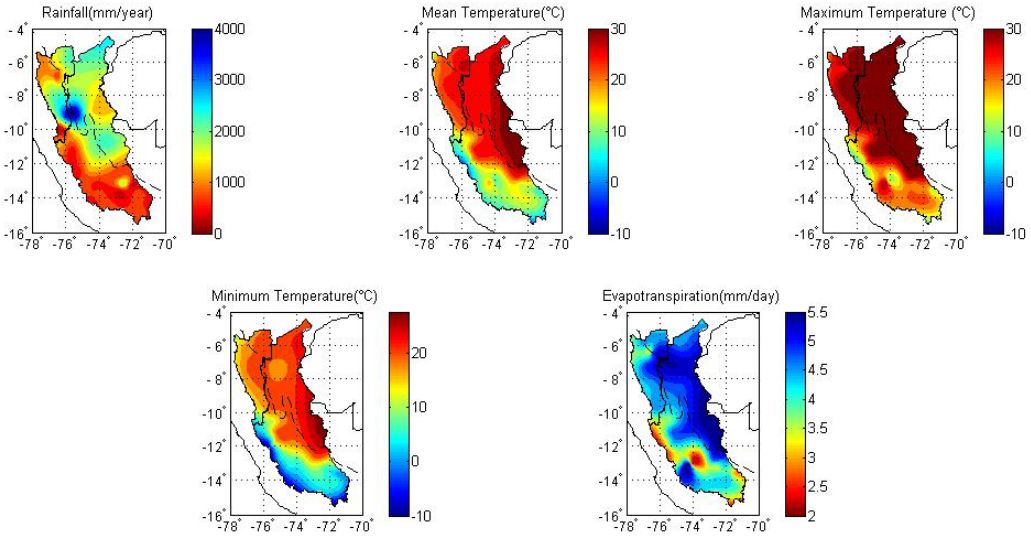

Figure 2. Mean (1965-2007) values of climate variables in Huallaga and Ucayali basins. The Andes and Rainforest region are limited by black dashed line. The Huallaga and the Ucayali basins are separated by a dark plain line. The Andes and Rainforest regions are limited by a black dashed line.

Three regions were considered for trend analysis: the Global zone of study, the Andes region (over 500 m a.s.l.) and the Rainforest region (below 500 m a.s.l.). Trends per decade, considering the 1965-2007 period, were calculated using Bravais-Pearson and Mann-Kendall correlations, using statistical significant level at 0.05 Then, the higher significance level between both methods is considered in the rest of the study. Results are reported in Table 3.
R data show heterogeneous non-significant evolutions (in mm per decade) for the three zones under study: annual, summer and autumn rainfall rates exhibit positive evolution whereas winter and spring rainfall rates exhibit negative evolution.

Annual Tmean data exhibit positive significant trends over the Global region except for the winter series in the Andes region. Trend values of Tmean for annual series (0.9°C per decade) is similar to Vuille et al., 2003. Annual, summer and spring Tmax series exhibit significant trends over Global and Andes regions whereas winter Tmax series shows significant trend only over the Rainforest region. Rainforest region presents significant positive trends for all the temporal Tmin series. The Global region shows significant positive trends for annual, summer and autumn temporal Tmin series whereas Andes region exhibits positive significant trends for annual and summer Tmin series.

Table 3. Rainfall, temperature and evapotranspiration trends (over the 1965-2007 period). Significant trends values (α at 0.05) are with asterisks (**). Values between brackets are years of mean-change using Pettitt method (α at 0.05). Max. Tem.: Maximum Temperature; Min. Tem.: Minimum Temperature; Mean. Tem.: Mean Temperature; Evp: Evapotranspiration.

		Rainfall mm/decade	Mean Tem. °C/decade	Max. Tem. °C/decade	Min. Tem. °C/decade	Evp mm/decade
Total	Annual	8.01	0.09**(1986)	0.11**(1976)	0.07**	4.75
	Summer	10.25	0.10**(1976)	0.12**(1976)	0.09**(1996)	4.45
	Autumn	4.64	0.09**	0.1	0.09**	2.79
	Winter	-2.3	0.07**	0.09	0.05	4.64
	Spring	-4.58	0.08**(1993)	0.12**(1993)	0.04	7.1
Andes	Annual	6.06	0.09**(1986)	0.12**(1976)	0.06**	6.31**
	Summer	7.6	0.11**(1986)	0.15**(1976)	0.08**(1996)	8.38(1976)
	Autumn	3.76	0.10**	0.11	0.09	3.32
	Winter	-2.34	0.06	0.09	0.04	4.53
	Spring	-2.96	0.07**(1993)	0.13**(1993)	0.02	9.00**
Rainforest	Annual	14.74	0.09**(1978)	0.07(1978)	0.11**(1981)	-0.5
	Summer	19.4	0.08**(1976)	0.02	0.15**(1986)	-8.77
	Autumn	7.7	0.08**(1979)	0.08	0.09**(1982)	1.01
	Winter	-2.16	0.09**(1981)	0.11**(1981)	0.08**(1981)	5.04
	Spring	-10.2	0.09**(1981)	0.08(1978)	0.11**(1981)	0.71

Ev fluctuations show mostly positive values except at annual and summer time scales in the Rainforest region (-0.5 and -8.77 mm per decade respectively). In particular, strong positive trends in evapotranspiration are calculated for the year, spring and summer in the Andes region.

Table 3 also shows the years of mean-change using Pettitt test (with a confidence interval α equal to 0.05). Temperatures series exhibit various years of mean-change. The Andes region is characterized by a mean-change around 1986 in Tmean series and around 1976 in Tmax. Rainforest region exhibits, on average, a mean-change at the end of the 1970's in mean, maximum and minimum temperature series.

To verify whether the fluctuations in the climatological variables occurred in recent years or before, we split the time series into three 15-year-long periods, namely: 1965-1980, 1981-1995 and 1996-2007. Average anomalies in these periods are reported in Figure 3 and Table 4.

R data show negative anomalies over the three regions in the 1965-1980 period. However, in the last two periods (1981-1995 and 1996-2007) different anomalies were computed in the Andes region (positive then negative) and in the Rainforest region (negative then positive). During recent years the Global region presents positive anomalies due to the increase highlighted over the Rainforest region (46 mm per year in the 1996-2007 period). Mean, maximum and minimum temperature show in general positive anomalies in the recent years (from 1981 to 2007 except the 1981-1995 period over Andes region), this split concords with mean-change found at the end of 1970's in some temperature series (Table 3).

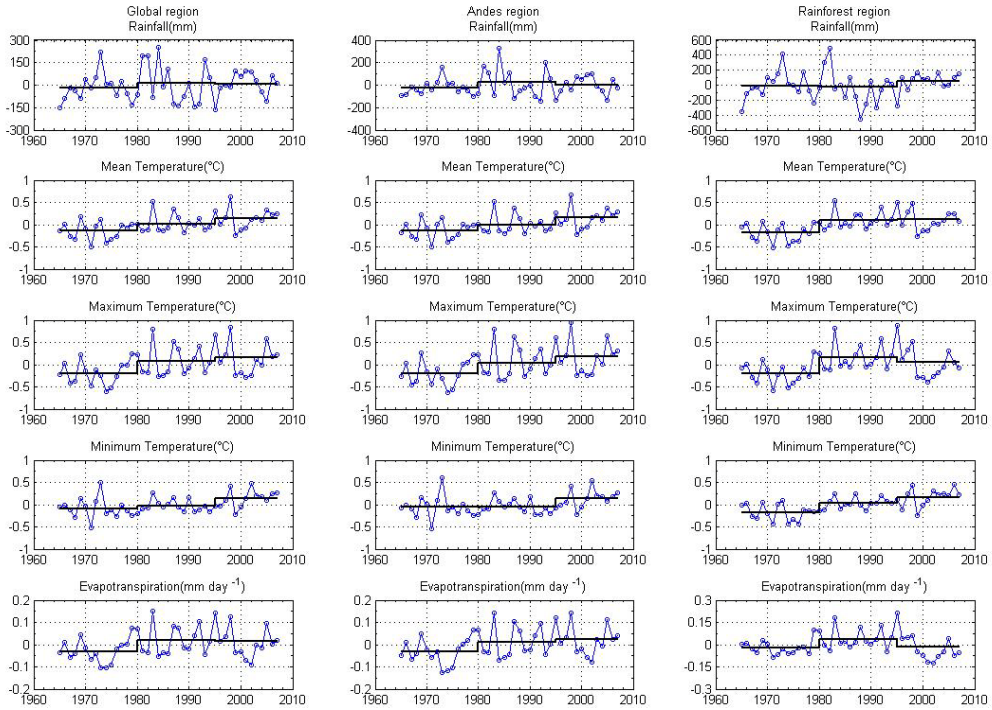

Figure 3. Mean Annual rainfall, mean temperature, minimum and maximum temperature and evapotranspiration anomalies for each period (1965-1980, 1981-1995 and 1996-2007 - stair lines). The left graphics stand for the entire region, the central graphics for the Andes region and the right graphics for the Rainforest region.

Table 4. Estimates of rainfall, temperatures and evapotranspiration anomalies over the three splits periods. Max. Tem.: Maximum Temperature; Min. Tem.: Minimum Temperature; Mean. Tem.: Mean Temperature; Evp: Evapotranspiration. Anomalies were calculated with respect to 1965-2007 period.

	Variables	1965-1980	1981-1995	1996-2007
Total	Rainfall (mm/year)	-20.54	13.93	7.62
	Mean Temp.(°C)	-0.14	0.02	0.14
	Max. Temp.(°C)	-0.20	0.07	0.15
	Min. Temp.(°C)	-0.09	-0.03	0.14
	Evp (mm/day)	-0.03	0.02	0.01
Andes	Rainfall (mm/year)	-23.47	26.50	-3.50
	Mean Temp.(°C)	-0.13	0.00	0.15
	Max. Temp.(°C)	-0.20	0.04	0.18
	Min. Temp.(°C)	-0.06	-0.05	0.13
	Evp (mm/day)	-0.03	0.01	0.02
Rainforest	Rainfall (mm/year)	-10.41	-29.56	46.12
	Mean Temp.(°C)	-0.19	0.09	0.11
	Max. Temp.(°C)	-0.20	0.15	0.05
	Min. Temp.(°C)	-0.18	0.03	0.17
	Evp (mm/day)	-0.02	0.04	-0.02

Ev fluctuations analyzed over the three regions are consistent with R anomalies in the 1965-1980 period. Ev positive anomalies were estimated over the last two periods (from 1981 to 2007) in the Global region and in the Andes. A singular negative anomaly is reported during the 1996-2007 period (-0.02 mm per) for the Rainforest region.

LOCAL TRENDS

Trend analysis is also applied to the 77 stations in order to highlight more localized effects over this region. Bravais-Pearson and Mann-Kendall statistical tests lead to very similar

results. For a given station, the confidence interval corresponds to the highest value of the two tests using $\alpha = 0.05$ for all the climate variables.

Rainfall data analysis

Fig. 4 highlights the spatial distribution of stations with significant positive or negative rainfall trends for the five temporal series (annual, summer, autumn, winter and spring). The percentages of stations with significant trends (positive and negative) for each season and each region are shown in Table 5. Very few stations (7 upon 82 rainfall stations) present significant trends. They may be positive or negative and they are unevenly distributed.

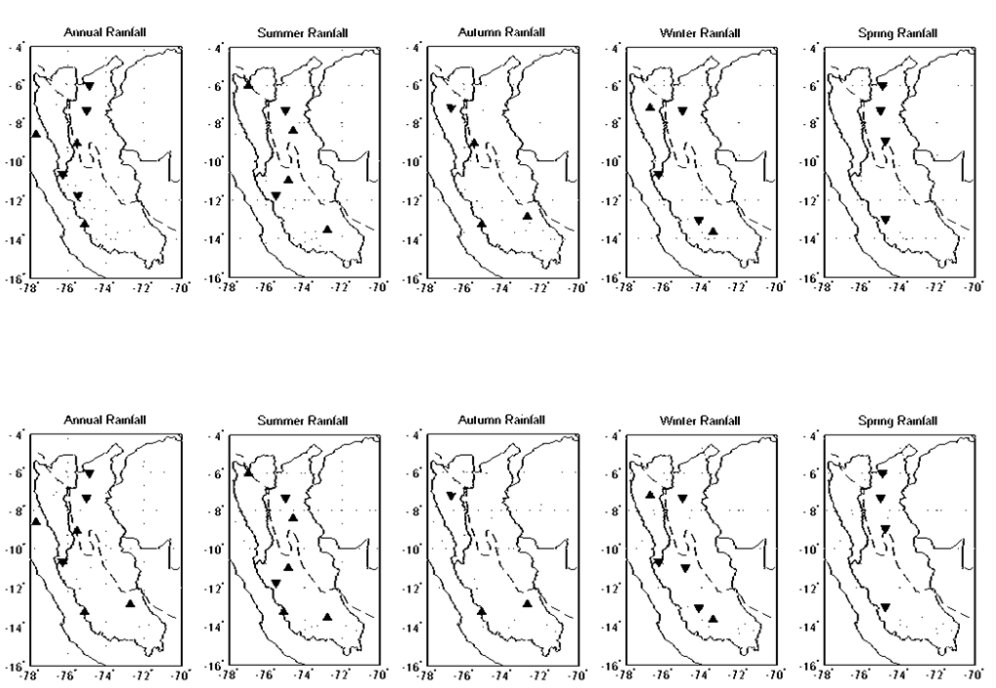

Figure 4. Presence of a local trend in Rainfall for the five period analyzed (annual, summer, autumn, winter and spring) over the 1965-2007 period. Stations with positive significant trend (α equal 0.05) are with an upward triangle and stations with negative significant trend (α equal 0.05) with a downward triangle Top: Bravais-Pearson methodology; Bottom: Mann-Kendall methodology. The Huallaga and the Ucayali basins are separated by a dark plain line. The Andes and Rainforest region are limited by a black dashed line.

Temperature data analysis

The spatial distribution of stations with significant Tmean trends considering mean-annual and seasonal series is depicted in Fig. 5 and Table 5 show that stations with significant Tmean trend are more numerous (about 40 to 50% of the stations) than those with trend in R. Significant trend are mainly positive and they are always located in the Andes region, over the Huallaga and Ucayali basins. The spatial distribution appears as highly similar considering annual-mean and seasonal series. Summer season shows a major percentage of stations with positive trends (until 59% of stations in the Andes region). Few negative trends are observed in winter in the Andes.

Table 5. Percentage of stations with significant trends (Pos.: positive and Neg.: negative), considering rainfall, temperatures and evapotranspiration series (1965- 2007) in the three analyzed regions. Percentages of stations were selected using the higher value of confidence level between Bravais Pearson and Mann-Kendall methods.

	Region	Trend	Annual	Summer	Autumn	Winter	Spring
Rainfall	Global	Pos.	7	10	3	3	2
		Neg.	5	3	2	5	7
	Andes	Pos.	7	11	4	2	2
		Neg.	4	2	0	4	7
	Rainforest	Pos.	8	8	0	8	0
		Neg.	8	8	8	8	8
Mean Temperature	Global	Pos.	48	56	42	40	40
		Neg.	2	0	2	8	4
	Andes	Pos.	49	59	41	38	35
		Neg.	3	0	3	8	5
	Rainforest	Pos.	45	45	45	45	55
		Neg.	0	0	0	0	0
Maximum Temperature	Global	Pos.	35	40	33	31	40
		Neg.	8	6	6	6	6
	Andes	Pos.	35	46	32	24	41
		Neg.	5	3	5	3	5
	Rainforest	Pos.	36	18	36	55	27
		Neg.	18	18	9	18	9
Minimum Temperature	Global	Pos.	38	44	35	23	31
		Neg.	6	6	4	10	6
	Andes	Pos.	32	38	32	22	22
		Neg.	8	8	5	11	8
	Rainforest	Pos.	32	38	32	22	22
		Neg.	8	8	5	11	8
Evapotranspiration	Global	Pos.	29	27	21	29	31
		Neg.	10	10	10	13	6
	Andes	Pos.	30	32	22	19	30
		Neg.	8	5	8	11	3
	Rainforest	Pos.	27	9	18	64	36
		Neg.	18	27	18	18	18

Spatially, stations with significant Tmax trends (α equal at 0.05) are shown in Fig. 6. These stations are located in the same region than previously. However, the percentages of stations with significant positive and negative trends are lower (30 to 40% - see Table 5). Most stations exhibit positive trends, especially in summer, except in the Rainforest region where negative trend are as frequent in summer for instance than positive ones (about 18%).

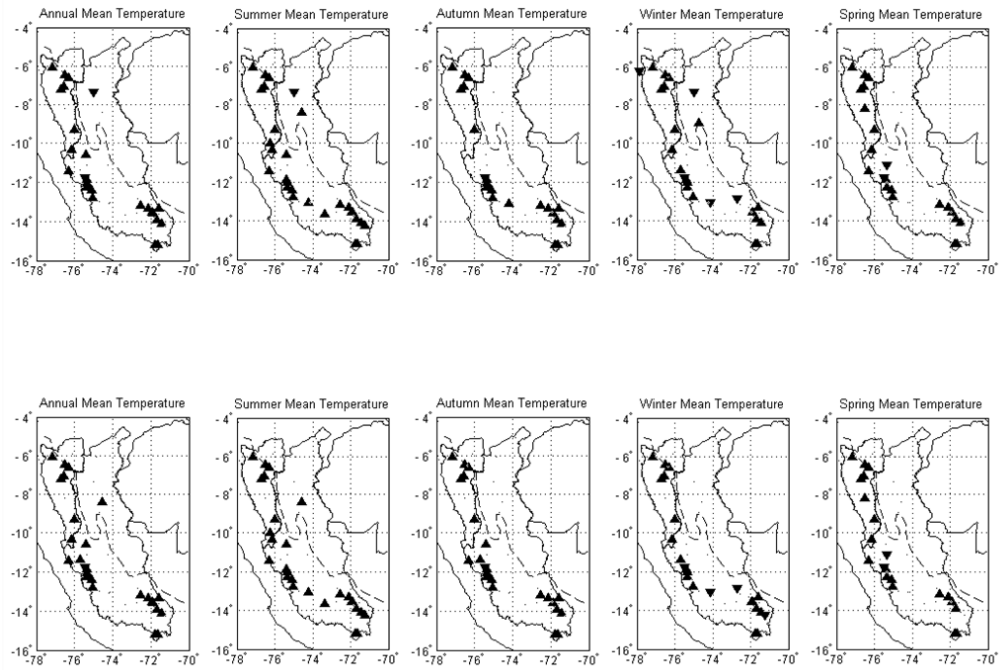

Figure 5. As in Figure 4, but for trends in Mean Temperature.

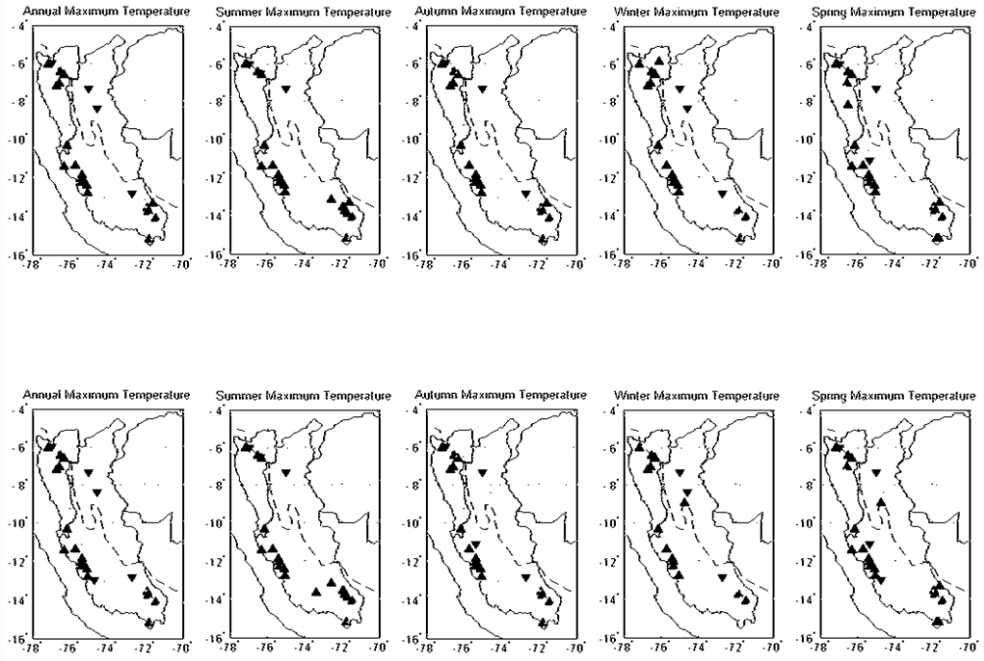

Figure 6. As in Figure 4, but for trends in Maximum Temperature.

Stations with significant Tmin trends are plotted in Fig.7. Most stations with significant trend exhibit an increase in temperature and are located in the Andes region. The percentage of stations with significant trend is higher in summer (around 40%) and lower in winter (20%). Some stations present significant negative trend, especially in winter, in the Ucayali basin.

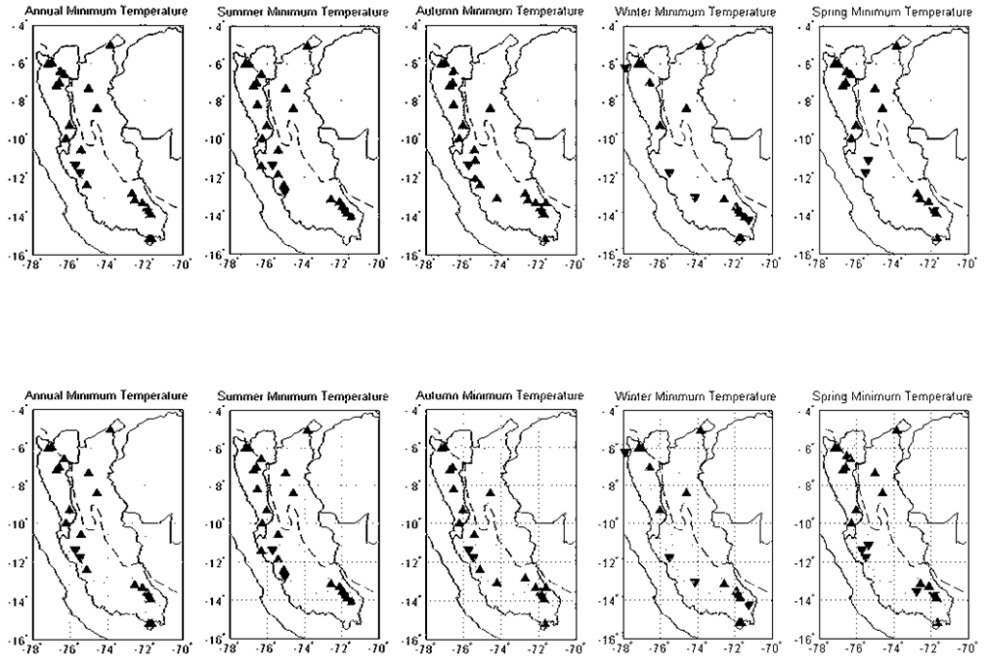

Figure 7. As in Figure 4, but for trends in Minimum Temperature.

Evapotranspiration trend analysis

The spatial distribution of significant positive and negative Ev trends is plotted in Fig. 8. Table 5 shows that about 30% of the stations present significant positive trends in the Global region. In the Andes, positive trends are regularly distributed along the year while they are concentrated in winter and spring in the rainforest. The Rainforest region exhibits singular significant negative trend in two stations over Ucayali basin in all the analyzed temporal series. One recalls that evapotranspiration computation is based on Equation 1 and is directly related with Tmean and Tmax as well as indirectly related with Tmin. Thus, Tmax and Ev series present equal percentage of stations with positive and negative significant trends in the Rainforest region considering summer season. This concordance is also observed spatially in the similar significant trends for Tmax and Ev plotted in Figures 6 and 8.

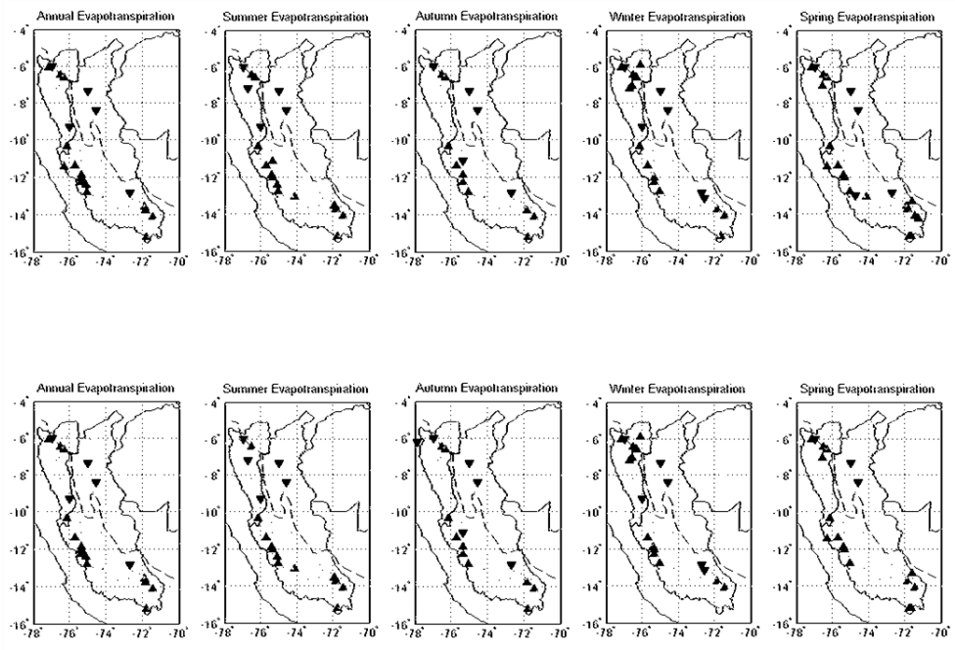

Figure 8. As in Figure 4, but for trends in Evapotranspiration.

STATIONS MEAN-CHANGE ANALYSIS

Table 6 reports the percentage of stations with significant mean-change classified in four periods: 1965-1970, 1971-1980, 1981-1990 and 1991-2008, considering rainfall, temperatures and evapotranspiration series. R mean-changes are observed mostly in the two last periods, 1981-1990 and 1991-2007. They are less frequent (about 10% of the cases) during the 1981-1990 period in the Rainforest but more abundant during the 1991-2007 period; this is consistent with the strong rainfall increase during the 1996-2007 period.

Tmean and Tmin series present higher percentages of stations with significant mean-change in the 1981-1990 period (until 36% for mean temperature and 55% for minimum temperature) while maximum temperature series shows a higher percentage of stations with significant mean-change in the 1971-1980 period (until 45%). Higher percentages of stations with significant mean-change in evapotranspiration are observed in the 1981-1990 period over Global and Andes regions (until 27%) while in the Rainforest region higher percentages appear during the 1991-2007 period (until 36%).

Table 6. Percentage of stations with significant year of mean-change for periods (α = 0.05) over the three analyzed regions. An: Annual; Su: Summer; Au: Autumn; Wi: Winter; Sp: Spring

		Global					Andes					Rainforest				
Variable	Period	An	Su	Au	Wi	Sp	An	Su	Au	Wi	Sp	An	Su	Au	Wi	Sp
Rainfall	1965-1970	0	0	0	0	0	0	0	0	0	0	0	0	0	0	0
	1971-1980	0	2	0	0	0	0	2	0	0	0	0	0	0	0	0
	1981-1990	9	9	9	3	3	11	11	9	4	4	0	0	8	0	0
	1991-2007	14	7	2	10	5	13	7	2	11	7	15	8	0	8	0
Mean Temp.	1965-1970	0	0	0	0	0	0	0	0	0	0	0	0	0	0	0
	1971-1980	17	21	6	13	19	14	19	3	11	19	27	27	18	18	18
	1981-1990	29	23	31	21	13	30	24	30	19	11	27	18	36	27	18
	1991-2007	13	10	6	13	21	14	11	8	11	22	9	9	0	18	18
Max. Temp.	1965-1970	0	0	0	0	0	0	0	0	0	0	0	0	0	0	0
	1971-1980	27	27	25	17	10	22	30	19	14	3	45	18	45	27	36
	1981-1990	17	15	10	13	33	16	14	11	5	41	18	18	9	36	9
	1991-2007	10	15	4	10	10	8	11	0	8	5	18	27	18	18	27
Min. Temp.	1965-1970	0	0	0	0	0	0	0	0	0	0	0	0	0	0	0
	1971-1980	4	2	2	4	6	5	3	3	3	8	0	0	0	9	0
	1981-1990	33	35	27	29	21	30	30	22	32	16	45	55	45	18	36
	1991-2007	17	23	8	8	15	19	30	11	8	11	9	0	0	9	27
Evp.	1965-1970	0	0	0	0	0	0	0	0	0	0	0	0	0	0	0
	1971-1980	19	21	15	21	10	16	24	14	11	8	27	9	18	55	18
	1981-1990	25	19	13	19	25	27	19	16	19	30	18	18	0	18	9
	1991-2007	10	13	6	2	8	5	5	0	0	3	27	36	27	9	27

ALTITUDES- TREND RELATIONSHIP AND SINGULAR REGIONS WITH HOMOGENEOUS TRENDS

Linear fluctuations calculated based on Bravais-Pearson method taking into consideration all the stations are compared together with station elevations (Fig. 9). Significant values are in red color circles. R trends exhibit no elevation-dependent pattern. Many cases of significant positive trend in Tmean are located overall in the Andes region (~ above 2000 m a.s.l.). On

the contrary, Ev trends present an elevation-dependent pattern, with an Ev positive trend at high altitudes. These results are confirmed by the values computed in Table 5.

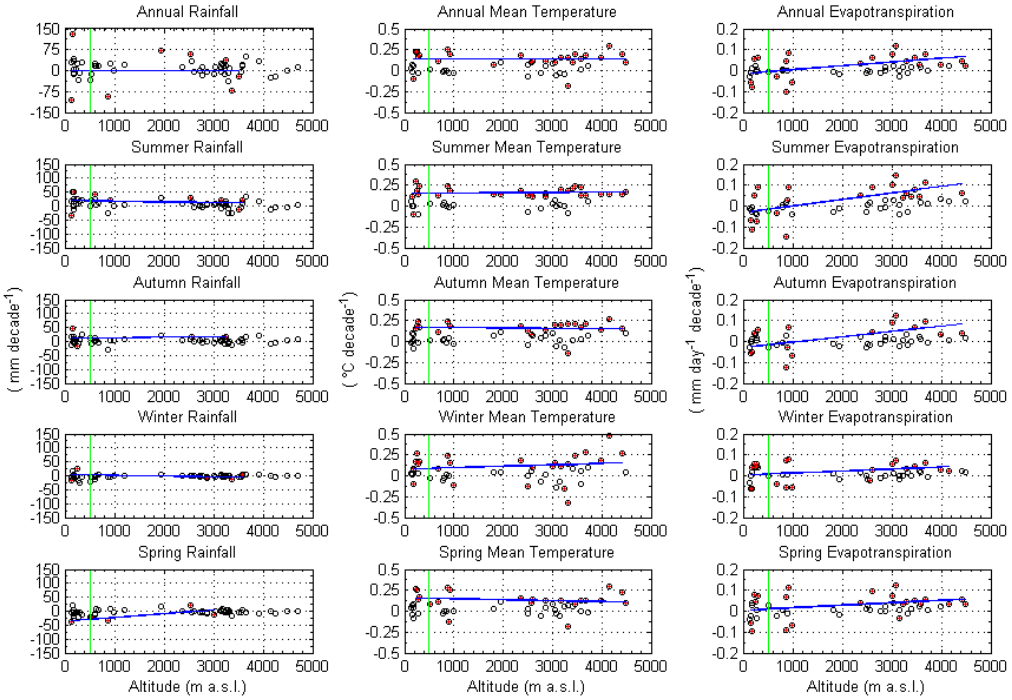

Figure 9. Local trends in mean annual or seasonal values (1965-2007) plotted as a function of station elevation for Rainfall, Mean Temperature and evapotranspiration. Significant values are in red circles. The Andes and Rainforest region are limited by a green vertical line. A linear trend is represented (blue line) following stations with significant trend.

Linear fluctuations values for all the stations, considering the 1965-2007 period, are interpolated and plotted for all the variables (R in mm per decade, Tmean, Tmax and Tmin in °C per decade and Ev in mm per decade) in Fig. 10.

R time series exhibit the highest negative fluctuations over the northern Rainforest region in the Ucayali and Huallaga basins (until -150 mm per decade). Positive fluctuations (until +110 mm per decade) are put in evidence at the limit between Andes and Rainforest over the Ucayali basin (~ 9°S- 75.5°W).

Temperature time series are characterized by strong positive fluctuations over the Andes region and light negative values over the Rainforest region. However, Tmin presents light negative fluctuations values in the Andes region over Ucayali basin (~ 12°S-76°W). The highest negative Ev fluctuations are put in evidence in the northern Rainforest region (Ucayali and Huallaga basins) following a similar pattern than rainfall. Other regions located on the western part of both basins are mostly characterized by a positive evapotranspiration fluctuation over the 1965-2007 period that follows temperature fluctuation.

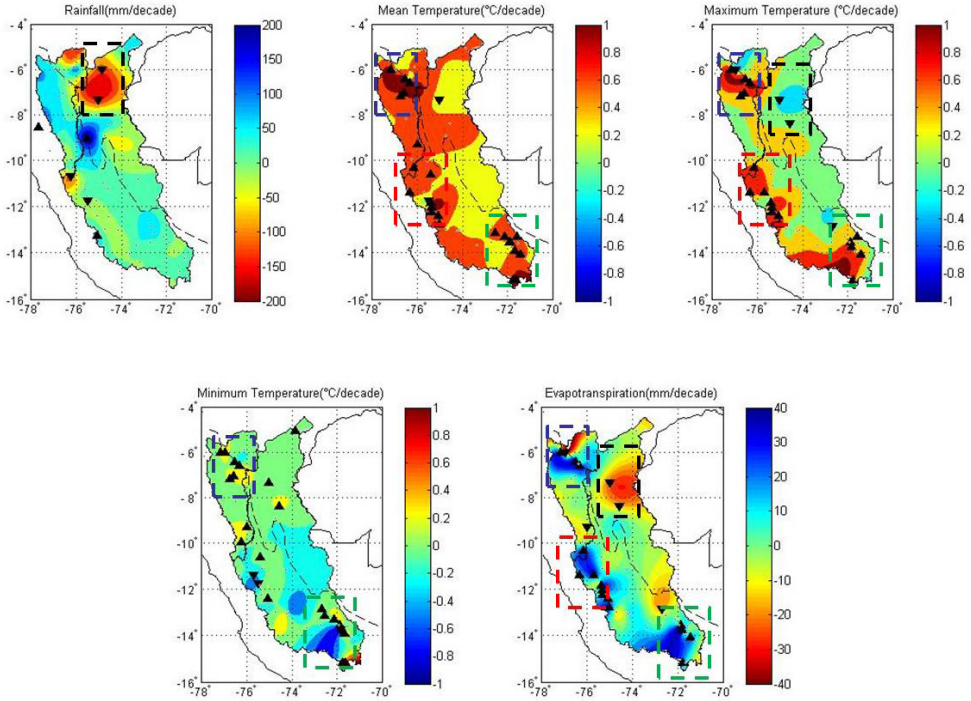

Figure 10. Annual interpolated linear trends using Bravais Pearson methodology for the 1965-2007 period in rainfall (mm per decade); mean, maximum and minimum temperature (° C per decade) and evapotranspiration (mm per decade). Positive significant trends (α equal 0.05) are represented by upward triangles and negative significant trends (α equal 0.05) by downward triangles. Dashed rectangles are regions with homogeneous significant trends. The Huallaga and the Ucayali basins are separated by a dark plain line. The Andes and Rainforest region are limited by a black dashed line.

In summary, stations with significant trends can be distinguished in four regions. Fig. 10 shows these four regions using colored rectangles. Rainfall decreases in the lowlands of the Ucayali basin (in the Rainforest region). In the same region are observed Tmean, Tmax and Ev negative trends (black dotted rectangle). The blue rectangle put together stations with similar significant positive trends in Tmean, Tmax, Tmin and Ev in the northern Huallaga basin. The red rectangle gathers stations with significant positive trends in Tmean, Tmax and Ev in the central Andean region (Mantaro sub-basin over Ucayali basin). Stations with significant positive trends in all the temperature's series and Ev are limited by the green rectangle located in the southern Andes region in Ucayali basin (close to highland in Urubamba basin). Figures 9 and 10 show the concordance for temperatures and Ev series between altitudes and spatial distribution of stations with significant trends located mostly in the Andes region.

RELATIONSHIP BETWEEN CLIMATE AND LARGE-SCALE OCEANIC PATTERNS

Vuille et al. (2003) and Espinoza et al. (2008) described the leading teleconnection patterns between rainfall or temperature in the Andes and the Amazon basin and the SST of the Pacific and the Atlantic Ocean. But these authors do not use the large dataset we gathered, including many Peruvian weather stations and calculated evapotranspiration data. For this reason, R, Tmean and Ev series at station scale are related to the index of the El Niño –Southern Oscillation, the SOI, and with the SST difference between the northern and the southern tropical Atlantic Ocean (NATL-SATL).

The stations with significant correlation coefficients (α equal to 0.05) between climate series and SOI are plotted in Fig. 11. Rainfall variability in some stations appears as in positive

relationship with SOI over the southern Ucayali basin (Andes region) especially during the rainy season (~ 23% of stations with significant correlation). These results show that rainfall is less (more) abundant during El Niño (La Niña). They concord with Vuille et al.(2003) and Espinoza et al.(2008). Though, in spring, there is more (less) rainfall during El Niño (La Niña) in some intra-Andean stations of the extreme south of the studied region.

In many stations, Tmean (mostly in the central and Northern Andes) and Ev (mostly in the Central and Southern Andes) appear as negatively correlated with SOI, especially at annual time scale and during summer and autumn seasons. Tmean and Ev are higher (lower) during El Niño (La Niña) years. These stations are the same than those with a positive trend, already highlighted in Fig. 10 (blue, red and green dotted rectangles for Tmean linear trends). Therefore, the Tmean increase may be associated with the stronger frequency of El Niño events since the end of the seventies (Trenberth et Hurell, 1994).

Fig. 12 shows stations with significant correlation coefficients between climatological series and NATL-SATL sea surface temperature. R series appear mostly in negative relationship with NATL-SATL SST, that is to say that rainfall is more (less) abundant when NATL (SATL) is cold. Significant correlation coefficients values are exhibited in the southern zone over Ucayali basin (Andes region) especially considering annual, summer and autumn rainfall time series. In nearly 40% of the stations there are significant correlations between rainfall and NATL-SATL during summer. Then, NATL-SATL SST appears to play a more important role than SOI on rainfall pattern in the southern Andean Ucayali. These results concord with the recent study by Espinoza et al.(2008).

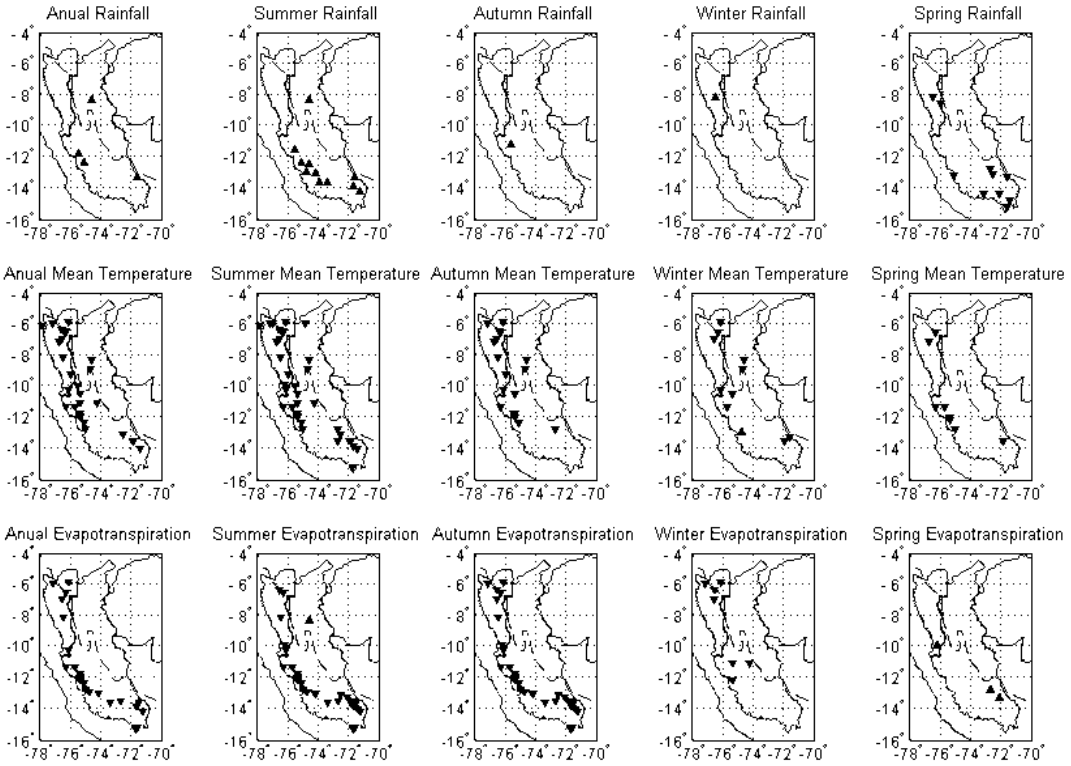

Figure 11. Stations with positive and negative significant correlation with SOI (p > 95%) over Huallaga and Ucayali basins for annual and seasonal rainfall, mean temperature and evapotranspiration. Positives correlations are represented by upward triangles and negative ones by downward triangles. The Huallaga and the Ucayali basins are separated by a dark plain line. The Andes and Rainforest region are limited by a black dashed line.

Tmean time series and Ev especially in the Andes appear as mostly positively correlated with NATL-SATL SST, overall for annual, summer and autumn temporal series. This means that

temperature and evapotranspiration are higher when the northern tropical Atlantic is warm and/or the southern tropical Atlantic is colder than usual. However, when considering the percentages of stations with significant correlation in Figures 11 and 12, it is obvious that SOI plays a more important role on mean temperature and evapotranspiration patterns than NATL-SATL, overall in the Andes region, in Huallaga and Ucayali basins.

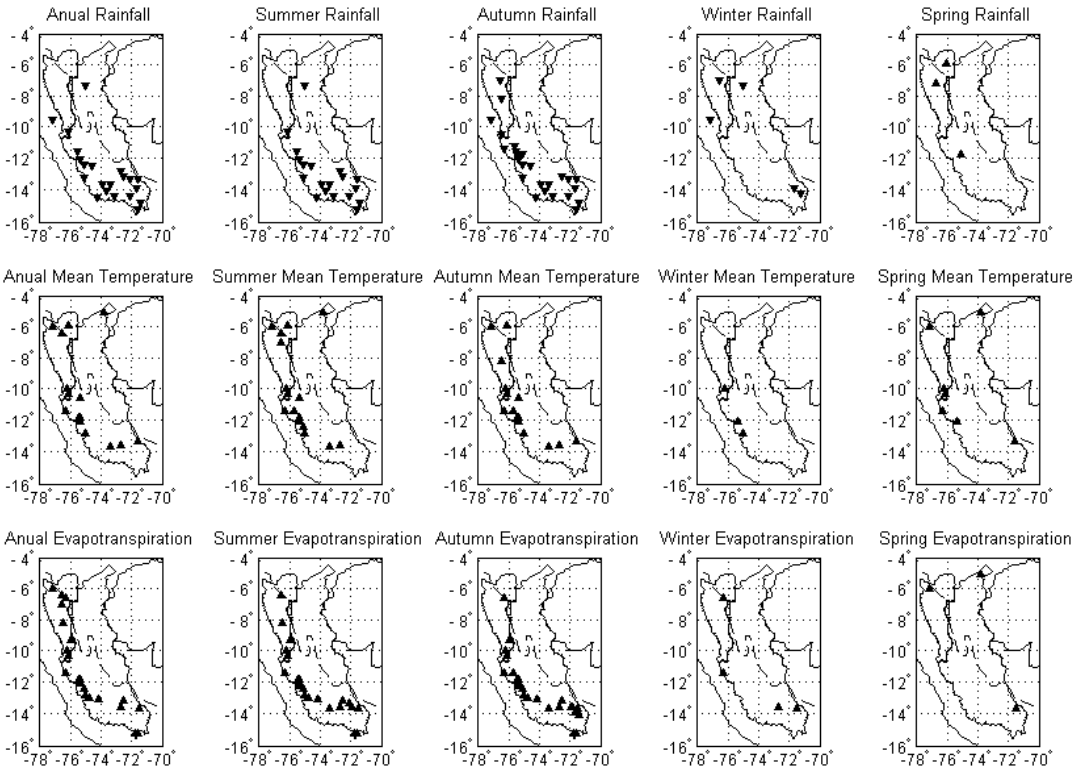

Figure 12. Stations with positive or negative significant correlations with NATL-SATL ($p > 95\%$) over Huallaga and Ucayali basins for annual and seasonal rainfall, mean temperature and evapotranspiration. Positives correlations are represented by upward triangles and negative ones by downward triangle. The Huallaga and the Ucayali basins are separated by a dark plain line. The Andes and Rainforest region are limited by a black dashed line.

CONCLUSION

This work is the first that describes recent trends in rainfall, temperatures and evapotranspiration over the Peruvian Amazonas-Andes basin (mainly Huallaga and Ucayali basins). It is based on an extended monthly database from on-site stations and covers the last 43 years (from 1965 to 2007).

Our main findings are summarized as follows:

- The mean warming over the Global Region is about +0.09°C per decade. This estimation is close to the 0.10-0.11°C increase per decade reported by Vuille et al.(2003) in the 1939-1998 along the tropical Andes and also in concordance with estimations of the global warming (~ 0.07 °C per decade over the last 100 years, Christensen et al., 2007). Moreover, significant years of mean-change for temperature series in the three regions are, on average, the end of the 1970's period that concord with the start of the strong frequency of El Niño events (Trenberth et Hurell, 1994). This is consistent with the fact that temperature is negatively correlated with the Pacific SOI index, that is to say that temperature is higher during El Nino years. At station-scale, significant Tmean trends related with the altitude of the stations (Figure

9) show more percentage of stations with significant positive trends in high altitudes than in low altitudes. These changes will have important consequences for eastern Andes glaciers and for communities located in high altitudes that rely on glacier-fed water (IGP, 2005 and Bradley et al., 2006). Some stations over the eastern Andes region show significant negative temperature trends while nearby stations exhibit positive trends. This opposition is clarified by the cloud cover changes (Vuille et al., 2003) and do not call in question again the global warming trend. It is noticeable that a major percentage of mean-changes at station-scale are first observed in Tmax (during the 1970s) then in Tmin series (during the 1980s) over the three analyzed regions. Thus, Tmean series present mean-changes in the 1980's decade. Significant trends (annual and spring season) and mean-change year (1976-summer season) in Ev are observed in the Andes; as temperature's series, they can be related to the start of a strong frequency of El Niño events at the end of the seventies.

- There is no trend in rainfall. Thought, roughly 10 % of the stations over the Global region exhibit a mean-change in the 1991-2007 period, when a significant mean-SST change is observed in the Northern Atlantic Ocean (Espinoza et al., 2008, Marengo et al 2008). The decline (increase) in rainfall in the Andes (Rainforest) observed at regional scale since the mid' nineties is consistent with the negative relationship between rainfall in the southern Andes and the SST gradient between the northern and the southern tropical Atlantic. Opposite rainfall anomalies between Andes and Rainforest have already been commented (Jones et Carvalho, 2002); at intraseasonal time scale they are associated with active and break phases in the South American monsoon. More, our findings are consistent with the results by Espinoza et al.(2008); they indicate that rainfall variability in western Amazon is observed at decadal and long term time scales and respectively associated with the Atlantic and Pacific SST pluriannual variability. Long term variability is related to the Pacific Decadal Oscillation (Marengo, 2004) and to the Pacific Pan Decadal Variability (PDV - Chen et al., 2008) that experience a change at the beginning of the nineties. Decadal variability that opposes the northwest and the south of the AB is associated with changes in the northern Atlantic SST that is warmer since the middle of the nineties (Espinoza et al 2008, Marengo et al 2008).

Future works about climatological trends in Peru will take into consideration the whole country with a special focus on extremes values, using daily data.

3.2 Variabilité spatiale des débits sur les bassins de l'Ucayali et de Huallaga

Cette étude malheureusement limitée du fait du faible nombre d'années disponibles repose en partie sur les résultats de Espinoza et al.(In Press) qui s'attachaient à l'étude de la variabilité spatiale sur la zone andine. Espinoza et al. (In Press) ont mis en évidence sur notre zone d'étude (voir Figure III-1) des tendances négatives sur les séries temporelles de débits annuels maximums et moyens (avec un niveau de confiance de 90%) ainsi que sur les séries temporelles de débits minimums (avec un niveau de confiance de 99%) sur le bassin du Rio Ucayali (station de Requena REQ) sur la période 1990-2005. Le Rio Huallaga termine son parcours dans le Rio Marañón, lui-même contrôlé à la station San Regis (SRE) située en aval de la jonction des rios Huallaga et Marañón. Les séries chronologiques de débits mesurés à SRE présentent des tendances positives avec un niveau de confiance de 99% pour les débits maximums et moyens, tandis que les débits minimums ne présentent pas de tendance significative. Cette variabilité s'avère plus contrastée entre le sud et le nord selon Espinoza et al. (In Press) et concorde avec la variabilité observée sur les séries chronologiques de

précipitations. Ainsi, les séries chronologiques de pluies présentent des tendances positives pour les mois de Mars-Avril-Mai et des tendances négatives pour les mois de Septembre-Octobre-Novembre dans le nord-ouest du bassin de l'Amazone depuis le début des années 1990. De plus, dans le sud de la zone d'étude, la diminution des précipitations de Décembre-Janvier-Février depuis le début des années 1980 explique en partie les diminutions des écoulements moyens annuels et la diminution de l'intensité des crues observée à l'exutoire de l'Ucayali. Cette variabilité hydrologique est directement liée à la variabilité à court et à long terme des température de surface des océans tropicaux Pacifiques et Atlantique nord (Marengo, 2004 et Espinoza et al., 2008).

Les séries de débits mesurés sur nos bassins d'étude (voir section 2.4), même en gardant à l'esprit le caractère parcellaire des données à notre disposition, montrent des tendances en accord avec le paragraphe précédent. Ainsi, sur la Figure III-2, nous avons représenté les différentes tendances obtenues : une tendance positive dans les séries temporelles de débits du fleuve Huallaga (bassin de Chazuta) et sur les débits mesurés à la station de San Regis SRE (voir Figure III-1) et une tendance négative dans les séries temporelles de débits du Rio Ucayali (bassin de Requena) observée sur différentes périodes. Cependant, les débits mesurés à l'exutoire des autres bassins situés dans la zone d'étude mettent en évidence des tendances annuelles difficiles à exploiter et à analyser car les données ne sont pas disponibles sur des périodes identiques et parfois sur des périodes très courtes. Enfin, nous observons aussi des tendances opposées en considérant les séries de débit de Mejorada (positive) et Pisac (négative), stations situées dans les Andes.

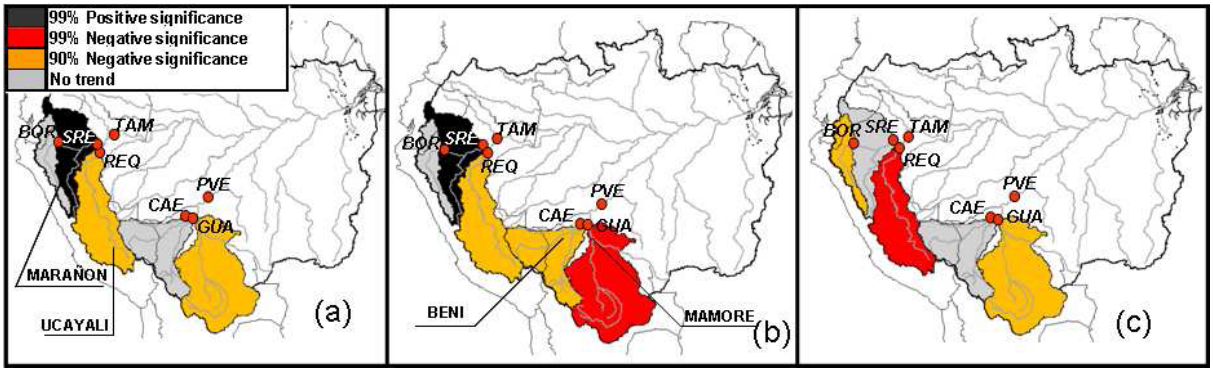

Figure III-1. Tendances mises en évidence sur les séries débits mesurés à l'exutoire des sous bassins Andins amazoniens pour la période 1990-2005, en considérant les grands bassins Tamishiyacu, TAM (Borja BOR, San Regis SRE et Requena REQ) ainsi que le bassin de Porto Velho pour a) les maxima annuels b) les moyennes annuelles, c) Les minima annuels. Les couleurs indiquent le signe et la le niveau de confiance de la tendance. D'après Espinoza et al., In Press.

En conclusion la variabilité des débits sur notre zone d'étude est marquée par une opposition entre le nord (Rios Huallaga et Marañón) et le sud (Rio Ucayali) en relation avec la variabilité pluviométrique déjà commentée dans Espinoza et al.(In Press). De plus, les débits mesurés mettent en évidence une grande variabilité spatio-temporelle difficile encore à interpréter du fait de la disponibilité réduite des données.

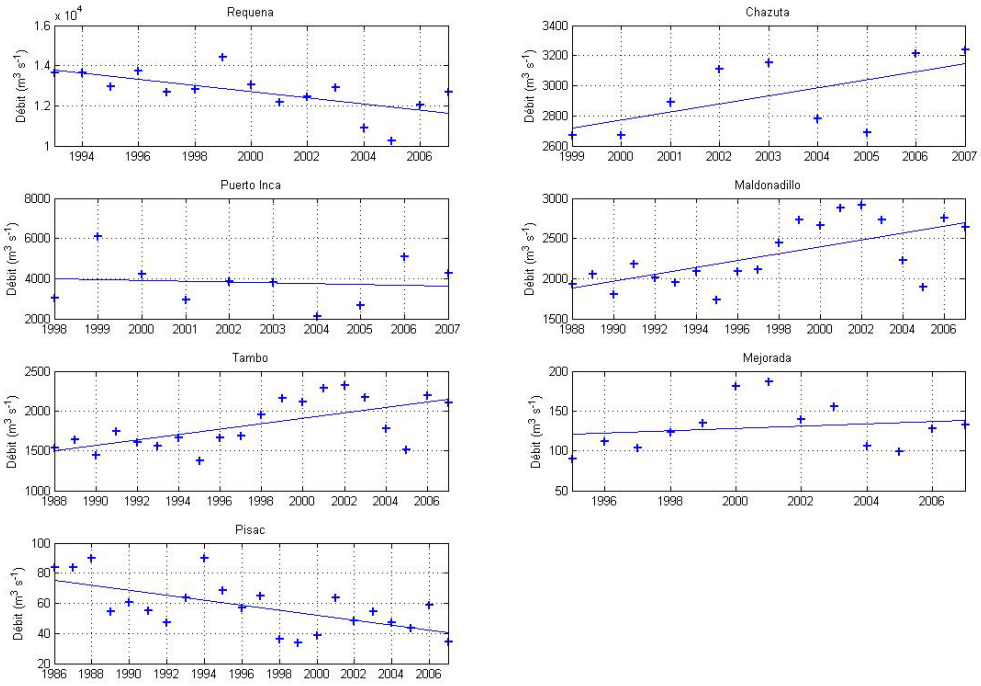

Figure III-2. Tendances annuelles mises en évidence sur les séries de débits considérés dans cette étude. La ligne bleue correspond à la tendance linéaire.

CHAPITRE 4

Modélisation du bilan hydrique au niveau mensuel et impact des changements climatiques sur les régimes hydrologiques des bassins des rios Ucayali et Huallaga

IV. CHAPITRE 4 .Modélisation de bilan hydrique au pas de temps mensuel et impact du changement climatique sur les régimes hydrologiques dans les basins des rios Ucayali et Huallaga

Pour comprendre quelles sont les interrelations entre la pluie et le débit, il est nécessaire de développer des modèles hydrologiques qui tentent d'expliquer ces processus. Ainsi, il existe dans la littérature diverse types de modèles hydrologiques ayant soit des bases conceptuelles (modèle statistique ou modèle à réservoirs, etc.) soit des bases physiques. Ces derniers se distinguent alors principalement par la grande quantité des données d'entrée nécessaires à leur fonctionnement. En prenant en compte la disponibilité limitée de données dans notre région d'étude (voir **Chapitre 2**), nous avons choisi de mettre en place une modélisation hydrologique conceptuelle à base de réservoirs. Le travail de modélisation des bilans hydriques sur les deux bassins d'étude a suivi un continuum tout au long de la thèse en fonction de la qualité et de la quantité des données disponibles. Au début de la thèse, nous ne disposions que des données hydroclimatologiques à la station de Requena sur le fleuve Ucayali. Ainsi, nous nous sommes initialement orientés vers des modèles semi-distribués en prenant en compte les sous bassins (voir section 4.1.2). Ensuite, avec la mise à disposition de données sur six stations intermédiaires, en complément de données hydroclimatologiques à la résolution spatiale de 0.25º par 0.25º, la modélisation hydrologique distribuée, au pas de temps mensuel, a été améliorée.

En utilisant les résultats de la modélisation hydrologique (en particulier les paramètres calés sur les données actuelles), il a été possible d'évaluer les impacts du changement climatique sur l'hydrologie en utilisant les sorties des modèles de circulation générale du IPCC.

4.1 Premiers essais de modélisation en utilisant des modèles de bilan hydrique mensuel

Dans cette section, nous décrivons le résultat des premiers essais de modélisation basés sur les données de la station de contrôle de Requena sur le Rio Ucayali. Ce travail á été soumis au « Hydrological Sciences Journal », et il est en révision.

4.1.2 Monthly water balance models in the Amazon drainage basin of Peru: Ucayali River basin

WALDO SVEN LAVADO CASIMIRO, DAVID LABAT, JEAN LOUP GUYOT, SANDRA ARDOIN-BARDIN & JUAN JULIO ORDOÑEZ

RÉSUMÉ

Le bassin péruvien amazonien est le lieu de naissance du fleuve Amazone, et c'est une région caractérisée par différentes conditions physiographiques et hydroclimatologiques. Les variables du cycle hydrologique dans cette région restent en grande partie inconnues et n'ont pas encore été étudiées, principalement en raison de l'inaccessibilité de la partie andine du bassin.

Pendant les dernières années, un effort important de rassemblement des données concernant les bassins des rios Ucayali et Marañón, couplé à plusieurs campagnes de mesure de débit,

rend maintenant possible de développer certaines analyses spécifiques, telles que l'étude du bilan hydrique et l'approche de modélisation hydrologique, aux résultats encourageants pour la période 1978-1999.

Dans le présent travail, le bilan hydrique du bassin du Rio Ucayali est réalisé au pas de temps mensuel, prenant en compte la semi-distribution spatiale du bassin et des sous-bassins. Nous comparons également l'exécution de trois modèles conceptuels de bilan hydrique (GR2M, ABCD et Vandewiele). Par la classique procédure de calage-validation, nous prouvons que ces modèles conceptuels sont bien adaptés aux différentes conditions physiographiques et climatiques de notre zone d'étude.

ABSTRACT

The Peruvian Amazon basin where the Amazon River originates is a region characterised by different physiographic and hydroclimatological conditions. The components of the hydrological cycle in this region remain largely unknown and have not yet been extensively studied mainly due to the inaccessible rural scenery.

During the last years, a strong data-collecting effort over the Ucayali and Marañon rivers coupled to several discharge measure campaigns makes now possible to develop some specific analysis such as water balance study and a promising hydrological modelling approach for the period 1978-1999.

In the present work, the water balance of the Ucayali river basin is developed on a monthly basis, taking into consideration the spatial semi-distribution of the basin and sub-basins. We also compare the performance of three conceptual water balance models (GR2M, ABCD and Vandewiele). Via a classical calibration-validation procedure, we show that these conceptual models are well adapted to the different physiographic and climatic conditions.

Key words: conceptual hydrological models, Amazon basin, water balance, Ucayali River, Peru.

INTRODUCTION

The Amazon Basin is the largest one in the planet, with a drainage area of 6 200 000 km^2 and average annual discharge of 6 300 km^3 of water to the Atlantic Ocean (Molinier et al., 1996; Marengo, 2006). Emanuel et Escurra (2000), mention that the Amazon River basin has almost 99% of all the existing resources in the Peruvian territory, and a study made by UNESCO (2006) considers that the annual water availability in this drainage basin is 2696 net mm, after having carried out the multi-annual water balance. The Ucayali River basin covers approximately 6% of the total Amazon basin, and 27% of the Peruvian territory (Fig. 1). This basin is characterized for presenting great altitudinal variations, ranging from 6306 m to 45 m above sea level.

Preliminary studies on the hydro-meteorological characteristics in this area (Gentry et Lopez-Parodi, 1980) exhibit significant negative trends in rainfall with reference to the 1961-1969 and 1970-1978 periods in the Pucallpa station. But Rocha et al.(1989) reject these results, finding significant positive rainfall trends for the 1957-1981 periods in the same station. Recent study have demonstrated that discharges and rainfall show a decreasing trend (Espinoza et al., 2006b).

In the Tamishiyacu station, discharges downstream the Ucayali River, after the junction of this last one with the Marañón River, show a decreasing trend - 0.81% per year for the 1970-1997 period, likewise average rainfalls up to this zone, show a decreasing trend of - 0.83% for the same analysis period. Espinoza et al.(2007) show that the discharges of the Ucayali River have a significant negative trend for the 1990-2005 period.

Documents on water balance models of the Amazon basin often deals with macro-scale level covering the entire Amazon basin (e.g. Russell et Miller, 1990; Miller et al., 1994; Marengo et al., 1994; Nijssen et al., 2001; Nijssen et al., 1997), and confront to the systematic underestimation problem of rainfall and discharges, due to the lack of information availability in the Amazon basin. In the Peruvian territory, there are documents about the hydrological characteristics, as we have described before, but there are few references about development of hydrological models. Only two works deal with this topic at our knowledge. The first one was developed by BCEOM (1999) that carries out modeling using the GR model (Edijatno et al., 1999), made in several basins of the Pacific Ocean, and the second one was developed by Ordoñez (2001) carried out over a sub-basin in our study area, using the IPH-MEN (Tucci, 1998).

The measurements of hydro-climatological variables in the Amazon basin are administrated by the National Meteorology and Hydrology Service SENAMHI (www.senamhi.gob.pe). Most part of the information is related to climate variables (rainfall, temperature, etc.), without having discharge measures, especially from the largest Peruvian Amazon rivers. Starting the year 2001, the HYBAM Program (IRD – SENAMHI – UNALM Convention, www.mpl.ird.fr/hybam) carries out gauging campaigns over the largest Amazon rivers in the Peruvian territory, as described by Yerren et al.(2004).

After four years, the project exhibits a consistent database that allow for the first time to estimate how much water flows through the Amazon-Solimoes Rivers in the Peruvian territory. It allows presenting in this contribution an extensive hydrological modelling of the Ucayali river basin based on monthly water balance and conceptual reservoir models.

AVAILABLE DATA

Ucayali River basin

The Ucayali River basin is situated in the central and eastern part of the Peruvian territory, exactly between 4.40°-15.64°S and 70.65°-76.80°W coordinates, it has an area of 354 341 km^2. The Ucayali is a main river that runs from south to north, across this basin; it has approximately 1452 km length (Fig. 1 and Table 1).

To better understand the hydrography and hydro-climatological characteristics of the Ucayali river basin, a subdivision into sub-basins was made. This subdivision into sub-basins, using the Requena station as basis, (the only station that has discharge measurements) was carried out using the Digital Elevation Model (DEM) provided by the National Aeronautics and Space Administration, NASA through the Shuttle Radar Topography Mission, SRTM (www2.jpl.nasa.gov/srtm); a description of this model is given by Farr et al.(2007). Based on this DEM the sub-basins outline was made. Validation was carried out based on the basin maps of Peru, from the Natural Resources Institute of Peru INRENA (www.inrena.gob.pe), as well as the basin maps generated by Mialocq et al.(2005) for this analysis zone.

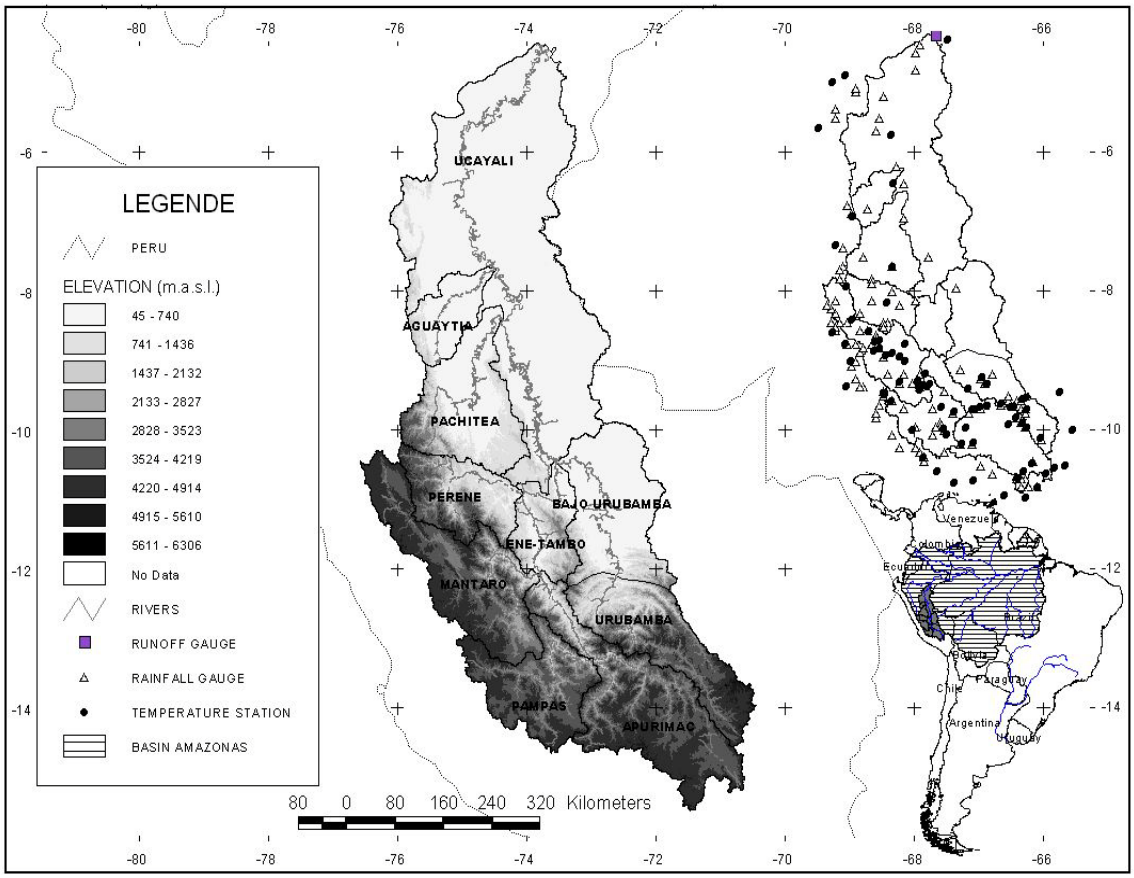

Figure 1. Location of the area of study; altitudes; sub-basins and used information.

Both the rainfall and evapotranspiration information from SENAMHI, was interpolated over each one of the sub-basins, to this end the Kriging interpolation method was used (Oliver et Webster, 1990). The algorithm described by Deutsch et Journel (1992) and included in the Spatial module of the software Hydraccess developed by Vauchel (2005b) is used to achieve this spatial interpolation.

Table 1. Characteristics of the Basin and Sub-basin of river Ucayali. Rainfall and Evapotranspiration: Mean Annual (1970-1999)

Sub-basin	Area (km2)	Length River (km)	Rainfall (mm)	Evapotranspiration (mm)
Urubamba	29283	354	1028	844
Bajo Urubamba	31424	267	1921	1206
Apurimac	42934	501	746	640
Pampas	24048	367	757	613
Mantaro	35545	577	721	637
Perene	19035	240	1130	844
Ene-Tambo	14159	268	1222	821
Pachitea	29592	287	2413	1270
Aguaytia	11622	199	2940	1498
Ucayali	116699	808	1889	1606
Total	354341	1452	1477	998

Rainfall

The rainfall data available in Peru has been digitized from SENAMHI database, collected by the HYBAM Project and already preliminary investigated by Espinoza et al.(2007). This information releases monthly rainfall and runoff and is completed by some stations collected by the study from UNESCO (2006).

All our information has been submitted to the Regional Vector Method RVM (Hiez, 1977 and Brunet-Moret, 1979) to analyze the quality of the data. Based on the obtained consistent spatial database, we estimate the mean annual rainfall for the basin around 1477 mm and the main rainfall of the sub-basins are summarised in Table 1. We note that the Pachitea and Aguaytia sub-basins highlight higher mean annual rainfall than the others sub-basins.

Evapotranspiration

Figure 1 shows the stations with temperature information that were used to compute monthly evapotranspiration. This information originates from SENAMHI and seizure from UNESCO (2006).

For this purpose, the Thornthwaite method was used (Thornthwaite, 1948b), because this evapotranspiration model only needs monthly temperature information. This estimation was developed for each sub-basin (Table 1). It can also be observed that mean annual evapotranspiration on the entire basin is 998 mm and that the Ucayali and Aguaytia sub-basins are characterised by higher annual evapotranspiration than the others sub-basin. In general, the difference of rainfall minus evapotranspiration used generally as water availability is of 479 mm in our basin of study.

Soils

In order to work with soil data, we have used the methodology described by Dieulin et al., 2006, based on the data from the Digital Soil Map of the World (FAO/UNESCO, 1981). FAO defines soil units depending on the horizons' depth and texture of its components, which are grouped in classes according to water holding capacity.

Table 2. Distribution of values of water holding capacity (S) in mm. Smin: minimum Water holding capacity; Smean: average Water holding capacity; Smax: maximum Water holding capacity.

Clase	Smin	Smean	Smax
A	200	250	300
B	150	175	200
C	100	125	150
D	60	80	100
E	20	40	60
F	0	10	20
W (Wetlands)	1000	1000	1000

The water holding capacity depends mainly on the granulometric characteristics of the soil and on the depth of the soil exploitation by the plant which is assimilated to the depth of the root. The method developed by FAO to compute the water holding capacity is based on the plants roots depth, plant coverage and the standardized suction limits (wilting point and field capacity). For each kind of soil, we have evaluated water holding capacity, using 3 values:

minimum, maximum and mean of the limits of the considered soil types. FAO does not give any information about the capacity value to be given to the Wetlands type. With the purpose to keep certain homogeneity with previous studies (Dray, 2001; Ouedraogo, 2001) the Wetlands type will be given the value of 1000 mm for water holding capacity. The different values obtained for water holding capacity are given in Table 2.

From the soil coverage map, and based on its water capacity, a disaggregation was made aimed at obtaining a coverage under the form of a sub-basin. This operation consists in allocating to a data grid, a capacity value equal to the mean surface - weighted of the polygons that cover the grid, that are in the limits of the basin (e.g. Dieulin et al., 2006). This way, weighted values were found for each sub-basin (Table 3), from this values the average value is used (Smean) as the Mean Soil water retention.

Table 3. Values of capacity of water capacity holding (S) en mm in the sub-basins from Ucayali. Smin: minimum Water holding capacity; Smean: average Water holding capacity; Smax: maximum Water holding capacity.

Sub basins	Smin	Smean	Smax
Vilcanota_Yavero	392.4	404.8	417.1
Urubamba	286.2	300.3	314.3
Apurimac	388.4	401.1	413.8
Pampas	376.4	389.0	401.6
Mantaro	390.5	403.4	416.3
Perene	347.9	361.5	375.2
Ene-Tambo	352.5	365.0	377.5
Pachitea	240.5	256.0	271.5
Aguatia	197.5	213.2	228.9
Ucayali Bajo	144.2	161.2	178.3
Ucayali	243.8	258.8	273.8

Discharges

The Amazon river, in the Obidos Station (Brazil) has a mean discharge of 209 000 $m^3.s^{-1}$ (Molinier et al., 1996), and in the Tamishiyacu station (Peru) has an average discharge of 27 500 $m^3.s^{-1}$ (Espinoza et al., 2006b). The average multi-annual discharge of the Ucayali River in the Requena station is 11 260 $m^3.s^{-1}$, it transfers approximately 41% of the total discharge that goes into the Amazon River. For the present study the discharges are obtained in millimetres using as reference the total area of our drainage area and just one discharge station is used, the Requena station.

MONTHLY WATER BALANCE MODELS

GR2M Model

The GR2M model (Niel et al., 2003) first developed by Kabouya (1990), and reviewed by Makhlouf & Michel (1994) is a two reservoirs conceptual model. The reservoir H has a capacity maximum A (Smean) that carries out the simulation of discharge on monthly basis, from rainfall data and mean monthly evapotranspiration over a basin. The concept pattern of the model is shown in Figure 2a, where the parameters of model are X1 and X2.

ABCD Model

The ABCD model developed by Thomas (1981) and applied for example by Mouehli (2003), is a four parameter model (A, B, C and D in Figure 2b), that is articulated around two reservoirs: a ground reservoir of maximum capacity A (Smean) and a linear reservoir of drainage G, characterized by the parameter D.

Vandewiele Model

This model has been explained and commented by Vandewiele et al.(1992), Xu (1992), Xu et Vandewiele (1994), Xu (1997) among others. This model is based on the water balance equation

$$Sm_t = Sm_{t-1} + P_t - EPT_t - Q \quad (1)$$

where Sm_{t-1} is the state of the soil moisture storage (Smean) at the end of month t-1 and P_t, EPT_t and Q are rainfall, actual evapotranspiration and runoff during month t, respectively. Actual evapotranspiration is computed according to Xu (1997) as

$$Et_t = \min(ETP_t(1 - a_1^{\frac{W_t}{EPT_t}}), W_t) \quad (2)$$

where a_1 is the first parameter and takes values between 0 and 1. $W_t=P_t+Sm_{t-1}$ is the available water. Monthly runoff is distinguished between slow runoff

$$Q_S=a_2(Sm_{t-1})^{b1} \quad (3)$$

where the parameters a_2 y b_1 are positive. Because of physical constraints, b_1 takes discrete values (namely 0.5, 1 or 2). Rainfall P_t causes a fast runoff Q_f depending on the parameters a_3 y b_2, alter a partial neutralization of the ETP, that reduces it to level Pn:

$$P_n = P_t - ETP_t(1 - \exp(-\frac{P_t}{ETP_t})) \quad (4)$$

$Q_f = a_3(Sm_{t-1})^{b2}P_n$, where a_3 y b_2 are positive, for the same criterion used in the aforementioned, b_2 also take discrete values (namely 0.5,1 or 2). Monthly runoff Q outside the basin is the sum of both runoffs: $Q=Q_s+Q_f$.

CALIBRATING AND VALIDATING THE MODELS

In this section, the calibration and validation procedures are described. After testing different sub-division of the discharge series, using the method described by Ardoin-Bardin (2004), we find that the best periods are: January 1978 – December 1993 for calibration and January 1994 – December 1999 for validation.

In order to use the optimisation criteria, we choose the objective form proposed by Perrin (2000) which is a modification of the coefficient explain for Nash et Sutcliffe (1970), here after called « Nash »:

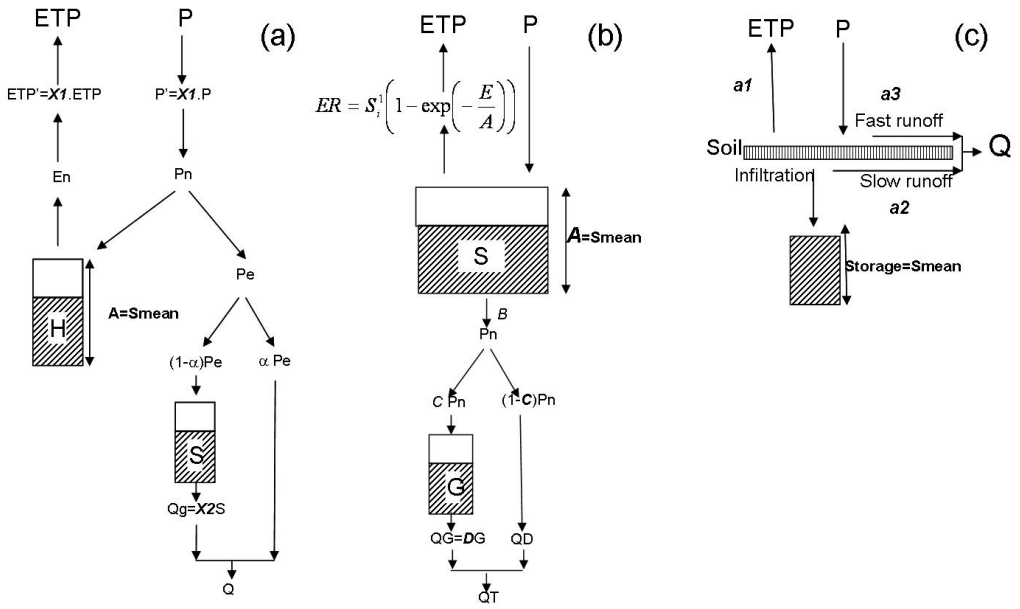

Figure 2. Scheme of the conceptual hydrological models used in this study: GR2M (a), ABCD (b) and Vandewiele(c).

$$Nash = 100\left[1 - \frac{\sum_{i=1}^{n}(\sqrt{Q_{\dot{a}}^{i}} - \sqrt{Q_{c}^{i}})}{\sum_{i=1}^{n}(\sqrt{Q_{o}^{i}} - \sqrt{Q_{m}^{i}})}\right] \qquad (5)$$

Where Q_o^i is the monthly observed discharge; Q_c^i is the monthly computed discharge; Q_m^i the the monthly mean observed discharge and i is the month considered.

The model is better when a Nash value is close to 100%. Nash et Sutcliffe (1970) say that there is nothing precise in the meaning of this criterion because the degrees of freedom of the model are unknown. However, it can be stated that a criterion of less than 60% does not provide a satisfactory agreement between the observed hydrograms and the ones simulated by the model (Niel et al., 2003).

Another important point to take into account is the approaches used to optimise the models, because of the lack of data for Ucayali River. We used two optimal approximations developed by Chennu (2005) that use as basis each station with rainfall information how input starting in the models, but our modification to his approaches consisted in taking as input the sub-basins in our study zone. The first approach ("Global approach") (Fig.3) shows a sub-division of the input precipitation (Pn) depending on each sub-basin and weighted by a factors αparameter to optimize in our models. The total input precipitation for the entire catchment will be:

$$PT=\alpha_1 P_1+\alpha_2 P_2+ \ldots\ldots \alpha_n P_n \qquad (6)$$

For running the models, we also used the total evapotranspiration (ET) and the total soil water holding capacity (Smean), both calculated for the entire catchment.

The second approximation ("Semi distributed approach") (Fig. 4), shows a sub-division of net precipitation (Pn), the evapotranspiration (En) and the soil water retention capacity (Smsn) for each sub-basin. The model run for each sub-basin and the total discharge is obtained by the amount of each sub-basin discharge weighted by a factors β parameter to optimize in our models:

$$QT=\beta_1*Q_1+\beta_2*Q_2+ \ldots\ldots \beta_n Q_n \qquad (7)$$

where n is the number of sub-basins.

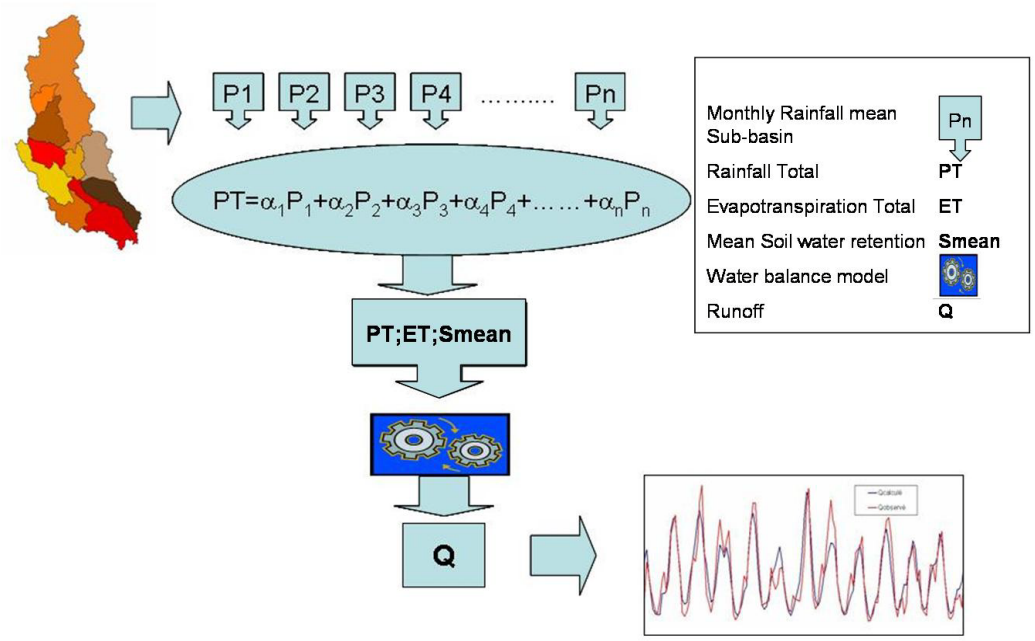

Figure 3. "Global approach" for the water balance models.

The second approximation ("Semi distributed approach") (Fig. 4), shows a sub-division of net precipitation (Pn), the evapotranspiration (En) and the soil water retention capacity (Smsn) for each sub-basin. The model run for each sub-basin and the total discharge is obtained by the amount of each sub-basin discharge weighted by a factors β parameter to optimize in our models:

$$QT=\beta_1*Q_1+\beta_2*Q_2+ \ldots\ldots \beta_n Q_n \qquad (8)$$

where n is the number of sub-basins.
In order to discriminate the best model, we have not only used the Nash coefficient. The Root Mean Square Error (RMSE) and the standard deviation of residuals (SD res.) are also calculated. RMSE is defined by:

$$RMSE = \frac{1}{n}\sqrt{\sum_{i=1}^{n}(Q_{\grave{a}}^{i} - Q_c^{i})} \qquad (9)$$

The residuals are the difference between observed and calculated models.

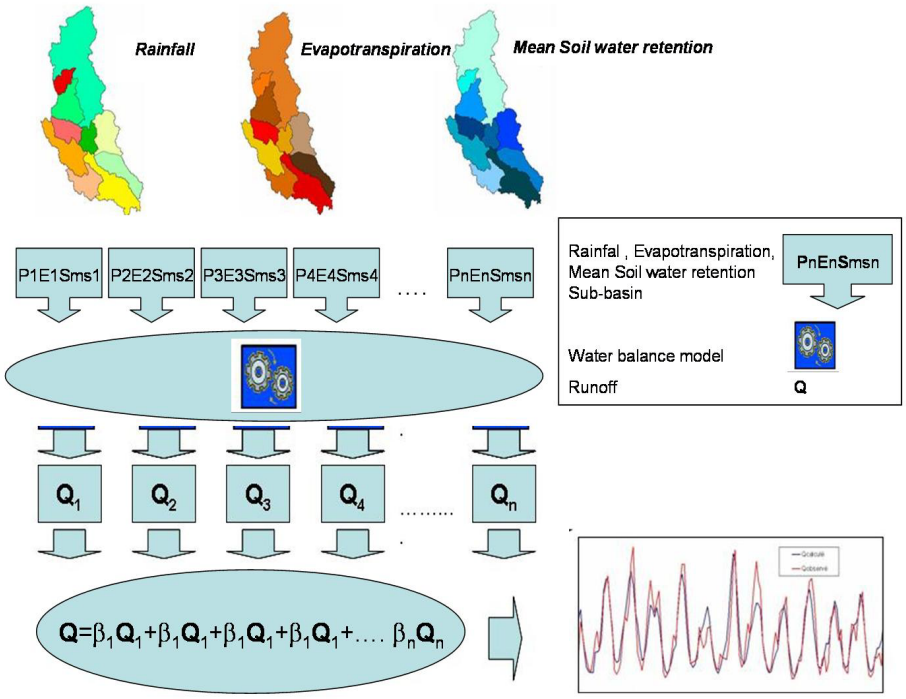

Figure 4. "Semi distributed" approach for the water balance models

Figures 5 and 6 show the results obtained with the two approaches. We note the well behaviour between the simulated and the observed runoff series, both on calibration and on validation periods. The Table 4 gives the statistical indices, so it's possible do determine the most appropriate hydrological model. Vandewiele model seems to be the best, since it presents the greater values of Nash and the smaller values of RMSE and SD residuals. GR2M and ABCD models present similar statistics.

The figures 7a to 7c show the scatter plot and the results of regression analysis for the three models used in the calibration analysis ("Semi distributed approach"). The values of R^2 are more than 0.6 and the Vandewiele model presents the greater values of R^2 (0.8). The seasonal hydrograph of the three models used with the "Semi distributed approach" is shown in Figures 7d and 7e. Vandewiele model presents the better seasonal averages calculated in the flood months (April and May) whereas both GR2M and ABCD model do not simulate well the flood months.

Table 4. Comparison of the results of the three models in reproducing historical runoff in the Ucayali Basin. (The best statistical values are in bold characters)

			Global approach			Semidistributed approach		
Calibration and Validation			GR2M	ABCD	Vandewiele	GR2M	ABCD	Vandewiele
Calibration 1978-1993	Nash		70.4	67.8	71.5	70.1	72.4	81.7
	Qmean	96.2	95.2	94.6	93.3	94.8	94.8	95.9
	RMSE		2.1	2.2	2.0	2.1	2.0	1.6
	SD res.		28.3	29.4	27.4	28.4	26.2	21.1
Validation 1994-1999	Nash		56.9	30.1	65.2	62.3	60.8	71.9
	Qmean	89.0	104.7	121.9	106.7	99.2	108.9	104.8
	RMSE		4.0	5.7	3.9	3.9	4.1	3.4
	SD res.		27.2	29.9	25.0	27.3	23.7	18.9

Qmean: Runoff average (mm); RMSE: Root Mean Square Error; SD res.: Standard Deviation of residuals

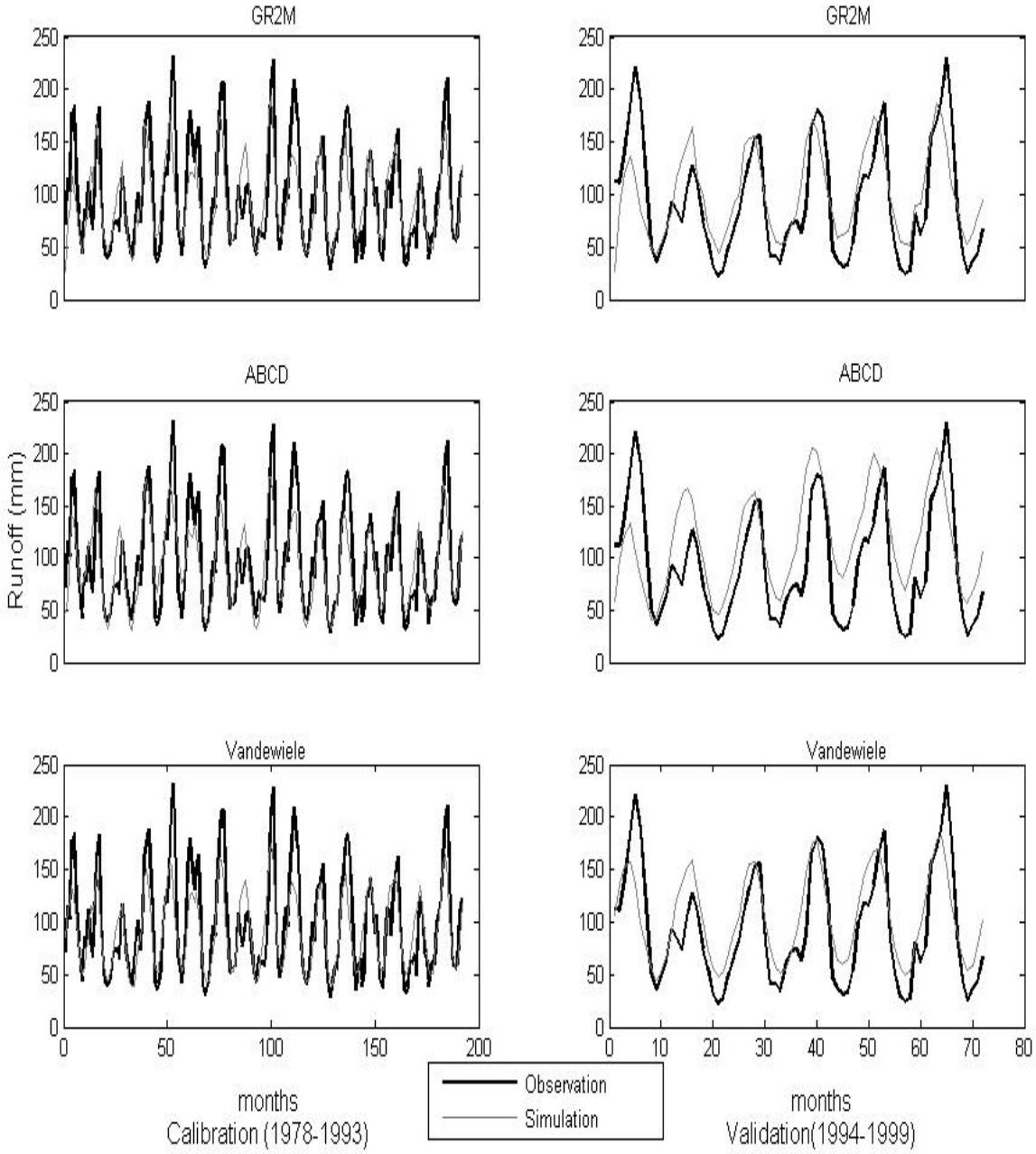

Figure 5. Calibration and validation according to "Global approach".

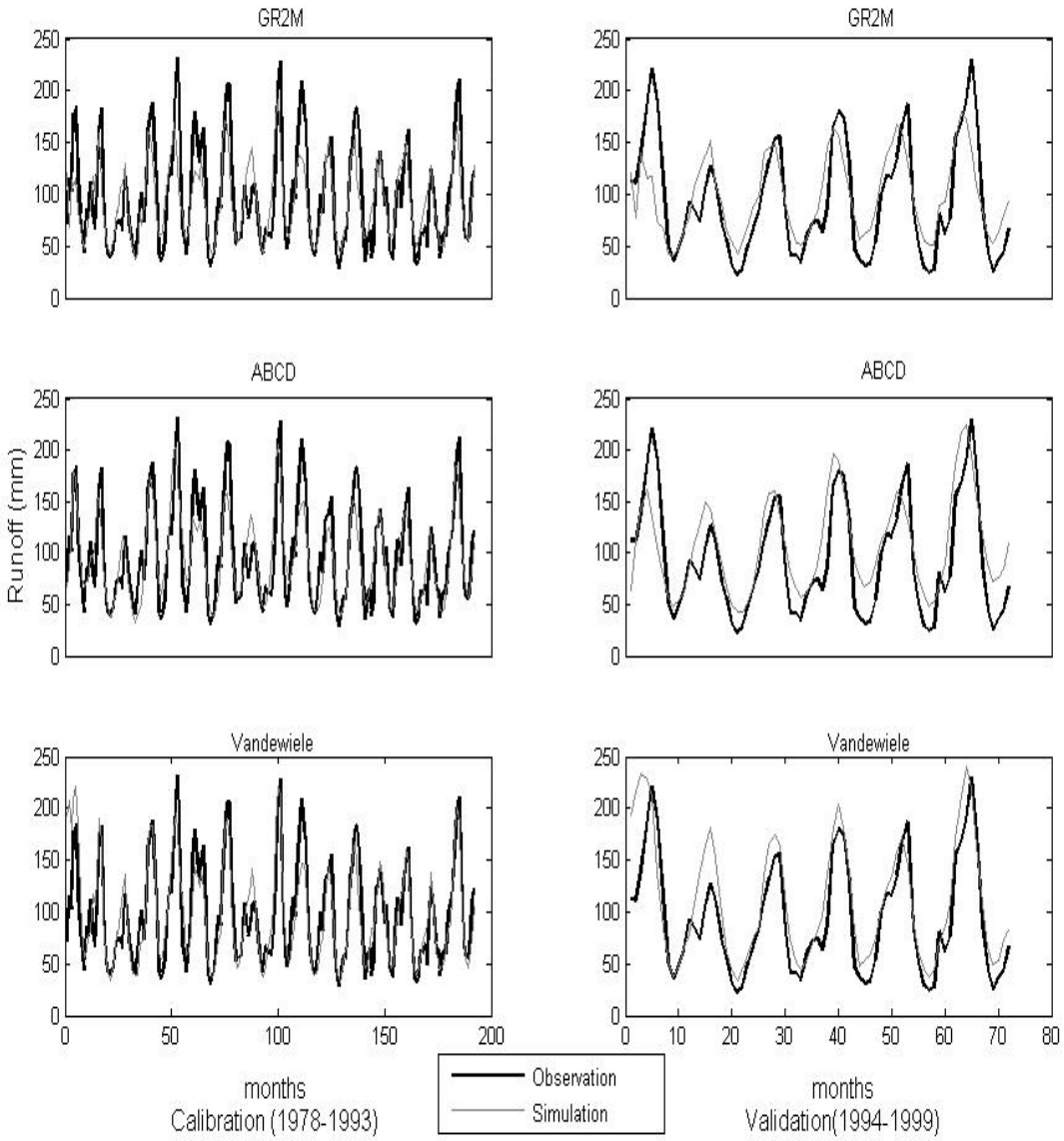

Figure 6. Calibration and validation according to "Semi distributed approach".

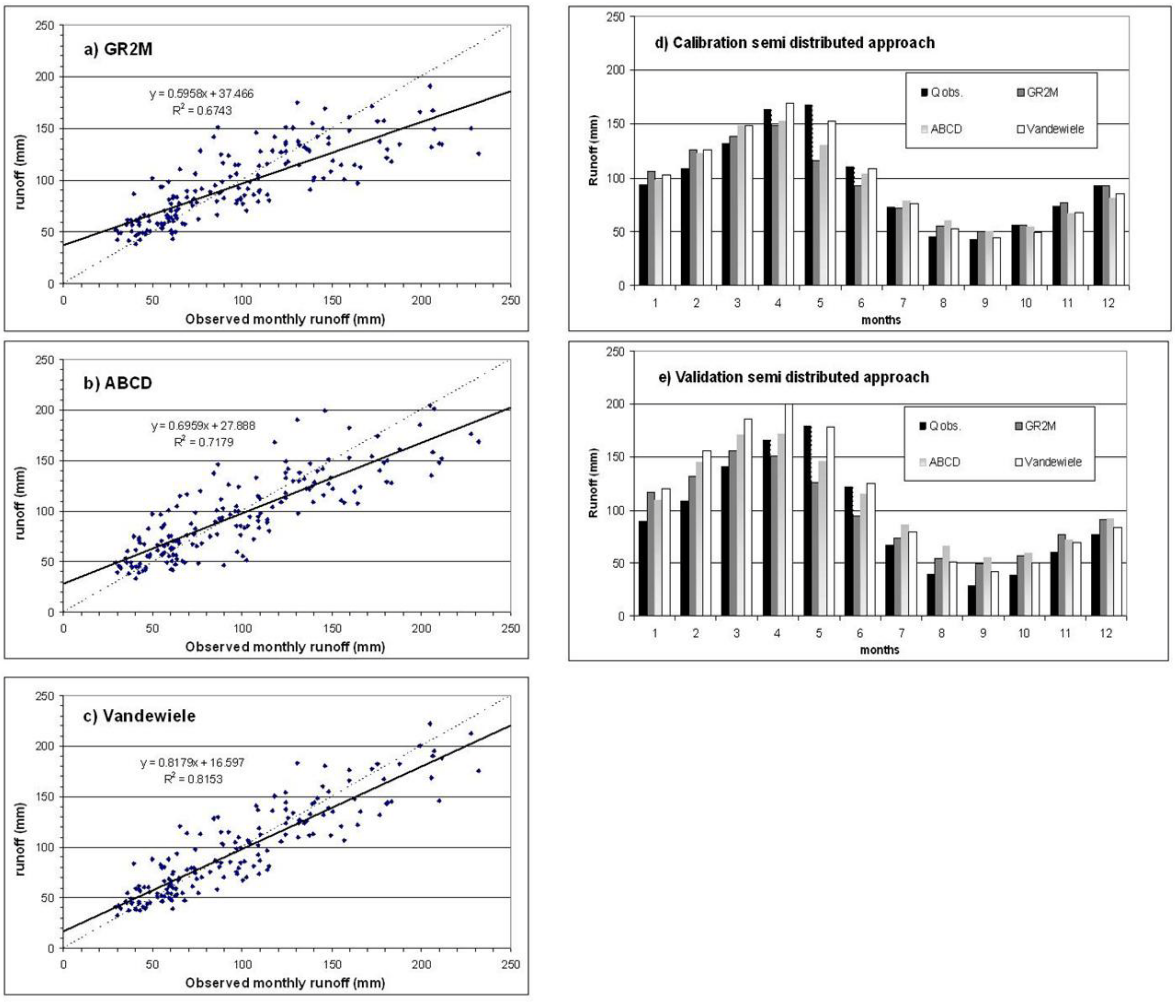

Figure 7. Scatter plots with regression equations of the monthly runoff calculated in calibration procedure with a) GR2M model, b) ABCD model and c) Vandewiele model and seasonal behaviour with the semi distributed approach for d) calibration and e) validation procedure.

CONCLUSIONS

The present work is the first one of its kind to include a large extension of the Amazon Basin in the Peruvian territory. Thanks to the last missions carried out by the HYBAM Project, it was possible to obtain discharge values of the large Amazon basins such as the Ucayali River now. This, together with the rainfall information analyzed from SENAMHI and recently documented for Espinoza *et al.* (2007b) and the last study made by UNESCO (2006), has enabled us to carry out this study.

The lack of runoff information makes it necessary to use this optimal approaches due to the extension of the basins, of course that the optimal idea is to present discharge values in each one of the existing sub-basins.

The evapotranspiration calculated in this work use only the Thornthwaite method because we have just temperature data but others methods will be necessary to do a best analysis of water balance models. Therefore, we present the first water balance modelling over the Ucayali river basin and sub-catchments.

From the results obtained, Vandewiele model seems to be well adapted at this hydrological context. “Semi-distributed approach” shows better results because it takes into account the heterogeneity of climatological and hydrological information at the sub-basin scale. The 3 models tested show Nash values above 60%. Like Niel et al. (2003) described, we can concluded that our models are reliable.

The present document represents the first step for a most important study that would include modelling all the Peruvian Amazon basins. The results obtained in this work can be matter of discussion, although is certain that it represent an advance in applying hydrological models to the Andean part of the Amazon Basin.

4.2 Modélisation au niveau mensuel sur sept sous-bassins des rios Ucayali et Huallaga, et évaluation des impacts du changement climatique sur le régime hydrologique

Une fois ce travail préliminaire de modélisation effectué, en considérant seulement la station de Requena (voir section antérieure), nous avons rassemblé des données de débits à l’exutoire de six sous bassins emboités : Chazuta, Puerto Inca, Tambo, Maldonadillo, Mejorada et Pisac. De plus, il a aussi été possible de construire une base de données à la résolution (0.25° x 0.25°) pour les précipitations, l’évapotranspiration et les sols. Aussi comme le montre l’article ci-dessous qui sera prochainement soumis, il a été possible d’estimer au pas de temps mensuel l’évaluation de l’impact des changements climatiques en utilisant trois modèles de l’IPCC (BCM2, CSMK3 et MIHR) et en considérant deux scenarios A1B et B1.

4.2.1 Monthly hydrological models to predict climatic change impacts on hydrology in the Peruvian Amazon-Andes basin.

WALDO SVEN LAVADO CASIMIRO, DAVID LABAT, JEAN LOUP GUYOT & SANDRA ARDOIN-BARDIN

RÉSUMÉ

Sur le plan hydroclimatologique, le bassin de l’ouest de l'Amazone, autour de la Cordillère des Andes reste encore mal documenté. Dans cette contribution, nous proposons une analyse du comportement hydrologique de deux bassins situés dans le bassin Amazonas-Andes péruvien qui incluent environ 10% de total du bassin amazonien. Cette contribution est basée sur l’utilisation de deux modèles hydrologiques conceptuels (GR2M et MWB3).

Durant ces dernières années, un effort de collecte et de rassemblement de données sur les bassins des rios Ucayali et Huallaga (données issues du réseau du Service National de Météorologie et d'Hydrologie) couplé à plusieurs missions de mesure de débit ont permis de développer une analyse spécifique mensuelle du bilan hydrique.

Les données d’entrées du modèle prennent en compte la distribution spatiale des précipitations, de l’évapotranspiration et de la capacité de rétention en eau des sols (WHC). L'algorithme Shuffled Complex Evolution Metropolis a été employé dans le processus de calibration. On observe que cet algorithme a bien estimé la distribution antérieure des paramètres des modèles et des paramètres optimaux des sous bassins choisis. Les modèles hydrologiques choisis reproduisent raisonnablement bien l'écoulement observé à la fois dans la procédure de calibration mais aussi dans la procédure de validation.

L'analyse de sensibilité montre que l'écoulement est moins sensible au paramètre α dans le modèle de GR2M et est moins sensible au paramètre a3 dans MWB3 dans la plupart des sous basins considérés. Les écoulements annuels simulés pour la période (2008-2099) utilisant deux techniques de downscaling (anomalies et horizons) suggèrent que les impacts du changement climatique sur l'hydrologie varient en fonction du sous bassin considéré mais aussi avec le modèle hydrologique utilisé. Ainsi, les écoulements du fleuve Ucayali à Requena montrent une augmentation (diminution) en utilisant le modèle hydrologique GR2M (MWB3) en considérant les scénarios climatiques A1B et B1 SRES. Les écoulements des sous bassins Chazuta, Maldonadillo et Pisac diminuent tandis que les écoulements des sous bassins Puerto Inca, Tambo et Mejorada augmentent. L'impact le plus important concerne le bassin du Tambo (modèle MWB3 et scénarios A1B). Les écoulements mensuels (2008-2099) montrent une tendance à l'augmentation pour tous les sous bassins excepté le bassin de Pisac en prenant en compte les deux scénarios de SRES et les deux modèles hydrologiques.

ABSTRACT

Whereas this is a region with a complex hydroclimatology, theWestern Amazon basin around Andes cordillera is still poorly documented. In this contribution, we propose an investigation of the hydrological behaviour of two basins located in the Peruvian Amazonas-Andes basin corresponding 10% of total Amazonian basin. This contribution is based on hydrological models using two water balance models (GR2M and MWB3).

During the last years, a strong data-collecting effort in the Ucayali and Huallaga rivers (data from Peruvian National Meteorology and Hydrology Service network) coupled to several discharge measurement missions have made possible to develop some specific analysis such as monthly water balance model study.

Inputs are taking into consideration the spatial distribution of rainfall, evapotranspiration and water holding capacity (WHC). The Shuffled Complex Evolution Metropolis algorithm was used in the calibration procedure. It is observed that this algorithm found well the prior distribution of model parameters and the optimal parameters of the selected watersheds.
Selected models reproduce reasonably well observed flow in the calibration and validation procedure. Sensitivity analysis demonstrates that flow is least sensible to α parameter in GR2M model and least sensible to a_3 parameter in MWB3 in the mostly of watersheds except in Puerto Inca.

Annual flows simulated from the future (2008-2099) using two simples downscaling techniques (Anomalies and Horizons) suggest that impacts of climatic change on hydrology vary with the watershed and with the hydrological model used. Requena River flow increase (decrease) using GR2M (MWB3) hydrological models considering A1B and B1 SRES scenarios. Chazuta, Maldonadillo and Pisac River flows decrease whereas in Puerto Inca, Tambo and Mejorada flows increase. The most important impact is for the Tambo (MWB3 model and A1B scenarios). Changes in monthly flows (2008-2099) suggest increase changes for entire watersheds except Pisac that depicts decrease and increase changes considering both SRES scenarios and both hydrological models.

Keywords: hydrological models, Amazon basin, monthly water balance, climatic change, Peru.

INTRODUCTION

The Amazon Basin (AB) is the largest one in the planet, with a drainage area of 6 200 000 km^2 and mean annual discharge at 209 000 $m^3 s^{-1}$ (~ 5% of all the above-water lands) (Molinier et al., 1996; Marengo, 2006). The AB is one of the regions with the highest rainfall and a major water vapour source in the world (Espinoza et al., 2008). Also, in the AB is possible has extremes events as dramatic drought observed in 2005 (Marengo et al., 2008; Zeng et al., 2008a).

Mostly studies related to climatic change impacts on hydroclimatology over AB focus on Brazil whereas Andeans countries remain still poorly documented. In Peru, measurements of the hydro-climatological variables in the Amazon-Andes basin (PAB) are administrated by the National Meteorology and Hydrology Service, SENAMHI (www.senamhi.gob.pe). Most part of hydrometeorological data is related to climate variables (rainfall, temperature, etc.). Since 2001, the HYBAM program realized in collaboration with SENAMHI, IRD and UNALM (www.ore-hybam.org) carries out flow measurement missions over the largest rivers in PAB (Yerren et al., 2004, Guyot et al., 2007). Results of flow measurement joined to meteorological observation by SENAMHI have permitted to achieve for the first time a data bank over PAB analyzed in this study.

Monthly hydrological models are valuable tools in water resources management, reservoir simulation, drought assessment or long-term drought forecasting (Mouelhi et al., 2006). Several conceptual monthly water balance models are available in the literature, between the models with least parameters, one can mention:

- MOSAZ model (Jayasuriya et al., 1991) explained by Boughton, 2005 who use two free parameters to represent monthly rainfall-runoff transformation over Australia
- GR2M model (Kabouya, 1990, Makhlouf et Michel, 1994, Mouelhi et al., 2006) frequently used over French catchments but also in Western Africa (Paturel et al., 1995; Niel et al., 2003 ; Paturel et al., 2003; Mahe et al., 2005); recently perform GR2M model using only two parameters. A similar two parameter model is developed for large basins over China to predicts the impacts of climate change (Xiong et Guo, 1999 and Guo et al., 2002b). Paturel et al. (2003) using GR2M and Water balance (WBM, Conway et Jones, 1999) models and several set of distributed input data (0.5° x 0.5°) over west Africa exhibit that GR2M model seems to be more robust than the WBM. Niel et al. (2003) observed better performance in spatially distributed data version than in lumped data version using GR2M model.
- Vandewiele et al. (1992) over the NOPEX region develop several series of models with three-parameters and modifications are applied over distinct countries and various climate conditions (see e.g. Vandewiele et Ni Lar, 1998; Xu et Vandewiele, 1995; Xu et al., 1996; Muller-Wohlfeil et al., 2003; Widén-Nilsson et al., 2007).
- ABCD model is applied over several catchments in the United States (Alley, 1985).

Finally, other conceptual monthly models with major number of parameters are found in the literature between them: IPH-MEN model used over large basin in the Amazon region (Tucci,

1998). Hydrological models developed before the early 1980s have a lumped structure and the spatial variation of hydrological variables and models parameters is generally not taken into account (Chen et al., 2007). Distributed models (conceptual basis) at monthly scales were developed on the early 2000s. Guo et al. (2002b) carries out a macro-scale and semi-distributed monthly water balance model (Xiong et Guo, 1999) over China. Recently Chen et al. (2007) over two basin located in central and southern China develop a distributed monthly hydrological model integrating topography and rainfall spatial variations, model is an hybrid of the Xinanjiang model (Zhao et al., 1980) and TOPMODEL (Beven et Kirkby, 1979), simulations results is capable of describing spatial and temporal variations of water balance components.

Literature on water balance models over the Amazon basin often deals with macro-scale level covering the entire Amazon basin (see e.g. Russell et Miller, 1990; Miller et al., 1994; Marengo et al., 1994; Nijssen et al., 1997; Nijssen et al., 2001;Coe et al., 2002; Costa et al., 2002; Coe et al., 2008; among others); and confront to the systematic underestimation problem of rainfall and discharges, due to the lack of information availability over the Amazon basin (Marengo, 2006), also hydrological models based mostly on land surface in the Amazon basin have been developed overall for the rainforest zone focus in Brazil (see e.g. Paz et al., 2006; Valeriano et al., 2006; Collischonn et al., 2007; Collischonn et al., 2008; Tomasella et al., 2008; Zeng et al., 2008b among others).

In Peru, only three works deal with this topic at our knowledge. The first one was developed by BCEOM (1999) that carries out modelling using the GR model (Edijatno et al., 1999), made in several basins in the Pacific drainage, the second was developed by Ordoñez (2001) carried out over a sub-basin in our study area (Pachitea basin), using the IPH-MEN (Tucci, 1998).

Global warming exhibit influence over some global flow patterns (Labat et al., 2004). Also, estimates of climate change as global observed and projected increases in temperature, sea level and rainfall variability are expected will have implications over flow regimes of many rivers around the world (Kundzewicz et al., 2007).

Water use of rivers in the PAB can be classified as agricultural irrigation; hydropower; domestic use; industrial and river navigation. This last principal transport way in villages located in the low zones from PAB. Peru is considered as the third country susceptible to climatic risk (Brooks et Adger, 2003), for this reason climatic changes can produce extreme hydroclimatologic impacts as floods. Hotspots of humanitarian risk relating to flooding (next 20-30 years) are identifies of occur over PAB (CARE, 2008). Also, recent studies describe glacier retreat product of global warming over High Mountain from PAB, as Vilcanota-Quelcaya cordillera (e.g. Silverio et Jaquet, 2005 and Mark et Seltzer, 2005).

Several studies employ as input General Circulation Models (called IPCC models in this study) and/or hypothetical scenarios (sensitivity of flow based in temperature and rainfall changes) coupled with hydrological models for simulate future hydrological processes (see e.g. Mimikou et al., 1991; Sefton et Boorman, 1997; Strzepek et Yates, 1997; Xu et Halldin, 1997; Arnell, 1999; Jose et Cruz, 1999; Limbrick et al., 2000 ; Xu, 2000; Zhang et al., 2000 ; Fontaine et al., 2001; Matondo et Msibi, 2001 ; Middelkoop et al., 2001 ; Guo et al., 2002a ; Menzel et Bürger, 2002 ; Yu et al., 2002 ; Dettinger et al., 2004 ; Drogue et al., 2004 ; Dibike

et Coulibaly, 2005 ; Andersson et al., 2006; Jones et al., 2006; Charles et al., 2007; Hagg et al., 2007; Jiang et al., 2007; Juen et al., 2007; Thodsen, 2007; Salathe et al., 2007; Steele-Dunne et al., 2008; Ardoin-Bardin et al., 2009). In order to explain climatic change impact on hydrology for this study future IPCC models data were used.

This paper has two aims. The first one is to fulfil and compare the performance of two conceptual monthly water balance models with least number of parameters for a context of limited data (rainfall and evapotranspiration) in 7 flow stations located over the PAB. To this end, statistical tests of comparison in models outputs during the calibration and validation procedures were used. Then, sensibilities of models in the selected watersheds were analyzed. The second aim of the paper is to explain climate change impacts over flow regimes (seasonal and annual future simulation, 2008-2099). The future climate change impacts in flows will be analysed using three IPCC models (2 scenarios) over the 2008-2099 period using calibrated parameters of hydrological models calculated before.

STUDY AREA AND AVAILABLE DATA

Hydroclimatological characteristics over PAB

The PAB region occupies 10% of the Amazon basin and is located in the Western Amazonas basin where two distinct natural regions are finding: Amazonian floodplain and Andes, the first consisting of relatively flat lowland plains, the latter formed by some of the steepest and tallest mountain ranges on earth. Hot tropical lowlands near sea level versus freezing cold tropical high mountain peaks at up to 6000m a.s.l. of elevation, nowhere in the world are such dramatic environmental contrasts lying closer together. Naturally, each of these two realms is subject to different, but in many aspects interrelated, sets of physical, geochemical and biologic parameters (ACTO, 2005).

According to UNESCO (2006), the estimate of mean annual rainfall over the PAB region in the 1969-1999 period is nearby 2060 mm. Moreover very high and low rainfall values (between 6000 and 250 mm/year) can be observed in close stations due to the leeward or windward position of stations (Espinoza et al., 2008); maximal rainfall rates occur between November to March and in the high Andes most of the rainfall is produced by convection (Garreaud et al., 2003). The moisture supply for this convection is predominantly the Amazon basin (Fuenzalida et Rutllant, 1987; Vuille et al., 1998; Chaffaut et al., 1998; Garreaud, 1999; Garreaud et al., 2003; Vizy et Cook, 2007).

Mean annual temperature characteristics over the PAB region appear indirectly related to elevation (lower altitude more temperature). Higher seasonal amplitude of mean temperature is observed over the highland close to Andes cordillera than over the rainforest (lowlands). Mean annual of temperature over the PAB region considering the 1969-1999 period is estimated at 23 °C with ranges of temperature from 6 °C to 19°C between 500 to 6 780 m a.s.l. (highlands) and from 19 °C to 30°C between 400 to 1 000 m a.s.l. (lowlands) (UNESCO, 2006).

Over the middle land and highland (around the Andes mountain) where lithosols predominate (Viera, 1975a), evapotranspiration is less than over the rainforest. Using Thornthwaite method

(Thornthwaite, 1948b) evapotranspiration is estimated at 1343 mm per year (~3.7 mm per day) in the PAB (UNESCO, 2006).

The Peruvian and Ecuadorian Amazon-Andes basin shows in the Tamishiyacu station an mean discharge of 25 000 $m^3.s^{-1}$, seasonal coefficient of variation of 0.24 and negative trend of -0.81% per year in the 1970-1997 period (Espinoza et al., 2006b). According to Espinoza et al. (In Press), annual flow trends over the 1990-2005 period show decreasing trend, significant at 99% level, for minimum discharges in Ucayali river and non significant increasing trend in maximum and mean discharges in Marañon river. Marañon river (upstream Hullaga river) in the San Regis station and Ucayali river in the Requena station exhibit the same annual discharge (~ 14 000 m^3 s^{-1} Guyot et al., 2007).

Watersheds and available data

Selected watersheds are inside Huallaga and Ucayali river basins and they are totally within Peru. Basins areas are of 89 654 km^2 over Huallaga river basin and 35 0287 km^2 over Ucayali river basin. Boundaries of watersheds are in function of flow station (Figure 1 and Table 1). Six watersheds are within the Ucayali river system, only Chazuta watershed is within Huallaga river system. In summary two watersheds are over the Andes zone (Mejorada within Mantaro basin and Pisac within Vilcanota basin) whereas the others seven watersheds (Requena, Chazuta, Puerto Inca, Maldonadillo, Tambo) are within the rainforest (lowland). Watersheds subdivision is based on the Digital Elevation Model (DEM) provided by the National Aeronautics and Space Administration (NASA) through the Shuttle Radar Topography Mission (SRTM - www2.jpl.nasa.gov/srtm). SRTM data is available at 3 arc second (~ 90m resolution). A detailed description of this DEM can be found in Farr et al., 2007.

Weather stations used in this work are part of the SENAMHI network. 77 weather stations were used: 58 for rainfall and 48 for temperatures (Figure 1), of which 24 stations are located over the Huallaga basin and 53 over the Ucayali basin. Rainfall and temperature data (mean, maximum and minimum) available is a monthly scale and includes the period from January 1965 to December 2007. A procedure for quality analysis in temperature data is first applied. After a visual detection of suspect outliers in monthly plots, box plots graphics are computed for the suspect month; doubtful temperature values are those that exceed the third quartile plus three times the interquartile range. Suspect outliers values are compared to values of the corresponding period in nearby stations (over similar physiographic zone). The data is discarded only if a mismatch is detected through both criteria. Gaps were filled up by a multiple correlation method between nearby geographical stations.

Rainfall data over the 1965-2003 period are also validated using the Regional Vector Method – RVM (Hiez, 1977 and Brunet-Moret, 1979) : four homogeneous regions with similar interannual variability are found over Ucayali and Huallaga basin (Espinoza et al., 2008).
Evapotranspiration standard is assumed by the FAO Penman-Monteith method (Allen et al., 1998). Lavado et al., submitted-a, exhibits satisfactory relationship between FAO Penman-Monteith and Hargreaves-Samani (HE) method (Hargreaves et Samani, 1985); the modified Hargreaves-Samani method (HEm) is used for our region of study, given by:

$$HE = \frac{0.0023(T + 17.8)(T\max - T\min)^{0.5} Ra}{\lambda} \quad (1)$$

$$HEm = 0.6484 * HE + 1.146 \quad (2)$$

Where HEm is Ev (mm per day), λ is the latent heat of vaporization (MJ kg^{-1}), T is mean temperature (°C), Tmax is maximum temperature (°C), Tmin is minimum temperature (°C), Ra is extraterrestrial radiation (MJ m^{-2} d^{-1}) computed following Allen et al. (1998) method . One notes that λ in this study is assumed as 2.45 MJ Kg^{-1} as suggested by Allen et al. (1998).

In order to work with soil data, we have used the methodology given by Dieulin et al., 2006, based on the data from the Digital Soil Map of the World (FAO/UNESCO, 1981). FAO defines soil units depending on the horizons' depth and texture of its components, which are grouped in classes according to water holding capacity. The water holding capacity depends mainly on the granulometric characteristics of the soil and on the depth of the soil exploitation by the plant which is assimilated to the depth of the root. The method developed by FAO to compute the water holding capacity is based on the plants roots depth, plant coverage and the standardized suction limits (wilting point and field capacity). For each type of soil, we have evaluated water holding capacity, using 3 values: minimum, maximum and mean of the limits of the considered soil types. Soil water holding capacity is named **WHC** in this study.

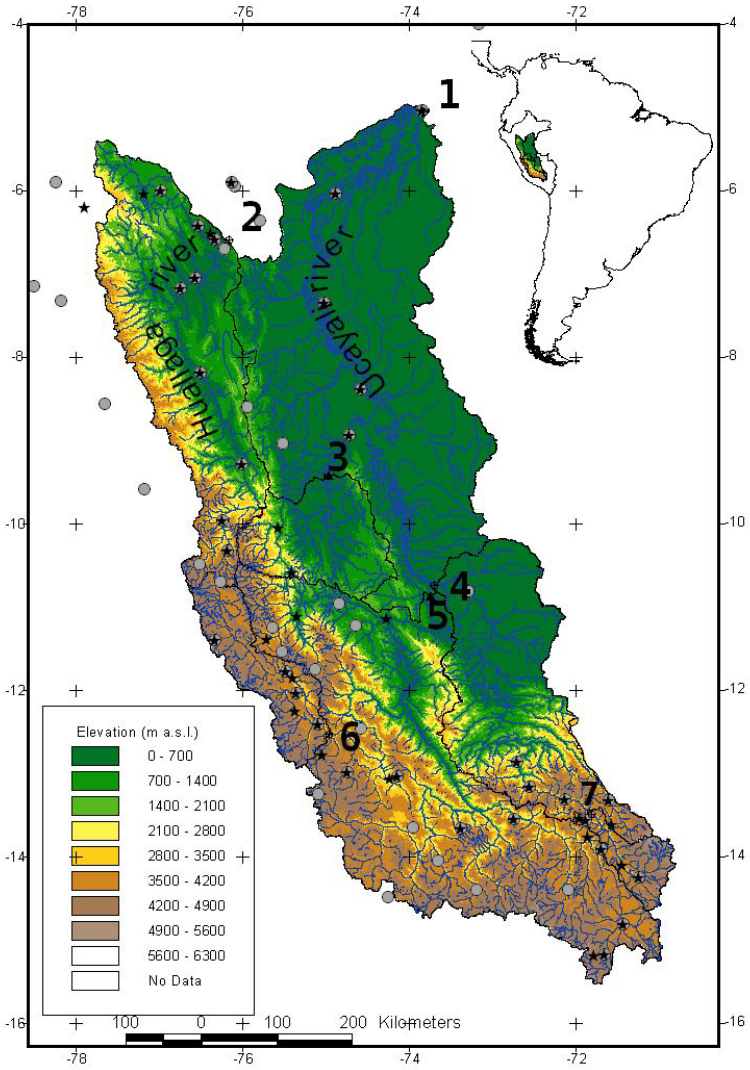

Figure 1. Hydrological network and elevations over the Ucayali and Huallaga basins, take into account Requena flow station (1 over Ucayali river) and Chazuta flow station (2 over Huallaga river); numbers are flow stations: 3 Puerto Inca station over Pachitea river; 4 Maldonadillo station over Urubamba river; 5 Tambo station over Tambo river; 6 Mejorada station over Mantaro river and 7 Pisac station over Vilcanota river. Circles markers are rainfall station and star markers are temperatures stations.

Table 1. Flow stations, locations, drainage area (Dr. Ar.) and flow record used in this study.

Code	Flow Station Watershed	River and Basin name	Latitude (°S)	Longitude (°W)	Altitude (m a.s.l.)	Dr. Ar. (Km2)	Flow record
1	Requena	Ucayali	5.05	73.84	200	354416	janv-1993/dec-2007
2	Chazuta	Huallaga	6.58	76.18	200	69463	janv-1999/dec--2007
3	Puerto Inca	Pachitea	9.38	74.96	249	22661	janv-1998/dec-2007
4	Maldonadillo	Urubamba	10.74	73.71	287	60301	janv-1988/dec-2007
5	Tambo	Tambo	10.85	73.71	290	135252	janv-1988/dec-2007
6	Mejorada	Mantaro	12.52	74.93	2819	17244	janv-1995/dec-2007
7	Pisac	Vilcanota	13.43	71.84	2971	7129	janv-1986/dec-2007

Summary of principal hydrometeorological characteristics, morphology, water holding capacity and land cover characteristics (Hansen et al., 1998) of the watersheds are shown in Table 2.

Table 2. Climatologic and physical characteristics of the two study basins and their nested watersheds. R: Rainfall; E: Evapotranspiration; WHC: soil water holding capacity; F: Flow

	Ucayali basin						Huallaga basin
Code	1	3	4	5	6	7	2
Watershed	Requena	Puerto Inca	Maldonadillo	Tambo	Mejorada	Pisac	Chazuta
Mean annual R (mm year^{-1})	1391	1633	985	754	456	315	1153
Mean annual E (mm month^{-1})	103	78	83	85	54	47	86
Mean annual F (m^3 s^{-1})	12691	3806	2289	1824	81	58	2934
Specific discharge (mm)	93	435	98	35	12	21	109
Total length of rivers (Km)	71807	4652	12571	25217	3388	1243	14136
Mean Altitud (m a.s.l.)	1813	1223	1877	3400	4263	4319	1773
Minimum Altitud (m a.s.l.)	45	175	185	208	2835	2964	180
Maximum Altitud (m a.s.l.)	6306	4922	6306	5777	5670	6306	5275
Slope (%)	21	26	27	32	21	28	33
Maximum WHC (mm)	207	111	177	135	98	94	127
Minimum WHC (mm)	174	83	152	105	75	79	99
Mean WHC (mm)	191	97	165	120	87	87	113
Land Cover: -Water (%)	1	0	1	1	1	2	0
-Evergreen Broadleaf (%)	57	73	57	16	2	0	58
-Woodland (%)	11	13	11	20	15	11	16
-Wooded Grassland (%)	7	3	7	14	13	13	8
-Grassland (%)	14	3	13	30	51	55	7

In order to generate future climate, data of models and scenarios emissions included in the recent report by the IPCC (Randall et al., 2007) were used. 2 DVD with IPCC models and scenarios data for South America (www.mad.zmaw.de) were acquired. IPCC data output involve 10 experiments, 3 of which were used in this study: climate of the 20th Century experiment (scenario 20C3M); 720 ppm stabilization experiment (scenario SRES A1B) and 550 ppm stabilization experiment (scenario SRES B1), for more description of scenarios see Nakicenovic et al. (2000). IPCC models and scenarios were selected for availability of rainfall and evapotranspiration (using equation 2) data and for the better resolution output. 20C3M was used to compare actual climatology (1965-2000) whereas two later experiments are future scenario data (2008-2100 in this study). Thus, three general circulation models given by IPCC were used: In the scenario 20C3M: BCM2 model (Bjerkness Centre for Climate Research, Norway) with resolution of 1.9° per 1.9°; CSMK3 model (Commonwealth

Scientific and Industrial Research Organisation (CSIRO) Atmospheric Research, Australia) with resolution roughly of 1.9° per 1.9° and MIHR (Center for Climate System Research (University of Tokyo), National Institute for Environmental Studies, and Frontier Research Center for Global Change (JAMSTEC), Japan) with resolution approximatly of 1.1° per 1.1°. The scenario SRES A1B use output data of BCM2, CSMK3 and MIHR models while the scenario SRES B1 use output data of CSMK3 and MIHR models. BCM2 model with scenario SRES B1 data was removed for exhibit doubtful data in maximum temperature variable.

MONTHLY HYDROLOGICAL MODELS

GR2M Model

The GR2M model version used in this study is given by Niel et al.(2003), and is based in GR2M (Edijatno et Michel, 1989 and Kabouya, 1990), and reviewed by Makhlouf et Michel (1994), this model is a two reservoirs conceptual model. The reservoir H has a capacity maximum A (WHC) that carries out the simulation of discharge at monthly scale, from rainfall data and mean monthly evapotranspiration over a basin. The concept pattern of the model is shown in Figure 2a, where the parameters of model are X1, X2 and α.

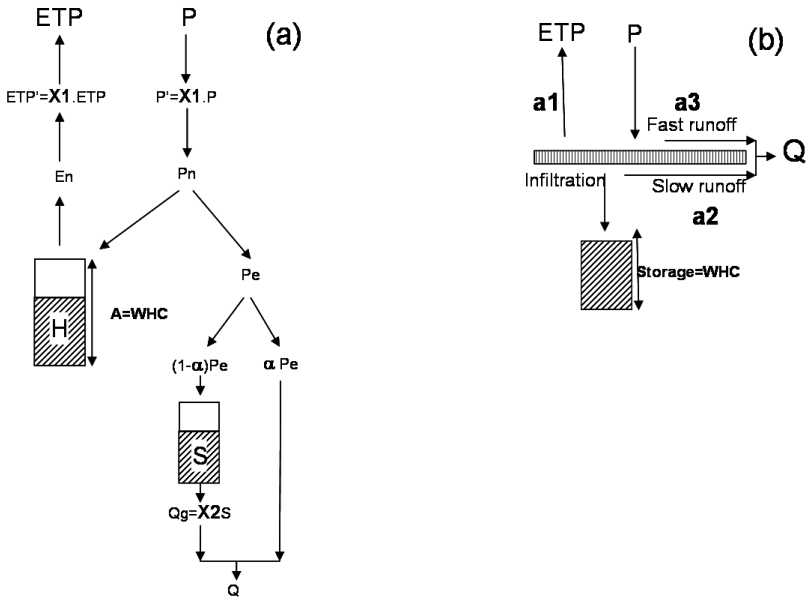

Figure 2. Scheme of Water balance models a) GR2M model with parameters X1, α and X2 b) MWB3 model with parameters a_1, a_2 and a_3. WHC: Soil water holding capacity.

MWB3 Model

This model is based in Vandewiele model(Vandewiele et al., 1992) and the version used in this study is given by Xu (1999). Figure 2b describe scheme of MWB3 model. This model is based on the water balance equation

$$Sm_t = Sm_{t-1} + P_t - EPT_t - Q \quad (3)$$

where Sm_{t-1} is the state of the soil moisture storage (WHC) at the end of month t-1 and P_t, EPT_t and Q are rainfall, actual evapotranspiration and runoff during month t, respectively. Actual evapotranspiration is computed according to Xu (1997) as:

$$Et_t = \min(ETP_t(1 - a_1^{\frac{W_t}{EPT_t}}), W_t) \quad (4)$$

where a_1 is the first parameter and takes values between 0 and 1. $W_t=P_t+Sm_{t-1}$ is the available water. Monthly runoff is distinguished between slow runoff

$$Q_S=a_2(Sm_{t-1})^2 \quad (5)$$

where the parameter a_2 is positive. Rainfall P_t causes a fast runoff Q_f depending on the parameter a_3, alter a partial neutralization of the ETP, that reduces it to level Pn:

$$P_n = P_t - ETP_t(1 - \exp(-\frac{P_t}{ETP_t})) \quad (6)$$

$$Q_f = a_3(Sm_{t-1})^2 P_n \quad (7)$$

where a_3 is positive. Monthly runoff Q outside the basin is the sum of both runoffs: $Q=Q_s+Q_f$.

METHODOLOGY

Distributed input data strategy and models parameterisation

Rainfall and evapotranspiration are spatially interpolates in cells from 0.25° by 0.25° (~ 27.8 per 27.8 km), based on Krigging method (Oliver et Webster, 1990,Deutsch et Journel, 1992,Vauchel, 2005b). Using the Digital Soil Map of the World (FAO/UNESCO, 1981) and based on its water capacity, we intersected these values in our region of study obtained at 0.25° by 0.25° grids of maximum, minimum and mean WHC, following the methodology given by Dieulin et al., 2006. Then, we have one distributed data set for rainfall and evapotranspiration. Also, three data set of WHC (minimum, mean and maximum). Figure 3 shows procedure of distributed input and output data used in this study.

GR2M parameters (see Figure 2a) are described as follow (Niel et al., 2003): X1 parameter is adjust multiplying in the same proportion to rainfall and evapotranspiration, and ranges from 0 to 1; α parameter multiplied to effective rainfall (Pe) is flow direct while the rest flow (1-α). Pe into the gravity drainage reservoir, α is ranges from 0 to 1; finally the discharge of second reservoir is defined through a parameter X2 with ranges from 0 to 1. MWB3 parameters (see Figure 2b) are described above and in order that all the parameters be expressed in the same order of magnitude (Vandewiele et al., 1993) cited by Niel et al. (2003) for this study a_1, a_2 and a_3 parameters in MWB3 models are ranges from 0 to 1.

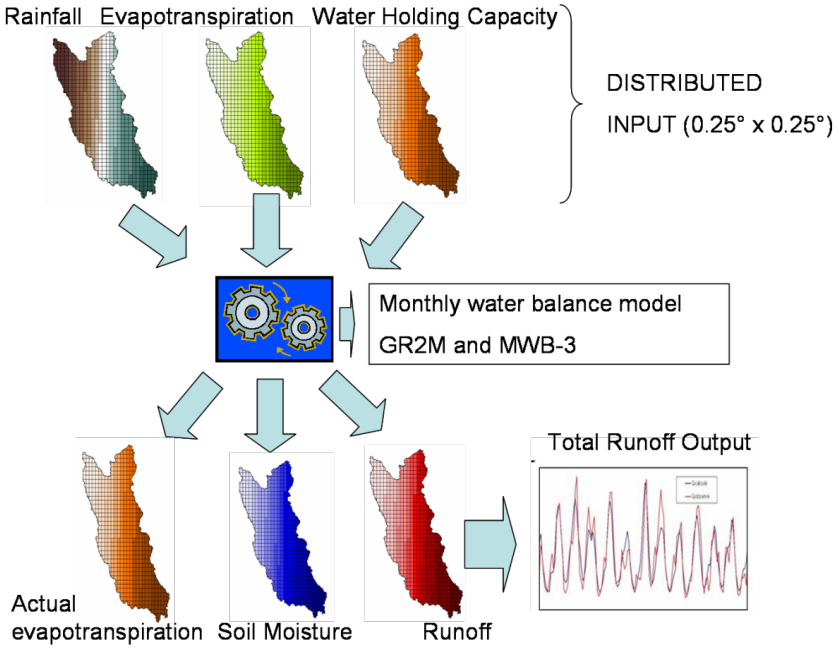

Figure 3. Procedure of distributed input and output of monthly water balance models used.

Calibration procedure

In this study automatic calibration is carry out using Shuffled Complex Evolution Metropolis algorithm (SCEM-UA), that is a modified version of the original SCE-UA global optimization algorithm (Duan et al., 1992) and use Metropolis Hastings strategy (Metropolis et al., 1953; Hastings, 1970), for detailed description of this method see Vrugt et al. (2003). SCEM-UA search strategy to generate a sequence of parameter sets $\{\theta_1, \theta_1, \ldots, \theta_n\}$ that adapts to the target posterior parameter distribution p(θ\y). The SCEM-UA algorithm starts with generating an initial population of *s* parameter sets sampled from the joint prior parameter distribution *p*(θ). The latter constrains the parameter space and represents the belief about the parameters before any data are collected. Independent uniform prior parameter distributions between realistic lower and upper bounds are typically adopted for each parameter in θ. This implies that the information in the data, expressed by the likelihood function, should dominate the form of the resulting posterior distribution. Note that the assumption of prior independence among the parameters is by no means necessary and can be relaxed only at the cost of making computations more burdensome.

Assuming that the residuals are mutually independent, normally distributed with a constant variance, the likelihood of a parameter set θ for describing the observed data (Q_o) is computed using Box et Tiao (1973):

$$L(\theta / Q_o, \beta) = \exp\left[-\frac{1}{2}\sum_{j=1}^{n}\left|\frac{Q_{oj} - \hat{Q}_{oj}(\theta)}{\sigma}\right|^2\right] \qquad (8)$$

in which $\hat{Q}_o$ is a n × 1 vector of models predictions, Q_o denote the time series of observed outputs (observed flow).The parameter of the error model, i.e., $\beta = \sigma$, is treated as a hyperparameter whose uncertainty is accounted for by marginalisation.

Once the SCEM-UA algorithm has converged to a limiting distribution, the covariance matrix of the parameters (P) within this distribution can be computed. This matrix P contains all the necessary information to infer the identifiability of the parameters and to assess how many parameters are supported by the data. According to Vrugt et al. (2003), the stationary posterior distribution corresponding to the likelihood criterion specified in equation 8 was estimated using a population size of 100 points in combination with a total of 10000 model evaluations. Moreover, we use a uniform distribution on θ as the prior distribution p(θ).

Models performance

In order to evaluate the performance of monthly water balance models different statistical tests are available in the literature. The correlation coefficient (R^2) is by far the most commonly used by the scientific community. Unfortunately, it exhibits some limitations that results in poor measure of model performance (Legates et McCabe, 1999). Therefore, it is essential to use other statistical tests to obtain the best goodness of fit. In hydrological models two test are commonly used: Nash-Sutcliffe efficiency **Nash** (Nash et Sutcliffe, 1970) and relative volume error expressed in percent **%V** . Moreover, two others statistical were used in this study: the root mean square (**RMSE**) and the seasonal relative bias (**SB**). Nash, %V, RMSE and SB are defined as:

$$Nash = 100 \times \left[1 - \frac{\sum_{j=1}^{n} \left(Q_{o,j} - Q_{s,j} \right)^2}{\sum_{j=1}^{n} \left(Q_{o,j} - \overline{Q_o} \right)^2} \right] \quad (9)$$

Where, $Q_{o,j}$ is the observed value; $\overline{Q_o}$ is the mean of the observed values; $Q_{s,j}$ is the model simulated values; n is the number of data points. The model is better when a Nash value is close to 100%. Nash et Sutcliffe (1970) say that there is nothing precise in the meaning of this criterion because the degrees of freedom of the model are unknown. However, it can be stated that a criterion of less than 60% does not provide a satisfactory agreement between the observed hydrograms and the ones simulated by the model (Niel et al., 2003).

$$\%V = 100 \times \left[\frac{\sum_{j=1}^{n} Q_{s,j} - \sum_{j=1}^{n} Q_{o,j}}{\sum_{j=1}^{n} Q_{o,j}} \right] \quad (10)$$

%V ideal is close to 0, positive values indicate over estimation and negative values indicate under estimation of simulated values for the models. The RMSE is frequently used to measure the differences between values simulated by a model and the observed values, being the measure of non-systematic variation between two data series used as an index for performance evaluation (Szilagyi et al., 2007). The RMSE is given by:

$$RMSE = \frac{1}{n} \sqrt{\sum_{j=1}^{n} (Q_{\grave{a},j} - Q_{s,j})} \quad (11)$$

Finally, a seasonal relative Bias (SB) is used to compare seasonal values:

$$SB = \frac{1}{n} \sum_{j=1}^{n} \left(Q_{os,j} - Q_{ss,j} \right) \quad (12)$$

Where, $Q_{os,j}$ are the seasonal observed values and $Q_{ss,j}$ is the model seasonal simulated values, n is equal to 12 (monthly averages of total data record). Larger value of RMSE and absolute SB indicate lesser accuracy of the model.

Simple downscaling approaches for future climate

Availability of future data describe above is a monthly scale; three IPCC models were interpolates to 0.25° per 0.25° over our region of study. In order of use IPCC outputs, two simple methods of downscaling were used following the methodology given by Ardoin-Bardin et al. (2009):

a)**Anomalies Scenarios**, given for the next equation:

$$Ano_{GCM,i,j} = \frac{\left(X_{GCM,i,j} - \overline{X}_{GCM,i}\right)}{\sigma_{GCM,i}} \quad (13)$$

Where: X_{GCM} is monthly value simulated for the IPCC models, $\overline{X}_{GCM}$ is mean monthly of simulated IPCC models in the reference period (1965-2000), σ_{GCM} is monthly standard deviation of simulated IPCC models in the reference period. Future climate (2008-2099) using anomalies scenarios are downscaling for rapport to observed data over the reference period as:

$$X_{SCEN,i,j} = \overline{X}_{ob,i} + (Ano_{GCM,i,j} \times \sigma_{ob,i}) \quad (14)$$

Where $\overline{X}_{ob}$ is mean observed monthly in the reference period, σ_{ob} is standard deviation observed monthly in the reference period.

b) **Horizons Scenarios**, given for the next equation:

$$\Delta_{HOR,i,j} = 100 \times \frac{\left(\overline{X}_{HOR,i} - \overline{X}_{REF,i}\right)}{\overline{X}_{REF,i}} \quad (15)$$

Where: $\overline{X}_{HOR}$ is monthly mean value for the simulated horizons given (2020, 2050 or 2080), $\overline{X}_{REF}$ is monthly mean value in the reference period. Future climate (2008-2099) using horizons scenarios are downscaling for rapport to observed data in the reference period as:

$$X_{SCEN,i,j} = X_{ob,i} \times \Delta_{HORi,j} \quad (16)$$

Where X_{ob} is mean observed monthly value for one year pull randomly in the reference period.

RESULTS

ANALYSIS OF MONTHLY WATER BALANCE MODELS

Initial soil water holding capacity (WHC)

Distributed data sets used in the monthly water balance models include: one set of rainfall, one set of evapotranspiration and three sets of WHC (minimum, mean and maximum); i.e. 3 runoff outputs for everyone selected watershed. In order to evaluate better initial WHC for each watershed, statistical R^2, Nash, %V, RMSE and SB were used. Table 3 exhibits these statistical and the better performance obtained (gray box), for calibration and validation procedure of hydrological models. Then, WHC minimum calculates better the observed flow for all the selected watersheds using GR2M model. MWB3 model exhibits in the watersheds as better initial input the: WHC maximum in Requena, Puerto Inca, Maldonadillo and Mejorada. WHC mean in Chazuta and Pisac whereas WHC minimum in Tambo.

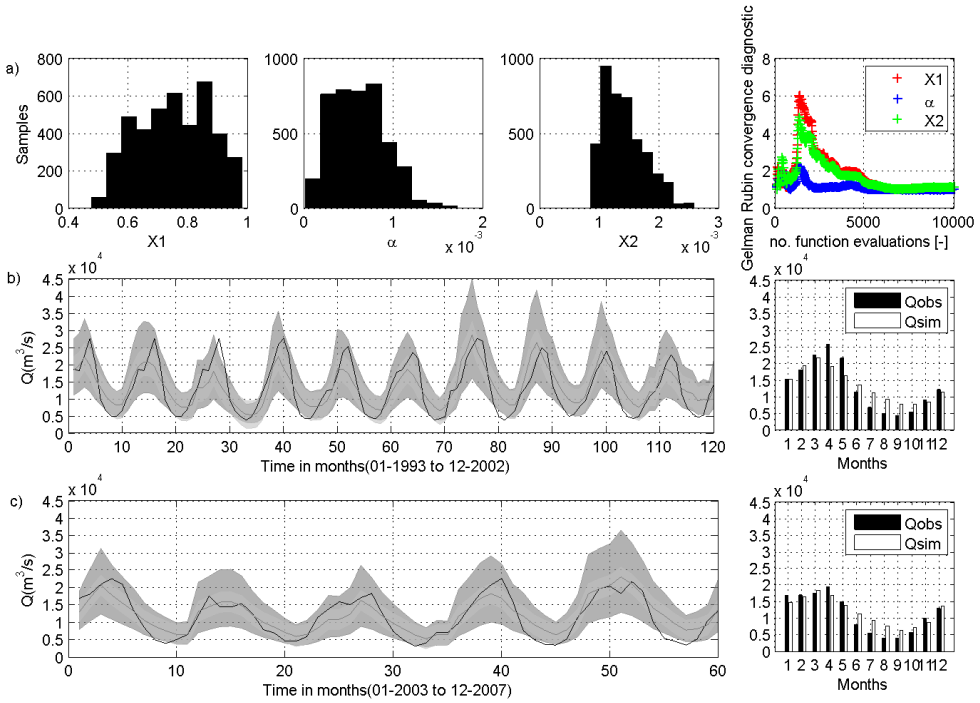

Figure 4. Calibration and validation procedure for GR2M model over the Ucayali basin (Requena watershed): a) histograms of parameters in the model and evolution of the Gelman and Rubin scale reduction). b): hydrograph prediction uncertainty for the calibration period (01/1993 to 12/2002) and monthly observed (Qobs) and simulated flows (Qsim). c): hydrograph prediction uncertainty for the validation period (01/2003 to 12/2007) and monthly observed (Qobs) and simulated flows (Qsim). Observed flows are represented by the black line. The gray line denotes simulated flow. The dark shaded area denotes the prediction uncertainty that results from parameter uncertainty. The light shaded area denotes the additional prediction uncertainty that results from model and measurement uncertainty.

Parameters optimization

SCEM-UA algorithm was carries-out with a 10 000 samples generated after convergence, this article non clear in detail sequence of SCEM-UA for more details see Vrugt et al. (2003). Convergence of samples was evaluated using the Scale Reduction score defined by Gelman et Rubin, 1992. If the scale reduction score is less than 1.2, samples is considered to be

converged; otherwise, more runs are needed. For illustrative purposes and due to the limit of the length of the paper only better models in the selected watershed are shown. Then, Figures 4a, 5a, 6a, 7a, 8a, 9a and 10a exhibit parameters histograms and Gelman Rubin convergence diagnostic. Convergences of Gelman Rubin diagnostic are before of 5000 simulations for all the watersheds except for Requena watershed (convergence after of 5000 simulations).

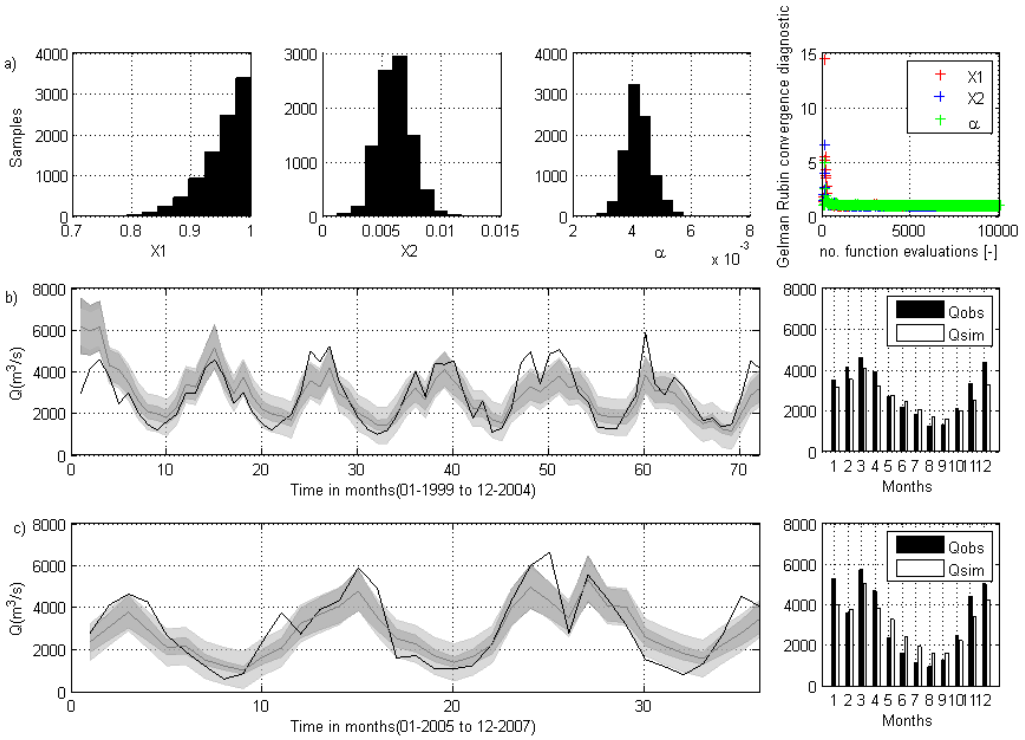

Figure 5. As in 4 but for GR2M model in the Huallaga basin (Chazuta watershed). Calibration period (01/1999 to 12/2004) and validation period (01/2005 to 12/2007).

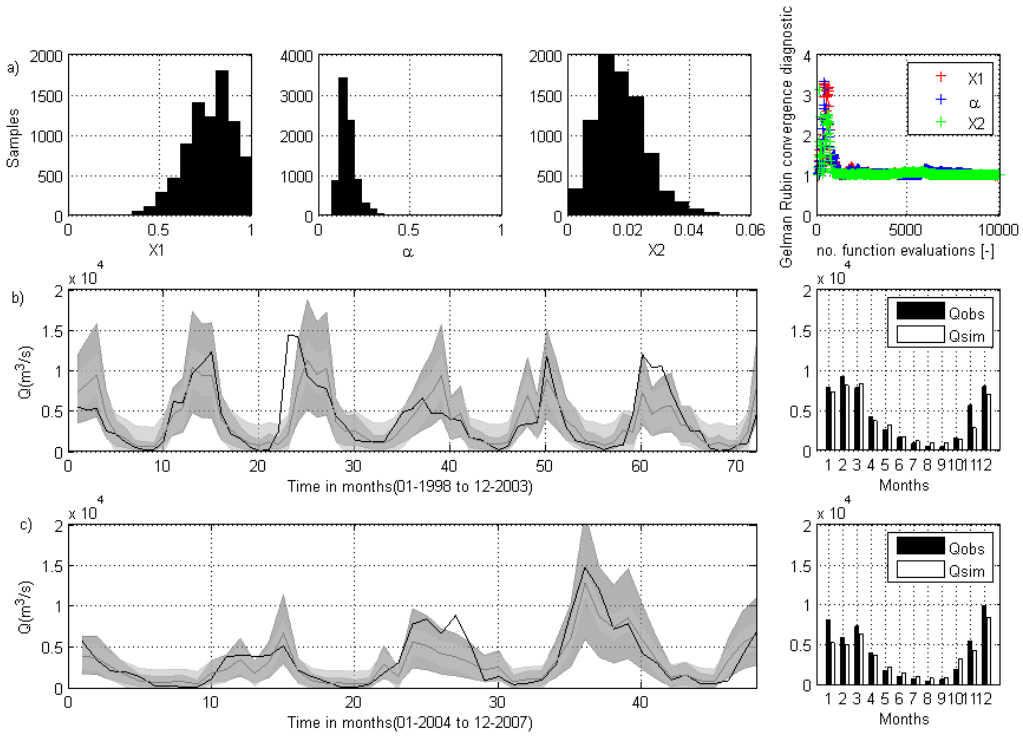

Figure 6. As in 4 but for GR2M model in the Pachitea basin (Chazuta watershed). Calibration period (01/1998 to 12/2003) and validation period (01/2004 to 12/2007).

GR2M model parameters samples exhibited non-normal distribution in Requena watershed (Figure 4a), the others watersheds exhibit normal distribution for parameters α and X2 whereas X1 parameter is distributed close to 1 with values in ranges from 0.75 to 1. MWB3 model parameters samples show mostly normal distribution for all the selected watersheds. That is to say, in the histograms of parameters samples for both models: boundary of parameters occupy relatively small range, except for GR2M in Requena watershed (Figure 4a), these results indicate better identification of parameters limits for MWB3 model than for GR2M model.

The summarising statistics of parameters samples using SCEM-UA optimization procedure for GR2M and MWB3 models are reported in Table 4. Then, the mostly of optimal parameters of GR2M and MWB3 models are close to mean statistical except over Puerto Inca watershed. Correlation coefficients of parameters samples show in Table 4 exhibit significant inverse relationship between X1 with α and X2. This correlation can be explained by the balance between the production and transfer functions during calibration procedure in GR2M model. Correlation coefficients for MWB3 parameters show inverse significant correlation between a_2 and a_3 parameters. This correlation can be explained by the compensation between slow and fast runoff, descript in the scheme of MWB3 model.

In French basins α parameter in GR2M model is considered equal to 0.2 (Makhlouf et Michel, 1994) and α equal to 0 for western and central Africa basins (Niel et al., 2003), α parameters estimated over PAB watersheds show distinct values and are essential in the calibration procedure.

Better monthly water balance model

The Table 3 report the better model for the selected watershed using statistical tests of model performance. Statistical tests exhibit close values for GR2M and MWB3 in the selected watersheds. However, found that GR2M model is better in Requena, Chazuta, Puerto Inca and Maldonadillo watersheds while Tambo, Mejorada and Pisac watersheds are better using MWB3 model. The calibration and validation periods for the selected watersheds are also shown in Table 3. Hydrographs of better models over the selected watershed are presented. Then, Figures 4b, 5b, 6b, 7b, 8b, 9b and 10b show a plot considering the calibration period from: observed flow (dark line), simulated flow (gray line), the prediction uncertainty associated with only parameter uncertainty (dark shaded area), the prediction uncertainty associated with the total error in terms of modelling simulations (light shaded area) and means monthly of observed and simulated flows. Similar last description is valid for the Figures 4c, 5c, 6c, 7c, 8c, 9c and 10c but considering validation period. Hydrographs of calibration and validation periods show that the simulated flow of the better models reproduce the observed flow reasonably well. Prediction uncertainty associated to parameter uncertainty and prediction uncertainty associated with the model simulations show large shaded area especially for GR2M over Requena, Chazuta and Puerto Inca watersheds. These last results can be linked for errors in input data or model structure (Feyen et al., 2007), other watershed show small shaded area associated to prediction uncertainty. Monthly means show for the calibration and validation periods (better models selected) mostly under estimation for the monthly floods (~ December to May) and over estimation for the monthly low water (~ June to November).

Sensitivity analysis

Sensitivity analysis was carried out for the selected watersheds to evaluate and quantify the effect of the parameters variations on model output, this methodology is adapted from St-Onge et al. (2007) and Chen et al. (2007). Relative changes of mean annual flow (ratio of flow change to annual mean flow simulated for the optimal parameter dF/F) g enerating of the relative changes of everyone parameter (ratio of parameter change to the calibrated optimal parameter dP/P) were used as indicator of the sensitivity of flow to parameter changes.

Sensitivity of GR2M and MWB3 models parameters for the selected watershed is shown in Figure 11. For the three parameters, X1 has the most significant effect on flow for all the selected watersheds (e.g. a 25% change in parameter X1 results approximately in 40% flow change over all the selected watersheds) and α has the least significant effect on flow for almost all the selected watershed except over Puerto Inca watershed where X2 parameter has the least significant effect on flow.

Sensitivity of MWB3 model parameters over the selected watershed show distinct effect on flow for the relative changes of parameters. Parameters magnitude effect on flow can be put in order as: a_2, a_1 and a_3 in Requena watershed. a_2, a_3, a_1 in Chazuta watershed. a_3, a_2, a_1 in Puerto Inca watershed and a_1, a_2, a_3 in Maldonadillo, Tambo, Mejorada and Pisac watersheds. Effect of change of rainfall and evapotranspiration amount on flow simulation was also experienced in GR2M and MWB3 models; rainfall had the most significant effect on annual flow. On average, a 25% change in rainfall, flow changed approximately 50% for GR2M

Table 3. Statistical values for GR2M and WBM-3 models in the calibration and validation procedure for the watershed selected. Better values are in gray box.

Watershed	River	Statistical	GR2M model						MWB3 model					
			Calibration			Validation			Calibration			Validation		
			WHCmin	WHCmed	WHCmax	WHCmin	WHCmed	WHCmax	WHCmin	WHCmed	WHCmax	WHCmin	WHCmed	WHCmax
		R^2	0.85	0.85	0.84	0.90	0.89	0.89	0.84	0.84	0.85	0.90	0.90	0.90
Requena	Ucayali	Nash	0.70	0.70	0.69	0.77	0.77	0.77	0.70	0.70	0.71	0.71	0.72	0.72
		%V	1.88	2.44	1.82	3.53	3.69	3.40	1.41	1.55	1.44	15.24	15.24	15.01
Cal: janv-1993/dic-2002		RMSE	29.46	29.50	29.58	20.86	21.28	20.99	29.26	29.09	29.02	23.51	23.29	23.19
Val: janv-2004/dic-2007		SB	19.41	19.66	19.62	14.86	15.03	14.85	18.17	18.09	18.15	15.69	15.46	15.13
		R^2	0.86	0.86	0.85	0.88	0.88	0.87	0.89	0.89	0.89	0.89	0.88	0.89
Chazuta	Huallaga	Nash	0.67	0.66	0.61	0.71	0.71	0.69	0.64	0.65	0.65	0.69	0.69	0.69
		%V	-7.89	-8.94	11.25	7.09	7.26	9.01	-6.22	-5.35	-5.93	-8.04	-6.84	-7.17
Cal: janv-1999/dic-2004		RMSE	27.70	28.19	30.12	33.12	32.90	34.43	29.96	29.46	29.49	34.41	34.02	34.02
Val: janv-2005/dic-2007		SB	17.41	17.76	19.48	23.68	23.55	25.46	23.34	22.86	22.75	21.95	21.54	21.37
		R^2	0.80	0.80	0.79	0.90	0.90	0.89	0.80	0.80	0.80	0.92	0.92	0.91
Puerto Inca	Pachitea	Nash	0.63	0.63	0.62	0.77	0.77	0.76	0.60	0.60	0.61	0.79	0.78	0.79
		%V	0.88	0.80	1.03	-10.67	-11.20	-10.95	-13.09	-13.68	-10.11	-20.00	-20.83	-17.77
Cal: janv-1998/dic-2003		RMSE	223.35	224.45	226.47	195.65	196.80	200.49	233.78	232.16	229.31	191.07	194.74	188.63
Val: janv-2004/dic-2007		SB	61.09	62.58	61.74	105.72	106.90	111.84	85.85	85.98	78.60	99.70	102.18	92.88
		R^2	0.89	0.89	0.89	0.91	0.91	0.90	0.86	0.87	0.87	0.90	0.90	0.90
Maldonadillo	Urubamba	Nash	0.80	0.79	0.78	0.82	0.81	0.81	0.75	0.75	0.75	0.79	0.79	0.79
		%V	0.60	0.53	0.05	-5.52	-5.05	-5.01	1.31	0.93	1.43	-3.54	-4.03	-3.54
Cal: janv-1993/dic-2002		RMSE	29.58	30.33	30.84	30.41	30.91	31.16	33.29	33.19	33.15	33.02	33.02	32.63
Val: janv-2004/dic-2007		SB	14.84	15.36	14.79	18.44	18.60	17.91	16.64	16.76	16.50	23.07	23.03	22.61
		R^2	0.88	0.88	0.88	0.92	0.91	0.90	0.92	0.92	0.92	0.94	0.94	0.94
Tambo	Tambo	Nash	0.77	0.76	0.75	0.78	0.76	0.74	0.85	0.85	0.85	0.87	0.86	0.86
		%V	4.17	6.46	8.19	11.52	13.02	14.00	1.42	1.73	1.84	-6.92	-7.43	-7.58
Cal: janv-1988/dic-2001		RMSE	11.53	11.88	12.46	11.39	12.61	12.39	9.33	9.32	9.34	8.94	9.07	9.22
Val: janv-2002/dic-2007		SB	7.24	7.69	7.70	8.44	8.76	8.76	4.17	4.23	4.32	5.25	5.30	5.43
		R^2	0.90	0.88	0.86	0.91	0.91	0.92	0.90	0.91	0.91	0.89	0.89	0.90
Mejorada	Mantaro	Nash	0.76	0.72	0.67	0.45	0.38	0.29	0.80	0.81	0.82	0.65	0.68	0.70
		%V	-7.10	-8.22	-9.47	-28.67	-31.53	-34.65	-3.82	-3.88	-3.12	-2.26	-2.87	-2.78
Cal: janv-1995/dic-2002		RMSE	3.67	3.98	4.29	3.89	4.15	4.44	3.36	3.28	3.20	3.09	2.97	2.87
Val: janv-2003/dic-2007		SB	1.32	1.41	1.57	3.23	3.55	3.90	1.79	1.70	1.60	2.09	1.99	1.88
		R^2	0.72	0.71	0.71	0.84	0.83	0.83	0.82	0.82	0.82	0.84	0.84	0.83
Pisac	Vilcanota	Nash	0.48	0.45	0.43	0.56	0.59	0.59	0.67	0.67	0.67	0.33	0.36	0.35
		%V	-13.23	-16.86	-18.91	21.78	17.15	14.56	-0.04	0.21	-0.78	34.02	34.03	33.58
Cal: janv-1986/dic-2001		RMSE	13.52	13.83	14.06	9.17	8.91	8.86	10.74	10.74	10.78	11.32	11.08	11.19
Val: janv-2002/dic-2007		SB	9.75	11.45	12.33	11.66	10.09	9.98	6.47	6.76	6.27	18.63	17.95	17.90

Table 4. Summarising statistics of Shuffled Complex Evolution Metropolis posterior parameter distribution for GR2M model and MWB3 model for the selected watershed (optimal parameter set, posterior mean, standard deviation St. Dev. and correlation coefficients between the generated simples).

Watershed	GR2M model							MWB3 model						
	Parameter	Optimal	Mean	St. Dev	X1	α	X2	Parameter	Optimal	Mean	St. Dev	a_1	a_2	a_3
Requena	X1	0.7319	0.7512	0.1196	1.0000			a_1	0.3709	0.3495	0.0503	1.0000		
	α	0.0006	0.0006	0.0003	-0.5604	1.0000		$a_2 \times 10^5$	0.3767	0.3791	0.0203	-0.2702	1.0000	
	X2	0.0014	0.0014	0.0003	-0.9590	0.4296	1.0000	$a_3 \times 10^7$	0.0634	0.0649	0.0163	-0.1980	-0.7307	1.0000
Chazuta	X1	0.9975	0.9524	0.0411	1.0000			a_1	0.7676	0.7570	0.0522	1.0000		
	α	0.0059	0.0060	0.0014	-0.2264	1.0000		$a_2 \times 10^5$	2.1593	2.1745	0.3219	-0.4926	1.0000	
	X2	0.0039	0.0042	0.0004	-0.5997	-0.5044	1.0000	$a_3 \times 10^7$	3.3716	3.4547	0.3951	-0.0119	-0.7419	1.0000
Puerto Inca	X1	0.9928	0.7701	0.1281	1.0000			a_1	0.6410	0.6819	0.1343	1.0000		
	α	0.1227	0.1627	0.0509	-0.8560	1.0000		$a_2 \times 10^5$	9.6018	11.0314	6.3554	-0.2878	1.0000	
	X2	0.0094	0.0175	0.0081	-0.4793	0.1543	1.0000	$a_3 \times 10^7$	35.7692	35.4923	3.7713	0.1155	-0.7481	1.0000
Maldonadillo	X1	0.9995	0.9377	0.0483	1.0000			a_1	0.5953	0.5938	0.0291	1.0000		
	α	0.0098	0.0110	0.0014	-0.6863	1.0000		$a_2 \times 10^5$	1.5875	1.5748	0.0954	-0.4790	1.0000	
	X2	0.0052	0.0058	0.0006	-0.8540	0.3051	1.0000	$a_3 \times 10^7$	0.6724	0.6732	0.0615	-0.0662	-0.6256	1.0000
Tambo	X1	0.9989	0.9699	0.0267	1.0000			a_1	0.5739	0.5696	0.0189	1.0000		
	α	0.0021	0.0022	0.0003	-0.3760	1.0000		$a_2 \times 10^5$	0.8556	0.8626	0.0511	-0.4934	1.0000	
	X2	0.0015	0.0015	0.0001	-0.6161	-0.3126	1.0000	$a_3 \times 10^7$	0.7845	0.7893	0.0561	-0.1258	-0.6480	1.0000
Mejorada	X1	0.9985	0.9818	0.0169	1.0000			a_1	0.7496	0.7323	0.0625	1.0000		
	α	0.0103	0.0106	0.0013	-0.2013	1.0000		$a_2 \times 10^5$	1.3705	1.4197	0.1636	-0.7138	1.0000	
	X2	0.0069	0.0071	0.0005	-0.4123	-0.5627	1.0000	$a_3 \times 10^7$	2.4884	2.5815	0.5570	-0.8507	0.3470	1.0000
Pisac	X1	0.9997	0.9615	0.0329	1.0000			a_1	0.7966	0.7903	0.0125	1.0000		
	α	0.0482	0.0486	0.0098	-0.2871	1.0000		$a_2 \times 10^5$	5.5317	5.6136	0.4005	-0.3273	1.0000	
	X2	0.0395	0.0430	0.0044	-0.6030	-0.4017	1.0000	$a_3 \times 10^7$	11.3186	11.5038	1.0089	-0.3939	-0.4774	1.0000

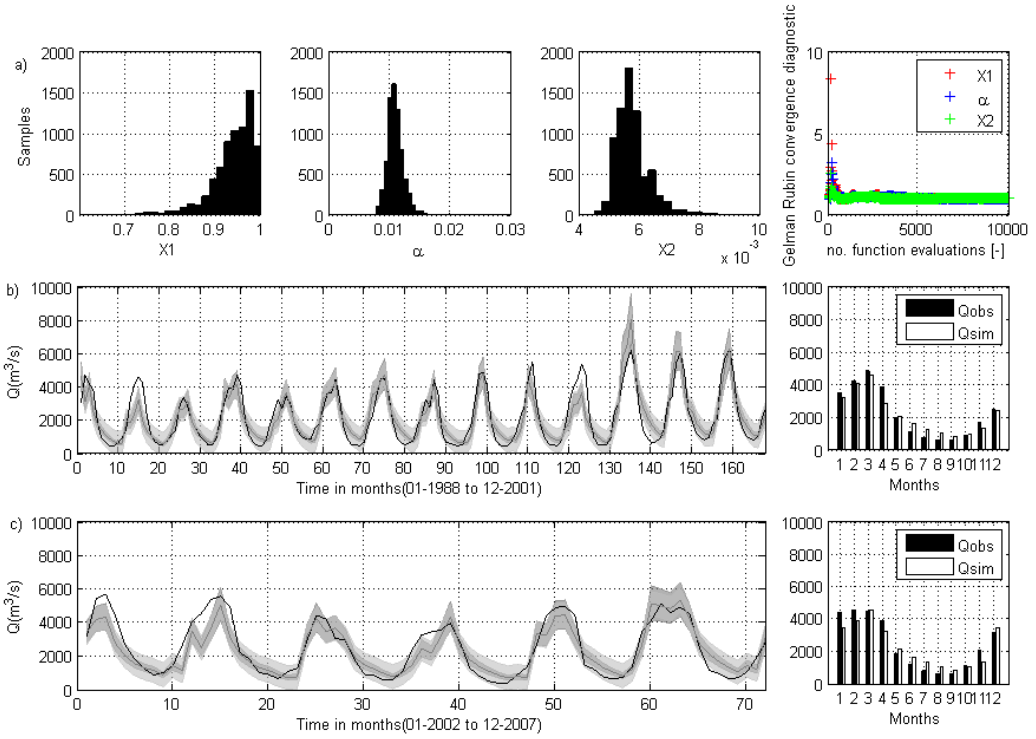

Figure 7. As in 4 but for GR2M model in the Urubamba basin (Maldonadillo watershed). Calibration period (01/1988 to 12/2001) and validation period (01/2002 to 12/2007).

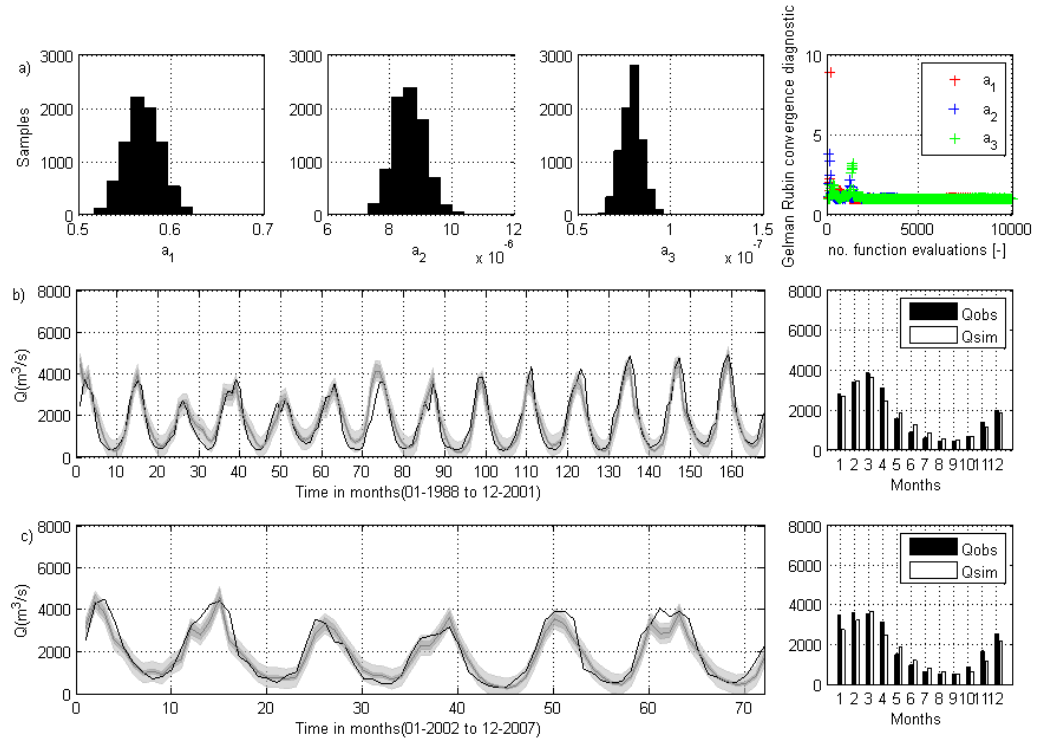

Figure 8. As in 4 but for MWB3 model in the Tambo basin (Tambo watershed). Calibration period (01/1988 to 12/2001) and validation period (01/2002 to 12/2007).

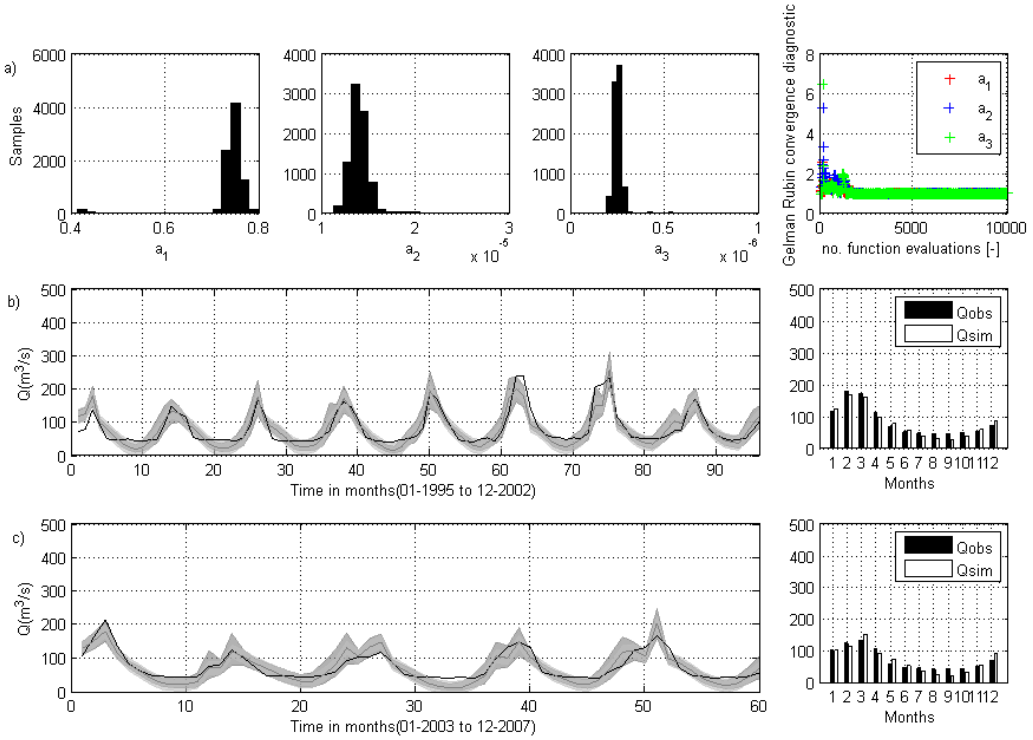

Figure 9. As in 4 but for MWB3 model in the Mantaro basin (Mejorada watershed). Calibration period (01/1995 to 12/2002) and validation period (01/2003 to 12/2007).

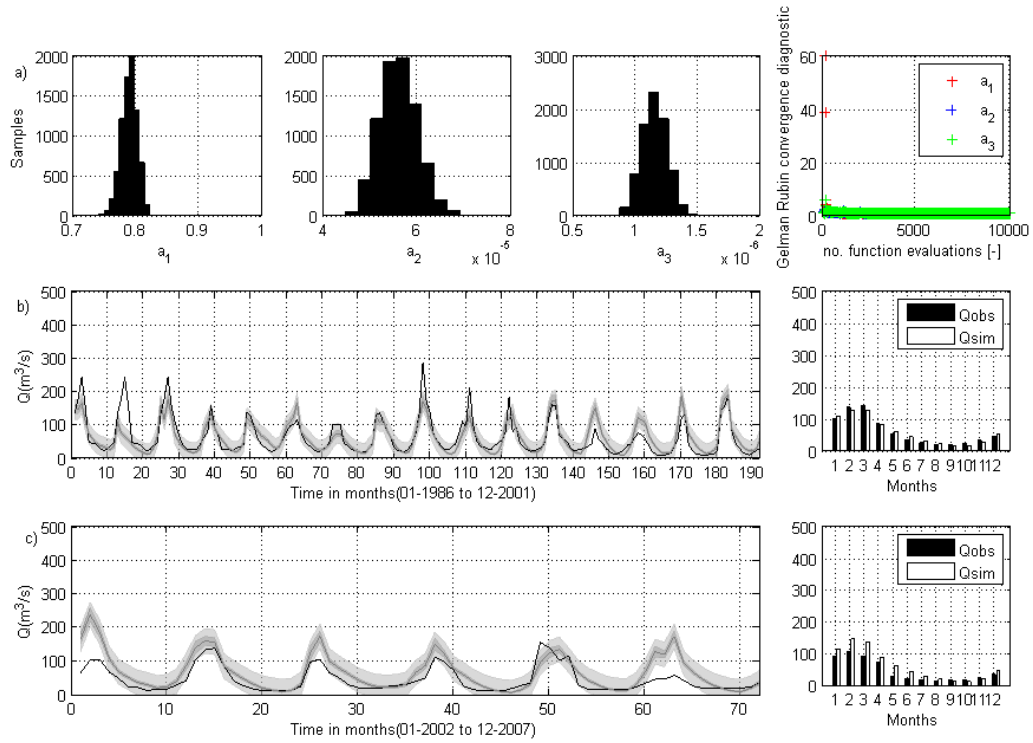

Figure 10. As in 4 but for MWB3 model in the Vilcanota basin (Pisac watershed). Calibration period (01/1986 to 12/2001) and validation period (01/2002 to 12/2007).

model whereas 25% change flow for MWB3 model. Same percentage of change is observed, on average, for evapotranspiration change for GR2M and MWB3 models: a 50% change in evapotranspiration change approximately -25% in flow.

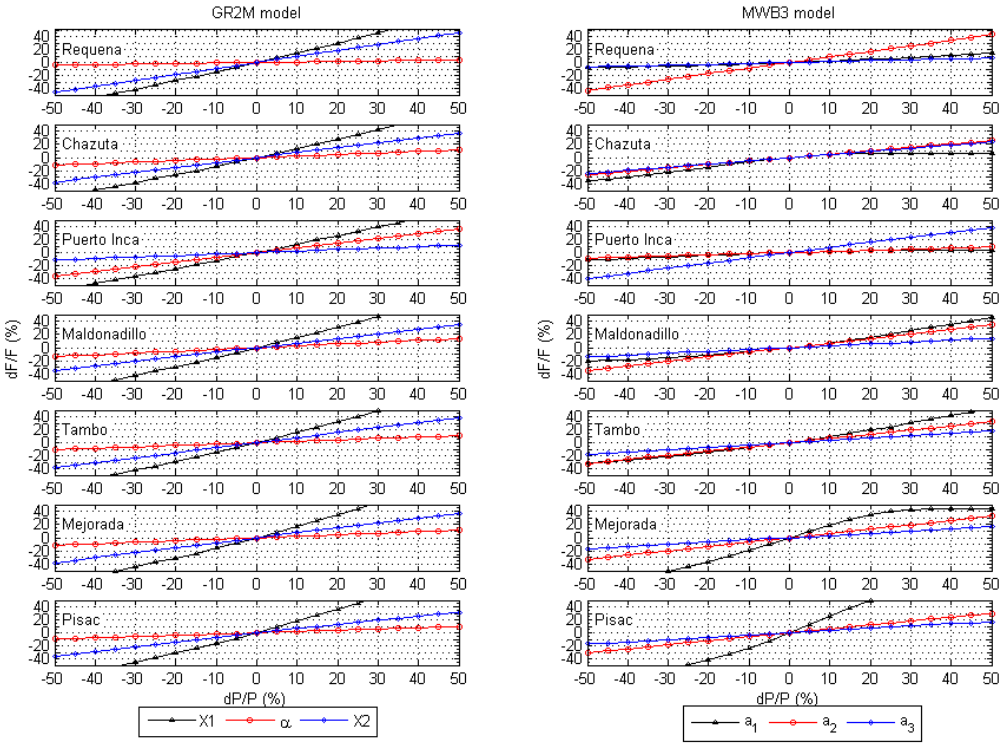

Figure 11. Sensitivity of the model simulated discharge (GR2M and MWB3) to the change of model parameter values for Requena, Chazuta, Puerto Inca, Maldonadillo, Tambo, Mejorada and Pisac watersheds. dF/F (%) is the relative change in the simulated discharge and dP/P(%) is the relative change in parameter values.

CLIMATIC CHANGE IMPACTS

Spatial comparison of 20C3M experiment with observed data

20C3M experiments of the IPCC models impose initial conditions for SRES A1B and SRES B1. In order to compare 20C3M output data with observed data (rainfall and evapotranspiration) in the 1965-2000 period, simple mean relative error in percentage for mean multi-annual values (RE) were estimated for BCM2, CSMK3 and MIHR IPCC models. Figure 12 shows spatial distribution of RE values over the selected watersheds used in this study considering rainfall and evapotranspiration data. It is observed that: a) Rainfall, on average, show that RE values is about from -50 to 300 for the three IPCC models (BCM2, CSMK3 and MIHR). Over estimation (mean multi-annual) of IPCC models output for rapport to observe data (until 300% RE value) are located, on average for the three models, mostly in Southern Tambo, Maldonadillo and Pisac. Others watersheds show, on average, similar and underestimation (mean multi-annual) values to compare IPCC output models and observe data (until -50% RE value). b) Considering evapotranspiration, on average, RE values are about from -15 to 50% for the IPCC models. The CSMK3 exhibits least range values of RE whereas BCM2 exhibits most range values of RE. Over estimation (mean multi-annual) of IPCC models output (until 50 RE value) are located, on average for the three models, mostly in the west of our zone of study center within Mejorada watershed. Others watersheds show,

on average, similar and underestimation (mean multi-annual) values to compare IPCC output models and observe data (until -15% RE value).

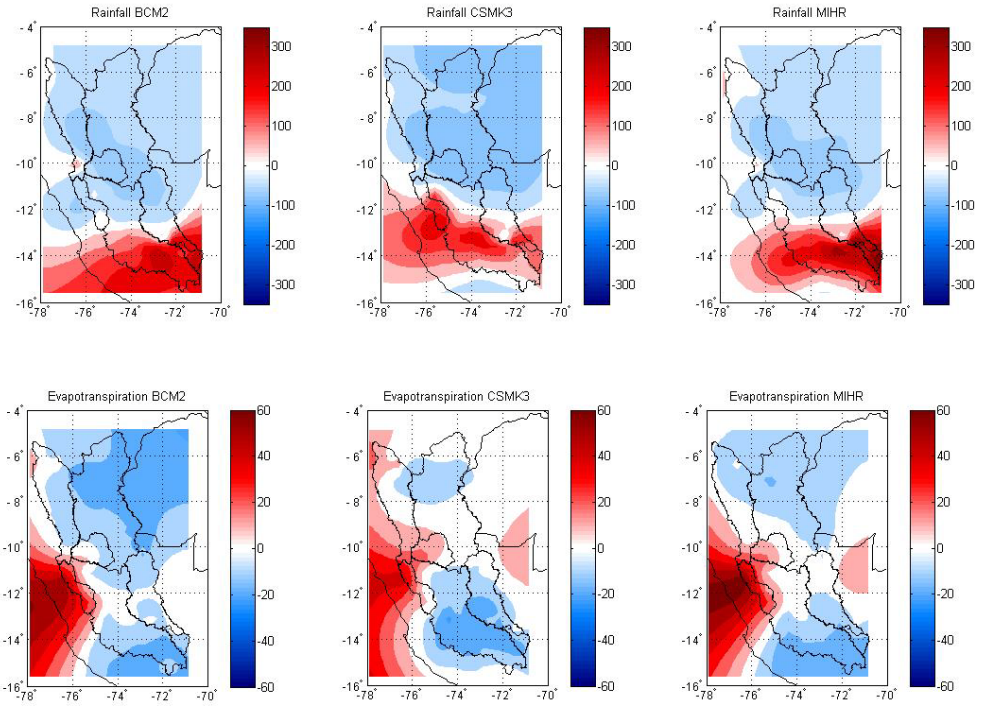

Figure 12. Mean annual relative error (%) in IPCC models (BCM2, CSMK3 and MIHR) for rapport with observed data (Rainfall and Evapotranspiration) considering mean multi-annual values over the 1965-2000 period.

Mean monthly rainfall and evapotranspiration

The accuracy of IPCC models was also assessed at the monthly step within the watersheds. Evapotranspiration in mm per month was plotted and compared (Figure 13). On average, it is observed that IPCC models represent well monthly cycle of observed data in all the selected watersheds but with overestimation and underestimation in some months for each model. For description purpose and for the limit of this paper, absolute value of SB (Equation 10) was calculated between observed and IPCC models in all the watersheds. It is observed that BCM2 is the better model for perhaps all the stations except for Mejorada watershed who presents to CSMK3 as the better model. Also, it is observed overestimations (underestimations) in Mejorada (Pisac) watersheds for all the IPCC models.

Monthly rainfall observed is plotted and compared with IPCC models within the watersheds (Figure 14). Contrary to evapotranspiration, rainfall shows majors overestimation and underestimation for all the months in each one IPCC model. It is observed that, on average, underestimations within Requena, Chazuta and Puerto Inca with better bias in June, July and August (until more of 50%). Using absolute value of SB, were calculated as the better IPCC models: BCM2 in Requena and Puerto Inca as well as MIHR in Chazuta. Maldonadillo exhibits underestimations and overestimations for all the models, underestimations are in July and August and overestimations are in April and November. Tambo shows, overestimations from August to May in all the IPCC models with underestimations from June to September for CSMK3 and MIHR models. Mejorada presents, on average, for the three IPCC models overestimations in May, November and December as well as underestimations in August and September. In Pisac the three IPCC models exhibit overestimations and using absolute value of SB is calculated as the better model the CSMK3.

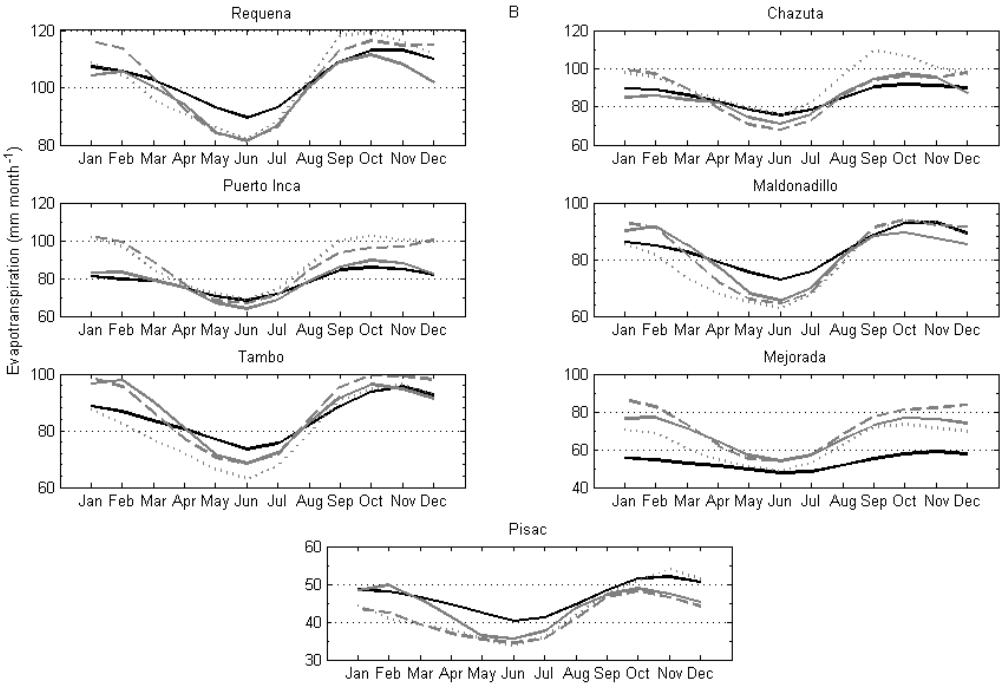

Figure 13 Comparison of monthly means (1965-2000) of evapotranspiration (mm per month) in the selected watersheds. Observed values are represented by the black line. The gray line denotes BCM2 model. The gray dashed line denotes CSMK3 model. The gray dotted line denotes MIHR model.

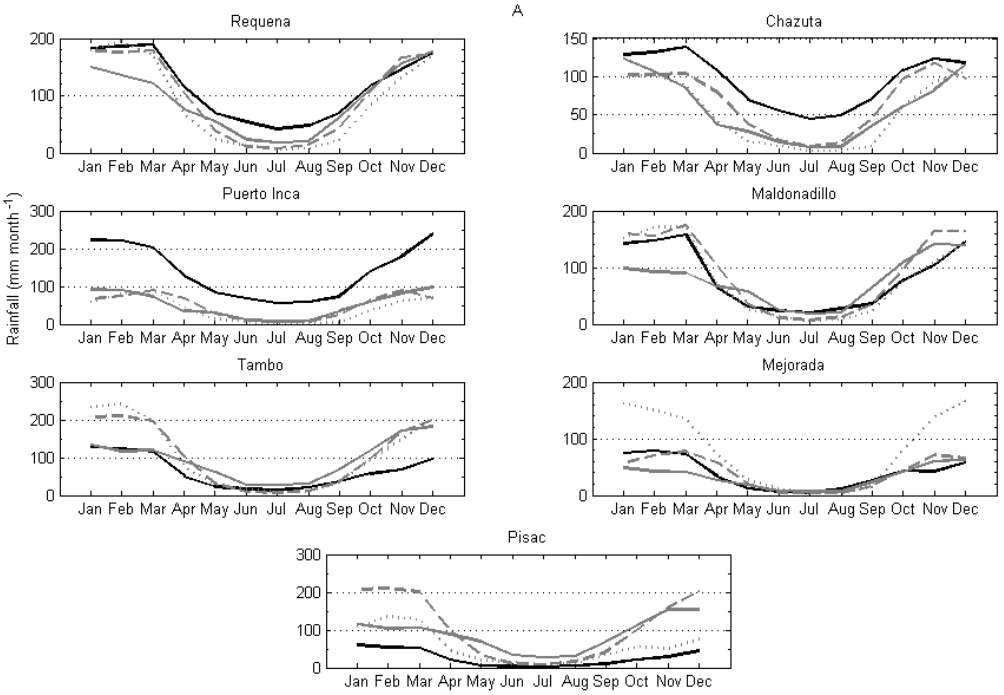

Figure 14 As in the Figure 13 but for rainfall (mm per month).

In summary, the three IPCC models used for this study represent well the monthly cycle of evapotranspiration and rainfall but with systematic bias between observed data with IPCC monthly values.

Rainfall and evapotranspiration projections (2008-2099)

Anomalies and Horizons downscalling methodologies are based in correct the monthly bias found in the latter section. Results calculated with these two methodologies report similar answers for the two methods. Then, in order to compare these were calculated the maximum, minimum, mean and the sensibility of the models (means ± standard deviation) of all the outputs (Downscalling methods and IPCC models). The Figures 15 and 16 show the mean annual observed values (1965-2007) and the future mean annual projection (2008-2099) considering the SCE A1B and SCE B1 in rainfall and evapotranspiration respectively. It is observed, that the variability of future annual rainfall rates (2008-2099) exhibit similar representation than observed data (1965-2007) while evapotranspirations present for the future projection positive trend in the major part of watersheds in accord with the global warming. Table 5 rapports the mean annual values (rainfall and evapotranspiration) in the observed period and the future projections (SCE A1B and SCE B1) split in 2008-2050 and 2051-2099 periods. Rainfall future projections considering the SCE A1B exhibit mostly values above the observed period in all the watersheds, except the 2051-2099 period within Maldonadillo as well as the two period (i.e. 2008-2099) in Pisac watershed. For the SCE B1 Chazuta, Maldonadillo and Pisac present values under the mean of observed period. Also, in the same scenario Requena and Tambo present values under the mean of observed data in the 2051-2099 period. The others watershed and periods show mostly values above the mean of observed period. Evapotranspiration projections show similar periods with values under and over the mean annual observed considering both scenarios. Thus, perhaps all the watersheds exhibit values over the mean of observed data while Chazuta, Puerto Inca and Mejorada show values under the mean of observed period in the 2008-2050 period.

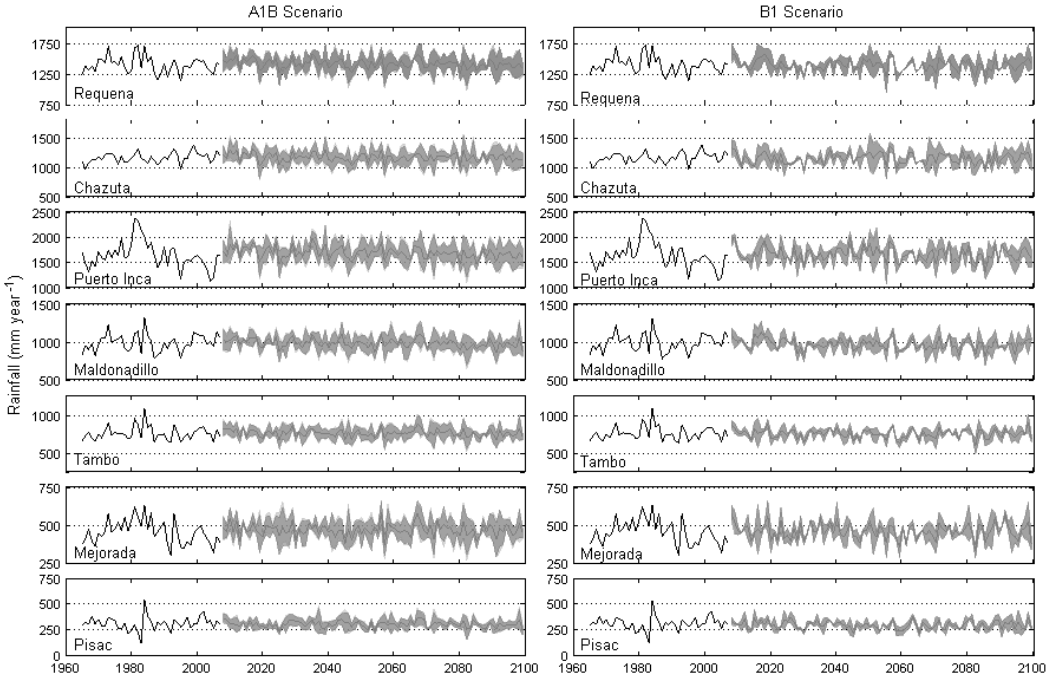

Figure 15. Time series of annual rainfall (mm per year) in the observed period (1965-2007) and future climate projections for the future period (2008-2099) for the A1B and B1 scenarios over the selected watersheds. Observed values are represented by the black line. The gray line denotes mean future climate projections (average of IPCC models and two methods of downscalling). The dark shaded area denotes the limits between maximums and minimums values of IPCC models calculated with the two methods of downscalling. The light shaded area denotes the means ± standard deviation of IPCC models calculated with the two methods of downscalling.

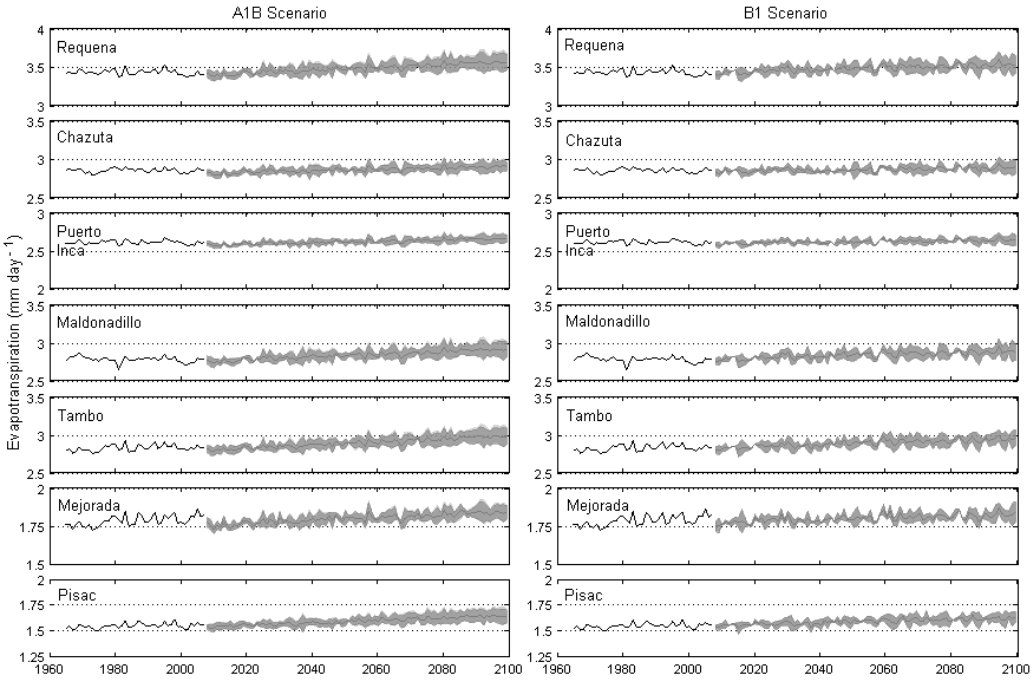

Figure 16. As in the Figure 15 but for evapotranspiration (mm per day).

Table 5. Mean annual of Rainfall (mm per year) and Evapotranspiration (mm per year) in the 1965-2000 period considering A1B and B1 scenarios. Blue text is over the mean multiannual observed and red text is under the mean multiannual observed.

		Requena	Chazuta	Puerto Inca	Maldonadillo	Tambo	Mejorada	Pisac
				Rainfall				
	Observed	1390.7	1152.9	1632.6	984.2	753.4	455.7	314.2
A1B	2008-2050	1420.1	1164.4	1706.4	991.8	759.6	467.8	310.9
	2051-2099	1396.4	1154.3	1661.6	968.4	754.0	471.3	304.4
B1	2008-2050	1398.9	1143.4	1677.5	977.6	755.6	465.7	305.4
	2051-2099	1372.5	1142.1	1637.2	952.4	742.7	456.3	295.9
				Evapotranspiration				
	Observed	1251.5	1041.2	951.4	1015.0	1031.7	651.6	566.6
A1B	2008-2050	1254.1	1036.1	946.4	1019.5	1037.5	648.7	571.8
	2051-2099	1284.7	1051.5	960.8	1048.8	1071.5	663.8	592.9
B1	2008-2050	1259.6	1040.0	949.8	1025.5	1041.7	651.5	573.9
	2051-2099	1280.4	1049.7	958.5	1045.1	1065.8	661.8	588.4

Table 6. Mean annual flow (m^3 per second) in the watersheds for GR2M and MWB3 models considering A1B and B1 scenarios. 2020s (average from 2008 to 2040); 2050s (average from 2041 to 2070); 2080s (average from 2071 to 2099). Blue text is over the mean multiannual observed and red text is under the mean multiannual observed.

	Requena	Chazuta	Pto. Inca	Maldonadillo	Tambo	Mejorada	Pisac
Observed	(1993-2007)	(1999-2007)	(1998-2007)	(1988-2007)	(1988-2007)	(1995-2007)	(1986-2007)
	12691.2	2934.5	3805.6	2289.3	1824.5	80.6	58.0
GR2M (A1B)							
2020s	14154.1	2963.6	4708.1	2253.6	1862.7	102.4	50.5
2050s	13679.9	2828.8	4601.5	2243.1	1831.1	101.9	51.5
2080s	13221.6	2883.5	4285.1	2146.6	1795.4	101.8	48.4
GR2M (B1)							
2020s	13802.3	2801.1	4459.8	2252.0	2080.8	101.3	54.8
2050s	13099.8	2845.6	4375.7	2155.1	1922.0	93.2	48.6
2080s	13170.0	2819.5	4391.2	2159.3	2012.6	102.0	50.9
MWB3 (A1B)							
2020s	14210.8	2868.8	4548.9	2379.7	2475.3	97.5	61.3
2050s	13211.1	2766.9	4424.6	2270.6	2349.8	95.4	59.5
2080s	12521.6	2766.9	4167.5	2165.1	2251.0	93.2	57.6
MWB3 (B1)							
2020s	12582.9	2608.6	4072.4	2135.9	2174.2	88.6	56.8
2050s	11832.0	2620.4	4151.9	2059.9	2113.0	84.7	53.9
2080s	11297.1	2559.8	3847.5	1953.3	2051.4	85.8	54.8

Impact of climatic change on hydrology

The monthly rainfall and evapotranspiration projected for the 2008-2099 period were based in Anomalies and Horizons methodologies (2 outputs), these methodologies involve three IPCC models (3 outputs) considering two scenarios (2 outputs). Moreover, we work with two hydrological models (2 outputs). It is to say, 24 outputs data. For this study, we consider as principals outputs the scenarios (A1B and B1) as well as the hydrological models (GR2M and MWB3). Thus, impact of climatic change on hydrology will be describe in function of these four outputs whereas of the others outputs will be calculated the mean, maximum and minimum taking as basis the scenarios and hydrological models.

Box plots of mean annual flows considering the horizons: 2020s (average from 2008 to 2040); 2050s (average from 2041 to 2070); 2080s (average from 2071 to 2099) for the SCE A1B and SCE B1 (GR2M and MWB3) were plotted in the Figure 17 and 18 respectively. It is observed, in the two figures that the horizons 2020s, 2050s and 2080s present major amplitude than observed periods in the watersheds for both hydrological models. Also, GR2M present major amplitude than MWB3 models in both figures.

In order to evaluate the means values and possible fluctuations in the horizons periods for rapport to observed period, multiannual horizons means were calculated and reported in the Table 6. It is observed that: a) Requena exhibits means in the horizons above the mean of the observed period (1993-2007) in the GR2M and for both scenarios (until +11.5% in the 2020s for SCE A1B). MWB3 for SCE A1B presents in the 2080s values under the observed period (-1%) while previous horizons show values above the observed period (until +12% in the 2020s). MWB3 for SCE B1 presents in all the horizons values under the observed period (until -11% in the 2080s). b) Chazuta watershed exhibits mostly values for the horizons under

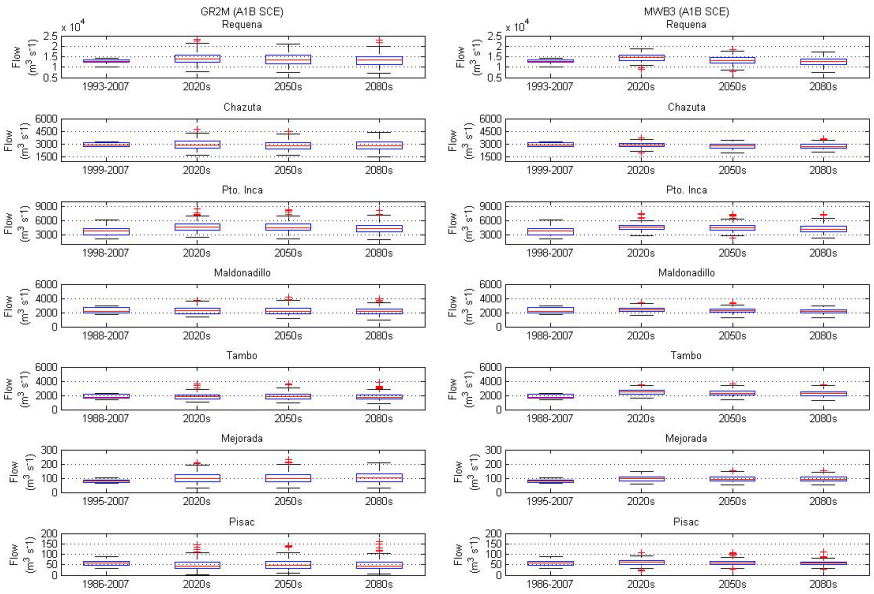

Figure 17. Boxplots of annual flow (m^3 per second) in the observed period and future climate projections explain as horizons: 2020s (average from 2008 to 2040); 2050s (average from 2041 to 2070); 2080s (average from 2071 to 2099) for the A1B scenario as well as for the GR2M and MWB3 models over the selected watersheds.

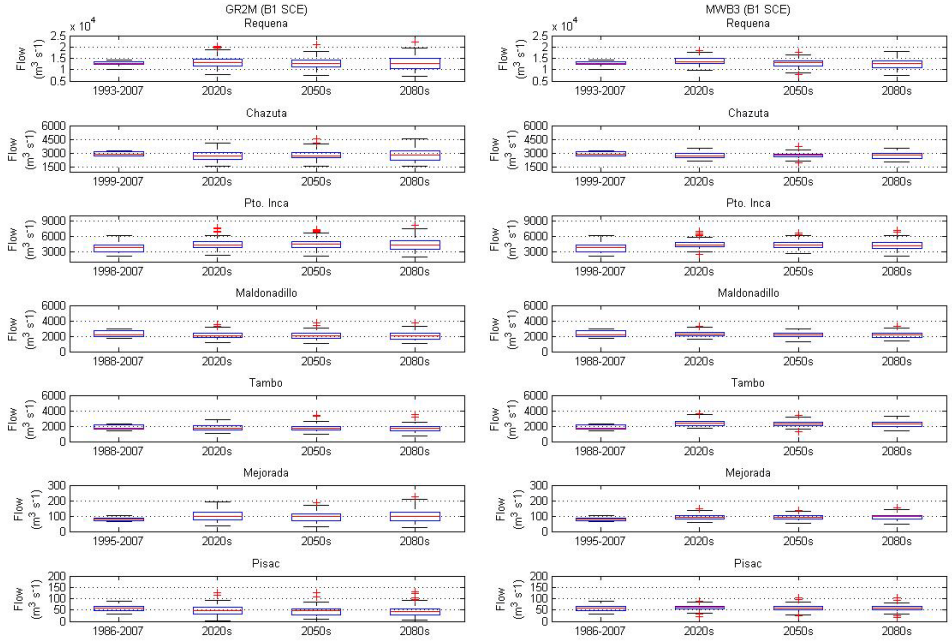

Figure 18. As in the Figure 17 but for the B1 scenario.

the observed period (1999-2007). MWB3 model for SCE B1 presents the least values (until -13% in the 2080s). c) Puerto Inca presents values above the observed period (1998-2007) in all the horizons, hydrological models and scenarios. The horizon 2020s presents majors values (until +24% for GR2M using A1B SCE). d) Maldonadillo watershed exhibits mostly values for the horizons under the observed period (1988-2007). MWB3 model for B1 SCE present the least values (until -15% in the 2080s). e) Tambo watershed exhibits mostly values for the horizons over the observed period (1988-2007). MWB3 model for A1B SCE present

the major values (until +36% in the 2020s). f) Mejorada watershed presents values for the horizons over the observed period (1995-2007). GR2M model for A1B SCE present the major values (until +27% in the 2020s). g) Pisac watershed shows mostly values for the horizons under the observed period (1986-2007). GR2M model for A1B SCE present the major values (until -16% in the 2080s).

The expected changes in monthly flow (as a percentage of observed flow) were calculated considering the future projection 2008-2050. These results were plotted in the Figures 19 and 20 for the A1B SCE and B1 SCE (GR2M and MWB3) respectively. In summary of these two figures, it is observed similar change in monthly flow in Requena, Chazuta, Puerto Inca, Maldonadillo and Tambo watersheds considering both scenarios and hydrological models. It is observed mostly positive changes in monthly flow with the major anomalies in the months of July, August and September. Puerto Inca watershed will be the most affecting for these changes (until ~ +200% in August and September). Mejorada watershed will present positive changes in monthly flow for almost all the months with major changes in January, May and June (~ +50%) considering all the hydrological models and scenarios. Pisac watershed will present changes in monthly flow, on average, negative anomalies in September, October, November, Mars and positive anomalies the others months considering all the hydrological models and scenarios. The best negative anomaly is in November (~ -50%) and the best positive anomaly is in June (~ +50%) considering all the models and scenarios.

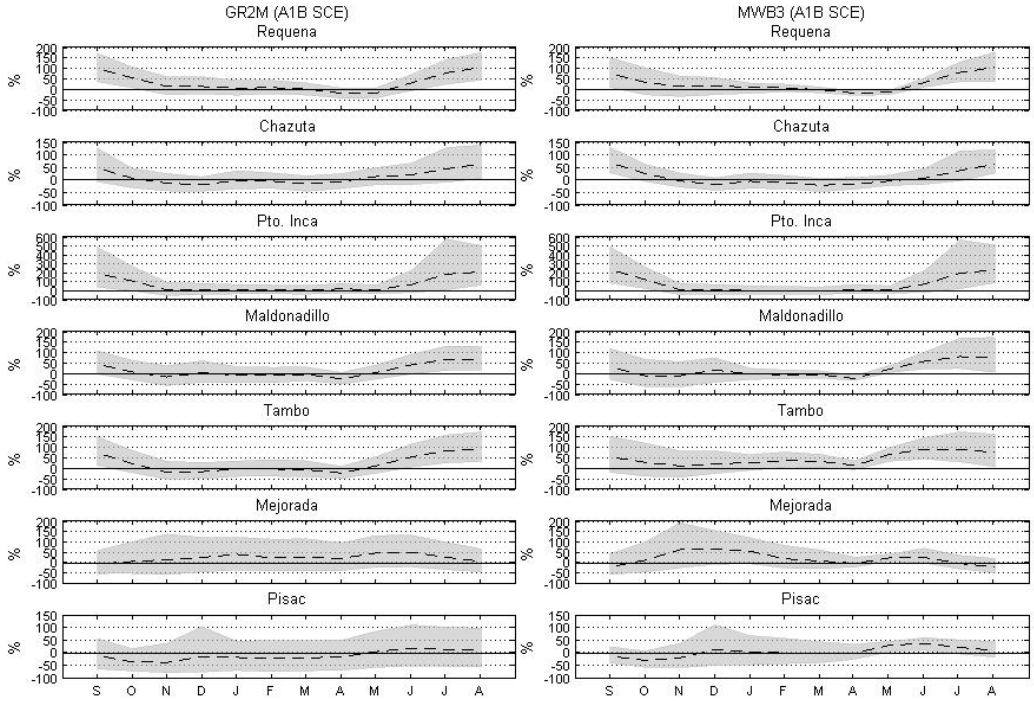

Figure 19. Change in simulated monthly flow (%) due to climatic change under the A1B scenario as well as GR2M and MWB3 models in the selected watersheds. The dashed dark line denotes the mean monthly value of IPCC models calculated with the two methods of downscalling. The light shaded area denotes the maximum and minimum monthly values of IPCC models calculated with the two methods of downscalling.

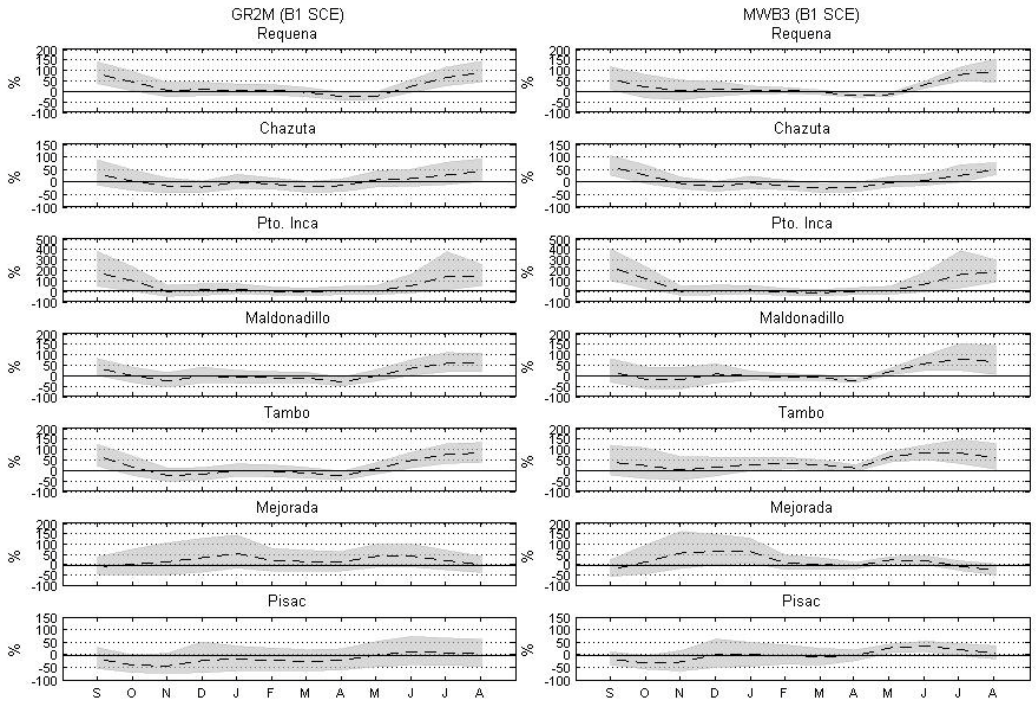

Figure 20. As in the Figure 19 but under B1 scenario as well as GR2M and MWB3 models in the selected watersheds.

SUMMARY AND CONCLUSIONS

The present work is the first one about conceptual monthly hydrological models using distributed data in the Peruvian Amazon-Andes basin to analyse climatic change impacts. Thanks to the last missions carried out by the HYBAM Project (IRD – SENAMHI – UNALM collaboration) and hydrological stations from SENAMHI network, seven large and small watersheds with flow data inside the Peruvian Amazon-Andes basin (Ucayali and Huallaga rivers system) were chosen for this study.

This study conclude that initial input maximum, mean and minimum soil water holding capacity (WHC) estimate by FAO / UNESCO (1981) using the methodology given by Dieulin et al. (2006) can be used as initial value for conceptual distributed hydrological models based on reservoirs. The minimum values of WHC in the calibration procedure using GR2M seem as the best for all the watersheds while for MWB3 the better are the minimum and maximum values of WHC minimum. The WHC as initial input is important to avoid the over-parameterisation and to reduce the dimensionality in the calibration procedure.

Using Shuffled Complex Evolution Algorithm (SCEM-UA) is possible estimate prior probability distributions of the parameters using the GR2M and MWB3 hydrological models. Distributions of parameters samples show that MWB3 model in the selected watersheds are mostly Gaussian while the distribution of parameters samples of GR2M model are close to one for X1 parameter and the others parameters (α and X2) are mostly Gaussian. Optimal parameters estimates during calibration procedure reproduce reasonably well observed flow for the selected watersheds showing nearby statistical values of comparison performance for GR2M and MWB3 model, better models can be classifies as: GR2M model over Requena, Chazuta, Puerto Inca and Maldonadillo watersheds whereas Tambo, Mejorada and Pisac watershed for MWB3 model.

Hydrographs through calibration and validation periods in the watersheds shown that both models are able of reproduce observed flows with reasonable accuracy. However, it is observed least accuracy in Pisac watershed (GR2M model) and most accuracy over Tambo watershed (MWB3 model). Mostly using both models seasonal values simulated are over estimate in monthly low water and under estimate in floods months.

Sensibility analyses exhibit the parameters more stables to effects in simulated flows for GR2M than MWB3 model. Thus, X1 parameter has the most significant effect on flow for the watersheds. MWB3 parameters exhibit distinct sensibility effects on flow, i.e. parameters estimated over the watersheds are distinct but mostly a_3 parameter has the most significant effect on flow.

Puerto Inca watershed is special watershed for carries out monthly hydrological model due to hydrological characteristics: rainfall (~ 1633 mm year $^{-1}$), specific discharge (~ 435 mm) and coefficient of variation of monthly seasonal flow (~ 0.43). These values are the most (rainfall and specific discharge) and the least (coefficient of variation) of all the watersheds. These characteristics have influence over optimal parameters estimates and parameters sensibility i.e. optimal parameters found in Puerto Inca are completely distinct that the others watershed. In addition, parameters sensibility in this watershed has special behaviours. Thus, for GR2M model α parameter play a special role in calibration procedure and a_3 parameter similar behaviour for MWB3 model. The regionalization of watersheds over the Peruvian Amazon-Andes basin appears difficult for the distinct values of the parameters obtained in the watersheds and for the missing of flow stations in sub-watersheds, future work will examine spatial distribution taking in consideration spatial variations from elevations and rainfall as the study by Chen et al. (2007) for estimate flow over ungauged watersheds.

Annual flows simulated from the future (2008-2099) suggest that possible impacts of climatic change on hydrology vary with watershed: a) for the Requena flow increase (decrease) using GR2M (MWB3) hydrological models considering A1B and B1 scenarios b) for the Chazuta, the Maldonadillo and the Pisac flows decrease while for the Puerto Inca, the Tambo and the Mejorada flows increase. The impact more marked is for the Tambo watershed (MWB3 model and A1B SCE). Changes in monthly flows (2008-2099) suggest increase changes for the entire watersheds except Pisac that depicts decrease and increase changes considering both scenarios and both hydrological models. July, August and September are the months with more marked impact (increase change) for the Requena, Chazuta, Puerto Inca, Maldonadillo and Tambo watersheds. Also, January, May and June are the months with major impact on hydrology (increase change) for the Mejorada watershed. The Pisac watershed exhibits decrease change from September to Mars and increase change from April to August. Puerto Inca watershed will be the most affecting for climatic change in monthly values.

Parameter uncertainty of hydrological models is by no means the only source of uncertainty in this study there is a 'cascade' of uncertainty associated with climate impact studies (Steele-Dunne et al., 2008). Future research activities are focused on work hydrological models at daily step and generate an ensemble of hydrological simulations based on different IPCC models and multiple future climate scenarios. The ultimate goal is to use these results as forcing data for the framework developed here to provide Peruvian engineers, planners and policy-makers with a significant ensemble of projected changes in flow with which to plan for the future.

CHAPITRE 5

Conclusion générale et perspectives

V. CHAPITRE 5. Conclusion générale et perspectives

5.1 Conclusion

Pour la première fois dans le cadre de cette étude, grâce au recueil de nombreuses données hydrométéorologiques et pédologiques (**Chapitre 2**), nous avons pu mettre en évidence et analyser les variabilités et tendances des variables hydrométéorologiques (**Chapitre 3**) et finalement développer des modèles hydrologiques au pas de temps mensuel afin d'évaluer l'impact des changements climatiques (**Chapitre 4**) sur les bassins des rios Ucayali et Huallaga.

Ce travail de thèse répond ainsi aux questions suivantes :

- *Quels sont les cycles annuels et saisonniers ainsi que la variabilité interannuelle et intra-saisonnière à moyen et long terme des principales composantes du cycle hydrologique sur les bassins des rios Huallaga et Ucayali ?*

- *Quelles sont les réserves disponibles en eau sur les bassins des rios Huallaga et Ucayali ?*

- *Quel est l'impact du changement climatique sur l'hydrologie des rios Huallaga et Ucayali ?*

Des éléments de réponse à la première question ont été apportés dans le **Chapitre 3** et des éléments de réponse aux deux autres questions ont été apportés dans le **Chapitre 4**.

Dans le **Chapitre 1** nous présentons une analyse des séries de pluies et de débit sur plusieurs bassins péruviens en examinant les tendances hydro-climatologiques. Nous observons dans le bassin Amazonien du Pérou (BAP) des tendances négatives significatives dans les bassins de cette région à la fois pour les débits mais aussi pour les précipitations. Au Pérou depuis quelques années des mesures de débits ont été réalisés en collaboration entre le SENAMHI et l'IRD au sein du programme HYBAM. Ainsi, les résultats de ces mesures ont été utilisés comme source de données pour développer cette thèse dans le cadre de deux bassins versant amazonien au Pérou : les bassins des rios Ucayali et Huallaga.

Dans le **Chapitre 2,** nous avons explicité les principales caractéristiques des bassins des rios Ucayali et Huallaga ainsi que présenté la base de données utilisée dans le cadre de cette thèse, qui s'est focalisé sur l'évolution climatique au pas mensuel, les données journalières étant malheureusement disponibles que de manières très parcellaire. De plus, une comparaison entre différentes méthodes empiriques d'estimation de l'évapotranspiration en prenant comme base la méthode de la FAO Penman-Monteith (Allen et al., 1998) a aussi été proposée. Nous avons montré que la méthode de Hargreaves (Hargreaves et Samani, 1985) s'avère être la plus adaptée à notre région d'étude pour estimer l'évapotranspiration, en proposant une équation régionale valide pour les bassins des rios Ucayali et Huallaga.

Nous avons aussi mis en évidence les relations entre la variabilité et les tendances des variables hydrométéorologiques (précipitation, température et évapotranspiration) sur les bassins de l'Ucayali et du Huallaga avec les variables océan-atmosphère dans le **Chapitre 3**. Le réchauffement sur notre zone d'étude est estimé à +0.09°C par décade. De plus, les ruptures de moyenne observées sur les séries de température à la fin des années 70 concordent avec les séquences d'événements de type « El Niño » (Trenberth et Hurell,

1994). Nous avons aussi démontré une corrélation négative entre les températures et l'index du Pacifique (Indice d'Oscillation du Sud, IOS), c'est-à-dire des températures plus élevées pendant les années El Niño. Ce réchauffement aura des conséquences importantes pour les glaciers orientaux des Andes et pour les communautés situées en altitude qui dépendent des eaux de ces glaciers (IGP, 2005 et Bradley et al., 2006). On observe d'abord un pourcentage important de ruptures de moyenne dans les séries de température maximum pendant les années 70 ainsi que dans les séries de température minimum pendant les années 80. Les séries de température moyenne présentent-elles des ruptures de moyenne significatives dans la décennie des années 80. On observe des tendances positives (au niveau des séries annuelles et des séries moyennées sur les trois mois de printemps) et des ruptures dans les séries d'évapotranspiration moyennées sur les trois mois d'été en 1976, et dans les séries d'évapotranspiration dans les Andes, ces ruptures pouvant être liées au début d'une fréquence forte d'événements El Niño à la fin des années 70. Par contre, aucune tendance n'est mise en évidence dans les séries de précipitation. Néanmoins, environ 10% des stations de notre région d'étude présentent des ruptures significatives dans la période 1991-2007, alors qu'une rupture dans les températures de surface de la mer (TSM) est observée dans l'Océan Atlantique Nord (Espinoza et al., 2008, Marengo et Camargo, 2008). Le déclin (resp. augmentation) des précipitations dans les Andes (resp. dans la Forêt tropicale de la plaine amazonienne) observé(e) depuis le milieu des années 90 est compatible avec le rapport négatif entre les précipitations dans les Andes méridionales et le gradient de TSM entre l'Océan Atlantique tropical nordique et méridional. Des anomalies opposées de précipitations entre les Andes et la Forêt tropicale ont été déjà commentées (Jones et Carvalho, 2002) à l'échelle de temps intra-saisonnière et sont souvent associées à l'activation ou la rupture de la mousson sud-américaine.

La production des ressources en eau sur les bassins des rios Ucayali et Huallaga, ainsi que l'impact du changement climatique sur l'hydrologie de ces bassins sont décrits dans le **Chapitre 4**. La production des ressources en eau sur les bassins des rios Ucayali et Huallaga est évaluée sur 7 sous-bassins : 6 situés dans le bassin de l'Ucayali et un situé dans le basin de l'Huallaga. Pour quantifier ces ressources en eau nous utilisons deux modèles hydrologiques au pas de temps mensuel (GR2M et MWB3) en considérant comme données d'entrés les grilles de 0.25° par 0.25 de pluie, évapotranspiration et capacité de rétention en eau des sols (CRE). L'utilisation des données de CRE (maximum, moyenne et minimum) de la FAO comme valeurs d'entrée dans les modèles de bilan hydrique au niveau mensuel a contribué à rendre plus physique ces modèles. Les valeurs de CRE minimum apparaissent comme optimum dans le processus de calibration du modèle GR2M, tandis que ce sont les valeurs de CRE minimum ou maximum qui conviennent pour le modèle MWB3. Les paramètres optimaux obtenus par calibration reproduisent raisonnablement bien l'écoulement observé à l'exutoire des bassins sélectionnés avec des coefficients de Nash équivalent pour les deux modèles. Plus finement, le modèle GR2M apparait comme le plus adapté pour les bassins de Requena, Chazuta, Puerto Inca et Maldonadillo tandis que le modèle MWB3 donne de meilleurs résultats pour les bassins de Tambo, Mejorada et Pisac.

L'impact des changements climatiques sur l'hydrologie a été évalué en utilisant les paramètres calibrés dans la section précédente, mais en utilisant comme données climatiques les sorties des modèles de l'IPCC (3 modèles : BCM2, CSMK3 and MIHR) correspondant aux scénarios A1B (stabilisation de la concentration en CO_2 à 720 ppm) et B1 (stabilisation de la concentration en CO_2 à 550 ppm). Les écoulements annuels simulés sur la période 2008-2099 suggèrent que les impacts du changement climatique sur l'hydrologie varient avec le bassin, le modèle hydrologique choisi, et le scénario :

- Le sous-basin Requena est caractérisé par une augmentation (resp. diminution) d'écoulement en utilisant les modèles GR2M (resp. MWB3) en considérant les scénarios A1B et B,

- Les bassins de Chazuta, Maldonadillo et Pisac voient leurs débits diminuer tandis que les bassins de Puerto Inca, Tambo et Mejorada voient leurs débits augmenter. L'impact le plus marqué concerne le bassin de Tambo (modèle MWB3 et scenario A1B).

Les changements simulés dans les écoulements mensuels sur la période 2008-2099 suggèrent une augmentation pour tous les sous-bassins, excepté le bassin de Pisac, en considérant les deux scénarios et les deux modèles hydrologiques. Juillet, Août et Septembre sont en général les mois caractérisés par les changements les plus marqués, avec une augmentation des débits pour les bassins de Requena, Chazuta, Puerto Inca, Maldonadillo et Tambo. Globalement ; le bassin de Puerto Inca apparaît comme le bassin le plus affecté par les changements climatiques au pas mensuel.

5.2 Perspectives

Les différents résultats de cette thèse ouvrent de nombreuses perspectives qui peuvent être déclinées selon quatre axes : validation des autres sources de données de pluie sur le bassin amazonien péruvien, modélisation hydrologique au pas de temps journalier, quantification de l'impact des changements d'usage du sol sur l'hydrologie et impact du changement climatique au niveau journalier sur l'hydrologie.

5.2.1 *Validation des autres sources de données de pluie sur le basin amazonien péruvien.*

Le réseau de stations pluviométriques des bassins amazoniens du Pérou est mal réparti, avec une grande majorité de stations situées dans les Andes. Une source de données des pluies importante à prendre en compte consisterait dans les données du Tropical Rainfall Measurement Mission (TRMM), disponibles au pas de temps journalier et mensuel, et pouvant être utilisées comme données d'entrée dans les modèles hydrologiques comme on le montre dans l'annexe B.

5.2.2 *La modélisation hydrologique au pas de temps journalier*

Une autre perspective qui s'ouvre avec ce travail consisterait à améliorer la modélisation hydrologique au pas de temps journalier. La validation de données de pluies du TRMM en particulier ouvre la voie au développement de travaux de modélisation hydrologique, objectif primordial du SENAMHI. Ceci permettrait aussi de tester et de comparer les résultats d'autres modèles conceptuels disponibles au pas journalier.

5.2.3 *L'impact des changements d'usage du sol sur l'hydrologie*

Dans la forêt tropicale péruvienne, le déboisement est évalué sur la période 2004-2005 a une surface de 1174 km^2 (Oliveira et al., 2007). Dans notre étude, nous utilisons les données de sol de la FAO comme condition initiale de capacité en eau de sols tout en négligeant de facto les changements d'usage des sols. Une étude de sensibilité avec différents scenarios d'occupation du sol permettraient par ailleurs d'évaluer les impacts hydrologiques.

5.2.4 *L'impact du changement hydrologique au niveau journalier sur l'hydrologie.*

Dans le cadre de cette thèse, nous nous sommes focalisés sur des données et modèles mensuels, mais une perspective serait bien sur d'évaluer les impacts des changements

climatiques sur l'hydrologie au niveau journalier. Pour réaliser cet objectif, des techniques de 'downscalling' au niveau journalier devrait être réalisées et les sorties appliquées sur des modèles hydrologiques opérant au pas de temps journalier. Ces résultats permettront ainsi de quantifier l'impact des changements climatiques sur les extrêmes hydrologiques (étiages et crues).

5.2.5 Autres perspectives

Enfin divers autres perspectives peuvent aussi être mentionnées telles que :

- Validation des données d'évapotranspiration (données des bacs type 'A' ou de lysimètres) par comparaison avec les équations empiriques d'évapotranspiration.
- Evaluation des méthodes d'interpolation des variables climatiques.
- Evaluation des tendances des extrêmes hydrométéorologiques en utilisant des données journalières sur de longues périodes pour évaluer les changements climatiques.
- Régionalisation des paramètres des modèles hydrologiques pour évaluer les comportements hydrologiques dans des bassins non jaugés.

Bibliographie

Abtew, W. (1996). Evapotranspiration measurements and modeling for three wetland systems in south Florida. Water Resources Bulletin, 32(3): 465-473.

Aceituno, P. (1988). On the functionning of the Southern Oscillation in the South American sector. Part 1 : surface climate. Mon. Wea. Rev., 116,: 505-524.

ACTO (2005). A proposal for defining the geographical boundaries of Amazonia. In: H.D. Eva et O. Huber (Editors), Synthesis of the results from an Expert Consultation Workshop organized by the European Commission in collaboration with the Amazon Cooperation Treaty Organization - JRC Ispra, 7-8 June 2005.

Ali, S., Ghosh, N.C. et Singh, R. (2007). Evaluating best evaporation estimate model for water surface evaporation in semi-arid region, India. Hydrological Processes

Allen, G.R., Periera, L.S., Raes, D. et Smith, M. (1998). Crop evapotranspiration: Guidelines for computing crop water requirements. FAO Irrigation and Drainage Paper 56. Food and Agricultural Orgainzation of the United Nations.

Alley, W.M. (1985). Water Balance Models in One-Month-Ahead Streamflow Forecasting. Water Resour. Res., 21(4): 597-606.

Andersson, L. *et al.* (2006). Impact of climate change and development scenarios on flow patterns in the Okavango River. Journal of Hydrology, 331(1-2): 43-57.

Ardoin-Bardin, S. (2004). Variabilité hydroclimatique et impacts sur les ressources en eau de grands bassins hydrographiques en zone soudano-sahélienne. , Université Montpellier II, Montpellier, France, 330 p. pp.

Ardoin-Bardin, S. *et al.* (2009). Using general circulation model outputs to assess impacts of climate change on runoff for large hydrological catchments in West Africa. Hydrological Sciences Journal-Journal Des Sciences Hydrologiques, 54(1): 77-89.

Arnell, N.W. (1999). The effect of climate change on hydrological regimes in Europe: a continental perspective. Global Environmental Change, 9(1): 5-23.

Baigorria, G.A., Villegas, E.B., Trebejo, I., Carlos, J.F. et Quiroz, R. (2004). Atmospheric transmissivity: distribution and empirical estimation around the central andes. Int. J. Climatol., 24: 1121-1136.

BCEOM (1999). Estudio hidrológico - meteorológico en la vertiente del Pacífico del Perú con fines de evaluación y pronóstico del fenómeno el niño para prevención y mitigación de desastres. Volumen I, Asociacion BCEOM – Sofi Consult S.A. - ORSTOM, Programa de apoyo a la emergencia Fenomeno del Niño. Contrato de prestamo n°4250-PE-BIRF, Presidencia de la Republica, Perú.

Beven, K. et Kirkby, M. (1979). A physically based variable contributing area model of basin hydrology. Hydrological Sciences Journal, 24: 43-69.

Boughton, W. (2005). Catchment water balance modelling in Australia 1960-2004. Agricultural Water Management, 71(2): 91-116.

Box, G.E.P. et Tiao, G.C. (1973). Bayesian Inference in Statistical Analysis. Addison-Wesley-Longman, Reading, MA.

Bradley, R.S., Vuille, M., Diaz, H.F. et Vergara, W. (2006). Threats to water supplies in the tropical Andes. Science, 312(5781): 1755-1756.

Bristow, K. et Campbell, G. (1984). On the relationship between incoming solar radiation and daily maximum and minimum temperature. Agricultural and Forest Meteorology, 31: 159-166.

Brooks, N. et Adger, N. (2003). Country level risk measures of climate-related natural disasters and implications for adaptation to climate change. Working Paper 26, Tyndall Centre for Climate Change Research.

Brunet-Moret, Y. (1979). Homogénéisation des précipitations Cahiers ORSTOM, Série Hydrologie., 16: 3-4.

Burn, D.H. et Elnur, M.A.H. (2002). Detection of hydrologic trends and variability. Journal of Hydrology, 255(1-4): 107-122.

CARE (2008). Humanitarian Implications of Climate Change: Mapping Emerging Trends and Risk Hotspots" Copyright © 2008 Cooperative for Assistance and Relief Everywhere, Inc. (CARE).

Chaffaut, I., Coudrian-Ribstein, A., Michelot, J.L. et Pouyaud, B. (1998). Précipitations d'altitude du Nord-Chili, origine des sources de vapeur et donnés isotopiques,. Bull. Inst. Fr. Etudes Andines, 27: 367-384.

Charles, S.P., Bari, M.A., Kitsios, A. et Bates, B.C. (2007). Effect of GCM bias on downscaled precipitation and runoff projections for the Serpentine catchment, Western Australia. International Journal of Climatology, 27(12): 1673-1690.

Chen, D.L., Gao, G., Xu, C.Y., Guo, J. et Ren, G.Y. (2005). Comparison of the Thornthwaite method and pan data with the standard Penman-Monteith estimates of reference evapotranspiration in China. Climate Research, 28(2): 123-132.

Chen, J., Del Genio, A.D., Carlson, B.E. et Bosilovich, M.G. (2008). The spatiotemporal structure of twentieth-century climate variations in observations and reanalyses. Part I: Long-term trend. J. Climate, 21: 2611-2633.

Chen, X., Chen, Y.D. et Xu, C.Y. (2007). A distributed monthly hydrological model for integrating spatial variations of basin topography and rainfall. Hydrological Processes, 21(2): 242-252.

Chiew, F.H.S., Kamaladasa, N.N., Malano, H.M. et McMahon, T.A. (1995). Penman-Monteith, FAO-24 reference crop evapotranspiration and class-A pan data in Australia. Agricultural Water Management, 28(1): 9-21.

Christensen, J.H. *et al.* (2007). Regional Climate Projections. In: Climate Change 2007: The Physical Science Basis. . Contribution of Working Group I to the Fourth Assessment Report of the Intergovernmental Panel on Climate Change [Solomon, S., D. Qin, M. Manning, Z. Chen, M. Marquis, K.B. Averyt, M. Tignor and H.L. Miller (eds.)]. Cambridge University Press, Cambridge, United Kingdom and New York, NY, USA.

Coe, M.T., Costa, M.H., Botta, A. et Birkett, C. (2002). Long-term simulations of discharge and floods in the Amazon Basin. Journal of Geophysical Research-Atmospheres, 107(D20).

Coe, M.T., Costa, M.H. et Howard, E.A. (2008). Simulating the surface waters of the Amazon River basin: impacts of new river geomorphic and flow parameterizations. Hydrological Processes, 22(14): 2542-2553.

Collischonn, B., Collischonn, W. et Tucci, C.E.M. (2008). Daily hydrological modeling in the Amazon basin using TRMM rainfall estimates. Journal of Hydrology, 360(1-4): 207-216.

Collischonn, W., Allasia, D., Silva, B.C.D. et Tucci, C.E.M. (2007). The MGB-IPH model for large-scale rainfall–runoff modelling / Le modèle MGB-IPH pour la modélisation pluie–débit à grande échelle. Hydrological Sciences Journal, 52(5): 878-895.

Conway, D. et Jones, P.D. (1999). Assessing the impact of future climatic change on the water resources and the hydrology of the Rio de la Plata basin, Argentina. Climatic Research Unit, University of East Anglia, UK.

Costa, M.H. et Foley, J.A. (1997). Water balance of the Amazon Basin: Dependence on vegetation cover and canopy conductance. Journal of Geophysical Research-Atmospheres, 102(D20): 23973-23989.

Costa, M.H. et Foley, J.A. (1999). Trends in the hydrologic cycle of the Amazon basin. Journal of Geophysical Research-Atmospheres, 104(D12): 14189-14198.

Costa, M.H. *et al.* (2002). A macroscale hydrological data set of river flow routing parameters for the Amazon Basin. Journal of Geophysical Research-Atmospheres, 107(D20).

Dettinger, M.D., Cayan, D.R., Meyer, M. et Jeton, A.E. (2004). Simulated hydrologic responses to climate variations and change in the Merced, Carson, and American River basins, Sierra Nevada, California, 1900-2099. Climatic Change, 62(1-3): 283-317.

Deutsch, C.V. et Journel, A.G. (1992). GSLIB Geostatistical Software Library and User's Guide. TIC: 224174., New York, New York: Oxford University Press.

Dibike, Y.B. et Coulibaly, P. (2005). Hydrologic impact of climate change in the Saguenay watershed: comparison of downscaling methods and hydrologic models. Journal of Hydrology, 307(1-4): 145-163.

Dieulin, C. (2005). Calcul des capacités en eau des sols (Water Holding Capacity - WHC) à partir de la carte des sols de la FAO, Note interne. HydroSciences Montpellier.

Dieulin, C., Boyer, J.F., Ardoin-Bardin, S. et Dezetter, A. (2006). The contribution of GIS to hydrological modelling. Climate Variability and Change-Hydrological Impacts, 68-74. IAHS Publ. 308, IAHS Press, Wallingford, UK, La Habana, Cuba, November 2006.

Dingman, S.L. (1994). Physical Hydrology. Upper Saddle River, NJ: Prentice Hall.

Dollfus, O. (1964). Cambios climáticos cuaternarios en los Andes Peruanos. Bol.Soc.Geogr. Lima, 83: 65-74 and 84: 78-83.

Doorenbos, J. et Pruitt., W.O. (1977). Guidelines for predicting crop water requirements. FAO Irrigation and Drainage Paper 24. Food and Agriculture Organization. Rome.

Dray, A. (2001). Prise en compte de l'evolution de la occupation du sol dans la modélisation des écoulements du Nakambé à Wayen (Burkina Faso), Rapport de stage ENSAR-IRD.

Drogue, G. *et al.* (2004). Simulating the spatio-temporal variability of streamflow response to climate change scenarios in a mesoscale basin. Journal of Hydrology, 293(1-4): 255-269.

Duan, Q., Sorooshian, S. et Gupta, V. (1992). Effective and Efficient Global Optimization for Conceptual Rainfall-Runoff Models. Water Resources Research, 28(4): 1015-1031.

Edijatno et Michel, C. (1989). Un modèle pluie–débit journalier à trois paramètres. La Houille Blanche, 2: 113-121.

Edijatno, Nascimento, N.O., Yang, X., Makhlouf, Z. et Michel, C. (1999). GR3J : a daily watershed model with three free parameters. Hydrological Sciences Journal, 44(2), 263-278., 44(2): 263-278.

Emanuel, C. et Escurra, J. (2000). Informe Nacional sobre la Gestión del Agua en el Perú, Comité asesor técnico de América del Sur – SAMTAC – Global Water Partnership (GWP). Lima.

Espinoza, J.C. *et al.* (2006a). La variabilité des débits du Rio Amazonas au Pérou. Climate variability and Change – Hydrological Impacts (Procceedings of the Fifth FRIEND World Conference held at Havana, Cuba, November 2006), IAHS Publ. 308, 2006, 424-429.

Espinoza, J.C. *et al.* (2006b). La variabilité des débits du Rio Amazonas au Pérou. Climate Variability and Change-Hydrological Impacts, 424 – 429. IAHS Publ. 308, IAHS Press, Wallingford, UK, La Habana, Cuba, November 2006.

Espinoza, J.C. *et al.* (2009a). Contrasting regional discharge evolutions in the amazon basin (1974 – 2004). Accepted by Journal of Hydrology.

Espinoza, J.C. *et al.* (2007). Hydroclimatic variability in the Andean region of the Amazon basin, Paper read at Changes to hydrologic extremes. IAHS, Perugia (Italia), juil-07.

Espinoza , J.C. *et al.* (In Press). Contrasting regional discharge evolutions in the Amazon basin (1974-2004). Journal of Hydrology, In Press, Accepted Manuscript.

Espinoza, J.C. *et al.* (2008). Spatio – Temporal rainfall variability in the Amazon Basin Countries (Brazil, Peru, Bolivia, Colombia and Ecuador). International Journal of Climatology, 9999(9999): n/a.

Espinoza, J.C. *et al.* (2009b). Spatio – Temporal rainfall variability in the Amazon Basin Countries (Brazil, Peru, Bolivia, Colombia and Ecuador). Accepted by International Journal of Climatology.

Espinoza, V.J.C. *et al.* (In Press). Contrasting regional discharge evolutions in the Amazon basin (1974-2004). Journal of Hydrology, In Press, Accepted Manuscript.

FAO/UNESCO (1981). CD-ROM :Soil Map of the World, Ten volumes. UN Food and Agriculture Organization, Rome, Italy.

Farr, T.G. *et al.* (2007). The Shuttle Radar Topography mission. Rev. Geophys., 45,: RG2004.

Feyen, L., Vrugt, J.A., Nuallain, B.O., van der Knijff, J. et De Roo, A. (2007). Parameter optimisation and uncertainty assessment for large-scale streamflow simulation with the LISFLOOD model. Journal of Hydrology, 332: 276-289.

Figueroa, S.N. et Nobre, C. (1990). Precipitation distribution over central and western tropical South America. Climanalise, 5: 36-44.

Fontaine, T.A., Klassen, J.F., Cruickshank, T.S. et Hotchkiss, R.H. (2001). Hydrological response to climate change in the Black Hills of South Dakota, USA. Hydrological Sciences Journal-Journal Des Sciences Hydrologiques, 46(1): 27-40.

Fontenot, R.L. (2004). An evaluation of reference evapotranspiration models in Louisiana, Lousiana State University and A&M College, Louisiana.

Fooladmand, H.R. et Ahmadi, S.H. (2008). Monthly spatial calibration of Blaney-Criddle equation for calculating monthly ETo in south of Iran. Irrigation and Drainage, 9999(9999): n/a.

Fuenzalida, H. et Rutllant, J. (1987). Origen del vapor de agua que precipita sobre el Altiplano de Chile, paper presented at II Congreso InterAmericano de Meteorología, Am. Meteorol. Soc., Buenos Aires.

Garreaud, R., Vuille, M. et Clement, A.C. (2003). The climate of the Altiplano: observed current conditions and mechanisms of past changes. Palaeogeography, Palaeoclimatology, Palaeoecology, 194: 5-22.

Garreaud, R.D. (1999). Multiscale Analysis of the Summertime Precipitation over the Central Andes. Monthly Weather Review, 127(5): 901-921.

Garreaud, R.D., Vuille, M., Compagnucci, R. et Marengo, J. (2008). Present-day South American climate. Palaeogeography, Palaeoclimatology, Palaeoecology, In Press, Corrected Proof.

Gavilán, P., Lorite, I.J., Tornero, S. et Berengena, J. (2006). Regional calibration of Hargreaves equation for estimating reference ET in a semiarid environment. Agricultural Water Management, 81(3): 257-281.

Geiger, R., Aron, R.H. et Toddhunter, P. (2003). The Climate Near The Ground, 6th Ed. New York: Rowman and Littlefield.

Gelman, A. et Rubin, D.B. (1992). Inference from iterative simulation using multiple sequences. Statistical Science 7(4): 457-472.

Gentry, A.H. et Lopez-Parodi, J. (1980). Deforestation and Increased Flooding of the Upper Amazon. Science, 210(4476): 1354-1356.

Georges, C. (2004). The 20th century glacier fluctuations in the Cordillera Blanca (Perú). Arctic, Antarctic, and Alpine Research, 36(1): 100-107.

Guo, S., Wang, J., Xiong, L., Ying, A. et Li, D. (2002a). A macro-scale and semi-distributed monthly water balance model to predict climate change impacts in China. Journal of Hydrology, 268(1-4): 1-15.

Guo, S.L., Wang, J.X., Xiong, L.H., Ying, A.W. et Li, D.F. (2002b). A macro-scale and semi-distributed monthly water balance model to predict climate change impacts in China. Journal of Hydrology, 268(1-4): 1-15.

Guyot, J.L., Bazán, H., Fraizy, P. et Ordoñez, J.J. (2007). Suspended sediment yields in the Amazon basin of Peru, first estimation. Water quality and sediment behaviour of the future : Predictions for the 21st Century (Webb B.W., Ed.), Perugia (Italia), 07/2007. IAHS Publ. 314, 1-8.

Hagg, W., Braun, L.N., Kuhn, M. et Nesgaard, T.I. (2007). Modelling of hydrological response to climate change in glacierized Central Asian catchments. Journal of Hydrology, 332(1-2): 40-53.

Hamon, W.R. (1961). Estimating potential evaporation. In: J.o.H. Division (Editor), Proceedings of the American Society of Civil Engineers, pp. 107-120.

Hansen, M., DeFries, R., Townshend, J.R.G. et Sohlberg, R. (1998). UMD Global Land Cover Classification, 1 Kilometer, 1.0, Department of Geography, University of Maryland, College Park, Maryland, 1981-1994.

Hansen, V.E., Israelsen, O.W. et Stringham, G.E. (1980). Irrigation Principles and Practices 4th Edition. . New York, NY: John Wiley and Sons, Inc.

Hargreaves, G.H. et Samani, Z.A. (1985). Reference crop evapotranspiration from temperature. Applied Engineering in Agriculture, 1(2): 96-99.

Hastings, W.K. (1970). Monte Carlo sampling methods using Markov chains and their applications. Biometrika, 57(1): 97-109.

Haylock, M.R. *et al.* (2006). Trends in Total and Extreme South American Rainfall in 1960-2000 and Links with Sea Surface Temperature. Journal of Climate, 19(8): 1490-1512.

Hiez, G. (1977). L'homogénéité des données pluviométriques. Cahiers ORSTOM, série Hydrologie, 14: 129-72.

IGP (2005). Vulnerabilidad Actual y Futura ante el Cambio Climático y Medidas de Adaptación en la Cuenca del Río Mantaro. Evaluación local Integrada de Cambio Climático para la Cuenca del Río Mantaro, 9972-824-13-6, Lima, Perú.

Jabloun, M. et Sahli, A. (2008). Evaluation of FAO-56 methodology for estimating reference evapotranspiration using limited climatic data: Application to Tunisia. Agricultural Water Management, 95(6): 707-715.

Jayasuriya, L.N., McMahon, T.A. et O'Neill, I.C. (1991). Development of a simplified two-parameter rainfall-runoff model with potential for ungauged catchment application. International Hydrology and Water Resources Symposium, 2: 498-503.

Jensen, M.E. et Haise, H.R. (1963). Estimating evapotranspiration from solar radiation. Journal of Irrigation and Drainage Division, ASCE, 89(LR4): 15-41.

Jensen, M.E., R.D.Burman et Allen, R.G. (1990). Evapotranspiration and Irrigation Water Requirements. Manuals and Reports on Engineering Practice, Nº 70, Committee on Irrigation Water Requirements of the Irrigation and Drainage Division of the American Society of Civil Engineers.

Jiang, T. *et al.* (2007). Comparison of hydrological impacts of climate change simulated by six hydrological models in the Dongjiang Basin, South China. Journal of Hydrology, 336(3-4): 316-333.

Johnson, A. (1976). The climate of Peru, Bolivia and Ecuador. Climates of Central and South America. World Survey of Climatology, Vol. 12. Elsevier Scientific Publishing Company; New York 147-218, Chap. 4.

Jones, C. et Carvalho, L.M.V. (2002). Active and Break Phases in the South American Monsoon System. J. Climate, 15: 905-914.

Jones, R.N., Chiew, F.H.S., Boughton, W.C. et Zhang, L. (2006). Estimating the sensitivity of mean annual runoff to climate change using selected hydrological models. Advances in Water Resources, 29(10): 1419-1429.

Jose, A.M. et Cruz, N.A. (1999). Climate change impacts and responses in the Philippines: water resources. Climate Research, 12(2-3): 77-84.

Juen, I., Kaser, G. et Georges, C. (2007). Modelling observed and future runoff from a glacierized tropical catchment (Cordillera Blanca, Peru). Global and Planetary Change, 59: 37-48.

Kabouya, M. (1990). Modélisation pluie-débit au pas de temps mensuel et annuel en Algérie septentrionale., Université Paris-Sud, Paris, France.

Kane, R.P. (2000). El Nino/La Nina relationship with rainfall at Huancayo, in the Peruvian Andes. International Journal of Climatology, 20(1): 63-72.

Kaser, G., Juen, I., Georges, C., Gomez, J. et Tamayo, W. (2003). The impact of glaciers on the runoff and the reconstruction of mass balance history from hydrological data in the tropical Cordillera Blanca, Peru. Journal of Hydrology, 282(1-4): 130-144.

Kendall, M. (1975a). Rank Correlation Methods. Charles Griffin: London; 202 pp.

Kendall, M.G. (1975b). Rank Correlation Methods. Charles Griffin, London.

Kundzewicz, Z.W. *et al.* (2007). Freshwater resources and their management. Climate Change 2007: Impacts, Adaptation and Vulnerability. Contribution of Working Group II to the Fourth Assessment Report of the Intergovernmental Panel on Climate Change, M.L. Parry, O.F. Canziani, J.P. Palutikof, P.J. van der Linden and C.E. Hanson, Eds., Cambridge University Press, Cambridge, UK, 173-210.

Labat, D., Godderis, Y., Probst, J.L. et Guyot, J.L. (2004). Evidence for global runoff increase related to climate warming. Advances in Water Resources, 27(6): 631-642.

Laraque, A., Ronchail, J., Cochonneau, G., Pombosa, R. et Guyot, J.L. (2007). Heterogeneous distribution of rainfall and discharge regimes in the Ecuadorian Amazon basin. Journal of Hydrometeorology, 8(6): 1364-1381.

Lavado, C.W.S., Labat, D., Guyot, J.L., Ardoin-Bardin, S. et Ordoñez, J.J. (2008). Monthly water balance models in the Amazon drainage basin of Peru: Ucayali River basin. Submitted Hydrological Sciences Journal.

Lavado, C.W.S. *et al.* (submitted-a). Comparison of reference evapotranspiration models with the standard FAO Penman-Monteith model in the Peruvian Amazon-Andes basin. Journal of Hydrology.

Lavado, C.W.S. *et al.* (Submitted-b). Recent trends in rainfall, temperature and evapotranspiration in the Peruvian Amazonas-Andes basin: Huallaga and Ucayali basins. International Journal of Climatology.

Legates, D.R. et McCabe, G.J. (1999). Evaluating the use of "goodness of fit" measures in hydrologic and hydroclimatic model validation. Water Resources Research, 35(1): 233-241.

Liebmann, B. et Marengo, J.A. (2001). Interannual variability of the rainy season and rainfall in the Brazilian Amazon basin. Journal of Climate, 14(22): 4308-4318.

Limbrick, K.J., Whitehead, P.G., Butterfield, D. et Reynard, N. (2000). Assessing the potential impacts of various climate change scenarios on the hydrological regime of the River Kennet at Theale, Berkshire, south-central England, UK: an application and evaluation of the new semi-distributed model, INCA. The Science of The Total Environment, 251-252: 539-555.

Linacre, E.T. (1977). A simple formula for estimating evaporation rates in various climates, using temperature data alone. Agricultural Meteorology, 18(6): 409-424.

Mahe, G., Paturel, J.-E., Servat, E., Conway, D. et Dezetter, A. (2005). The impact of land use change on soil water holding capacity and river flow modelling in the Nakambe River, Burkina-Faso. Journal of Hydrology, 300(1-4): 33-43.

Makhlouf, Z. et Michel, C. (1994). A two-parameter monthly water balance model for French watersheds. Journal of Hydrology, 162(3-4): 299-318.

Makkink, G.F. (1957). Testing the Penman formula by means of lysimeters. Journal of the Institution of Water Engineering, 11(3): 277-288.

Mann, H.B. (1945). Non-parametric test againest trend. Econometrica, 13: 245-259.

Marengo, J. (2006). On the hydrological cycle of the amazon basin: A historical review and current state-of-the-art. Revista Brasileira de Meteorologia, 21(3): 1-19.

Marengo, J.A. (1992). Interannual Variability of Surface Climate in the Amazon Basin. International Journal of Climatology, 12(8): 853-863.

Marengo, J.A. (1995). Variations and change in south American streamflow. Climatic Change, 31(1): 99-117.

Marengo, J.A. (2004). Interdecadal variability and trends of rainfall across the Amazon basin. Theoretical and Applied Climatology, 78(1): 79-96.

Marengo, J.A. et Camargo, C.C. (2008). Surface air temperature trends in Southern Brazil for 1960-2002. International Journal of Climatology, 28(7): 893-904.

Marengo, J.A., Miller, J.R., Russell, G.L., Rosenzweig, C.E. et Abramopoulos, F. (1994). Calculations of river-runoff in the GISS GGM: impact of a new land-surface parameterization and runoff routing model on the hydrology of the Amazon River. Climate Dynamics, 10(6): 349-361.

Marengo, J.A. *et al.* (2008). The drought of Amazonia in 2005. Journal of Climate, 21: 495-516.

Marengo, J.A., Tomasella, J. et Uvo, C.R. (1998a). Trends in streamflow and rainfall in tropical South America: Amazonia, eastern Brazil, and northwestern Peru. Journal of Geophysical Research, 103(D2): 1775–1784.

Marengo, J.A., Tomasella, J. et Uvo, C.R. (1998b). Trends in streamflow and rainfall in tropical South America: Amazonia, eastern Brazil, and northwestern Peru. Journal of Geophysical Research-Atmospheres, 103(D2): 1775-1783.

Mark, B.G. et Seltzer, G.O. (2005). Evaluation of recent glacier recession in the Cordillera Blanca, Peru (AD 1962-1999): spatial distribution of mass loss and climatic forcing. Quaternary Science Reviews, 24(20-21): 2265-2280.

Matondo, J.I. et Msibi, K.M. (2001). Estimation of the impact of climate change on hydrology and water resources in Swaziland. Water International, 26(3): 425-434.

Melice, J. et Roucou, P. (1998). Decadal time scale variability recorded in the Quelccaya summit ice core ä18O isotopic ratio series and its relation with the sea surface temperature. Climate Dynamics, 14: 117-132.

MEM (1979). Evaluación del potencial hidroeléctrico nacional. Ministerio de Energia y Minas. Lima, Perú.

Menzel, L. et Bürger, G. (2002). Climate change scenarios and runoff response in the Mulde catchment (Southern Elbe, Germany). Journal of Hydrology, 267(1-2): 53-64.

Metropolis, N., Rosenbluth, A.W., Rosenbluth, M.N., Teller, A.H. et Teller, E. (1953). Equation of State Calculations by Fast Computing Machines. The Journal of Chemical Physics, 21(6): 1087-1092.

Mialocq, L., Acuña, M., Seyler, F., Yerren, J. et Guyot, J.L. (2005). Extraction of the topographic limits of the Andean and Amazonian river basins from SRTM., Isotope tracers and remote sensing techniques for assessing water cycle variability, IAHS, Foz de Iguaçu, April 2005.

Middelkoop, H. *et al.* (2001). Impact of climate change on hydrological regimes and water resources management in the rhine basin. Climatic Change, 49(1-2): 105-128.

Miller, J.R., Russell, G.L. et Caliri, G. (1994). Continental-Scale River Flow in Climate Models. Journal of Climate, 7(6): 914-928.

Mimikou, M., Kouvopoulos, Y., Cavadias, G. et Vayianos, N. (1991). Regional hydrological effects of climate change. Journal of Hydrology, 123(1-2): 119-146.

Molinier, M., Guyot, J.-L., Oliveira, E.d. et Guimarães, V. (1996). Les régimes hydrologiques de l'Amazone et de ses affluents. L'hydrologie tropicale: géoscience et outil pour le développement, 209-222. IAHS Publ. 238. IAHS Press, Wallingford, UK.

Molion, L.C.B. (1987). Micrometeorology of an Amazonian Rainforest. In: The Geophysiology of Amazonia, R. E. Dickinson (Ed.): 255-270.

Molion, L.C.B. (1991). Climate Variability And Its Effects On Amazonian Hydrology, International Seminar on Hydrology and Water Management of the Amazon Basin. UNESCO publication, Manaus, Brazil.

Montecinos, A. et Aceituno, P. (2003). Seasonality of the ENSO-Related Rainfall Variability in Central Chile and Associated Circulation Anomalies. Journal of Climate, 16(2): 281-296.

Mouehli, S. (2003). Vers une chaîne cohérente de modèles pluie-débit conceptuels globaux aux pas de temps pluriannuel, annuel, mensuel et journalier, Université Paris VI, Paris, France., 323 p. pp.

Mouelhi, S., Michel, C., Perrin, C. et Andréassian, V. (2006). Stepwise development of a two-parameter monthly water balance model. Journal of Hydrology, 318(1-4): 200-214.

Muller-Wohlfeil, D.I., Xu, C.Y. et Iversen, H.L. (2003). Estimation of monthly river discharge from Danish catchments. Nordic Hydrology, 34(4): 295-320.

Nakicenovic, N. *et al.* (2000). Special report on emissions scenarios, International Panel on Climate Change. Cambridge University Press, Cambridge, UK.

Nash, J.E. et Sutcliffe, J.V. (1970). River flow forecasting through conceptual models part I -- A discussion of principles. Journal of Hydrology, 10(3): 282-290.

New, M., Hulme, M. et Jones, P. (2000). Representing Twentieth-century Space-time Climate Variability. Part II: Development of 1901–1996 Monthly Grids of Terrestrial Surface Climate. J. Climate 13: 2217–2238.

Niel, H., Paturel, J.-E. et Servat, E. (2003). Study of parameter stability of a lumped hydrologic model in a context of climatic variability. Journal of Hydrology, 278(1-4): 213-230.

Nijssen, B., Donnell, G.M., Lettenmaier, D.P., Lohmann, D. et Wood, E.F. (2001). Predicting the Discharge of Global Rivers. Journal of Climate, 14(15): 3307-3323.

Nijssen, B., Lettenmaier, D., Liang, X., Wetzel, S. et Wood, E. (1997). Streamflow simulation for continental-scale river basins. Water Resources Research, 33: 711-724.

Nordin, C.F., Meade, R.H., Gentry, A.H. et Lopez-Parodi, J. (1982). Deforestation and Increased Flooding of the Upper Amazon. Science, 215(4531): 426-427.

Oliveira, P.J.C. *et al.* (2007). Land-Use Allocation Protects the Peruvian Amazon. Science, 317(5842): 1233-1236.

Oliver, M.A. et Webster, R. (1990). Kriging: a method of interpolation for geographical information system
Int. J. Geographical Information Systems, 4(3): 313-332.

Olson, J.S., Watts, J.A. et Allison, L.J. (1985). Major world ecosystem complexes ranked by carbon in live vegetation: A database. NDP-017, Carbon Dioxide Inf. Cent., Oak Ridge Natl. Lab., Oak Ridge, Tenn.

ONERN (1981). Mapa de Capacidad de Uso Mayor de las Tierras del Peru. Land Use Map of Peru. Oficina Nacional de Evaluación de Recursos Naturales (ONERN).Lima, Perú.

Ordoñez, J.J. (2001). Análisis hidrometeorológico y aplicación del modelo de simulación IPH-MEN en la cuenca del Pachitea, Universidad Agraria La Molina, Lima, Perú.

Ouedraogo (2001). Contribution à l'étude de l'impact de la variabilité climatique sur les ressources en eau en Afrique de l'ouest. Analyse des conséquences d'une sécheresse persistante : normes hydrologiques et modélisation régional, Université Montpellier II, Montpellier II, France.

Paturel, J.E. *et al.* (2003). The influence of distributed input data on the hydrological modelling of monthly river flow regimes in West Africa. Hydrological Sciences Journal-Journal Des Sciences Hydrologiques, 48(6): 881-890.

Paturel, J.E., Servat, E. et Vassiliadis, A. (1995). Sensitivity of conceptual rainfall-runoff algorithms to errors in input data -- case of the GR2M model. Journal of Hydrology, 168(1-4): 111-125.

Paz, A.R., Collischonn, W. et da Silveira, A.L.L. (2006). Improvements in large-scale drainage networks derived from digital elevation models. Water Resources Research, 42(8).

Peñaherrera, C. (2004). V Geografía In: Enciclopedia Temática del Perú. Orbis Ventures S.A.C.

Penman, H.L. (1948). Natural evaporation from open water, bare soil, and grass. Proceedings of the Royal Society of London, A193: 120-146.

Pettitt, A.N. (1979). A Non-Parametric Approach to the Change-Point Problem. Applied Statistics, 28(2): 126-135.

Popova, Z. et Pereira, M.K.L.S. (2006). Validation of the FAO methodology for computing ETo with limited data. Application to south Bulgaria. Irrigation and Drainage, 55(2): 201-215.

Pouyaud, B. *et al.* (2005). On the future of the water resources from glacier melting in the Cordillera Blanca, Peru. Hydrological Sciences Journal-Journal Des Sciences Hydrologiques, 50(6): 999-1022.

Priestley, C.H.B. et Taylor, R.J. (1972). On the assessment of surface heat flux and evaporation using large-scale parameters. Monthly Weather Review, 100(2): 81-92.

Pulgar, V.J. (1941). Geografía del Perú : las ocho regiones naturales del Perú Lima : Edit. Universo.

Randall, D.A. *et al.* (2007). Cilmate Models and Their Evaluation. In: Climate Change 2007: The Physical Science Basis. Contribution of Working Group I to the Fourth Assessment Report of the Intergovernmental Panel on Climate Change [Solomon, S., D. Qin, M. Manning, Z. Chen, M. Marquis, K.B. Averyt, M.Tignor and H.L. Miller (eds.)]. Cambridge University Press, Cambridge, United Kingdom and New York, NY, USA.

Remanenko, V.A. (1961). Computation of the autumn soil moisture using a universal relationship for a large area. Proc. of the Ukrainian Hydrometeorological Research Institute, No.3, Kiev.

Richey, J.E., Nobre, C. et Deser, C. (1989). Amazon River Discharge and Climate Variability: 1903 to 1985. Science, 246(4926): 101-103.

Rigsby, C.A., Baker, P.A. et Aldenderfer, M.S. (2003). Fluvial history of the Rio Ilave valley, Peru, and its relationship to climate and human history. Palaeogeography, Palaeoclimatology, Palaeoecology, 3061: 1-21.

Robson, A., Bardossy, A., Jones, D. et Kundzewicz, Z.W. (2000). Chapter 5: Statistical Methods for testing for change. In: Z.W.R. Kundzewicz, A. (Editor), Detecting Trend and Other Changes in Hydrological Data, WMO/TD 1013. Geneva, 157 pp.

Rocha, H.R.d., Nobre, C.A. et Barros, M.C. (1989). Variabilidade natural de longo prazo no ciclo hidrologico da Amazonia. Climanálise, 4(12): 36-42.

Roche, M. *et al.* (1990). Hétérogénéité des précipitations sur la cordillère des Andes boliviennes, Hydrology in Mountainous Regions. I - Hydrological Measurements; the Water Cycle, IAHS 193, 381-388.

Rome-Gaspaldy, S. et Ronchail, J. (1998). La pluviométrie au Pérou pendant les phases ENSO et LNSO. Bulletin de l'Institut Française d'Etudes Andins., 27,: 675 – 685.

Romero, C.C., Baigorria, G.A. et Stroosnijder, L. (2007). Changes of erosive rainfall for El Nino and La Nina years in the northern Andean highlands of Peru. Climatic Change, 85: 343-356.

Ronchail, J. *et al.* (2002). Interannual rainfall variability in the Amazon basin and sea-surface temperatures in the equatorial Pacific and the tropical Atlantic Oceans. International Journal of Climatology, 22(13): 1663-1686.

Ropelewski, C.F. et Halpert, M.S. (1987). Global and regional scale precipitations patterns associated with El Nino-Southern Oscillation. Mon. Wea. Rev., 115,: 1606-1626.

Ruiz, R.R., Torres, H.G. et Aguirre, M.N. (2008). Delimitación y codificación de unidades hidrográficas del Perú, Autoridad Nacional del Agua-Ministerio de Agricultura.

Russell, G.L. et Miller, J.R. (1990). Global river runoff calculated from a global atmospheric general circulation model. Journal of Hydrology, 117(1-4): 241-254.

Rutllant, J., Fuenzalida, H. et Aceituno, P. (2003). Climate dynamics along the arid northern coast of Chile: the 1997-1998 Dinamica del clima de la Region de Antofagasta (DICLIMA) experiment. J. Geophys. Res., 108(D17).

Salathe, E.P., Mote, P.W. et Wiley, M.W. (2007). Review of scenario selection and downscaling methods for the assessment of climate change impacts on hydrology in the United States pacific northwest. International Journal of Climatology, 27(12): 1611-1621.

Salati, E. (1987). The forest and the hydrological cycle. In Dickenson, R. (Ed.), The Geophysiology of Amazonia. (pp. 273-294). New York, New York, U.S.A.: John Wiley and Sons.

Sefton, C.E.M. et Boorman, D.B. (1997). A regional investigation of climate change impacts on UK streamflows. Journal of Hydrology, 195(1-4): 26-44.

SENAMHI (1993). Atlas de evaporación del Perú, Servicio Nacional de Meteorología e Hidrologia, Lima, Perú.

SENAMHI (2003). Atlas de energia solar del Peru, Servicio Nacional de Meteorologia e Hidrologia Lima, Peru.

SENAMHI (2005). Mapa Climatico del Peru, Servicio Nacional de Metorologia e Hidrologia, Lima, Peru.

Shuttleworth, W.J. (1988). Evaporation from Amazonian rainforest. In: Proceedings Roy. Soc. Lond. B. , 233: 321-346.

Silverio, W. et Jaquet, J.-M. (2005). Glacial cover mapping (1987-1996) of the Cordillera Blanca (Peru) using satellite imagery. Remote Sensing of Environment, 95(3): 342-350.

St-Onge, L., Bonn, F., Rousseau, A.N., Van Cu, P. et My, N.Q. (2007). Modelling the water balance of the BaBe Lake watershed, Vietnam, using physical data from remotely sensed images and climatological data. Hydrological Sciences Journal-Journal Des Sciences Hydrologiques, 52(4): 654-670.

Steele-Dunne, S. *et al.* (2008). The impacts of climate change on hydrology in Ireland. Journal of Hydrology, 356(1-2): 28-45.

Strzepek, K.M. et Yates, D.N. (1997). Climate change impacts on the hydrologic resources of Europe: A simplified continental scale analysis. Climatic Change, 36(1-2): 79-92.

Synder, R.L. (1992). Equation for evaporation pan to evapotranspiration conversions. Journal of Irrigation and Drainage Engineering, 118(1): 977-980.

Szilagyi, J., Gribovszki, Z. et Kalicz, P. (2007). Estimation of catchment-scale evapotranspiration from baseflow recession data: Numerical model and practical application results. Journal of Hydrology, 336(1-2): 206-217.

Tapley, T.D. et Waylen, P.R. (1989). A Mixture Model of annual precipitation in Peru. The Professional Geographer, 41(1): 62-71.

Tapley, T.D.J. et Waylen, P.R. (1990). Spatial variability of annual precipitation and ENSO events in western Peru. Hydrological Sciences Journal, 35, : 429-445.

Tapley, T.D.J. et Waylen, P.R. (1990). Spatial variability of annual precipitation and ENSO events in western Peru. Hydrological Sciences Journal, 35, : 429-445.

Thodsen, H. (2007). The influence of climate change on stream flow in Danish rivers. Journal of Hydrology, 333(2-4): 226-238.

Thornthwaite, C.W. (1948a). An approach toward a rational classification of climate. Geogr. Rev., 38(1): 55-94.

Thornthwaite, C.W. (1948b). An approach toward a rational classification of climate. Geogr. Rev., 38(1): 55-94.

Tomasella, J. *et al.* (2008). The water balance of an Amazonian micro-catchment: the effect of interannual variability of rainfall on hydrological behaviour. Hydrological Processes, 22(13): 2133-2147.

Trenberth, K. et Hurell, J. (1994). Decadal atmosphere-ocean variations in the Pacific. Climate Dynamics, 9: 303-319.

Trenberth, K.E. *et al.* (2007). Observations: Surface and Atmospheric Climate Change. Climate Change 2007: The Physical Science Basis. Contribution of Working Group I to the Fourth Assessment Report of the Intergovernmental Panel on Climate Change, Cambridge, United Kingdom and New York, NY, USA.

Tucci, C.E.M. (1998). *Modelos Hidrológicos*. Editora da UFRGS, 2ª edição, Porto Alegre, Brazil.

Turc, L. (1961). Evaluation des besoins en eau d'irrigation, evapotranspiration potentielle, formule climatique simplifee et mise a jour. Annales Agronomiques, 12(1): 13-49.

UNESCO (2006). Balance hídrico superficial del Perú a nivel multianual. Documentos Técnicos del PHI-LAC, Nº1.

Valeriano, M.M. *et al.* (2006). Modeling small watersheds in Brazilian Amazonia with shuttle radar topographic mission-90 m data. Computers & Geosciences, 32(8): 1169-1181.

Vandewiele, G.L. et Ni Lar, W. (1998). Monthly water balance models for 55 basins in 10 countries. Hydrological Sciences Journal-Journal Des Sciences Hydrologiques, 43(5): 687-699.

Vandewiele, G.L., Xu, C.-Y. et Ni Lar, W. (1992). Methodology and comparative study of monthly water balance models in Belgium, China and Burma. Journal of Hydrology, 134(1-4): 315-347.

Vandewiele, G.L., Xu, C.-Y. et Ni Lar, W. (1993). Methodology for constructing monthly water balance on basin scale, secodnd ed., Laboratory of Hydrology, Vrije Universiteit Brussel.

Vauchel, P. (2005a). Hydraccess : Logiciel de gestion et traitement de données hydro-météorologiques, version 2.1.4.

Vauchel, P. (2005b). Hydraccess : Logiciel de gestion et traitement de données hydro météorologiques, version 2.1.4. Téléchargeable sur www.mpl.ird.fr/hybam.

Viera, L.S. (1975a). Manual da Ciência do solo, 464 pp. Ed. Agronômica Ceres, São Paulo, Brasil.

Viera, L.S. (1975b). Manual da Ciência do solo, 464 pp. Ed. Agronômica Ceres, São Paulo, Brasil.

Vizy, E.K. et Cook, K.H. (2007). Relationship between Amazon and high Andes rainfall. Journal of Geophysical Research-Atmospheres, 112(D7).

Vrugt, J.A., Gupta, H.V., Bouten, W. et Sorooshian, S. (2003). A Shuffled Complex Evolution Metropolis algorithm for optimization and uncertainty assessment of hydrologic model parameters. Water Resources Research, 39(8).

Vuille, M. et Bradley, R.S. (2000). Mean annual temperature trends and their vertical structure in the tropical Andes. Geophysical Research Letters, 27(23): 3885-3888.

Vuille, M., Bradley, R.S. et Keimig, F. (2000). Interannual climate variability in the Central Andes and its relation to tropical Pacific and Atlantic forcing. Journal of Geophysical Research-Atmospheres, 105(D10): 12447-12460.

Vuille, M., Bradley, R.S., Werner, M. et Keimig, F. (2003). 20th century climate change in the tropical Andes: Observations and model results. Climatic Change, 59(1-2): 75-99.

Vuille, M. *et al.* (2008a). Climate change and tropical Andean glaciers: Past, present and future. Earth-Science Reviews, 89(3-4): 79-96.

Vuille, M., Hardy, D.R., Braun, C., Keimig, F. et Bradley, R.S. (1998). Atmospheric circulation anomalies associated with 1996/1997 summer precipitation events on Sajama ice cap, Bolivia. Journal of Geophysical Research-Atmospheres, 103(D10): 11191-11204.

Vuille, M., Kaser, G. et Juen, I. (2008b). Glacier mass balance variability in the Cordillera Blanca, Peru and its relationship with climate and the large-scale circulation. Global and Planetary Change, 62(1-2): 14-28.

Watson, I. et Burnett, A.D. (1995). Hydrology: An environmental approach. Boca Raton, FL: CRC Press.

Waylen, P. et Poveda, G. (2002). El Niño-Southern Oscillation and aspects of western South American hydro-climatology. Hydrological Processes, 16(6): 1247-1260.

Waylen, P.R. et Caviedes, C.N. (1986). El Nino and annual floods on the north Peruvian littoral. Journal of Hydrology, 89(1-2): 141-156.

Widén-Nilsson, E., Halldin, S. et Xu, C.-y. (2007). Global water-balance modelling with WASMOD-M: Parameter estimation and regionalisation. Journal of Hydrology, 340(1-2): 105-118.

Xiong, L.H. et Guo, S.L. (1999). A two-parameter monthly water balance model and its application. Journal of Hydrology, 216(1-2): 111-123.

Xu, C.-Y. (1992). Monthly water balance models in different climatic regions., Vrije Universiteit, Brussels, Belgium.

Xu, C.-Y. et Singh, V.P. (2001). Evaluation and generalization of temperature-based methods for calculating evaporation. Hydrological Processes, 15(2): 305-319.

Xu, C.Y. (1997). Application of Water Balance Models to Different Climatic Regions in China for Water Resources Assessment. Water Resources Management, 11(1): 51-67.

Xu, C.Y. (1999). Estimation of Parameters of a Conceptual Water Balance Model for Ungauged Catchments. Water Resources Management, 13: 353-368.

Xu, C.Y. (2000). Modelling the effects of climate change on water resources in central Sweden. Water Resources Management, 14(3): 177-189.

Xu, C.Y. et Halldin, S. (1997). The effect of climate change on river flow and snow cover in the NOPEX area simulated by a simple water balance model. Nordic Hydrology, 28(4-5): 273-282.

Xu, C.Y., Seibert, J. et Halldin, S. (1996). Regional water balance modelling in the NOPEX area: development and application of monthly water balance models. Journal of Hydrology, 180(1-4): 211-236.

Xu, C.Y. et Singh., V.P. (2000). Evaluation and generalization of radiation-based methods for calculating evaporation. Hydrological Processes, 14(2): 339-349.

Xu, C.Y. et Vandewiele, G.L. (1994). Sensitivity of monthly rainfall-runoff models to input errors and data length. Hydrological Sciences Journal, 39(2): 157-176.

Xu, C.Y. et Vandewiele, G.L. (1995). Parsimonious monthly rainfall-runoff models for humid basins with different input requirements. Advances in Water Resources, 18(1): 39-48.

Yerren, J., Lavado, W., Fraizy, P. et Guyot, J. (2004). Les régimes hydrologiques dans le bassin amazonien du Pérou. (Los regimenes hidrológicos en la Cuenca Amazónica del Perú). Surface hydrology and water chemistry, LBA, Brasilia.

Yu, P.S., Yang, T.C. et Wu, C.K. (2002). Impact of climate change on water resources in southern Taiwan. Journal of Hydrology, 260(1-4): 161-175.

Zbigniew, K.W. et Robson, A.J. (2004). Change detection in hydrological records: a review of the methodology : Detecting change in hydrological data. Hydrol. Sci. J., 49(1): 7-19.

Zeng, N. *et al.* (2008a). Causes and impacts of the 2005 Amazon drought. Environmental Research Letters, 3.

Zeng, N., Yoon, J.H., Mariotti, A. et Swenson, S. (2008b). Variability of basin-scale terrestrial water storage from a PER water budget method: The Amazon and the Mississippi. Journal of Climate, 21: 248-265.

Zhang, W.C., Ogawa, K., Ye, B.S. et Yamaguchi, Y. (2000). A monthly stream flow model for estimating the potential changes of river runoff on the projected global warming. Hydrological Processes, 14(10): 1851-1868.

Zhang, X.B., Harvey, K.D., Hogg, W.D. et Yuzyk, T.R. (2001). Trends in Canadian streamflow. Water Resources Research, 37(4): 987-998.

Zhao, R., Zhuang, Y., Fang, L., Liu, X. et Zhang, Q. (1980). The Xinanjiang model. In Hydrological Forecasting, IAHS Publication No. 129. . IAHS Press: Wallingford; 351–356.

Zhou, J. et Lau, K. (1998). Does a monsoon climate exist over South America? Journal of Climate, 11: 1020-1040.

ANNEXE A

TRMM rainfall data estimation over the Peruvian Amazon-Andes basin and its assimilation into monthly water balance models

Dans cette annexe, une étude de modélisation hydrologique au niveau mensuel en utilisant des données TRMM (Tropical Rainfall Measurement Mission) est présentée sur les bassins des rios Urubamba et Tambo.

Publié dans :

New Approaches to Hydrological Prediction in Data Sparse Regions (Proc. of Symposium HS.2 at the Joint IAHS & IAH Convention, Hyderabad, India, September 2009). IAHS Publ. 333, 2009.

TRMM RAINFALL DATA ESTIMATION OVER THE PERUVIAN AMAZON-ANDES BASIN AND ITS ASSIMILATION INTO A MONTHLY WATER BALANCE MODEL

WALDO SVEN LAVADO CASIMIRO, DAVID LABAT, JEAN LOUP GUYOT, JOSYANE RONCHAIL & JUAN JULIO ORDOÑEZ

ABSTRACT

The Peruvian Amazon-Andes basin corresponds to about 10% of the total Amazonian basin and is characterized by sparse rainfall data, particularly over the lowland zone (rainforest). We compare the 3B43 product of the Tropical Rainfall Measuring Mission (TRMM) with raingauge data over two sub-basins (Urubamba and Tambo) in the Ucayali basin located in the Peruvian Amazon-Andes basin. The spatial distribution of the 3B43 product is 0.25° × 0.25° (approx. 27.8 × 27.8 km) and data are at a monthly scale. The period of comparison between on-site rainfall and 3B43 TRMM data is from January 1998 to December 2007. Comparison between on-site rainfall observations and 3B43 product is carried out using correlation coefficient and relative error. Improvement of the TRMM rainfall data is then proposed based on on-site rainfall data. After analysis of the 3B43 product, three sets of distributed rainfall data (*in situ*, TRMM and on-site TRMM improved) were used as input in a GR2M monthly water balance model to simulate discharge at Urubamba and Tambo. Classical statistical overcalibration and validation procedure show a better accuracy in flow simulations, using only original TRMM data over Urubamba basin and improved data over Tambo basin.

Key words Amazon basin; TRMM; Andes; Peru; monthly water balance model

INTRODUCTION

The Amazon Basin (AB) is the largest basin on the planet, with a drainage area of 6 200 000 km^2 and mean annual discharge at 209 000 m^3 s^{-1} (~5% of all the above-water lands) (Molinier *et al*., 1996; Marengo, 2006). AB is one of the regions with the highest rainfall in the world and a major water vapour source (Espinoza *et al*., 2009). Also, over the AB it is possible to have extreme events such as the dramatic drought observed in 2005 (Marengo *et al*., 2008; Zeng *et al*., 2008).

Rainfall stations over Peruvian Amazon basin (~10% of total Amazonian basin) are poorly distributed. Mean rainfall at basin scale over this region is mostly underestimated (Guyot, pers. comm.). Rainfall 3B43 product of **Tropical Rainfall Measuring Mission** has been used with good results over distinct parts of the world by e.g. Sorooshian *et al*. (2000), Adeyewa & Nakamura (2003), Chiu *et al*. (2006), Dinku *et al*. (2007) and Islam & Uyeda (2007), who compare or improve on-site rainfall land data. Introduction of TRMM rainfall products in hydrological and water balance models has been already documented (see e.g. Wilk *et al*., 2006; Collischonn *et al*., 2008; Su *et al*., 2008).

In Peru measurements of hydro-climatological variables over the Amazon basin are administered by the National Meteorology and Hydrology Service SENAMHI (www.senamhi.gob.pe). Most of the hydrometeorological data are related to climate variables (rainfall, temperature, etc.). Since 2001, the HYBAM project (www.ore-hybam.org) has carried out flow measurement missions over the largest Amazon-Andes rivers in the Peruvian territory (Yerren *et al*., 2004, Lavado *et al*., 2009c). Results of flow measurements along with meteorological observation from SENAMHI have, for the first

time, allowed the development of a complete database over the Peruvian Amazon-Andes region (PAB) which has been used in this study. This complete database has enabled monthly hydrological models to be developed for the first time in the Peruvian Amazon zone (Lavado *et al*., 2009a,d). This paper compares on-site rainfall data with 3B43 TRMM rainfall data. Improvements of the original 3B43 TRMM data are also compared. The assimilation of these three data sets of rainfall in the GR2M monthly water balance models was evaluated.

AVAILABLE DATA AND METHODS

Two sub-basins (Urubamba and Tambo) in Ucayali basin were used in this study (Fig. 1 and Table 1). Watershed boundaries were plotted at base from Maldonadillo and Tambo hydrological gauging stations. Watershed subdivisions were made using the Digital Elevation Model (DEM) provided by the US National Aeronautics and Space Administration (NASA) through the Shuttle Radar Topography Mission, SRTM (www2.jpl.nasa.gov/srtm).

Weather stations used in this work are part of the Peruvian National Meteorology and Hydrology Service, SENAMHI (www.senamhi.gob.pe) network: 24 rainfall stations were used (Fig. 1). Rainfall and temperature data (mean, maximum and minimum) are available at the monthly scale and includes the period from January 1998 to December 2007.

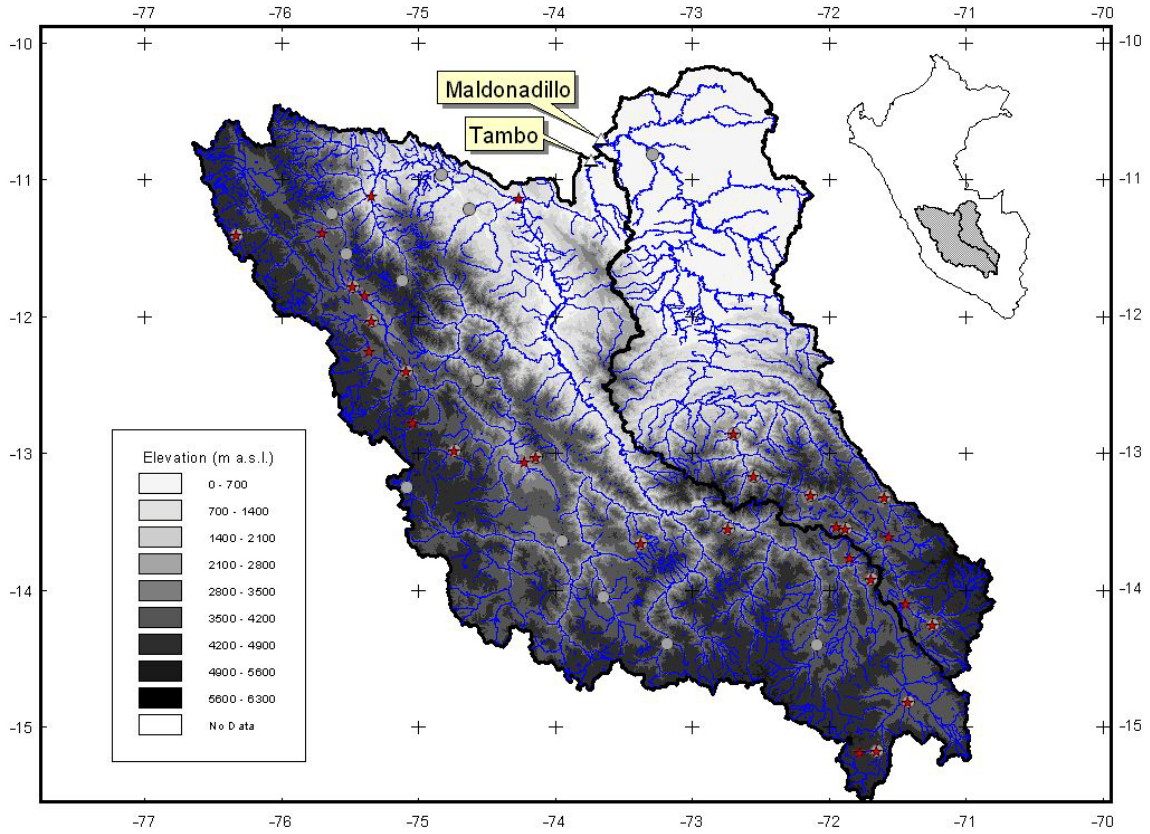

Fig. 1 Location of the study region. Basins boundary takes as a base the Tambo and Maldonadillo gauging station. Circles are rainfall stations, stars are temperature stations.

Table 1 Flow stations, locations, drainage area (Dr. Ar.) and flow record used in this study.

Flow Station	River	Latitude (°S)	Longitude (°W)	Altitude (m a.s.l.)	Dr. Ar. (km^2)	R (mm $year^{-1}$)	E (mm $year^{-1}$)	F (m^3 s^{-1})
Maldonadillo	Urubamba	10.74	73.71	287	60301	985	996	2289
Tambo	Tambo	10.85	73.71	290	135252	754	1020	1824

R: Rainfall; E: Evapotranspiration; F: Flow.

Lavado *et al*. (2009b), presented a satisfactory relationship between the FAO Penman-Monteith and Hargreaves-Samani (HE) methods (Hargreaves & Samani, 1985); the modified Hargreaves-Samani method (HEm) is used for our region of study, given by:

$$\mathrm{HE} = \frac{00023(T + 17.8)(T\,\mathrm{max} - T\,\mathrm{min})^{0.5}\,\mathrm{Ra}}{\lambda} \quad (1)$$

$$\mathrm{HEm} = 0.6484\mathrm{HE} + 1.146 \quad (2)$$

where HEm is evapotranspiration (mm d^{-1}); T is mean temperature (°C); Tmax is maximum temperature (°C); Tmin is minimum temperature (°C); and Ra is extraterrestrial radiation (MJ m^{-2} d^{-1}). The formula to compute Ra is given by Allen *et al*. (1998) and λ is latent heat of vaporization (MJ kg^{-1}); λ in this study is assumed as 2.45 MJ Kg^{-1} (Allen *et al*., 1998).

In order to work with soil data, we have used the methodology described by Dieulin *et al*. (2006), based on the data from the Digital Soil Map of the World (FAO/UNESCO, 1981). Soil water holding capacity is named WHC in this study.

Spatial distribution of the 3B43 TRMM product is at 0.25° × 0.25° (~ 27.8 × 27.8 km) and is at monthly scale since January 1998. The period of comparison between measured point rainfall and 3B43 TRMM product is from January 1998 to December 2007.

Improvement of TRMM rainfall data was made from on-site rainfall stations, using the following equations (Collischonn, 2006):

$$P'(x_i, y_i) = P(x_i, y_i) - P_m(x_i, y_i) \quad (3)$$

where $P'(x_i, y_i)$ is the fluctuation of TRMM with on-site rainfall; $P(x_i, y_i)$ is on-site rainfall estimate located over the cell (x_i, y_i); $P_m(x_i, y_i)$ is the rainfall estimate from TRMM over the cell (x_i, y_i). Conceptually, the methodology interpolates values of P', instead of on-site rainfall $P(x_i, y_i)$, because we consider that the variability of the first is lower than the second. Thus:

$$\hat{P}'(x, y) = \sum_{i=1}^{n} \lambda_i \cdot P'(x_i, y_i) \quad (4)$$

where $\hat{P}'(x, y)$ is the fluctuation (or residual) interpolated in the cell (x, y). For any (x, y) location, TRMM rainfall is improved using the following equation:

$$\hat{P}(x, y) = P_m(x, y) + \hat{P}'(x, y) \quad (5)$$

In summary, three sets of rainfall data were used for our analysis: on-site rainfall (Obs.R); TRMM rainfall data (TRMM); and improved rainfall (Obs.R TRMM).

The GR2M model version used in this study is described by (Niel *et al*., 2003, and is based on GR2M (Edijatno & Michel, 1989; Kabouya, 1990), and reviewed by Makhlouf & Michel (1994), this model is a two reservoir conceptual model.

Rainfall and evapotranspiration are spatially interpolated over cells from 0.25° × 0.25° (~ 27.8 × 27.8 km), based on the kriging method. The soil water holding capacities from the Digital Soil Map of the World (FAO/UNESCO, 1981) were interpolated over our region of study to obtain values at 0.25° × 0.25° grids, following the methodology given by Dieulin *et al*., 2006).

In this study, an automatic calibration is carried out using Shuffled Complex Evolution Metropolis algorithm (SCEM-UA), that is a modified version of the original SCE-UA global optimization algorithm (Duan *et al*., 1992) using the Metropolis Hastings strategy (Metropolis *et al*., 1953; Hastings, 1970), for detailed description of this method see Vrugt *et al*. (2003).

In hydrological models two test are commonly used: Nash-Sutcliffe efficiency (Nash; Nash & Sutcliffe, 1970) and relative volume error expressed in percent (%V), where $Q_{o,j}$ is the observed value; $\overline{Q_o}$ is the mean of the observed values; $Q_{s,j}$ is the model simulated values; and n is the number of data points:

$$\text{Nash} = 100 \times \left[1 - \frac{\sum_{j=1}^{n} \left(Q_{o,j} - Q_{o,j} \right)^2}{\sum_{j=1}^{n} \left(Q_{o,j} - \overline{Q_o} \right)^2} \right] \tag{6}$$

$$\%V = 100 \times \left[\frac{\sum_{j=1}^{n} Q_{s,j} - \sum_{j=1}^{n} Q_{o,j}}{\sum_{j=1}^{n} Q_{o,j}} \right] \tag{7}$$

RESULTS

In order to compare TRMM rainfall (3B43 product) and on-site rainfall data from 1998 to 2007, the statistics: Pearson correlation coefficient and relative error ((TRMM – Obs.R)/Obs.R) between both sets of data were compared (see Fig. 2).

In general, similar interpolated maps were estimated using both data sets considering the mean multi-annual for the 1998-2007 period over the two basins analysed. However, underestimation of rainfall are observed using TRMM data mostly in the lower zones of the Urubamba basins (region with sparse distribution of rainfall stations, see Fig. 1). Correlation coefficients are mostly significant (α = 0.05) with better values over the boundary region of the two basins analysed.

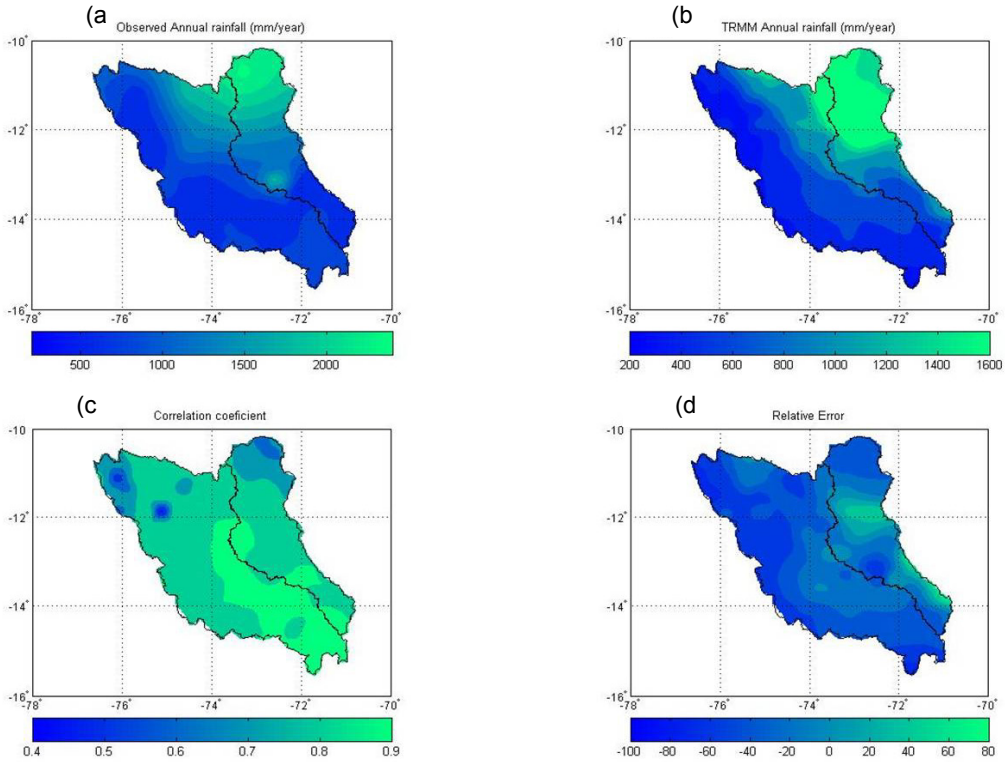

Fig. 2 (a) Interpolated mean multi-annual (1998–2007) for on-site rainfall data; (b) as in (a) but using TRMM rainfall data (1998–2007); (c) Pearson correlation coefficients between on-site and TRMM monthly rainfall data (January 1998–December 2007); and (d) as in (c) but by relative error statistic.

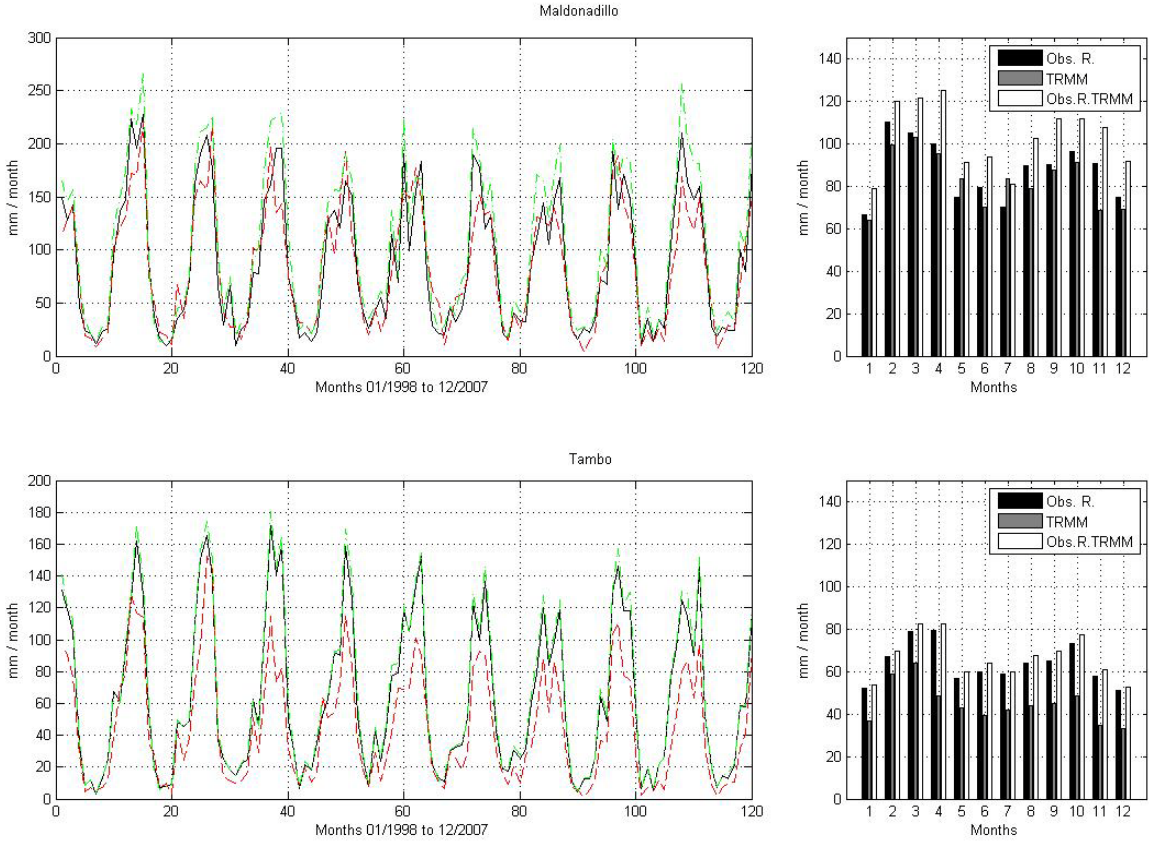

Fig. 3 Top: Comparison between mean monthly rainfall data sets interpolated over Maldonadillo basin. Bottom: Comparison between mean monthly rainfall data sets interpolated over Tambo basin. Black line is on-site rainfall data, dashed line is TRMM rainfall data and dotted dashed line is improved observed rainfall TRMM data.

Underestimation from using TRMM data are shown in interpolated relative error as well; negative values are located mostly over the western zone of the two basins analysed. Figure 3 shows comparison of the mean areal value of the three data sets of rainfall used over Maldonadillo and Tambo basins; on average, good estimations were exhibited for Maldonadillo basin and under estimations were evident over Tambo basins. Nevertheless, improved rainfall data (Obs.R TRMM) show good relationship with on-site rainfall data.
Table 2, shows statistical Nash and %V for the two basins analysed as well as for the three sets of rainfall data. Figures 4 and 5 show parameter samples and hydrographs during the calibration and validation procedures. In summary, introduction of TRMM rainfall data without improvements into GR2M model over Maldonadillo basin gave good results in simulating monthly flow (Nash equal to 0.84 and %V equal to 2.22 during calibration procedure), but non-acceptable results over Tambo basin (Nash equal to 0.57 and %V equal to 12.23 during calibration procedure). Using improved rainfall data (Obs. R TRMM) led to good results for both basins.

Table 2 Comparison of Nash and relative volume error (%V) for the three sets of rainfall used. Better values are shown in bold.

Rainfall set	Statistic	Maldonadillo:		Tambo:	
		Cal.	Val.	Cal.	Val.
Obs.R	Nash	0.80	0.87	**0.92**	**0.92**
	%V	0.57	3.90	**0.01**	**8.83**
TRMM	Nash	0.84	0.81	0.57	0.40
	%V	2.22	7.38	12.23	32.35
Obs.R TRMM	Nash	**0.92**	**0.92**	0.86	0.82
	%V	**0.66**	**8.04**	1.35	5.31

CONCLUSION

TRMM data and its improvement data (Obs. R TRMM) appear to describe well the hydrological regimens over sparse regions in the Peruvian Amazon-Andes but on-site rainfall data is indispensable for validating and improving rainfall data sets. Future work in this region will focus on improving TRMM daily-data (3B42 product) using observed information as well as hydrological models at daily time-scale.

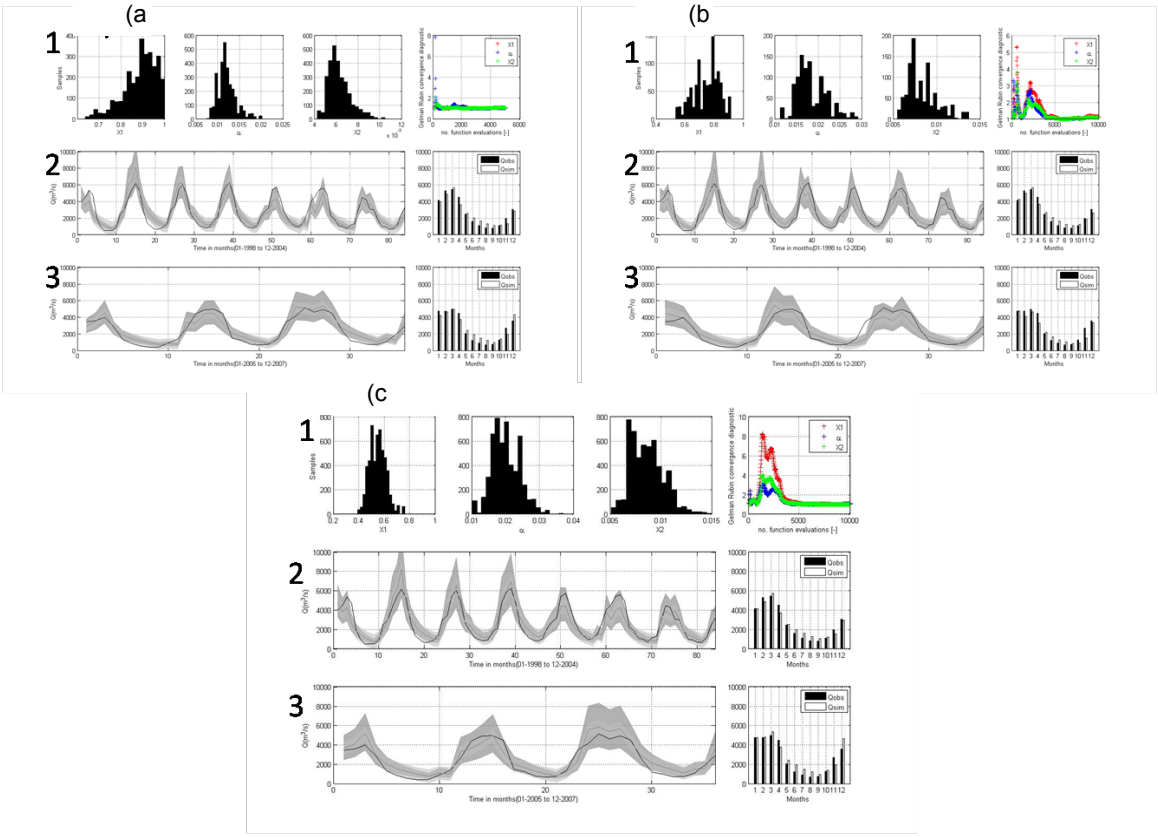

Fig. 4 Calibration and validation procedure for GR2M model over the Maldonadillo basin: (a) Using on-site rainfall data set: 1: histograms of parameters in the model and evolution of the Gelman and Rubin scale reduction. 2: hydrograph prediction uncertainty for the calibration period (01/1998 to 12/2004) and monthly observed (Qobs) and simulated flows (Qsim). 3: hydrograph prediction uncertainty for the validation period (01/2005 to 12/2007) and monthly observed (Qobs) and simulated flows (Qsim). (b) as in (a) but by TRMM rainfall data. (c) as in (a) but for improved observed rainfall TRMM data. Observed flows are represented by the black line. The grey line denotes simulated flow. The dark shaded area denotes the prediction uncertainty that results from parameter uncertainty. The light shaded area denotes the additional prediction uncertainty that results from model and measurement uncertainty.

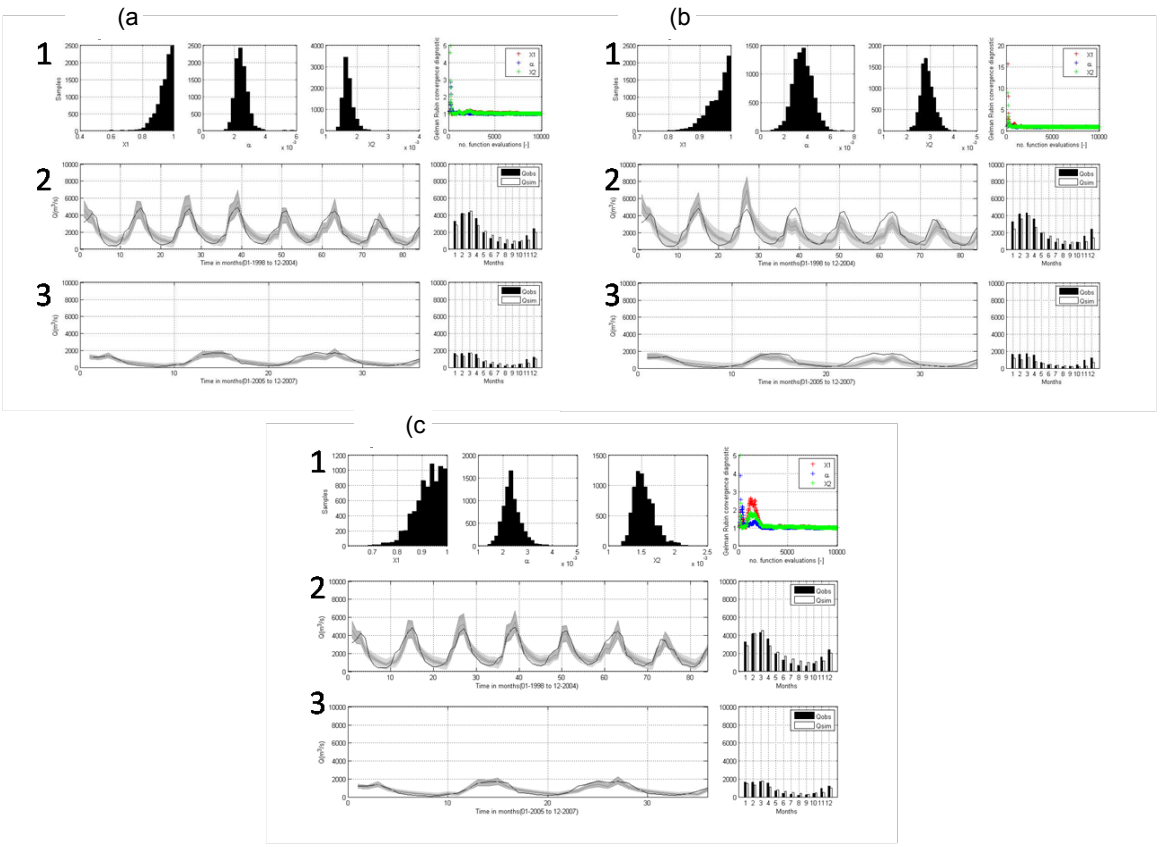

Fig. 5 Same as Fig. 4 but for Tambo basin.

REFERENCES

Adeyewa, Z. D. & Nakamura, K. (2003) Validation of TRMM radar rainfall data over major climatic regions in Africa. *J. Appl. Met.* **42**(2), 331–347.

Allen, G. R., Periera, L. S., Raes, D. & Smith, M. (1998) Crop evapotranspiration: guidelines for computing crop water requirements. *FAO Irrig. Drain. Paper 56*. Food and Agricultural Orgainzation of the United Nations, Rome, Italy.

Collischonn, B. (2006) Uso de precipitação estimada pelo satélite TRMM em modelo hidrológico distribuído, Universidade Federal do Rio Grande do Sul, Porto Alegre.

Collischonn, B., Collischonn, W. & Tucci, C. E. M. (2008) Daily hydrological modeling in the Amazon basin using TRMM rainfall estimates. *J. Hydrol.* **360**(1-4), 207–216.

Chiu, L. S., Liu, Z., Vongsaard, J., Morain, S., Budge, A., Neville, P. & Bales, C. (2006) Comparison of TRMM and water district rain rates over New Mexico. *Adv. Atmos. Sci*. **23**(1), 1–13.

Dieulin, C., Boyer, J. F., Ardoin-Bardin, S. & Dezetter, A. (2006) The contribution of GIS to hydrological modelling. In: *Climate Variability and Change—Hydrological Impacts* (Proc. Conf. La Habana, Cuba, November 2006), 68–74. IAHS Publ. 308, IAHS Press, Wallingford, UK.

Dinku, T., Ceccato, P., Grover-Kopec, E., Lemma, M., Connor, S. J. & Ropelewski, C. F. (2007) Validation of satellite rainfall products over East Africa's complex topography. *Int. J. Remote Sens.* **28**(7-8), 1503–1526.

Duan, Q., Sorooshian, S. & Gupta, V. (1992) Effective and efficient global optimization for conceptual rainfall–runoff models. *Water Resour. Res.* **28**(4), 1015–1031.

Edijatno & Michel, C. (1989) Un modèle pluie–débit journalier à trois paramètres. *La Houille Blanche* **2**, 113–121.

Espinoza, J. C., Ronchail, J., Guyot, J. L., Filizola, N., Noriega, L., Lavado, W., Pombosa, R. & Romero, R. (2009) Spatio–temporal rainfall variability in the Amazon Basin countries (Brazil, Peru, Bolivia, Colombia and Ecuador). *Int. J. Climatol.(accepted)*.

FAO/UNESCO (1981) CD-ROM *:Soil Map of the World*, Ten volumes. UN Food and Agriculture Organization, Rome, Italy.

Hargreaves, G. H. & Samani, Z. A. (1985) Reference crop evapotranspiration from temperature. *Appl.Engng Agric.* **1**(2), 96-99.

Hastings, W. K. (1970) Monte Carlo sampling methods using Markov chains and their applications. *Biometrika* **57**(1), 97–109.

Islam, M. N. & Uyeda, H. (2007) Use of TRMM in determining the climatic characteristics of rainfall over Bangladesh. *Remote Sens. Environ.* **108**(3), 264–276.

Kabouya, M. (1990) Modélisation pluie–débit au pas de temps mensuel et annuel en Algérie septentrionale. These de doctorat Université Paris-Sud, Paris, France.

Lavado, C. W. S., Labat, D., Guyot, J. L., Ardoin-Bardin, S. & Ordoñez, J. J. (2009a) Monthly water balance models in the Amazon drainage basin of Peru: Ucayali River basin. *Hydrol. Sci. J. (submitted)*

Lavado, C. W. S., Labat, D., Guyot, J. L., Boulet, G., Ordoñez, J. J. & Solis, O. (2009b) Comparison of reference evapotranspiration models with the standard FAO Penman-Monteith model in the Peruvian Amazon-Andes basin. *J. of Hydrol*. *(submitted)*

Lavado, C. W. S., Labat, D., Guyot, J. L., Ronchail, J., Espinoza, J. & Ordoñez, J. (2009c) Recent trends in rainfall, temperature and evapotranspiration in the Peruvian Amazon-Andes basin: Huallaga and Ucayali basins. *Int. J. Climatol. (submitted)*.

Lavado, C. W. S., Labat, D., Guyot, J. L., Vrugt, J. & Ordoñez, J. (2009d) Monthly water balance models to predict possible climatic change impacts using three IPCC AR-4 models in the Peruvian Amazon-Andes basin. *J. Hydrology*. *(submitted)*

Makhlouf, Z. & Michel, C. (1994) A two-parameter monthly water balance model for French watersheds. *J. Hydrol.* **162**(3-4), 299–318.

Marengo, J. (2006) On the hydrological cycle of the Amazon basin: a historical review and current state-of-the-art. *Revista Brasileira de Meteorologia* **21**(3), 1–19.

Marengo, J. A., Nobre, C. A., Tomasella, J., Oyama, M. D., De Oliveira, G. S., De Oliveira, R., Camargo, H., Alves, L. M. & Brown, I. F. (2008) The drought of Amazonia in 2005. *J. Climate* **21**, 495–516.

Metropolis, N., Rosenbluth, A. W., Rosenbluth, M. N., Teller, A. H. & Teller, E. (1953) Equation of state calculations by fast computing machines. *J. Chem. Phys.* **21**(6), 1087–1092.

Molinier, M., Guyot, J.-L., Oliveira, E. D. & Guimarães, V. (1996) Les régimes hydrologiques de l'Amazone et de ses affluents. L'hydrologie tropicale: géoscience et outil pour le développement, Paris, Mai 1995. In: IAHS Series of Proceedings and Reports. Vol. 238. pp. 209–222.IAHS Press, Wallingford, UK.

Nash, J. E. & Sutcliffe, J. V. (1970) River flow forecasting through conceptual models, Part I. A discussion of principles. *J. Hydrol.* **10**(3), 282–290.

Niel, H., Paturel, J.-E. & Servat, E. (2003) Study of parameter stability of a lumped hydrologic model in a context of climatic variability. *J. Hydrol.* **278**(1-4), 213–230.

Sorooshian, S., Hsu, K. L., Gao, X., Gupta, H. V., Imam, B. & Braithwaite, D. (2000) Evaluation of PERSIANN system satellite-based estimates of tropical rainfall. *Bull. Am. Met. Soc.* **81**(9), 2035–2046.

Su, F. G., Hong, Y. & Lettenmaier, D. P. (2008) Evaluation of TRMM Multisatellite

Precipitation Analysis (TMPA) and its utility in hydrologic prediction in the La Plata Basin. *J. Hydromet.* **9**(4), 622–640.

Vrugt, J. A., Gupta, H. V., Bouten, W. & Sorooshian, S. (2003) A Shuffled Complex Evolution Metropolis algorithm for optimization and uncertainty assessment of hydrologic model parameters. *Water Resour. Res.* **39**(8) 1201.

Wilk, J., Kniveton, D., Andersson, L., Layberry, R., Todd, M. C., Hughes, D., Ringrose, S. & Vanderpost, C. (2006) Estimating rainfall and water balance over the Okavango River Basin for hydrological applications. *J. Hydrol.* **331**(1-2), 18–29.

Yerren, J., Lavado, W., Fraizy, P. & Guyot, J. (2004) Les régimes hydrologiques dans le bassin amazonien du Pérou. (Los regimenes hidrológicos en la Cuenca Amazónica del Perú). III LBA Scientific Conference. Surface hydrology and water chemistry, LBA, Brasilia.

Zeng, N., Yoon, J. H., Marengo, J. A., Subramaniam, A., Nobre, C. A., Mariotti, A. & Neelin, J. D. (2008) Causes and impacts of the 2005 Amazon drought. *Environ. Res. Lett.* **3,** 014002.

ANNEXE B

Spatio-temporal rainfall variability in the Amazon basin countries (Brazil, Peru, Bolivia, Colombia and Ecuador)

Dans cette annexe, une étude complète de la variabilité des pluies sur le bassin Amazonien à été développé dans le cadre de programme HYBAM et les services hydrométéorologiques de Brésil, Pérou, Bolivie, Colombie et Equateur

Publié dans :

International Journal of Climatology.

INTERNATIONAL JOURNAL OF CLIMATOLOGY
Int. J. Climatol. (2008)
Published online in Wiley InterScience
(www.interscience.wiley.com) DOI: 10.1002/joc.1791

Spatio-temporal rainfall variability in the Amazon basin countries (Brazil, Peru, Bolivia, Colombia, and Ecuador)

Jhan Carlo Espinoza Villar,[a,b]* Josyane Ronchail,[b] Jean Loup Guyot,[c] Gerard Cochonneau,[c] Filizola Naziano,[d] Waldo Lavado,[e] Eurides De Oliveira,[f] Rodrigo Pombosa[g] and Philippe Vauchel[h]

[a] *HydroGéodynamique du Bassin Amazonien (HYBAM)/IRD. UNALM - Lima, Peru, Université Paris 6 and LOCEAN (IRD, CNRS, MNHN, UPMC) /IPSL, Boite 100, 4 Place Jussieu, 75252 Paris Cedex 05, France*
[b] *Université Paris 7 and LOCEAN*
[c] *LMTG (IRD-CNRS-UPS Toulouse), IRD CP 7091, Lago Sul, 71619-970 Brasilia (DF), Brazil*
[d] *UEA and I.PIATAM, Av. Ramos Ferreira, 199, 69010-120 Manaus-AM, Brazil*
[e] *SENAMHI/LMTG, Casilla 11 1308, Lima 11, Peru*
[f] *ANA, Setor Policia, CEP 70610-200, Brasilia, Brazil*
[g] *INAMHI, Quito, Ecuador, Iñaquito 700 y Correa, Quito, Ecuador*
[h] *LMTG (IRD-CNRS-UPS Toulouse), IRD, Casilla 18-1209, Lima 18, Peru*

ABSTRACT: Rainfall variability in the Amazon basin (AB) is analysed for the 1964–2003 period. It is based on 756 pluviometric stations distributed throughout the AB countries. For the first time it includes data from Bolivia, Peru, Ecuador, and Colombia. In particular, the recent availability of rainfall data from the Andean countries makes it possible to complete previous studies. The impact of mountain ranges on rainfall is pointed out. The highest rainfall in the AB is observed in low windward regions, and low rainfall is measured in leeward and elevated stations. Additionally, rainfall regimes are more diversified in the Andean regions than in the lowlands. Rainfall spatio-temporal variability is studied based on a varimax-rotated principal component analysis (PCA). Long-term variability with a decreasing rainfall since the 1980s prevails in June–July–August (JJA) and September–October–November (SON). During the rainiest seasons, i.e. December–January–February (DJF) and March–April–May (MAM), the main variability is at decadal and interannual time scales. Interdecadal variability is related to long-term changes in the Pacific Ocean, whereas decadal variability, opposing the northwest and the south of the AB, is associated with changes in the strength of the low-level jet (LLJ) along the Andes. Interannual variability characterizes more specifically the northeast of the basin and the southern tropical Andes. It is related to El Niño-Southern Oscillation (ENSO) and to the sea surface temperature (SST) gradient over the tropical Atlantic. Mean rainfall in the basin decreases during the 1975–2003 period at an annual rate estimated to be −0.32%. Break tests show that this decrease has been particularly important since 1982. Further insights into this phenomenon will permit to identify the impact of climate on the hydrology of the AB. Copyright © 2008 Royal Meteorological Society

KEY WORDS rainfall variability; rainfall regimes; Amazon basin; Andes; South American climate; Peru; Ecuador; Bolivia; Colombia; ENSO; PDO; LLJ

Received 24 July 2007; Revised 24 September 2008; Accepted 27 September 2008

1. Introduction

The Amazon basin (AB) extends between 5°N and 20°S and from the Andes to the Atlantic Ocean, covering approximately 6 000 000 km^2. Its fresh water contribution to the global ocean is 15% and its average discharge at the delta is 209 000 m^3/s (Molinier *et al*., 1996). The basin is divided into three great morphological units: 44% of its surface belongs to the Guyanese and Brazilian shields, 45% to the Amazon plain, and 11% to the Andes. This basin covers seven countries: Brazil (63%), Peru (16%), Bolivia (12%), Colombia (6%), Ecuador (2%), and Venezuela and Guyana (1%).

The AB is one of the regions with the highest rainfall in the world and a major water vapour source (Johnson, 1976; Ratisbona, 1976; Salati *et al*., 1978; Figueroa and Nobre, 1990). Also, it can undergo dramatic drought as observed in 2005 (Marengo *et al*., 2008; Zeng *et al*., 2008). Nonetheless, owing to a lack of information, few studies describe the spatio-temporal rainfall variability in the AB countries, except for Brazil. Cooperation programmes between Institut de Recherche pour le Développement/Institute for Research and Development (IRD) and local institutions have permitted, for the first time, the integration of data from the different Amazonian

* Correspondence to: Jhan Carlo Espinoza Villar, LOCEAN (IRD, CNRS, MNHN, UPMC)/IPSL, Boite 100, 4 Place Jussieu, 75252, Paris Cedex 05, France. E-mail: jhan-carlo.espinoza@locean-ipsl.upmc.fr

countries, highlighting a group of pluviometric stations unavailable so far, specially in the Amazon regions of the Andean countries (Bolivia, Peru, Ecuador, and Colombia). Nevertheless the need to consider comprehensive data set is important in the Andean regions. Rainfall tends to decrease with altitude, but the windward or leeward exposure of the stations to the dominant moist wind makes it difficult to find a simple relationship between rainfall and altitude (Johnson, 1976; Roche *et al*., 1990; Guyot, 1993; Pulwarty *et al*., 1998; Buytaert *et al*., 2006; Ronchail and Gallaire, 2006; Laraque *et al*., 2007). On the contrary, in Brazil, the spatio-temporal rainfall variability has been more widely studied and published than in the Andean countries. The highest values (3000–3500 mm/year) may be found in the northwest of the basin, on the border with Brazil, Colombia, and Venezuela, where the general large-scale relief shape, like the large concavities of the Andes eastern slope, creates favourable conditions for air convergence and large rainfall (Ratisbona, 1976; Salati *et al*., 1978; Nobre, 1983; Salati and Vose, 1984; Figueroa and Nobre, 1990). Abundant rainfall is also registered near the Amazon River delta where the sea-breeze effect is important (Salati *et al*., 1978). Salati *et al*. (1978) calculated a mean of 2400 mm/year in the central region of the AB and Marquez *et al*. (1980) and Fisch *et al*. (1998) a mean 2300 mm rainfall for the Brazilian AB. Different studies, for the whole AB, give values from 2000 to 3664 mm, with the greater part between 2000 and 2200 mm, as found by Marengo and Nobre (2001). Callède *et al*. (2008) report a 2230-mm mean annual rainfall for the AB down to Óbidos (1.93 °S 55.50 °W, 800 km from the Amazon River delta), based on 163 rainfall gauges, including stations in the Andean countries, for the 1943–2003 period.

Rainfall regimes in the Brazilian Amazon show an opposition between the north and the south with rainy months in austral winter and summer, respectively (Ratisbona, 1976; Salati *et al*., 1978; Kousky *et al*., 1984; Horel *et al*., 1989; Figueroa and Nobre, 1990; Nobre *et al*., 1991, among others). A rainy period is observed in MAM in regions close to the Amazon River delta. A better distribution of rainfall over the year characterizes regions towards the border of Peru, Colombia, and Brazil. Among the limited number of studies devoted to the spatial variability of rainfall regimes in the Andean AB that of Johnson (1976) is worth mentioning as this author analyses the seasonal regime of 107 rainfall gauges in Bolivia, Peru, and Ecuador. In Bolivia and southern Peru there exists a rainy period in austral summer and a dry period in winter, which is more intense in the west, inside the Andes (Johnson, 1976; Roche *et al*., 1990; Guyot, 1993; Aceituno, 1998). Laraque *et al*. (2007) complement the work by Johnson (1976) and detail the wide variability of regimes in the Ecuadorian AB based on 47 rainfall gauges, with opposite regimes in nearby zones. A better yearly rainfall distribution can be observed in the lowlands in the northeast of Peru (Weberbauer, 1945; Nicholson, 1948; Broggy, 1965).

Interannual rainfall variability in the AB partially depends on El Niño-Southern Oscillation (ENSO; Kousky *et al*., 1984; Aceituno, 1988; Marengo, 1992; Marengo and Hastenrath, 1993; Moron *et al*., 1995; Uvo *et al*., 1998; Liebmann and Marengo, 2001; Ronchail *et al*., 2002, among others). In particular, below normal rainfall is recorded in the north and northeast of the AB during El Niño events, whereas excess rainfall occurs during La Niña. This signal decreases towards the west and the south of the basin, and an inverse and weak signal can be observed in the Amazon plain of Bolivia (Ronchail, 1998; Ronchail *et al*., 2002, 2005; Ronchail and Gallaire, 2006), which may be related to the ENSO signal observed in the southeast of South America (the south of Brazil, Uruguay, and the northeast of Argentina). In the tropical Andes of Bolivia and the southern Andes of Peru, rainfall is below normal during El Niño event (Francou and Pizarro, 1985; Aceituno, 1988; Tapley and Waylen, 1990; Rome and Ronchail, 1998; Ronchail, 1998; Vuille *et al*., 2000; Garreaud and Aceituno, 2001; Ronchail and Gallaire, 2006), and the glacier meltdown accelerates during these years (Wagnon *et al*., 2001; Francou *et al*., 2003), while no clear signal can be found during La Niña events. In the north of the Peruvian Andes, no clear signal is found (Tapley and Waylen, 1990; Rome and Ronchail, 1998). The rainfall anomaly is not so pronounced in Ecuador (Rossel *et al*., 1999) with a slight rainfall increase during El Niño event for Ronchail *et al*. (2002) and Bendix *et al*. (2003) and a deficit for Vuille *et al*. (2000). The signal is also weak in the Colombian Amazon, where rainfall is abnormally abundant during La Niña events (Poveda and Mesa, 1993).

Long-term variability in the AB has been extensively reported in the literature. Chen *et al*. (2001) find a rainfall increase in the AB countries since the 1960s using data from Global Historical Climatology Network (GHCN). This is in line with the increase in humidity convergence, described by Chu *et al*. (1994) and Curtis and Hastenrath (1999). Nevertheless, this trend is not valid for Callède *et al*. (2004), who rebuilt a pluviometric series for the period 1945–1998 based on 43 pluviometric posts, and observe an slightly decreasing trend for the period, with the exception of high values recorded from 1965 to 1975. Marengo (2004) also finds this slight rainfall decrease in Brazil for the same period using data from Climate Research Unit (CRU), Climate Prediction Center Merged Analysis of Precipitation (CMAP), and 300 pluviometric stations from different local institutions. Also, Marengo and Nobre (2001) and Marengo (2004) show an opposition between the long-term rainfall evolution in northern and southern Amazon. In general, less rainfall has been recorded in the north since the late 1970s, whereas the opposite occurs in the south. These results are consistent with Ronchail (1996), with respect to rainfall in Bolivia and with Ronchail *et al*. (2005), who show an increase in the water level of the Madeira River during the 1970s. These findings may also be observed at the centre of Argentina (Agosta *et al*., 1999, among others), and in the discharge of the Paraná River in Paraguay

DOI: 10.1002/joc

(Genta *et al*., 1998; Robertson and Mechoso, 1998, etc.). Marengo (2004) attributes the rainfall increase in the southern Amazon to an intensification of the northeast trade winds and to the increase in water vapour transport from the tropical North Atlantic to the centre of the Amazon. For a shorter period (1978–1998) using CMAP data, Matsuyama *et al*. (2002) also present a decreasing rainfall trend in the north and an increasing trend in the south. Conversely, Zhou and Lau (2001) report a rainfall decrease as from 1986 to 1987 in the southwest of the basin, and an increase in the north. To account for this, the authors put forward the warming of the tropical South Atlantic and the shift of the intertropical convergence zone (ITCZ) to the south.

Rainfall variability is related to changes in the ocean and the atmosphere as mentioned before. However, it has also been linked to deforestation. In the AB, deforestation has been considered as virtually non-existent till 1960 (Houghton *et al*., 2000), and the beginning of the 1970s (0.34% of total land area being deforested in 1976, Callède *et al*., 2008). A compilation of the major works on the impact of deforestation on the AB rainfall has been presented by D'Almeida *et al*. (2007). It shows that the models developed at a macro-scale (>105 km^2) and simulating a general deforestation, evaluate a 0.40–1.70 mm/day rainfall decrease (Nobre *et al*., 1991; Henderson-Sellers *et al*., 1993; Dirmeyer and Shukla, 1994; Polcher and Laval, 1994; etc). Deforestation also causes the dry season to extend (Shukla *et al*., 1990; Nobre *et al*., 1991) and a strong rainfall decrease during the dry season (Silva Días *et al*., 2002). Nevertheless, the present human activity in the AB generates an intense deforestation in the southern and eastern basin principally and little deforestation in other regions, in particular, in the NW (Le Tourneau, 2004). That is why meso-scale deforestation models (102–105 km^2) are relevant. On the one hand, they point out a rainfall decrease (Eltahir and Bras, 1994; etc), as well as a rainfall increase, as a result of increased albedo and causing convergence and convection in deforested zones (Chen and Avissar, 1994; Avissar and Liu, 1996; etc), particularly during the dry season (Wang *et al*., 2000; Durieux *et al*., 2003).

The aim of this paper is to provide a comprehensive study of spatio-temporal rainfall variability, using a new set of enriched data mainly originating from Peru, Bolivia, Ecuador, and Colombia. Likewise, it aims to identify the trend and evolution with time of the average annual rainfall in the basin countries. Within the framework of the Hydrology and Geodynamics of the Amazon Basin (HYBAM) programme, a rainfall variability analysis has been developed to assess the impact on discharge and sediment transport in the AB (Guyot, 1993; Gautier *et al*., 2006). This article first presents the data and the related spatial distribution, as well as an explanation of the different methods applied. The first part of the results focusses on spatial rainfall variability, then on regimes. In both cases the analysis is more detailed for Andean regions. Then, the space time interannual and pluriannual variability is analysed in relation to atmospheric circulation and to regional modes of ocean and atmosphere variability. Finally, the mean rainfall variability and trends are described for the whole AB during the 1975–2003 period. Discussions and conclusions are provided in the last section.

2. Data and methods

The HYBAM programme (http://www.mpl.ird.fr/hybam) has elaborated a monthly rainfall database, from *in situ* stations belonging to different institutions in charge of the meteorological and hydrological monitoring: Agência Nacional de Águas (Water National Office – ANA, Brazil), Servicio Nacional de Meteorología e Hidrología (National Meteorology and Hydrology Service – SENAMHI, Peru and Bolivia), Instituto Nacional de Meteorología e Hidrología (National Meteorology and Hydrology Institute – INAMHI, Ecuador) and Instituto de Hidrología, Meteorología y Estudios Ambientales (Hydrology, Meteorology, and Environmental Studies Institute – IDEAM, Colombia). Brazilian data are freely available at http://www.ana.gov.br. Data from SENAMHI, IDEAM, and INAMHI are available on request. The database made up of a total of 1446 pluviometrical stations on a monthly basis has been submitted to the regional vector method (RVM) (Hiez, 1977 and Brunet-Moret, 1979) to assess its quality. Thus, for the same climatic zone experiencing the same rainfall regime, it is assumed that annual rainfall in the stations of the zone is proportional in-between stations, with little random annual variation as a result of rainfall distribution in the zone. The basic idea of the RVM is as follows: instead of comparing pairs of stations by correlation or double mass, a fictitious station is created as some 'sort of average or vector' of all stations in the zone, to be compared with every station (Hiez, 1977; Vauchel, 2005). To calculate this 'Vector' station, the RVM applies the concept of extended average rainfall to the work period, which is an estimation of the average possible value that would have been obtained through continuous observations during the study period. On the basis of the above, the least squares method is applied to find the regional annual pluviometric indexes $\boldsymbol{Z}_i$ and the extended average rainfall $\boldsymbol{P}_j$. This may be calculated by minimizing the sum of Equation (1), where i is the year index, j the station index, $\boldsymbol{N}$ the number of years, and $\boldsymbol{M}$ the number of stations. $\boldsymbol{P}_{ij}$ stands for the annual rainfall in the station j, year i; $\boldsymbol{P}_j$ is the extended average rainfall period of $\boldsymbol{N}$ years; and finally, $\boldsymbol{Z}_i$ is the regional pluviometric index of year i. The series of chronological indexes $\boldsymbol{Z}_i$ is called 'regional annual pluviometric indexes vector'.

$$\sum_{i=1}^{N}\sum_{j=1}^{M}\left(\frac{\boldsymbol{P}_{ij}}{\boldsymbol{P}_j}-\boldsymbol{Z}_i\right). \tag{1}$$

Two methods have been developed in parallel by Brunet-Moret (1979) and Hiez (1977), the main difference being the way in which the calculation of the

DOI: 10.1002/joc

extended average rainfall $\boldsymbol{P}_j$ is carried out. The first one considers that the extended average of a station is calculated using the mean observed values, after deleting outliers, i.e. data differing most from those of nearby stations for a particular year. The second one considers that the extended average of a station is calculated on the basis of the most frequent values (the mode) in accordance with the neighbouring stations. Therefore, there is no need to eliminate the data that differ considerably from the average, as it is carried out in the first method. In this study, Brunet-Moret's method has been applied, and the comparison with the other method has not yielded noticeable differences. On basis of these concepts, it is possible to analyse the data following an iterative process of station selection within a specific climatic region. The selection is supported by climatological maps and the description of rainfall regimes, as reported in previous studies. The iterative process calculates the vector, revises the results, separates inconsistent stations, calculates the vector once more, etc. Rejected stations close to the border of a region may present the behaviour of a neighbouring region. As a result, they are taken into account to calculate the vector of a new climatic region. Each resulting region is associated with a 'regional vector' that represents the interannual pluviometric variability in the region, and it is also similar to the behaviour of all the stations which are part of this region. Consequently, this vector is a good indicator of the climatic variability in the region. Thus for each year, this index requires data in at least five stations, to find the longest analysis periods per region. The application of the RVM in the AB led to 756 stations (52% of the total) with data lasting more than 5-year continuous periods, and less probabilities of errors in their series (Figure 1). On average, the data availability period is from 1975 to 2003, but, in the Andean countries, the series are generally longer and started in 1960 in Peru and in 1950 in Bolivia. In Colombia and Brazil, most records started between 1975 and 1980, with very few stations with data prior to 1965.

The seasonal variability is analysed by means of percentage of rainfall on a quarterly basis from December–January–February (DJF) to September–October–November (SON). The seasonal variation coefficient (sVC) is calculated using the mean monthly rainfall. Likewise, the interannual variation coefficient (iVC) is computed using annual rainfall values.

The different seasonal regimes are analysed based on rainfall indexes that relate monthly rainfall to annual rainfall. Thus, stations can be classified according to their annual cycle and not on an amount of water. Equation (2) is used to calculate this index, where $\boldsymbol{I}_i$ is the monthly index for the month i, $\boldsymbol{PP}_i$ the monthly rainfall for month i, and $\boldsymbol{PP}_{\mathrm{A}}$ the total annual rainfall.

$$\boldsymbol{I}_i = \frac{\boldsymbol{PP}_i}{\boldsymbol{PP}_{\mathrm{A}}/12} \tag{2}$$

An ascendant hierarchical classification (AHC) is applied to the monthly rainfall indexes to define the optimum number of clusters. The Ward method is applied to maximize inter-class variance. The K-means method is then applied based on the number of groups found through AHC. This method relies on consecutive iterations permitting to decrease intra-group inertia and to increase inter-group inertia. The number of iterations was 10, 15, and 25. Although groups can be created based on AHC, K-means permits to obtain several classifications and to identify stable and unstable stations (belonging to different clusters in different iterations). Only those stations belonging to the same cluster in every iteration were used to define the regimes.

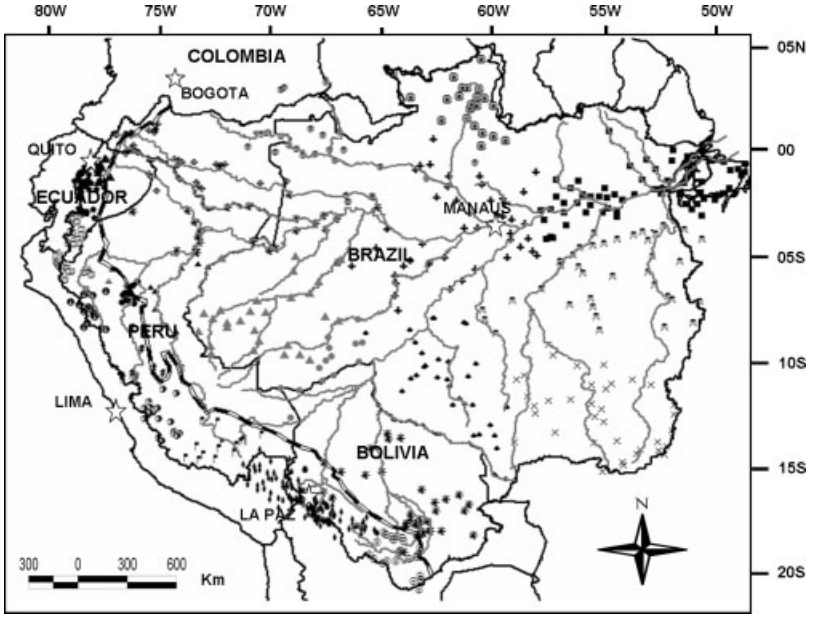

Figure 1. Limit of the Amazon basin (solid line) and of the Andean regions above 500 m (black and white line) and location of the rainfall gauges approved by the regional vector method (756 stations with more than 5-year records). The 25 symbols represent the groups of stations from which the 25 vectors were created.

DOI: 10.1002/joc

To measure the average rainfall in the basin and its interannual evolution, the Kriging interpolation method is applied. This method consists in establishing a variogram for each spatial point. This variogram evaluates the influence of the 16 closest stations according to distance. The Kriging method is the only one to take into consideration a possible spatial data gradient.

Spatial and temporal structures of interannual rainfall variability are studied based on a varimax-rotated principal components analysis (PCA) (Dillon and Goldstein, 1984) on the RVM pluviometric indexes. The use of the RVM indexes rather than initial data allows long time series (1964–2003) to be considered. The applied PCA is of the varimax-type. It circumvents the exaggerated influence of variables (vectors) with a high contribution to the factors.

The analysis of rainfall trend relies on correlation coefficients; the Pearson coefficient which is parametric measures the lineal correlation among variables, whereas Spearman and Kendal coefficients are non-parametric and based on range and range probability of the data occurrence order, respectively (Kendall, 1975; Siegel and Castellan, 1988).

Breaks and changes in the series are evaluated through different methods. The Bayesian Buishand method is based on changes of the series average; the critical values for the identification of breaks are based on Monte Carlo method which remains valid even for variables with a distribution different from normal (Buishand, 1982). The Pettitt method is a non-parametric test based on changes in the average and the range of the series subdivided into sub-series (Pettitt, 1979). It is considered one of the most complete tests for the identification of changes in time series (Zbigniew, 2004). Lee and Heghinian Bayesian test uses the average as an indicator of change thanks to an *a posteriori* Student's distribution (Lee and Heghinian, 1977). Finally, Hubert segmentation is based on the significant difference of average and standard deviation among periods; it is particularly well-suited to the search for multiple changes in series (Hubert *et al*., 1989).

Geopotential, wind, and humidity data originates from the European Center for Medium Range Weather Forecast (ECMWF) (Uppala *et al*., 2005) reanalysis project. The ECMWF ERA-40 reanalysis data used in this study has been obtained from the ECMWF data server. Reanalysis data result from a short-term operational forecast model and from the observation of various sources (land, ship, aircraft, satellite…). Data are provided four times a day, on a 2.5° latitude X 2.5° longitude global grid, at 23 pressure levels. The vertically integrated water vapour flux is derived from the specific humidity and the horizontal wind between the ground and 500 hPa (Rao *et al*., 1996).

Several regional climatic indexes are used to characterize the temporal patterns resulting from the analysis of annual rainfall. The Southern Oscillation Index (SOI) is the standardized pressure difference between Tahiti and Darwin. The Multivariate ENSO index (MEI) monitors ENSO in the Pacific using sea-level pressure, zonal and meridional components of the surface wind, sea surface temperature, surface air temperature and total cloudiness fraction of the sky (Wolter and Timlin, 1993). Both indexes are from the Climatic Prediction Centre of the National Oceanic and Atmospheric Administration (CPC-NOAA:http://www.cdc.noaa.gov/). Sea surface temperature (SST) data are also from the CPC-NOAA. Monthly SSTs (1950–2000) are provided for the northern tropical Atlantic (NATL, 5–20°N, 60–30°W) and the southern tropical Atlantic (SATL, 0–20°S, 30°W–10°E). The standardized SST difference between the NATL and SATL is computed to feature the SST gradient in this oceanic basin. The Pacific Decadal Oscillation (PDO) Index is defined as the leading component of North Pacific monthly SST variability, poleward of 20°N for the 1900–1993 period (Mantua *et al*., 1997: http://jisao.washington.edu/pdo/). When PDO is positive, water is colder in the central and western Pacific and warmer in the eastern Pacific; with a negative PDO, the reverse is observed. This negative and positive PDO 'events' tend to last from 20 to 30 years. The PDO index has been mainly positive since 1976.

The management of the pluviometric database, as well as the application of the RVM and the calculation of the average rainfall in the basin, has been carried out using the HYDRACCESS software, developed within the framework of the HYBAM programme (free download at www.mpl.ird.fr/hybam/outils/hydraccess_en.htm; Vauchel, 2005). The calculation of changes in the series is made using the KHRONOSTAT software (free download at www.mpl.ird.fr/hydrologie/gbt/projets/iccare/khronost.htm; IRD, 2002).

3. Spatio-temporal rainfall variability in the Amazon basin

Rainfall gauges approved by RVM display a heterogeneous spatial distribution in the AB countries (Figure 1). In Brazil, stations are evenly distributed. However, as the dense forest leads to poor access, the pluviometric stations have been mainly located along the rivers and highways. In the Andean countries there exists a great number of stations, often featuring long series, especially in mountainous regions, where access is easier than in the lowlands. On the contrary, stations are few and far between in the lowland regions of Peru, Ecuador, and Bolivia, on the border of Peru and Brazil, and in the northeast region of the basin, on the Brazilian border with Guyana and Surinam (Figure 1).

3.1. Spatial variability of annual rainfall

Particularly rainy regions (3000 mm/year and more) are located in the northeast, in the Amazon delta, close to the Atlantic Ocean (Figure 2), exposed to the ITCZ and in the northwest of the basin (Colombia, north of the Ecuadorian Amazon, northeast of Peru, and northwest of Brazil). Rainfall is also abundant towards the southeast, close to the average position of the South Atlantic Convergence

DOI: 10.1002/joc

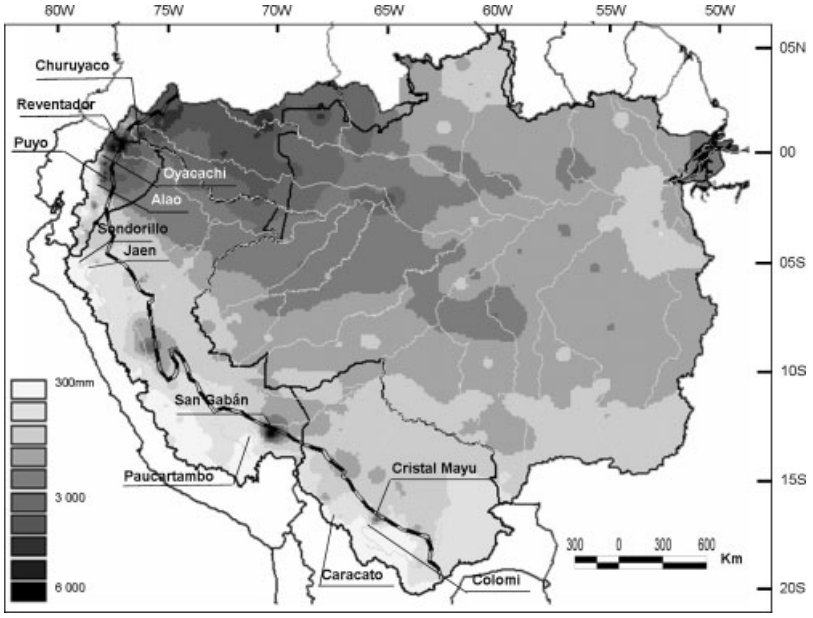

Figure 2. Mean 1975–2003 annual rain (mm/year). The pluviometric stations mentioned in the text are indicated. Andean regions above 500 m are limited by a black and white line.

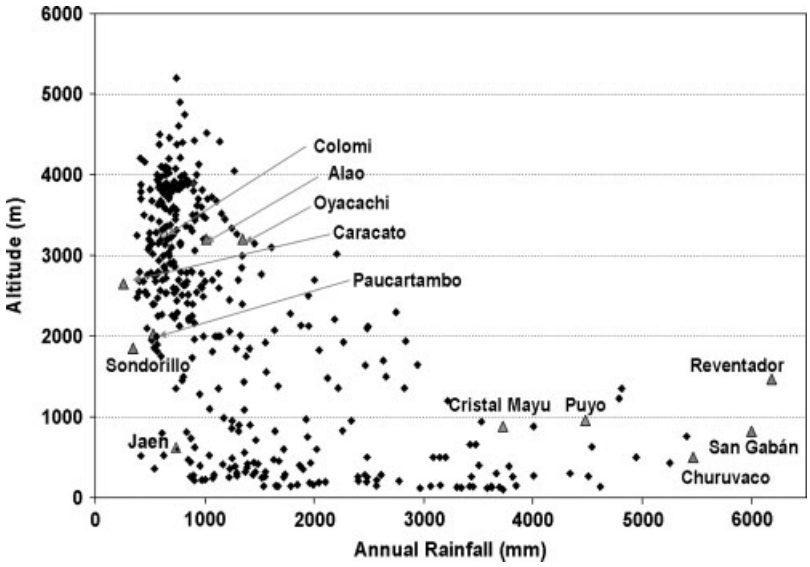

Figure 3. Relationship between altitude (m asl) and annual rainfall (mm) for the 391 stations of the Andean countries (Bolivia, Peru, Ecuador, and Colombia). The stations mentioned in the text are indicated.

Zone (SACZ), established during austral summer from the northwest of the Amazon to the Subtropical South Atlantic. Rainfall decreases towards the Tropics reaching more than 2000 mm/year in the southeast of Brazil and less than 1500 mm/year in the Peruvian–Bolivian plain and in the Roraima Brazilian state which is protected from the Atlantic humid flows by the Guyanese shield. This distribution is consistent with the results of Ratisbona (1976), Salati *et al*. (1978), Marquez *et al*. (1980), Figueroa and Nobre (1990), Fisch *et al*. (1998), and Marengo (2004), among others. However, our rainfall map yields more information about the Andean countries. Figure 2 clearly shows lower rainfall in the high Andes regions, mainly in the centre and south. Figure 3 displays the relationship between annual rainfall and altitude for 391 stations located in the Andes. Only a limited number of stations are located over 2000 m asl with an excess of 1500 mm/year and, in general less than 1000 mm/year is measured over 3000 m asl. The same situation is found by Guyot (1993) and Ronchail and Gallaire (2006) in Bolivia and by Laraque *et al*. (2007) in Ecuador. At low elevation, abundant rainfall is related to the moist warm air and to the release of high quantity of water vapour over the first eastern slope of the Andes. The stations registering more than 3000 mm/year are located at less than 1500 m asl (Figure 3). As a result, rainfall diminishes with altitude. Nonetheless, the least rainy stations such as Caracato (2650 m asl) in the Bolivian Andes with

DOI: 10.1002/joc

255 mm/year and Sondorillo in the Andes of northern Peru, (1850 m asl) with 345 mm/year, are not the highest (Figure 3). Indeed, the prevailing eastern direction of the moist trade winds and the exposure of the stations on the leeward side of the mountains, account for low precipitation levels measured at low altitudes. For example, little rain is registered in Jaén (620 m asl, 700 mm/year) which is surrounded by high mountains mainly towards the east (Figure 3). This is why a strong spatial variability is observed under 2000 m asl where rainfall varies from 500 to 3000 mm/year (Figure 3). Extreme values approved by the RVM analysis are in positions that favour strong air uplift, as Churuyacu (500 m asl) in Colombia with 5500 mm, close to a steep slope and Reventador (1470 m asl) in Ecuador with 6200 mm, located on a remote volcano. Also there exists a very rainy zone in the southeast of the Peruvian Amazon. For example, San Gabán station (820 m asl) gets an average of 6000 mm (Figure 3), and maximum values may be as high as 9000 mm/year (in 1967). It is located in a concavity in the Carabaya Mountain Range (south of Peru), close to steep slopes. It should also be mentioned that the RVM analysis has resulted in the rejection of several stations, particularly in very humid regions of the Andean countries. These stations located in remote areas feature scree and mudslide. As a result very scarce records have been kept. Thus, values in excess of 5000 mm in Chaparé, east of Cochabamba, as mentioned by Roche *et al*. (1990) in Bolivia, have not been included on the map (Figure 2).

Then, it is clear that the highest and lowest annual rainfall values in the AB are registered in the Andean region (Figures 2 and 3). Some cases illustrate the high spatial rainfall variability. In Ecuador, the Reventador station (1470 m asl; 6200 mm) is 80 km from Oyacachi (3200 m asl) whose annual rainfall is 1400 mm; the spatial variation between both stations is thus 58 mm/km. Also, between Puyo (960 m asl, with 4500 mm) on the border of the Andes, and Alao (3200 m asl, with 1000 mm) situated in an embanked valley, at a distance of 55 km, there is a 63 mm/km difference. In Peru, San Gabán (820 m asl; 6000 mm) is 110 km from Paucartambo (2030 m asl, with 530 mm). It is situated in a valley behind the Carabaya Mountain Range. In this case there is a 50 mm/km difference between both stations. In Bolivia, Cristal Mayu (880 m asl, with 4000 mm) is located 46 km away from Colomi (3280 m asl and 630 mm); the difference is still higher, 73 mm/km. The preceding examples show the important role of relief in determining the annual rainfall (Figure 3).

3.2. Seasonal cycle

The seasonal cycle is assessed with maps showing the quarterly percentage of rainfall (Figure 4) and using the AHC and K-means cluster analysis based on monthly rainfall indexes (Figure 5). AHC analysis enables the definition of an optimum number of nine clusters corresponding to nine regimes and the K-means technique gathers together stations experiencing the same regime. The seasonal cycle is also described using quarterly maps showing the mean 1979–1998 geopotential height at 850 hPa and the vertically integrated water vapour transport (Figure 6).

Figure 5(a) and (c) evidence a clear opposition between the tropical northern and southern regions of the Amazon in austral summer (DJF) and austral winter [June–July–August (JJA)]. In JJA the percentage of annual rainfall

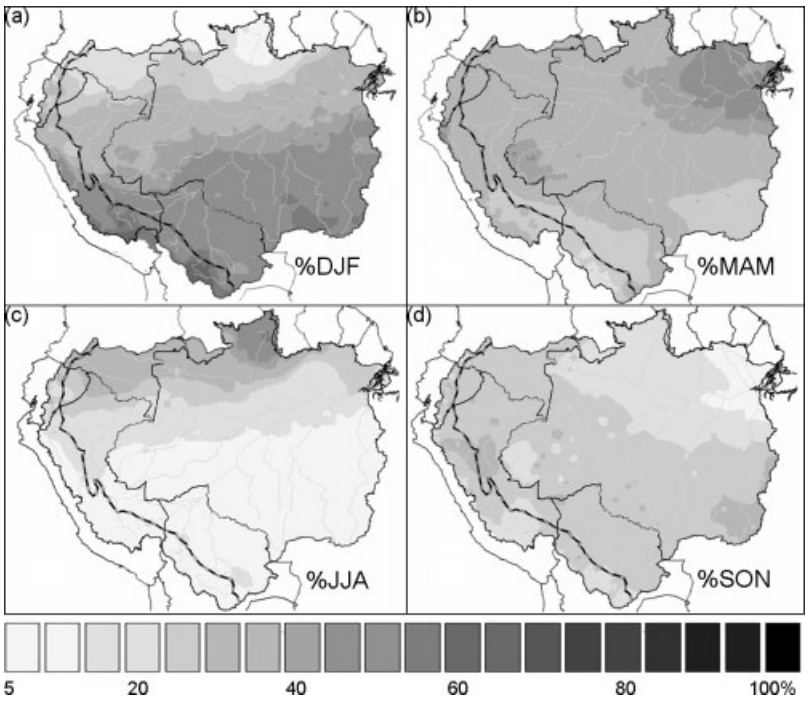

Figure 4. Quarterly percentages of rainfall (%) in (a) December–January–February (DJF), (b) March–April–May (MAM), (c) June–July–August (JJA), and (d) September–October–November (SON). The Andean regions above 500 m are limited by a black and white line.

DOI: 10.1002/joc

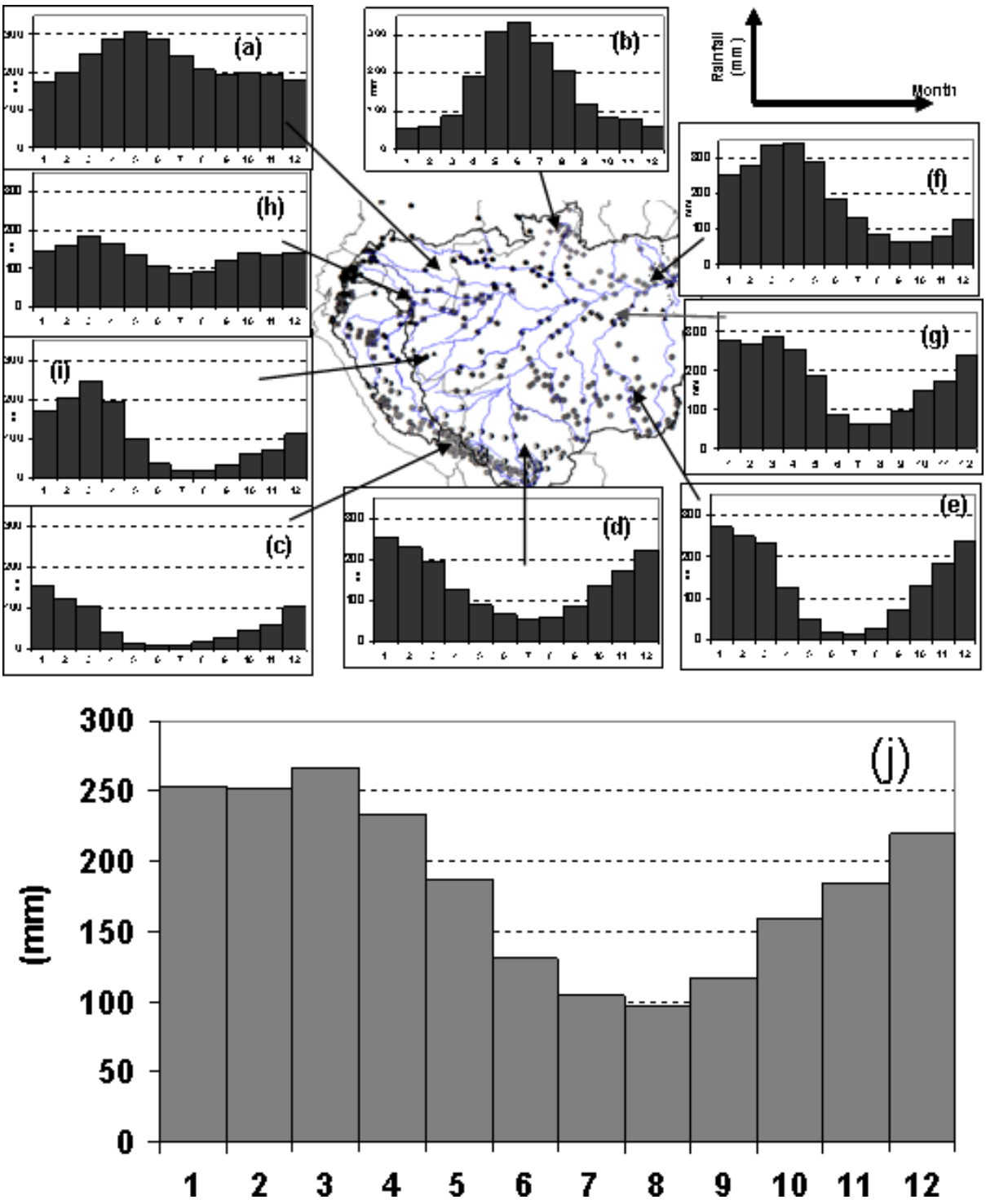

Figure 5. (a)–(i) Annual regimes, resulting from AHC and K-means classifications on a monthly rainfall index in 756 stations. Each symbol on the map corresponds to a regime. Each graph represents the average monthly rainfall of all the stations belonging to a class. (j) Annual regime of the average 1975–2003 rainfall in the Amazon basin at the delta. This figure is available in colour online at www.interscience.wiley.com/ijoc

is over 50% in the northern region (north of Brazil and Colombia), and below 20% in the south (south of Brazil, Peru, and Bolivia). The opposite is true in summer (DJF). Tropical regimes are also depicted in Figure 5(b) (Northern Hemisphere tropical regime) and in Figure 5(c)–(e) (Southern Hemisphere tropical regimes). In the Northern Hemisphere, particularly in the State of Roraima (Brazil), the rainfall peak in JJA is related to the warming of the continent and of the tropical Atlantic and eastern Pacific Ocean surface temperature (Pulwarty *et al*., 1998). To the south, the rainy season in austral summer is related to continent warming (Fu *et al*., 1999), to a low geopotential height in the Chaco region and to the onset of the South American monsoon (SAMS) and the related low-level jet (LLJ) along the Andes (Figure 6(a); Zhou and Lau, 1998; Saulo *et al*., 2000;

DOI: 10.1002/joc

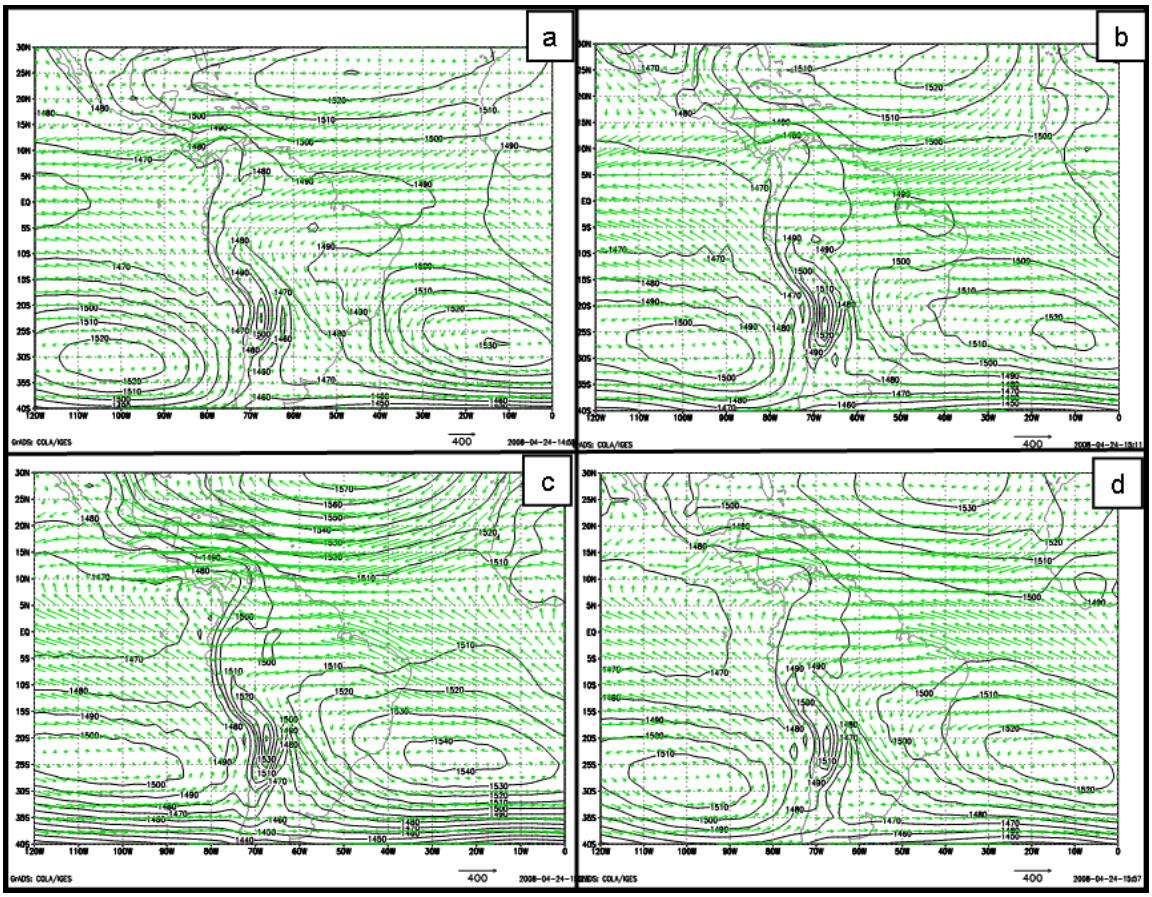

Figure 6. Mean 1964–2002 850 hPa geopotential height (m) and vertically integrated water vapour flux (kg/m/s) between the ground and 500 hPa wind in (a) January, (b) April, (c) July, and (d) October. The figures use ECMWF data. This figure is available in colour online at www.interscience.wiley.com/ijoc

Marengo *et al*., 2004). On the contrary, the dry season in JJA is related to high geopotential height values and to the retreat of the SAMS (Figure 6(c)). In the south, tropical regimes differ according to the length of the dry season. In the tropical Andes, it lasts from May to September (Figure 5(c)); only 5% of the annual rainfall can be registered during this period. In the lowlands the dry season is shorter, lasting from June to August. In the Bolivian plain the dry season is rainier (Figure 5(d)) than in the Mato Grosso (Figure 5(e)). This is because extra-tropical perturbations skim through the Bolivian lowlands during winter (Figure 6(c)) (Oliveira and Nobre, 1986; Ronchail, 1989; Garreaud, 2000; Seluchi and Marengo, 2000).

In the northeastern AB, autumn [March–April–May (MAM)] and spring (SON) are the most different seasons (Figure 4(b) and (d), respectively); more than 50% of annual rainfall can be measured in MAM, whereas less than 10% occurs in SON. This 'tropical maritime' regime involves a region from the Amazon delta to approximately 1000 km in the centre of the basin, at the confluence of the Amazon and Madeira River (Figure 5(f)). In this region, seasonality is mainly controlled by the Atlantic Ocean. In particular, the precipitations peak in austral autumn is related to the heating of the equatorial Atlantic and to the southernmost position of the ITCZ (Fu *et al*., 1999; Fu *et al*., 2001). On the contrary, in austral spring, the dry season is associated with the northward shift of warm waters and of the ITCZ.

In the northwest of the basin, in regions close to the equatorial line, rainfall distribution over the year is more uniform, with percentages close to 25% during each quarter (Figure 4). In Ecuador, the very low rainfall seasonality is related to deep convection on the always warm surface (Fu *et al*., 1999) and to the geopotential height that is very low from austral spring to austral autumn (Figure 6(b)). However, two different regimes can be highlighted from the upper Negro basin to the lowlands of Ecuador; on the windward slopes of the Andes, a unimodal regime with a slight peak at the end of the austral autumn (Figure 5(a)) is due to enhanced convection after the equinox and to a strong zonal water vapour transport (Figure 6(b)) (Laraque *et al*., 2007). A bimodal regime, with peaks near the equinoxes (April and October) and a slight decrease in austral winter is depicted in the intra-Andean basins in Peru and Ecuador, and in the Amazon plain, on the border of Peru, Brazil, and Colombia (Figure 5(h)). The semi-annual rainfall cycle results from the zonal oscillation of the continental ITCZ, associated with the semi-annual cycle of radiation and temperature (Horel *et al*., 1989; Figueroa and Nobre, 1990; Poveda, 2004; Poveda *et al*., 2006).

DOI: 10.1002/joc

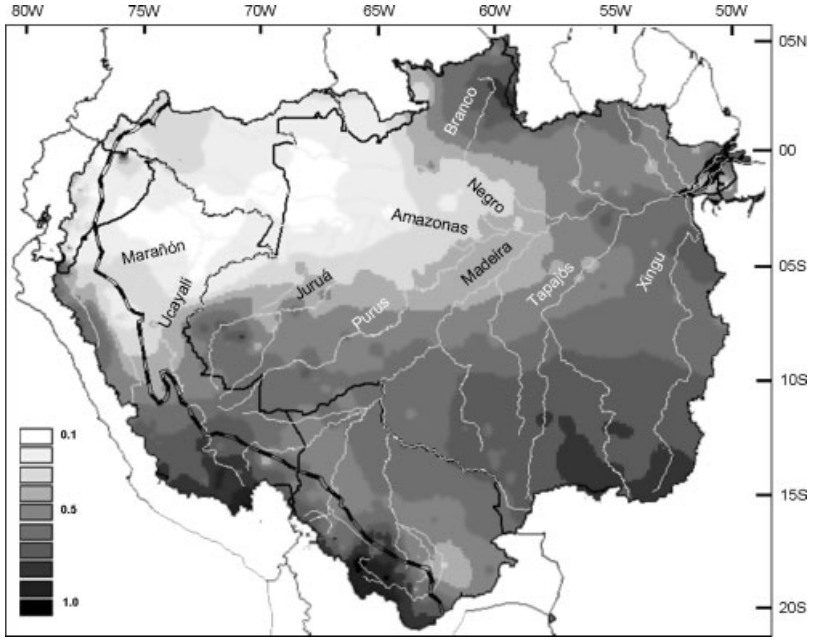

Figure 7. Seasonal variability coefficient (sVC): coefficient of variation computed on mean 1975–2003 monthly rainfall values. The Andean regions above 500 m are limited by a black and white line. The rivers mentioned in the text are named.

Finally, transition regimes prevail between 5 and 10 °S. In the central and eastern regions of the basin, an intermediate regime, between southeast (Figure 5(e)) and northeast (Figure 5(f)), is characterized by a rainy period from December to April (Figure 5(g)). In Peru, in the plain and the Andes, an intermediate regime between the southern tropical regime (Figure 5(c) and (d) and the northern bimodal regime in the north (Figure 5(h)), features a rainier season in March and a dry season from June to September (Figure 5(i)).

These results are similar to those described in previous studies for Brazil (Ratisbona, 1976; Salati *et al*., 1978; Kousky *et al*., 1984; Horel *et al*., 1989; Nobre *et al*., 1991; Marengo, 1992; Zhou and Lau, 2001; Ronchail *et al*., 2002). However new pieces of information are provided for the Andean regions, which had remained poorly documented.

The sVC (Figure 7) shows the important seasonal variability of rainfall with values over 0.6 in inner and tropical Andean regions, in the southern Andes of Peru (in the region of Apurimac, in the upper Ucayali basin) and in southwestern Bolivia (in the region of Sucre, in the upper Mamore Basin). From the south of the Bolivian lowland to southern Peru, in a corridor between the Andes and the Brazilian shield, the relatively low seasonal variability is due to winter rainfall related to extra-tropical perturbations. A strong sVC may be noticed in other tropical regions of the basin, particularly in the southeast (Mato Grosso) and in the north of Brazil (Roraima). In the northeast of the basin, close to the Amazon delta, there is also a major seasonal variation with an sVC value in excess of 0.5. Between 5°N and 5 °S, a strong decrease in sVC is observed from 60 °W towards the west, with values under 0.1, mainly in the lowland forests of Peru and Colombia and in the west of the Brazilian Amazon (Figure 7). This evidences the constant presence of rainfall in this region, confirming what is shown in Figures 4 and 5(a) and (h). In the northern part of Peru, there is an important east–west increase in sVC between the Amazon plain and the regions close to the Andes, as well as between the north and the south (throughout the Ucayali basin).

The Amazon basin of Peru and Ecuador down to Tamshiyacu (4.00 °S and 73.16 °W) extends over a surface of 726 400 km^2, with 53% over 500 m asl (Mialocq *et al*., 2005 and Espinoza *et al*., 2006). It experiences a high spatial variability of annual rainfall regimes (Figure 8).

The southern part of the basin displays a clear south tropical regime with a long dry season from May to September, such as Antabamba station (14.37 °S 72.88W; 3900 m asl, Figure 8(a)), with an annual cycle beginning in August and a rainy period from December to March. In the upper basin of the Huallaga and Ucayali Rivers, a tropical humid regime at Quillabamba station (12.86 °S 72.69 °W; 1128 m asl, Figure 8(b)) features a much longer and intense rainy period (from December to May). At Pozuzo (10.05 °S 75.55 °W; 258 m asl) in the north, at a lower altitude, a higher rainfall value and a shorter dry period (JJA) is observed (Figure 8(c)). In the north, in the upper Marañón River (Figure 8(d)), an intermediate regime between southern Tropics and the equator features a very rainy period from January to April, as in Julcán station (8.05 °S 78.50 °W; 3450 m asl). In the regions close to the equatorial line, longer rainy seasons are noticed; for example, the Gualaquiza station (3.40 °S 78.57 °W; 750 m asl, Figure 8(e)) close to the Andes presents a rainy season from February to July and no dry period. Towards the east in Iquitos (3.75 °S 73.25 °W; 125 m asl, Figure 8(f)), a more uniform regime

DOI: 10.1002/joc

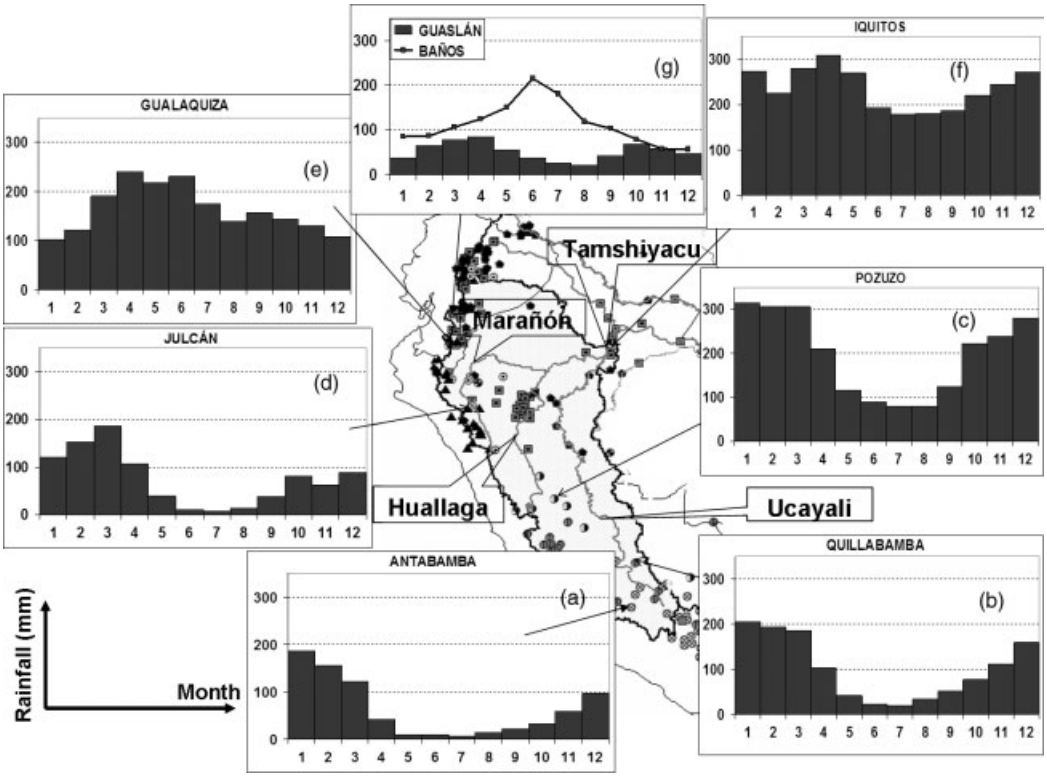

Figure 8. Rainfall regimes in eight stations in the Peruvian and Ecuadorian Amazon basin. Each symbol on the map corresponds to a regime as in Figure 5. The main rivers are named.

is depicted with a slight rainfall decrease from June to September, and a very weak sVC, as shown in Figure 7.

The spatial variability of rainfall regimes may be even greater as shown in studies about Ecuador. Stations with different regimes coexist in the same basin because of their different exposures to the easterlies. For example the minimum rainfall in Guaslan, in an intra-Andean basin, coincides with the rainfall peak in Baños, located on a windward slope (Figure 8(g)). This is due to an increase in the water vapour transport, in austral winter, which causes rainfall peaks in windward stations (Laraque *et al*., 2007; Bendix, Personal Communication).

The average monthly rainfall calculated for the whole AB (Figure 5(j)) presents a rainy period from December to April (between 220 and 270 mm/month) and less rainfall from July (105 mm) to August (95 mm). The sVC (0.34) is low and shows the influence of the northwest region, which, although not so extended, is very rainy and exhibits a low seasonality (Figures 2 and 5). Nevertheless, this rainfall cycle, with a drier season in winter, also reflects the influence of the extended southern tropical regions, from 5 °S to the south of the basin, characterized by a marked dry season around July and August (Figure 5).

3.3. Interannual variability

The interannual rainfall variability resulting from the iVC is particularly important in the mountainous regions of the Andean countries (Figure 9(a)), in the Tropics (Chaco and Roraima) and close to the Amazon delta. High values of iVC are also found on the elevated border of Peru and Brazil (Fitzcarrald Arch, 400–500 m asl, upper Juruá and Purus Rivers, see Figure 9(a)). Regions with lower interannual variability are situated along the northwest–southeast axis of the AB, where rainfall is abundant. Isolated high values may be related to particular local conditions.

The interannual–seasonal variability ratio (iVC/sVC) highlights a major uniformity of rainfall distribution during the year in the western equatorial regions of the AB (0°–05 °S and 65°–77 °W) (Figure 9(b)). In this region, interannual variability is three times higher than seasonal variability (iVC/sVC up to 3.0). On the contrary, in the south and east of the Amazon, seasonal variability exceeds interannual variability.

Interannual variability is also addressed using a varimax-rotated PCA on rainfall index vectors resulting from the RVM analysis. On the one hand, the advantage of this procedure lies in the use of data summarizing the interannual variability of homogeneous zones already specified by the RVM. Thus, 25 different regions are defined, from which 9 belong to the Brazilian Amazon plain and 16 are located in the Andean countries (Figure 1). In Brazil, regionalization is similar to that found by Hiez *et al*. (1991). On the other hand, the use of annual pluviometric indexes from RVM allows the analysis period to be extended to 1964–2003 (see Chapter 2).

PCAs are computed on a quarterly rainfall, i.e. DJF, MAM, JJA, and SON. The first three components of

DOI: 10.1002/joc

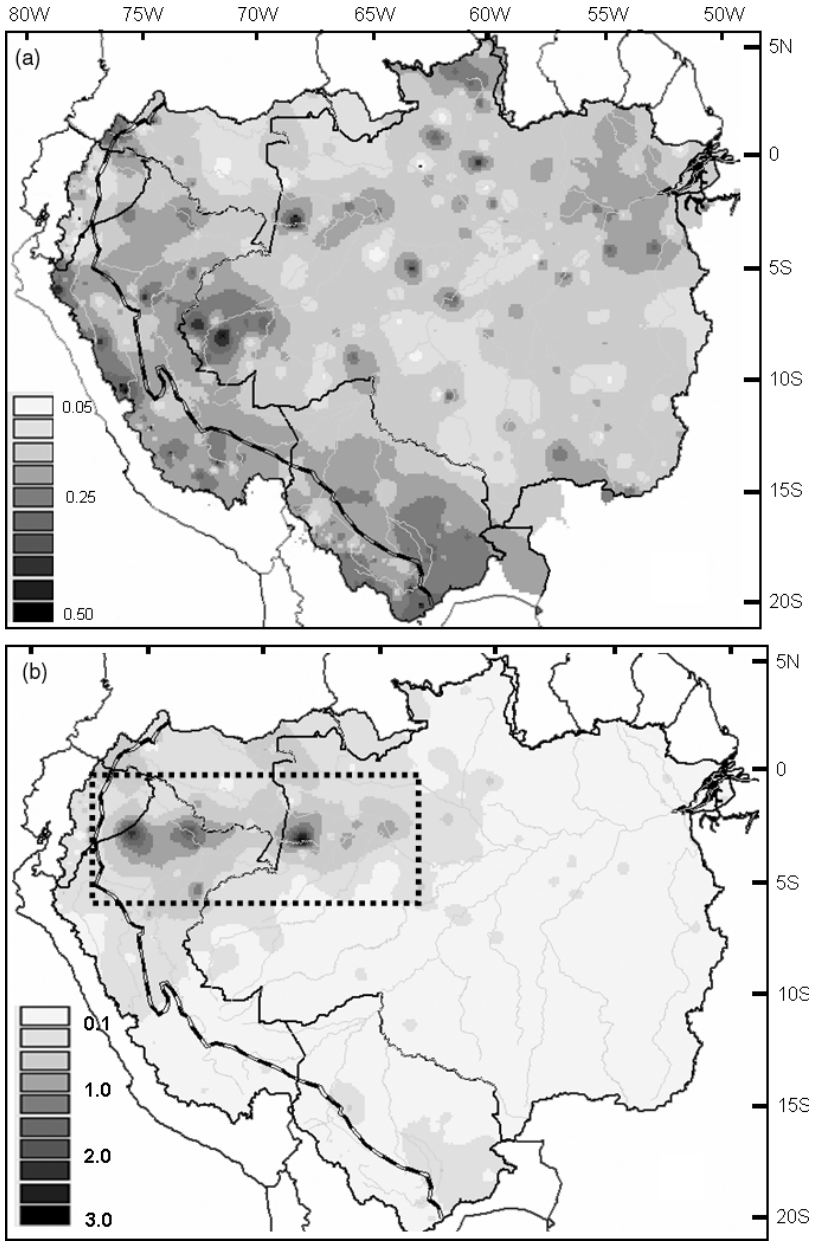

Figure 9. (a) Interannual variability coefficient (iVC): coefficient of variation of annual 1975–2003 rainfall. (b) Ratio between the interannual variability coefficient and the seasonal variability coefficient. In the dotted rectangle is the region where the interannual variability is more important than the seasonal variability. The Andean regions above 500 m are limited by a black and white line.

the PCAs generally summarize 45–50% of total rainfall variability.

In JJA and SON, experiencing little rainfall except in the northwest, the main variability is pluridecadal, with a change at the end of the 1970s in JJA (Figure 10) and the beginning of the 1980s in SON (not shown). The first principal components (PCs) account for 26 and 18% of the explained variance in JJA and SON, respectively. High rainfall is registered during the first period in the whole AB. The signal is very strong in the northwest, whereas it is weak in the south. Low rainfall characterizes the second period. We use the ERA-40 reanalysis to take into account the differences in atmospheric circulation between both periods. Figure 11(a) displays the differences in the 850 hPa geopotential height and wind between 1986–1997, the driest period, and 1967–1976, the rainiest period. After the 1970s, an enhanced geopotential height can be observed over the western Amazon and the tropical Atlantic. Water vapour diverges from these regions leading to a reduced rainfall. Interestingly, as a low geopotential height prevails over eastern Brazil, water vapour converges towards this region (Figure 11(b)). Given the fact that El Niño events are related to dryness in northern Amazon and that a strong frequency of El Niño events has been observed since the end of the 1970s (Trenberth and Hurrell, 1994), it is assumed that the rainfall decrease in the north of the basin after that date can be attributed to the warming of the tropical Pacific. The time series of the first PC in JJA is negatively correlated with the JJA multivariate

DOI: 10.1002/joc

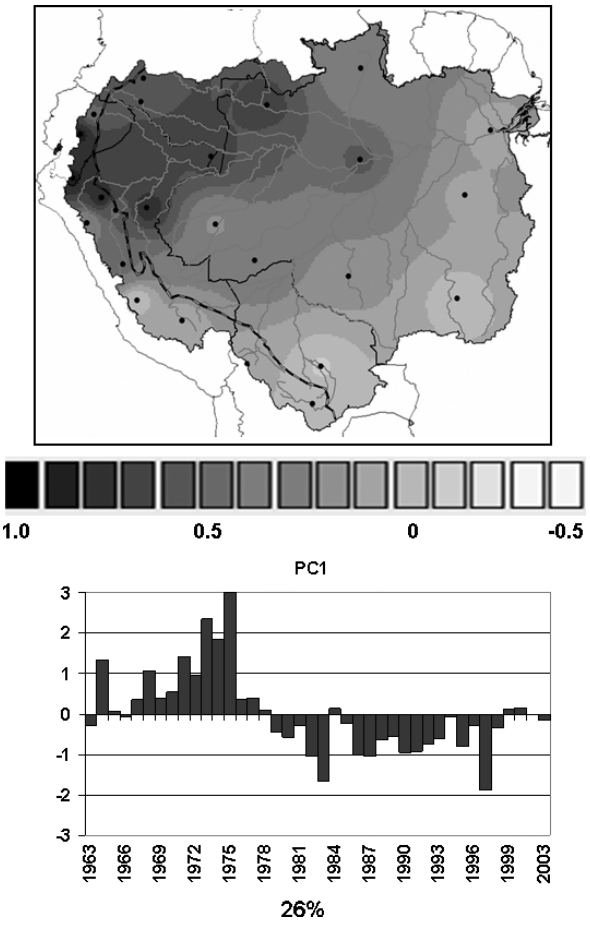

Figure 10. Spatial and temporal patterns associated with the first principal component resulting from a PCA analysis on JJA rainfall in 25 vectors (part 2).

ENSO index (MEI) and PDO indexes ($r = -0.69$ and -0.66, respectively, both correlations being significant at the 99% level; Figure 12). Partial correlations show that both indicators combine to account for 65% of the total rainfall variance. At an interannual time scale, positive MEI values are associated with very low rainfall over the basin (1983, 1997), whereas negative MEI values are concomitant with high rainfall (1973, 1975). At a pluriannual time scale, low PDO values during the 1960s and 1970s are associated with high rainfall. The opposite can be observed during the 1980s and 1990s. Marengo (2004) and Marengo *et al*. (2008) already mentioned connections between the long-term rainfall variability in the AB and the PDO.

The aforementioned long-term variability is also present in MAM and DJF seasons and but it is not the main mode of variability. Pluriannual variability in DJF and MAM, the rainiest seasons in many regions (Figure 5), is observed at a decadal time scale. PC1 in DJF (27% of variance) and PC2 in MAM (16%) show the same time space modes of variability. In MAM, rainfall is important (weak) in the northwest (southeast) of the basin during the 1970s and 1990s, and the opposite can be noticed from the beginning of the 1980s till the beginning of the 1990s with a higher than normal rainfall in the southeast (Figure 13). The rainfall increase in southeastern Amazon at the end of the 1970s is related to a negative geopotential height (Figure 14(a)) over southern Amazon where there is an intensification of the northwest wind along the Andes and of the LLJ and to the convergence of water vapour from the Atlantic and northwest Amazon (Figure 14(b)). On the contrary, stronger than normal geopotential height prevails over northwestern Amazon where water vapour diverges. The rainfall increase in northwestern Amazon during the last decade is related to a reduced northwest wind and LLJ and to an increased water vapour convergence over the north (Figure 14(d)), promoted by a positive geopotential anomaly over most of the continent south of the equator line (Figure 14(c)). In DJF and MAM, the PC loadings are very weakly correlated to the PDO ($r = -0.38$, $p > 0.95$ in MAM). These results are consistent with Ronchail (1996) who finds a similar pluriannual variability in Bolivia and with Marengo and Nobre (2001) and Marengo (2004) who show opposite long-term evolutions in the north and south of the Brazilian AB. Also Lau and Wu (2006) describe a similar spatio-temporal pattern, with an increase in the annual rainfall along the tropical Andes, whereas the annual rainfall decreases in the eastern and southern parts of the Amazon, between 1979–1990 and 1991–2002. However, our study yields some insights into the seasonality of the pluriannual rainfall evolution.

In DJF and MAM, an interannual variability represented by PC2 in DJF and PC3 in MAM accounts for 13 and 10% of rainfall variance, respectively (Figure 15). Strong positive values are displayed during the 1970s, in 1984–1985–1986, 1989, and 1995 (many of them La Niña years), and negative values in 1983, 1992–1993, and 1998 (most of them El Niño events). An opposition is pointed out between, on the one hand, the south of the Andean region (Peruvian and Bolivian Altiplano) and the northeast (in DJF) and east (in MAM) of the AB, and on the other, the southeast of the basin in DJF (the southwest in MAM) and the northwest of the AB. The two PCs are related to the interannual variability of ENSO and of the SST gradient between the NATL and the SATL (Figure 16). Correlation values between the DJF and MAM PCs and the seasonal MEI are -0.55 (significant at the 99% level), indicating that during El Niño events, rainfall is less abundant in the tropical Andes and in the east of the AB, as already described by Kousky *et al*. (1984), Aceituno (1988), Marengo (1992), Marengo and Hastenrath (1993), Moron *et al*. (1995), Ronchail (1998), Liebmann and Marengo (2001), and Ronchail *et al*. (2002), among others. El Niño events are associated with a rising motion over the eastern regions of the equatorial Pacific Ocean and subsidence over the northern AB (Kousky *et al*., 1984). Additionally, Garreaud and Aceituno (2001) show that the northward position of the Bolivian High during El Niño events prohibits the uplift of moist air towards the Altiplano, preventing rainfall in this region. On the contrary, rainfall tends to be slightly more abundant during El Niño events in western and

DOI: 10.1002/joc

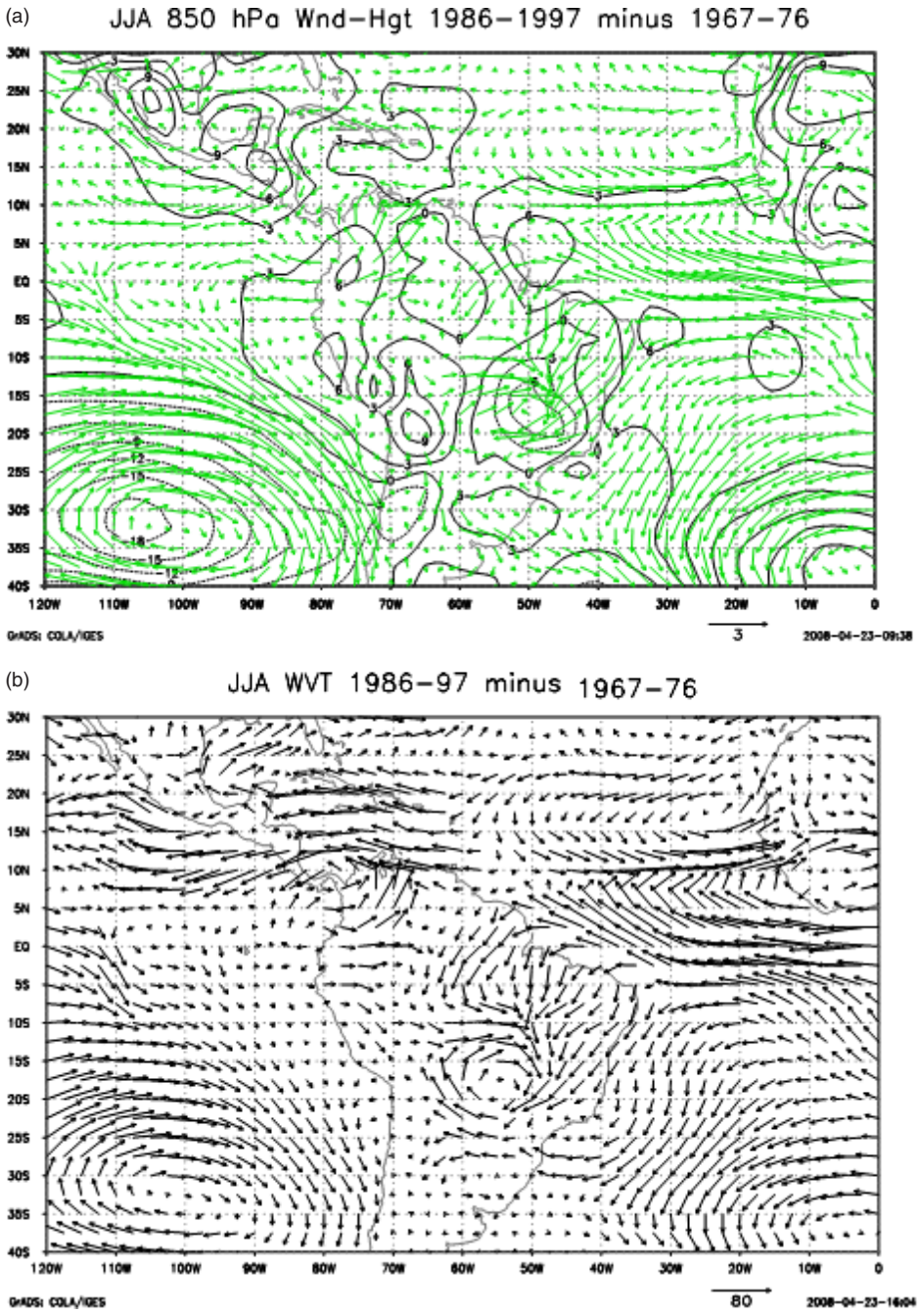

Figure 11. JJA differences between 1986–1997 and 1967–1976 in (a) 850 hPa geopotential height (m) and wind (m/s), (b) vertically integrated water vapour flux (kg/m/s) between the ground and 500 hPa. The figures use ECMWF data. This figure is available in colour online at www.interscience.wiley.com/ijoc

southern Amazon, as reported by Ronchail (1998), Ronchail *et al.* (2002, 2005), Bendix *et al.* (2003), Grimm (2003, 2004), and Ronchail and Gallaire (2006).

The correlation between these PCs and the annual difference between the northern and SATL SSTs is also significant at the 99% level ($r = -0.59$ in DJF and $r = -0.48$ in MAM). Figure 16 shows that when this gradient is positive, i.e. when the north tropical Atlantic is warmer and/or the south tropical Atlantic is colder than usual, rainfall is less abundant in the northeast of the basin, as previously pointed out and explained by Molion (1987, 1993), Marengo (1992), Moron *et al.* (1995), Nobre and Shukla (1996), and Ronchail *et al.* (2002), among others. Tropical Atlantic Ocean warming causes a rising motion over this ocean and subsidence in the south of the AB, a shift to the north of the ITCZ and less rainfall over northeastern Amazon. The opposite can be noticed when the Atlantic SST gradient is negative.

The partial correlations between, on the one hand, PC2 in DJF and SOI or MEI and NATL–SATL on the other, are significant, indicating that both climatic indicators are complementary to account for interannual variability. Together they make up 50% of rainfall variability as described by PC2 in DJF.

DOI: 10.1002/joc

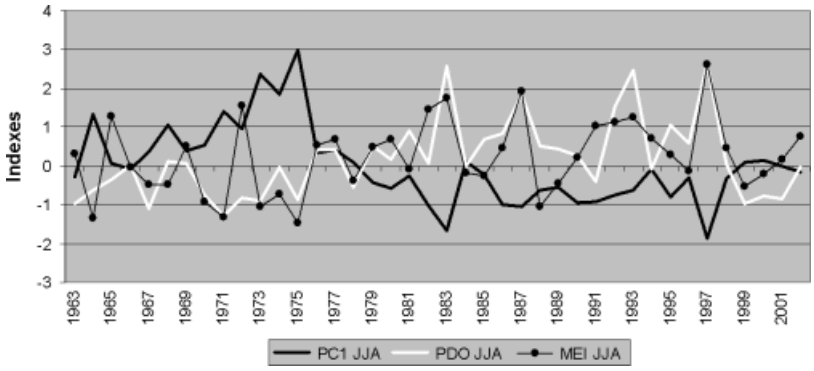

Figure 12. 1963–2003 time evolution of the first PC of a PCA analysis on JJA rainfall and JJA PDO and MEI indexes.

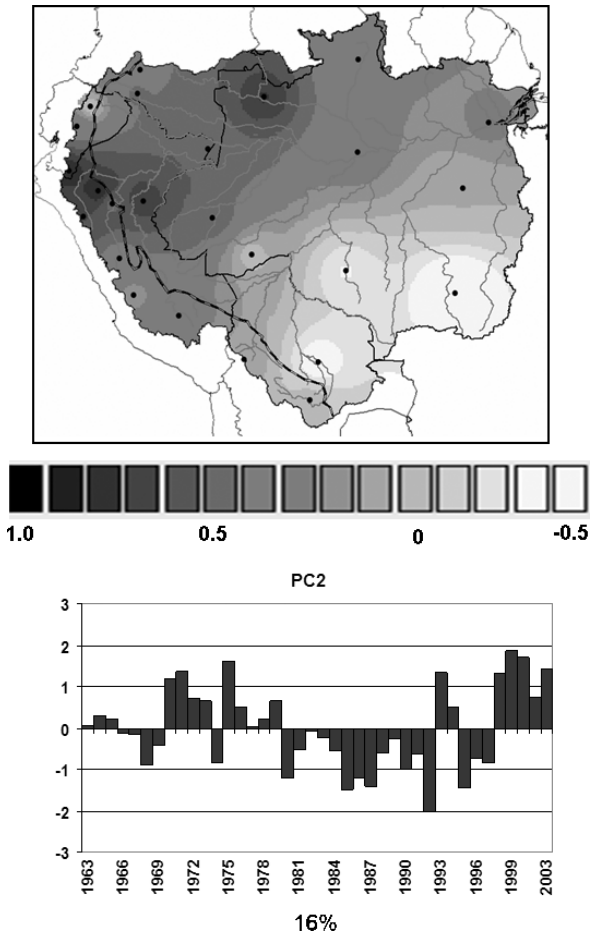

Figure 13. Spatial and temporal patterns associated with the second principal component resulting from PCA analysis on MAM rainfall in 25 vectors (part 2).

3.4. Mean rainfall in the basin

Mean interannual rainfall for the whole basin (Figure 17(a)) is of 2200 mm/year for a standard deviation of 138 mm and a variation coefficient of 0.06. The maximum value, as recorded in 1975 (during a La Niña year), is 2460 mm, whereas the minimum value, recorded in 1992, is 1815 mm (during an El Niño event).

Trend tests evidence a rainfall decrease during the 1975–2003 period (significant at the 95% level). The Pearson's, Spearman's and Kendall's coefficient values are −0.47, −0.50, −0.33, respectively. This is consistent with the negative trend reported by Marengo (2004) in Brazil. The annual rainfall decrease percentage is −0.30%/year (−30% rainfall in 100 years). This is lower than the average calculated in the Peruvian and Ecuadorian Amazon: −0.83%/year for the 1970–1997 period (Espinoza *et al*., 2006). All break tests applied to the mean annual rainfall agree with a change in 1982 (Table I), related to the time evolution of the JJA and SON rainfall PC1s (Figure 10) that shows lower rainfall values since 1983 in the north of the basin. The first period, before 1982, outlines an average of 2296 mm/year and the second one, after 1982, of 2160 mm/year. Another change is reported by the Buishand and Pettitt tests in 1989 (with slightly lower values after the break), in partial agreement with the rainfall increase in the northwest observed in PC1 in DJF and PC2 in MAM at the beginning of the 1990s (Figure 13). The first period, before 1989, totals 2250 mm/year average and the second, after 1989, 2139 mm.

At a quarterly time scale, it clearly appears that rainfall decreases in DJF, JJA, and SON during the 1975–2003 period, with trends being significant at the 95, 90, and 99% level, respectively (Figure 17(b)). In other words annual rainfall decrease is due to the strong negative trend observed in JJA and SON (Figure 10) in the extreme northwest of the basin that remains rainy during these seasons (Figure 5(a), (b), and (h)). At the end of the century, a positive trend developed from 1992 to 2003 in MAM (at the 95% significance level) which is consistent with the MAM PC2 (Figure 13), whereas a weak negative trend was found in SON and no trend in DJF and JJA (Figure 17(b)). From a hydrological standpoint, a major finding is the increasing rainfall amplitude which has been observed between SON and MAM since 1992 (Callède *et al*. 2004; Espinoza *et al*., 2008).

4. Conclusions

For the first time, a database with *in situ* pluviometric information gathers together 1446 original rain gauges from five countries that form the better part of the AB. Monthly rainfall data have been collected for the 1964–2003 period within the HYBAM programmes, in

DOI: 10.1002/joc

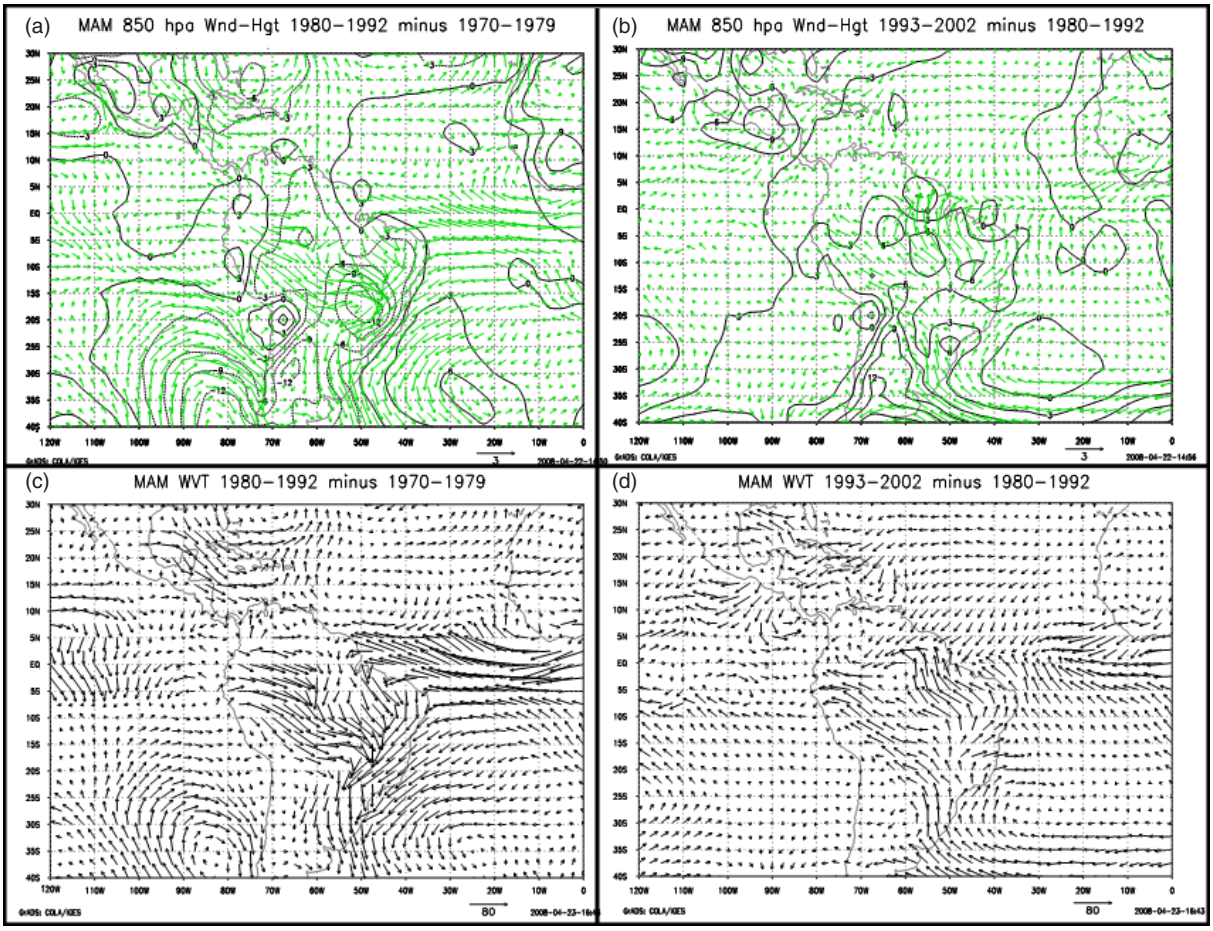

Figure 14. MAM differences between (a) 1980–1992 and 1970–1979 850 hPa geopotential height (m) and wind (m/s), (b) 1980–1992 and 1970–1979 vertically integrated water vapour flux (kg/m/s) between the ground and 500 hPa, (c) 1993–2002 and 1980–1992 850 hPa geopotential height (m) and wind (m/s), (d) 1993–2002 and 1980–1992 vertically integrated water vapour flux (kg/m/s) between the ground and 500 hPa. The figures use ECMWF data. This figure is available in colour online at www.interscience.wiley.com/ijoc

collaboration with the different institutions in charge of the meteorological and hydrological monitoring in the Amazonian countries. Rainfall data have been controlled using the RVM. The resulting database (756 stations for the 1964–2003 period) shows that the main data contribution is from the highlands of the Andean countries (Peru, Bolivia, Ecuador, and Colombia). Additionally, the stations are unevenly distributed, with a smaller number of posts in the plain of the Andean countries because of the remoteness of these regions.

In the Andean regions of the AB, very high and low rainfall values (between 6000 and 250 mm/year) are recorded in nearby stations, as observed in the Himalaya chain by Dobremez (2001). The strong spatial variability is due to rainfall decrease with altitude and to the leeward or windward position of the stations. The highest rainfall in the AB is observed in low windward regions (over 6000 mm/year) and conversely, low rainfall is measured in leeward and elevated stations (under 530 mm/year). In the lowlands, the northwest and northeast equatorial regions are the rainiest zones, with values over 3000 mm/year. Less rainfall is measured in the tropical regions. These results complement what is shown in many studies about rainfall distribution in the Brazilian Amazon and in particular a focus is given on east–west and north–south rainfall gradients in Peru.

Rainfall regimes evidence the strong opposition between the northern and southern Tropics, because of the alternating warming of each hemisphere and to American monsoons. Next to the Amazon delta, a MAM maximum and a SON minimum are associated with seasonal migration of the ITCZ. In the northwest equatorial region there is a better rainfall distribution within the year with quarterly percentages of rain close to 25%. In the equatorial Andes, the distribution of rainfall regimes is highly complex and associated with the stations exposure: bimodal regimes in intra-Andean basins are found close to unimodal regimes in windward stations. This particular subject is more widely developed in Laraque *et al.* (2007). Various intermediate regimes are described between equatorial and tropical regions; a focus on Peru is also proposed as very little information is available to this day.

The RVM has supported not only the analysis of data quality, but also the creation of homogeneous regions, exhibiting the same interannual rainfall variability, and computation of 25 indexes (vectors) that summarize the pluviometric variability of 25 regions. PCA has been

DOI: 10.1002/joc

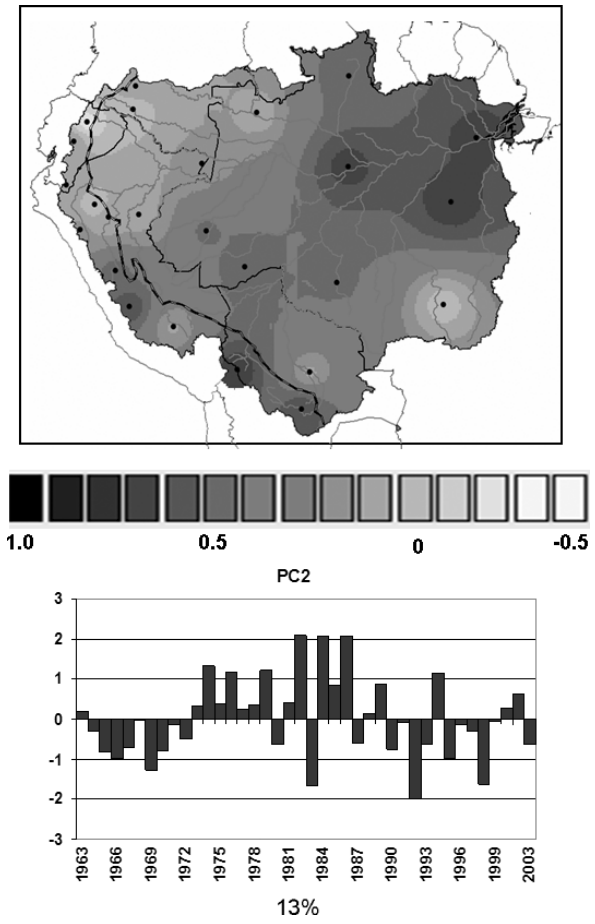

Figure 15. Spatial and temporal patterns associated with the second principal component resulting from a PCA analysis on DJF rainfall in 25 vectors (part 2).

performed on quarterly indexes to identify the main spatial and temporal rainfall patterns. Three main modes of spatio-temporal variability have been defined and the related spatial patterns are widely dependent on the Andean country indexes. A long-term variability characterizes rainfall evolution from June to November. It shows a rainfall decrease since the end of the 1970s–beginning of the 1980s, in the whole basin and especially in the northwest. This change is due to the long-term increase of the near surface geopotential height over the western part of the Amazon. It is also associated with the long- and short-term variability in the Pacific Ocean (PDO and ENSO). During the rainiest seasons, DJF and MAM, the long-term variability is interrupted at the beginning of the 1990s, featuring a clear NW–SE opposition, with more rainfall in the NW during the 1970s and 1990s and less rainfall during the 1980s; the opposite occurring in the SE. This variability is driven by reduced water vapour transport by the northwest wind along the Andes and the LLJ during the 1990s, which promotes rainfall in the northwest. The opposite conditions causing enhanced rainfall in the south are observed during the 1980s. Finally, an interannual variability in DJF and MAM is related to the Pacific and Atlantic interannual variability. Rainfall is less (more) abundant in the northeastern AB during El Niño (La Niña) events and when the SST gradient is positive (negative) in the tropical Atlantic. Rainfall is also less abundant over the southern tropical Andes during El Niño, whereas, on the contrary, it tends to be more abundant in the western and southern AB.

The mean rainfall at the outlet of the basin exhibits an average of 2200 mm/year for the 1975–2003 period. This value is consistent with different results yielding values between 2000 and 2200 mm for the AB (Marengo and Nobre, 2001; Marengo, 2004; Callède *et al*., 2008). The trend during this period is significantly negative and break tests indicate changes in 1982 and 1989 with less rainfall afterwards. The seasonal mean rainfall over the basin shows different evolutions for the 1975–2003 period. Rainfall diminishes dramatically during the drier seasons (JJA and SON) and not so much in DJF and MAM. Opposite trends appear after 1992; rainfall increases in MAM, whereas it decreases in SON. The resulting increase in rainfall amplitude is consistent with the pluriannual variability shown by MAM PC2, i.e. with high rainfall values in the NW and low rainfall values in the south after 1992, and with the break detected in 1989 in the mean rainfall of the basin.

Rainfall decrease is related to changes in the ocean and atmosphere as seen before. However, it may also be associated with deforestation. Unlike what could have been expected, a strong 1975–2003 rainfall decrease is observed during the dry season in the north of the basin, very rainy and undeforested, whereas it is weak in the south which is the most deforested region. To conclude, the assumed deforestation impact on rainfall does not seem to have taken place as expected in the

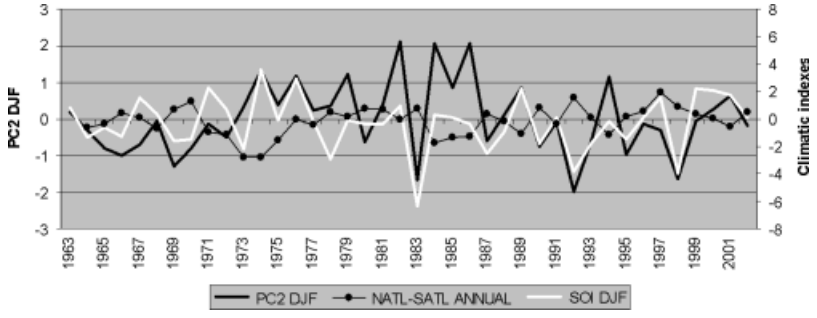

Figure 16. 1963–2003 time evolution of the second PC of a PCA analysis on DJF rainfall, DJF SOI index, and annual NATL–SATL index.

DOI: 10.1002/joc

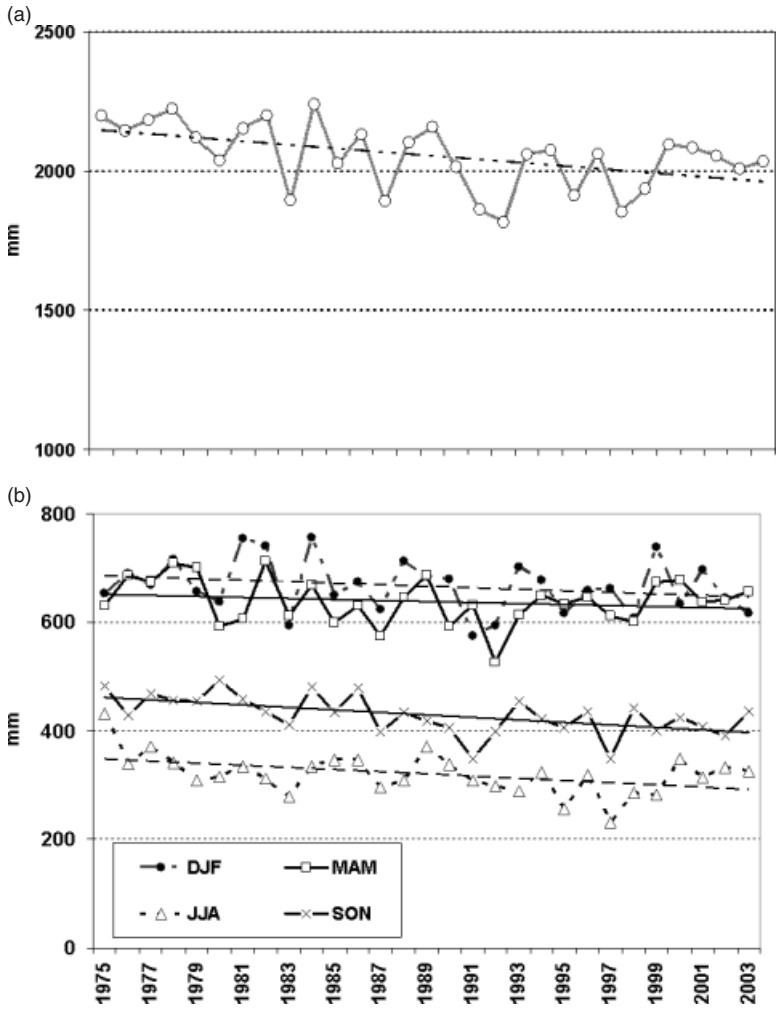

Figure 17. (a) 1975–2003 evolution of the average annual rainfall (mm) in the Amazon basin at the delta and trend line (significant at the 99% level). (b) 1975–2003 evolution of the average quarterly rainfall (mm) in the Amazon basin at the delta and trend lines DJF, JJA, and SON have significant trends at the 95, 90, and 99% levels, respectively. In MAM there is no significant trend.

Table I. Results of the break-detecting tests applied on the mean annual rainfall in the AB. 'X' indicates a break in the series. Mean, Standard Deviation and Variation Coefficient are given for the 1975–1982 and 1983–2003 periods.

TEST	1975	1980	1985	1990	1995	2000	2003
BUISHAND		**X**		**X**			
PETTITT		**X**	**X**	**X**			
LEE ET HEGNINIAN		**X**					
HUBERT		**X**					
Mean rainfall (mm)	**2158**				**2015**		
Standard Deviation (mm)	**59**				**112**		
Variation Coefficient	**0.03**				**0.06**		

most deforested areas. Nevertheless, this issue will have to be further addressed in the future.

Our results are in line with those of Zhou and Lau (2001) who reported interannual, decennial, and interdecadal rainfall variability in South America during the 1979–1995 period. Nonetheless, the introduction of data from the Andean countries, where variability reaches a peak, has a major impact on the spatial structure of rainfall variability. In particular, our study complements the north–south rainfall variability reported by Marengo (1992, 2004).

The description of two modes of long-term rainfall variability leads to a better understanding of runoff evolution in the main stream of the Amazon River (Callède *et al*., 2004, 2008, and Espinoza *et al*., 2008), particularly with respect to the intensification of runoff extremes, without taking into account the changes in land use. These results make it possible to identify the location

DOI: 10.1002/joc

with the main spatial temporal rainfall variability in the AB and as a consequence, highlight those regions where future researches aiming to define the causes of rainfall variability will be conducted. It will be done in order to address such issues as that of knowing whether rainfall variability is related to climate variability, or to climatic change, or to changes in land use such as deforestation. A better insight into regional rainfall variability is also conducive to a greater understanding of the regional runoff variability in the sub-basins of the Amazon, and especially the frequent major floods and very weak low-flows that have recently been observed (Marengo *et al*., 2008; Zeng *et al*., 2008).

Acknowledgements

The authors would like to express their special thanks to the Institute of Research for the Development (IRD) and the French National Center for Scientific Research (CNRS) through the National Program 'Fluid Envelopes and Environment' (LEFE) for funding this research. ECMWF ERA-40 data used in this study have been provided by ECMWF from the ECMWF data server. The authors are grateful to IDEAM (Instituto de Hidrología, Meteorología y Estudios Ambientales – Colombia), SENAMHI (Servicio Nacional de Meteorología e Hidrología – Bolivia and Peru), INAMHI (Instituto Nacional de Meteorología e Hidrología – Ecuador), and ANA (Agência Nacional de Águas – Brazil) for sharing their knowledge of local climate with the authors and for providing the rainfall data. The authors are grateful to the reviewers whose comments and suggestions considerably helped to improve the manuscript.

References

Aceituno P. 1988. On the functioning of the southern oscillation in the South American sector: surface, climate. *Monthly Water Review* **116**: 505–524.

Aceituno P. 1998. Climate elements of the South American Altiplano. *Revista Geofisica – IPGH* **44**: 37–55.

Agosta E, Compagnucci R, Vargas W. 1999. Cambios en el régimen de la precipitación estival en la región centro-oeste Argentina. *Meteorológica* **24**: 63–84.

Avissar R, Liu Y. 1996. Three-dimensional numerical study of shallow convective clouds and precipitation induced by land surface forcings. *Journal of Geophysical Research* **101**: 7499–7518.

Bendix J, Gämmerler S, Reudenbach C, Bendix A. 2003. A case study on rainfall dynamics during El Niño/La Niña 1997/99 in Ecuador and surrounding areas as inferred from GOES-8 and TRMM – PR observation. *Erdkunde* **57**: 81–93.

Broggy JA. 1965. Climatología general. *Boletín de la sociedad geográfica de Lima* **84**: 30–35.

Brunet-Moret Y. 1979. Homogénéisation des précipitations. *Cahiers ORSTOM, Série Hydrologie* **16**: 3–4.

Buishand TA. 1982. Tests for detecting a shift in the mean of hydrological time series. *Journal of Hydrology* **58**: 51–69.

Buytaert W, Celleri R, Willems P, De Bièvre B, Wyseure G. 2006. Spatial and temporal rainfall variability in mountain areas: A case study from the south Ecuadorian Andes. *Journal of Hydrology* **329**: 413–421.

Callède J, Guyot JL, Ronchail J, L'Hôte Y, Niel H, de Oliveira E. 2004. Evolution du débit de l'Amazone à Obidos de 1902 à 1999. *Hydrological Sciences Journal* **49**: 85–97.

Callède J, Ronchail J, Guyot JL. 2008. Déboisement amazonien: son influence sur le débit de l'Amazone à Óbidos (Brésil). *Revue des Sciences de l'Eau/Journal of Water Science* **21**: 59–72.

Chen F, Avissar R. 1994. Impact of land-surface moisture variability on local shallow convective cumulus and precipitation in large-scale models. *Journal of Applied Meteorology* **33**: 1382–1401.

Chen TC, Yoon JH, St. Croix KJ, Takle ES. 2001. Suppressing impacts of the Amazon deforestation by the global circulation change. *Bulletin of the American Meteorological Society* **82**: 2210–2216.

Chu PS, Yu ZP, Hastenrath S. 1994. Detecting climate change concurrent with deforestation in the Amazon basin: Which way has it gone? *Bulletin of the American Meteorological Society* **75**: 579–583.

Curtis S, Hastenrath S. 1999. Trend of upper-air circulation and water vapor in the equatorial South America and adjacent oceans. *International Journal of Climatology* **19**: 863–876.

D'Almeida C, Vörösmarty CJ, Hurtt GC, Marengo JA, Dingman SL, Keim BD. 2007. The effects of deforestation on the hydrological cycle in Amazonia: a review on scale and resolution. *International Journal of Climatology* **27**: 633–647.

Dillon W, Goldstein M. 1984. *Multivariate analysis. Methods and applications*. John Wiley and Sons; New York 157–186.

Dirmeyer P, Shukla J. 1994. Albedo as a modulator of climate response to tropical deforestation. *Journal of Geophysical Research* **99**: 20863–20877.

Dobremez JF. 2001. La Montagne du biologiste. *Revue de Géographie Alpine* **2**: 93–100.

Durieux L, Toledo Machado LA, Laurent H. 2003. The impact of deforestation on cloud cover over the Amazon arc of deforestation. *Remote Sensing of Environment* **86**: 132–140.

Eltahir EAB, Bras RL. 1994. Precipitation recycling in the Amazon Basin. *Quarterly Journal of the Royal Meteorological Society* **120**: 861–880.

Espinoza JC, Fraizy P, Guyot JL, Ordoñez JJ, Pombosa R, Ronchail J. 2006. La variabilité des débits du Rio Amazonas au Pérou. *Climate Variability and Change-Hydrological impacts* **308**: 424–429, IAHS Publ.

Espinoza JC, Guyot JL, Ronchail J, Cochonneau G, Filizola N, Fraizy P, Noriega L, de Oliveira E, Ordoñez JJ, Vauchel P. 2008. Contrasting regional discharge evolutions in the Amazon basin (1974–2004). *Journal of Hydrology* (Submitted).

Figueroa SN, Nobre CA. 1990. Precipitation distribution over central and western tropical South America. *Climanalise* **6**: 36–40.

Fisch G, Marengo JA, Nobre CA. 1998. Uma revisão geral sobre o clima da Amazõnia. *Acta Amazônica* **28**: 101–126.

Francou B, Pizarro L. 1985. El Niño y las sequías en los altos Andes centrales (Perú y Bolivia). *Bulletin de l'Institut Français d'Etudes Andines* **14**: 1–18.

Francou B, Vuille M, Wagnon P, Mendoza J, Sicart JE. 2003. Tropical climate change recorded by a glacier in the central Andes during the last decades of the 20th century: Chacaltaya, Bolivia. *Journal of Geophysical Research* **108**(D5): 4059. DOI:10.129/2002JD002473.

Fu R, Dickinson RE, Chen MX, Wang H. 2001. How the tropical sea surface temperatures influence the seasonal distribution precipitation in equatorial Amazonia? *Journal of Climate* **14**: 4003–4026.

Fu R, Zhu B, Dickinson RE. 1999. How the atmosphere and land surface influence seasonal changes of convection in the tropical Amazon? *Journal of Climate* **12**: 1306–1321.

Garreaud R. 2000. Cold air incursions over Subtropical South America: Mean structure and dynamics. *Monthly Weather Review* **128**: 2544–2559.

Garreaud R, Aceituno P. 2001. Interannual rainfall variability over the South American Altiplano. *Journal of Climate* **14**: 2779–2789.

Gautier E, Brunstein D, Vauchel P, Roulet M, Fuertes O, Guyot JL, Darrozes J, Bourrel L. 2006. Temporal relations between meander deformation, water discharge and sediment fluxes in the floodplain of the Rio Beni (Bolivian Amazonia). *Earth Surface Processes and Landforms* **32**: 230–248.

Genta J, Perez-Iribarren G, Mechoso G. 1998. A recent increasing trend in streamflow of rivers in southern South America. *Journal of Climate* **11**: 2858–2862.

Grimm AM. 2003. The El Niño impact on the summer monsoon in Brazil: regional processes versus remote influences. *Journal of Climate* **16**: 263–280.

Grimm AM. 2004. How do La Niña events disturb the summer monsoon system in Brazil? *Climate Dynamics* **22**: 123–138.

Guyot JL. 1993. Hydrogéochimie des fleuves de l'Amazonie bolivienne, *Editions de l'ORSTOM. Paris*, 261.

Henderson-Sellers A, Dickinson RE, Durbidge TB, Kennedy PJ, McGuffie K, Pitman AJ. 1993. Tropical deforestation: modeling local- to regional-scale climate change. *Journal of Geophysical Research* **98**: 7289–7315.

DOI: 10.1002/joc

Hiez G. 1977. L'homogénéité des données pluviométriques. *Cahier ORSTOM, série Hydrologie* **14**: 129–172.

Hiez G, Cochonneau G, Sèchet P, Medeiros Fernandes U. 1991. Aplicação do método do Vetor Regional : analise da pluviometria anual da bacia amazônica. *IX Simposio Brasileiro de Recursos Hidricos*. *ABRH* **1**: 367–377.

Horel JD, Hahmann AN, Geisler JE. 1989. An investigation of the annual cycle of convective activity over the tropical Americas. *Journal of Climate* **2**: 1388–1403.

Houghton RA, Skole DL, Nobre CA, Hackler JL, Lawrence KT, Chomentowski WH. 2000. Annual fluxes of carbon from deforestation and regrowth in the Brasilian Amazon. *Nature* **403**: 301–304.

Hubert P, Carbonnel JP, Chaouche A. 1989. Segmentation des séries hydrométéorologiques. Application à des séries de précipitations et de débits de l'Afrique de l'Ouest. *Journal of Hydrology* **110**: 349–367.

Institut de Recherche pour le Développement (IRD). 2002. KHRONOSTAT: Software for statistical analysis of chronological series, www.mpl.ird.fr/hydrologie/gbt/projets/iccare/khronost.htm.

Johnson AM. 1976. The climate of Peru, Bolivia and Ecuador. *Climates of Central and South America, World Survey of Climatology*, Vol. 12. Elsevier Scientific Publishing Company; New York 147–218, Chap. 4.

Kendall MG. 1975. *Rank Correlation Methods*. Griffin.

Kousky VE, Kayano MT, Cavalcanti IFA. 1984. A review of the southern oscillation: oceanic, atmospheric circulation changes and related anomalies. *Tellus* **36A**: 490–504.

Laraque A, Ronchail J, Cochonneau G, Pombosa R, Guyot JL. 2007. Heterogeneous distribution of rainfall and discharge regimes in the Ecuadorian Amazon basin. *Journal of Hydrometeorology* **8**: 1364–1381.

Lau KM, Wu HT. 2006. Detecting trends in tropical rainfall characteristics, 1979–2003. *International Journal of Climatology* **27**: 979–988.

Lee AFS, Heghinian SM. 1977. A shift of the mean level in a sequence of independent normal random variables-A bayesian approach. *Technometrics* **19**: 503–506.

Le Tourneau FM. 2004. Jusqu'au bout de la forêt? Causes et mécanismes de la déforestation en Amazonie brésilienne. *M@ppemonde* **75**, http://mappemonde.mgm.fr/num3/articles/art04307.html.

Liebmann B, Marengo JA. 2001. Interannual variability of the rainy season and rainfall in the Brazilian Amazonia. *Journal of Climate* **14**: 4308–4318.

Mantua NJ, Hare SR, Zhang Y, Wallace JM, Francis RC. 1997. A Pacific interdecadal climate oscillation with impacts on salmon production. *Bulletin of the American Meteorological Society* **78**: 1069–1079.

Marengo JA. 1992. Interannual variability of surface climate in the Amazon basin. *International Journal of Climatology* **12**: 853–863.

Marengo JA. 2004. Interdecadal variability and trends of rainfall across the Amazon basin. *Theoretical and Applied Climatology* **78**: 79–96.

Marengo JA, Hastenrath S. 1993. Case studies of extreme climatic events in the Amazon basin. *Journal of Climate* **6**: 617–627.

Marengo JA, Nobre CA. 2001. General characteristics and variability of climate in the Amazon basin and its links to the global climate system. In *The Biochemistry of the Amazon basin*, Clain ME, Victoria RL, Richey JE (eds). Oxford University Press; UK, 17–41.

Marengo JA, Nobre CA, Tomasella J, Oyama MD, de Oliveira GS, de Oliveira R, Camargo H, Alves LM. 2008. The drought in Amazonia in 2005. *Journal of Climate* **21**: 495–516.

Marengo JA, Soares WR, Saulo C, Nicolini M. 2004. Climatology of the Low Level Jet East of the Andes as derived from the NCEP-NCAR reanalysis. Characteristics and temporal variability. *Journal of Climate* **17**: 2261–2280.

Marquez J, Salati E, Marden Dos Santos J. 1980. A divergência do campo fluxo de vapor d'água e as chuvas na região amazônica. *Acta Amazônica* **10**: 133–140.

Matsuyama H, Marengo JA, Obregón GO, Nobre CA. 2002. Spatial and temporal variabilities of rainfall in tropical South America as derived from climate prediction center merged analysis of precipitation. *International Journal of Climatology* **22**: 175–195.

Mialocq L, Acuña M, Seyler F, Yerren J, Guyot JL. 2005. Extraction of the topographic limits of the Andean and Amazonian rivers basin from SRTM. *Paper presented at the workshop on: Isotope tracers and remote sensing techniques for assessing water cycle variability, VII th. IAHS Scientific Assembly*, Foz do Iguaçu, 3–9 April 2005.

Molinier M, Guyot JL, Oliveira E, Guimarães V. 1996. Les régimes hydrologiques de l'Amazone et de ses affluents. *L'hydrologie Tropicale: Géoscience et outil pour le Développement* **238**: 209–222, Paris, Mai 1995. *IAHS Publ.*.

Molion LCB. 1987. Climatologia dinâmica da região Amazônica: mecanismos de precipitação. *Revista Brasileira de Metodologia* **2**: 107–117.

Molion LCB. 1993. Amazonian rainfall and its variability. *Hydrological and Water Management in the Humid Tropics*. Cambridge University press: Cambridge; 99–111.

Moron V, Bigot S, Roucou P. 1995. Rainfall variability in subequatorial America and Africa and relationships with the main sea-surface temperature modes (1951–1990). *International Journal of Climatology* **15**: 1297–1322.

Nicholson C. 1948. Ensayo de la clasificación de los climas del Perú. *Boletín de la Sociedad Geográfica de Lima* **65**: 3–8.

Nobre CA. 1983. Amazonia and Climate. *Proc. Of the WMO technical conf. on climate for Latin America and the Caribbean*. Colombia WMO, 409–416.

Nobre CA, Sellers P, Shukla J. 1991. Amazonian deforestation and regional climate change. *Journal of Climate* **4**: 957–988.

Nobre P, Shukla J. 1996. Variation of sea surface temperature, wind stress and rainfall over the tropical Atlantic and South America. *Journal of Climate* **9**: 2469–2479.

Oliveira AS, Nobre CA. 1986. Meridional penetration of frontal systems in South America and its relation to organized convection in the Amazon, *Publication INPE*-3407-PRE/676.

Pettitt AN. 1979. A non-parametric approach to the change-point problem. *Applied Statistics* **28**: 126–135.

Polcher J, Laval K. 1994. A statistical study of the regional impact of deforestation on climate in the LMD GCM. *Climate Dynamics* **10**: 205–219.

Poveda G. 2004. La hidroclimatología de Colombia: Una síntesis desde la escala interdecadal hasta la escala diurna. *Revista de la Academia da Ciencias* **28**: 201–222.

Poveda G, Mesa OJ. 1993. Metodologías de predicción de la hidrología colombiana considerando el evento de El Niño Oscilación del Sur (ENOS), *Atmósfera. Sociedad Colombiana de Meteorología*, **17**.

Poveda G, Waylen P, Pulwarty R. 2006. Annual and Inter-annual Variability of Present Climate in Northern South America and Southern Mesoamerica. *Palaeogeography, Palaeoclimatolgy, Palaeoecology* **234**(1): 3–27.

Pulwarty RS, Barry RG, Hurst CM, Sellinger K, Mogollon LF. 1998. Precipitation in the Venezuelan Andes in the context of regional climate. *Meteorology and Atmospheric Physics* **67**: 217–237.

Ratisbona LR. 1976. The climate of Brazil. *Climates of Central and South America, World Survey of Climatology*, Vol. 12. Elsevier Scientific Publishing Company; New York, 219–293, chap. 5.

Rao VB, Cavalcanti IFA, Hada K. 1996. Annual variation of rainfall over Brazil and water vapor characteristics over South America. *Journal of Geophysical Research* **101**: 26539–26551.

Robertson AW, Mechoso CR. 1998. Interanual and decadal cycles in river flow of southeastern of South America. *Journal of Climate* **11**: 2570–2581.

Roche MA, Aliaga A, Campos J, Pena J, Cortes J, Rocha N. 1990. Hétérogénéité des précipitations sur la cordillère des Andes boliviennes, *Hydrology in Mountainous Regions. I – Hydrological Measurements; the Water Cycle*, IAHS **193**, 381–388.

Rome S, Ronchail J. 1998. La pluviométrie au Pérou pendant les phases ENSO et LNSO. *Bulletin de l'Institut Française d'Etudes Andines* **27**: 675–685.

Ronchail J. 1989. Advections Polaires en Bolivie: mise en évidence et caractérisation des effets climatiques. *Hydrologie Continentale* **4**: 49–56.

Ronchail J. 1996. Variabilité pluridécénale des précipitations en Bolivie. Essai de mise en relation avec les températures de surface océaniques de l'Atlantique extra-tropical. *Publication de l' Association Internationale de Climatologie* **9**: 504–511.

Ronchail J. 1998. Variabilité pluviométrique en Bolivie lors de phases extrêmes de l'Oscillation Australe du Pacifique (1950–1993). *Bulletin de l'Institut Français d'Etudes Andines* **27**: 687–698.

Ronchail J, Bourrel L, Cochonneau G, Vauchel P, Phillips L, Castro A, Guyot JL, de Oliveira E. 2005. Climate and inundation in the Mamoré basin (South-Western Amazon – Bolivia). *Journal of Hydrology* **302**: 223–238.

Ronchail J, Cochonneau G, Molinier M, Guyot JL, Goretti de Miranda Chaves A, Guimarães V, de Oliveira E. 2002. Rainfall variability in the Amazon Basin and SSTs in the tropical Pacific and Atlantic oceans. *International Journal of Climatology* **22**: 1663–1686.

DOI: 10.1002/joc

Ronchail J, Gallaire R. 2006. ENSO and rainfall along the Zongo valley (Bolivia) from the Altiplano to the Amazon basin. *International Journal of Climatology* **26**: 1223–1236.

Rossel F, Goulven PL, Cadier E. 1999. Areal distribution of the influence of ENSO on the annual rainfall in Ecuador. *Revue des Sciences de l'Eau/Journal of Water Science* **12**: 183–200.

Salati E, Marquez J, Molion LC. 1978. Origem e distribuição das chuvas na Amazônia. *Interciencia* **3**: 200–205.

Salati E, Vose PB. 1984. Amazon basin: a system in equilibrium. *Science* **225**: 129–138.

Saulo AC, Nicolini M, Chou SC. 2000. Model characterization of the South American low-level flow during the 1997–1998 spring-summer season. *Climate Dynamics* **16**: 867–881.

Seluchi M, Marengo JA. 2000. Tropical-midlatitude exchange of air masses during summer and winter in South America: climates aspects and examples of intense events. *International Journal of Climatology* **20**: 1167–1190.

Shukla J, Nobre CA, Sellers P. 1990. Amazon deforestation and climate change. *Science* **247**: 1322–1325.

Siegel S, Castellan NJ. 1988. *Non – Parametric Statistics for the Behavioural Sciences*. McGraw-Hill; USA.

Silva Dias MAF, Rutledge S, Kabat P, Silva Dias PL, Nobre CA, Fisch G, Dolman AJ, Zipser E, Garstang M, Manzi AO, Fuentes JD, da Rocha HR, Marengo JA, Plana-Fattori A, S'a LDA, Alval'a RCS, Andreae MO, Artaxo P, Gielow R, Gatti L. 2002. Cloud and rain processes in a biosphere-atmosphere interaction context in the Amazon Region. *Journal of Geophysical Research* **107**, DOI 10.1029/2001JD000335.

Tapley TD, Waylen PR. 1990. Spatial variability of annual precipitation and ENSO events in western Peru. *Hydrological Sciences Journal* **35**: 429–445.

Trenberth KE, Hurrell JW. 1994. Decadal atmosphere – ocean variations in the Pacific. *Climate Dynamics* **9**: 303–319.

Uppala SM, Kållberg PW, Simmons AJ, Andrae U, da Costa Bechtold V, Fiorino M, Gibson JK, Haseler J, Hernandez A, Kelly GA, Li X, Onogi K, Saarinen S, Sokka N, Allan RP, Andersson E, Arpe K, Balmaseda MA, Beljaars ACM, van de Berg L, Bidlot J, Bormann N, Caires S, Chevallier F, Dethof A, Dragosavac M, Fisher M, Fuentes M, Hagemann S, Hólm E, Hoskins BJ, Isaksen L, Janssen PAEM, Jenne R, McNally AP, Mahfouf JF, Morcrette JJ, Rayner NA, Saunders RW, Simon P, Sterl A, Trenberth KE, Untch A, Vasiljevic D, Viterbo P, Woollen J. 2005. The ERA-40 re-analysis. *Quarterly Journal of the Royal Meteorological Society* **131**: 2961–3012.

Uvo CB, Repelli CA, Zebiak SE, Kushnir Y. 1998. The relationship between Tropical Pacific and Atlantic SST and northeast Brazil monthly precipitation. *Journal of Climate* **11**: 551–562.

Vauchel P. 2005. Hydraccess: Software for Management and processing of Hydro – meteorological data software, Version 2.1.4. Free download www.mpl.ird.fr/hybam/utils/hydracces.htm.

Vuille M, Bradley R, Keiming F. 2000. Interannual climate variability in the clentral Andes and its relation to tropical Pacific and Atlantic forcing. *Journal of Geophysical Research* **105**: 12447–12460.

Wagnon P, Ribstein P, Francou B, Sicart JE. 2001. Anomalous heat and mass budget of Glacier Zongo, Bolivia, during the 1997/98 E1 Niño year. *J. Glaciol.* **47**: 21–28.

Wang J, Bras RL, Eltahir EAB. 2000. The impact of observed deforestation on the mesoscale distribution of rainfall and clouds in Amazonia. *Journal of Hydrometeorology* **1**: 267–286.

Weberbauer A. 1945. *El Mundo Vegetal de los Andes Peruanos, Studio Fitogeográfico*. Ministerio de Agricultura: Lima. Perú.

Wolter K, Timlin MS, 1993. Monitoring ENSO in COADS with a seasonally adjusted principal component index. *Proc. of the 17th Climate Diagnostics Workshop*, Norman, OK, NOAA/N MC/CAC, NSSL, Oklahoma Clim. Survey, CIMMS and the School of Meteor., Univ. of Oklahoma, 52–57.

Zbigniew WK. 2004. Change detection in hydrological records – a review of the methodology. *Hydrological Sciences Journal* **49**: 7–119.

Zeng N, Yoon J, Marengo J, Subramaniam A, Nobre C, Mariotti A, Neelin JD. 2008. Causes and impact of the 2005 Amazon drought. *Environmental Research Letters* **3**: 9.

Zhou J, Lau KM. 1998. Does a monsoon climate exist over South America? *Journal of Climate* **11**: 1020–1040.

Zhou J, Lau KM. 2001. Principal modes of interannual and decadal variability of summer rainfall over South America. *International Journal of Climatology* **21**: 1623–1644.

DOI: 10.1002/joc

AUTEUR: Waldo Sven LAVADO CASIMIRO.

TITLE : Monthly water balance modeling and evaluation of climate change impact over the Peruvian Amazonas basin.

SUMMARY

First, we describe the main features of the basins of Huallaga and Ucayali rivers, as well as the hydrological database used an we put in evidence a warming in our zone of study (estimated at +0.09°C per decade). Moreover, the ruptures observed in the series of average temperature at the end of the Seventies are in accordance with the sequences of "El Niño". We showed a negative correlation between the temperatures and the index of the Pacific (Southern Oscillation Index, SOI). On the other hand, no tendency is highlighted in the precipitation series. Nevertheless, approximately 10% of the stations in our area of study present significant ruptures during the 1991-2000 decade.

Then, the production of water resources in the basins of Huallaga and Ucayali rivers is evaluated over 7 sub-basins: 6 located in the Ucayali basin and one located in the Huallaga basin. To quantify water resources, we use two hydrological models at monthly step (GR2M and MWB3). The use of water holding capacity data of FAO soils (maximum, mean and minimum) as input of the hydrological models, contributed to propose physical interpretations to these models. The optimal parameters obtained by calibration procedure reproduce reasonably well the flow observed in the selected basins. The impacts of climate change on hydrology were evaluated using as climatic data the outputs of the IPCC models (BCM2, CSMK3 and MIHR), corresponding to the scenarios A1B and B1. The annual flows simulated in the 2008-2099 period suggest that the impacts of climate change on hydrology vary with the basin, the hydrological model chosen, and the scenario: The Requena sub-basin is characterized by an increase (respectively a reduction) of flow using GR2M model (respectively MWB3) considering the A1B and B1 scenarios. The Chazuta, Maldonadillo and Pisac basins exhibit flows decreasing while the basins of Puerto Inca, Tambo and Mejorada show flows increasing. The changes simulated in monthly flows over the 2008-2099 period suggest an increase for all the sub-basins, except the Pisac basin. July, August and September are in general the months characterized by the most marked changes, with an increase in flows for Requena, Chazuta, Puerto Inca, Maldonadillo and Tambo basins.

KEYWORDS: Amazonas basin; Peru; hydroclimatic variability; hydrological models; climate change.

FIELD : Hydrology.

AUTEUR: Waldo Sven LAVADO CASIMIRO.

TITRE : Modélisation du bilan hydrique à pas de temps mensuel pour l'évaluation de l'impact du changement climatique dans le bassin Amazonien du Pérou.

DIRECTEURS DE THESE : Jean Loup GUYOT et David LABAT.

LIEU ET DATE DE SOUTENANCE : OMP Toulouse le 16 Février 2010.

RESUME en français

En premier lieu, nous décrivons les principales caractéristiques des bassins des rios Ucayali et Huallaga, ainsi que la base de données utilisée. Nous avons ainsi mis en évidence le réchauffement sur notre zone d'étude (estimé à +0.09°C par décade). De plus, les ruptures observées sur les séries de température moyenne à la fin des années 70 concordent avec les séquences d'événements de type « El Niño ». Nous avons aussi démontré une corrélation négative entre les températures et l'indice du Pacifique (Indice d'Oscillation du Sud, IOS). Par contre, aucune tendance n'est mise en évidence dans les séries de précipitation. Néanmoins, environ 10% des stations de notre région d'étude présentent des ruptures significatives dans la période 1991-2000.

La production des ressources en eau sur les bassins des rios Ucayali et Huallaga est évaluée pour 7 sous-bassins : 6 situés dans le bassin de l'Ucayali et un situé dans le basin du Huallaga. Pour quantifier ces ressources en eau, nous utilisons deux modèles hydrologiques au pas de temps mensuel (GR2M et MWB3). L'utilisation des données de capacité de rétention en eau des sols (maximum, moyenne et minimum) de la FAO, comme valeurs d'entrée dans les modèles hydrologiques, a contribué à rendre plus physique ces modèles. Les paramètres optimaux obtenus par calibration reproduisent raisonnablement bien l'écoulement observé à l'exutoire des bassins sélectionnés.

L'impact des changements climatiques sur l'hydrologie ont été évalué en utilisant comme données climatiques les sorties des modèles de l'IPCC (BCM2, CSMK3 et MIHR), correspondant aux scénarios A1B et B1. Les écoulements annuels simulés sur la période 2008-2099 suggèrent que les impacts du changement climatique sur l'hydrologie varient avec le bassin, le modèle hydrologique choisi, et le scénario: Le sous-basin Requena est caractérisé par une augmentation (respectivement une diminution) d'écoulement en utilisant les modèles GR2M (respectivement MWB3) en considérant les scénarios A1B et B. Les bassins de Chazuta, Maldonadillo et Pisac voient leurs débits diminuer tandis que les bassins de Puerto Inca, Tambo et Mejorada voient leurs débits augmenter.

Les changements simulés dans les écoulements mensuels sur la période 2008-2099 suggèrent une augmentation pour tous les sous-bassins, excepté le bassin de Pisac. Juillet, Août et Septembre sont en général les mois caractérisés par les changements les plus marqués, avec une augmentation des débits pour les bassins de Requena, Chazuta, Puerto Inca, Maldonadillo et Tambo.

MOTS-CLES : bassin Amazonien ; Pérou ; variabilité hydroclimatique ; modélisation hydrologique ; changement climatique.

DISCIPLINE : Hydrologie.

LMTG - UMR 5563 UR 154 CNRS Université Paul Sabatier IRD
Observatoire Midi-Pyrénées
14, Avenue Edouard Belin - 31400 Toulouse